Investigating copper binding to bacterial metallothioneins SmtA and MymT

Maria Tareen

A thesis submitted in partial fulfilment of the requirements for the degree of Doctor of Philosophy in Chemistry

Department of Chemistry

April 2014

Table of contents

Table of contents

Table of contents

Table of contents

Table of contents

Table of contents

Table of contents

List of figures

List of figures

List of figures

List of figures

List of tables

Acknowledgments

I would like to express my profound and cordial gratitude to my supervisor Dr Claudia Blindauer, for giving me this opportunity to undertake this research project. Her scholarly guidance and keen observations enabled me to complete this research work objectively and comprehensively.

I am extremely grateful to all members of the Blindauer group (both past and present) for all their help and guidance; Oksana, Jin, James, Esther, Greg, Jie, Fran, Amira and Tanvir. A big thanks to the Dixon and Bugg group members for all our interesting discussions and laughs; Mike, Dhadchi, Muhammad, Fay, Leo, Rahman and Peter. I am especially thankful to all members of Chemical Biology Research Facility for their help in lab and for the use of instruments.

I express my deepest gratitude to Ann Smith, Dr. Ivan Prokes, Dr Lijiang Song and Phil Aston, without their help it would be impossible to carry out this work. Also thanks to Prof Ben Gold for sending me MymT peptide and Prof. Alison Rodger for useful CD discussions and letting me use her CD spectrometer. I would like to thank my advisors Dr Ann Dixon and Prof Greg Challis for their constructive feedback over the past few years. Special thanks to Prof Martin Wills and Dr David Josey for their massive support.

I pay my greatest tributes to my family and friends for all their love and encouragement, in particular Zeina, Freeha, Gulnaz, Khadija, Sohail, Rashmi and Mariam for always on my side. I owe a great deal to Dharmesh for constant support

and helping me throughout my project- thanks for all those chips lunches and reassurance after my injury.

Finally I dedicate this thesis to my parents who inspired me and encouraged me to think of highest idea of life and provided me with all the assistance I ever needed regardless of their busy routine.

Declaration

I hereby declare that this thesis, submitted in partial fulfilment for the degree of Doctor of Philosophy, represents my own work and has not been previously submitted to this or any other institution for any other qualification. Work was conducted under the supervision of Dr Claudia Blindauer. All sources of information have been acknowledged by means of reference.

Maria Tareen

April 2014

Abbreviations

aa	Amino acids
ACN	Acetonitrile
AU	Absorbance units
BMRB	Biological magnetic resonance databank
BCS	Bathocuproin disulfonate
CD	Circular dichroism
1D	One-dimensional
2D	Two-dimensional
3D	Three-dimensional
dH_2O	distilled water
DTT	Dithiothreitol
DTNB	5,5'-dithiobis-(2-nitrobenzoic acid)
ESI-MS	Electrospray ionisation mass spectrometry
EDTA	Ethylenediaminetetraacetic acid
FT	Fourier transform
g	Grams
HPLC	High performance liquid chromatography
hr	Hours

Abbreviations

HSQC	Heteronuclear single quantum coherence
Hz	Hertz
IPA	Isopropanol
IPTG	Isopropyl β-D–1-thiogalactopyranoside
ICP-OES	Inductively coupled plasma-optical emission spectroscopy
kDa	kilo Dalton
kHz	Kilo Hertz
MALDI-TOF	Matrix-assisted laser desorption ionisation time of flight
mg	Milligram
MHz	Mega Hertz
mL	Millilitre
mM	Millimolar
ms	Millisecond
NMR	Nuclear magnetic resonance
nm	Nanometre
NOE	Nuclear Overhauser enhancement
NOESY	Nuclear Overhauser spectroscopy
ppm	Parts per million
RF	Radio frequency
RT	Room temperature
s	Seconds
SDS	Sodium dodecyl sulphate
T_1	Longitudinal relaxation time
T_2	Transversal relaxation time

Abbreviations

TFA	Trifluoroacetic acid
TOCSY	Total correlation spectroscopy
TRIS	Tris (hydroxymethyl) aminomethane
TOF	Time of flight
UV	Ultraviolet
w/v	Weight per volume

Greek symbols

ε	Extinction coefficient
λ	Wavelength
µg	Micro gram
µL	Micro litre
µM	Micro molar

Amino acid abbreviations

Amino acid	Single letter	Short code	Molecular formula	Structure
Aspartate	D	Asp	$C_4H_7NO_4$	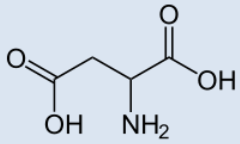
Glutamate	E	Glu	$C_5H_9NO_4$	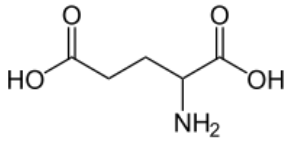
Lysine	K	Lys	$C_6H_{14}N_2O_2$	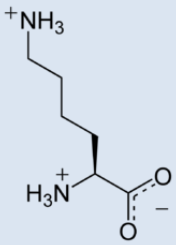
Arginine	R	Arg	$C_6H_{14}N_4O_2$	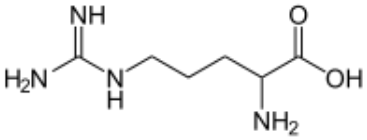
Histidine	H	His	$C_6H_9N_3O_2$	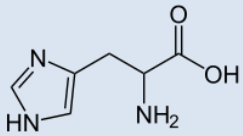
Serine	S	Ser	$C_3H_7NO_3$	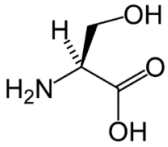
Threonine	T	Thr	$C_4H_9NO_3$	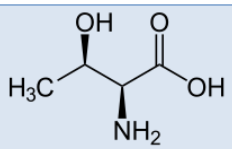

Abbreviations

Glutamine	Q	Gln	$C_5H_{10}N_2O_3$	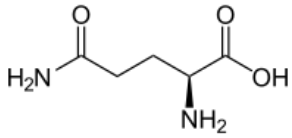
Asparagine	N	Asn	$C_4H_8N_2O_3$	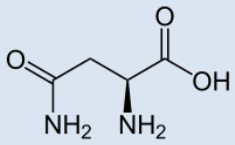
Tyrosine	Y	Tyr	$C_9H_{11}NO_3$	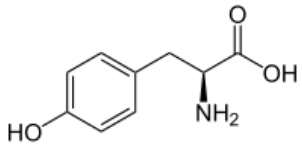
Alanine	A	Ala	$C_3H_7NO_2$	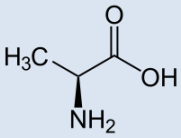
Valine	V	Val	$C_5H_{11}NO_2$	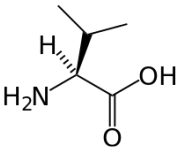
Leucine	L	Leu	$C_6H_{13}NO_2$	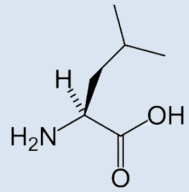
Isoleucine	I	Ile	$C_6H_{13}NO_2$	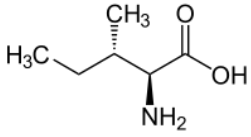
Methionine	M	Met	$C_5H_{11}NO_2S$	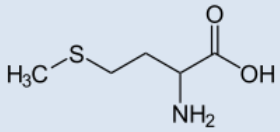

Phenylalanine	F	Phe	$C_9H_{11}NO_2$	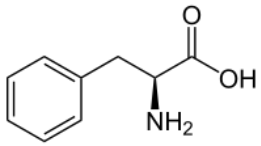
Tryptophan	W	Trp	$C_{11}H_{12}N_2O_2$	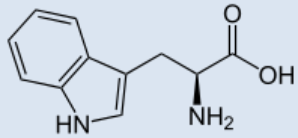
Glycine	G	Gly	$C_2H_5NO_2$	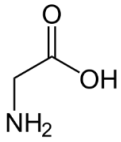
Cysteine	C	Cys	$C_3H_7NO_2S$	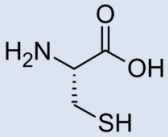
Proline	P	Pro	$C_5H_9NO_2$	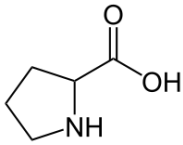

Summary

Metallothioneins are characterized as a group of small proteins with low molecular weight and high content of cysteinyl residues and their synthesis is induced by metal ions (e.g., Zn or Cd). The physicochemical properties of Zn-, Cd-, and Cu-containing MTs have been studied. However, copper metallothioneins (Cu-MTs) have been examined less intensively, with only two MTs containing Cu(I) having been structurally characterized to date i.e., yeast MT and *Neurospora crassa* MT.

The present study focuses on the stoichiometry and structural effects of binding of Cu(I) to the natively zinc binding MT (SmtA) from the cyanobacterium *Synechococcus elongatus* PCC7942. For this purpose, a Cu(I) titration study of Zn_4SmtA was anaerobically performed utilizing the collective detection of ESI-MS, UV-Vis absorbance and ^{1}H-^{15}N NMR spectroscopy, and fully exchanged Cu(I)-SmtA was also generated from the apo-protein. ESI-MS data confirmed the presence of predominantly monomeric Cu_7SmtA. UV-vis titrations of Zn_4SmtA showed that up to 7 Cu(I) displace Zn(II) from the protein, which was further studied in more detail by Cu(I) titrations of Zn_4SmtA monitored with ^{1}H-^{15}N and ^{111}Cd-^{15}H NMR spectroscopy. The extensive NMR analysis showed the unfolding of protein on Cu(I) addition with absence of inertness towards Cu(I) exchange and that the protein undergoes significant conformational changes on Cu(I) addition.

Preliminary characterization of MymT from *Mycobacterium tuberculosis* was also done and the composition of the metal cluster in the dominant Cu_5MymT species was proposed and cooperativity was established by ESI-MS analyses, although structural characterisation was impeded by the highly dynamic nature of the protein.

1

Introduction

The focus of the research undertaken was to study the copper binding properties of two bacterial metallothioneins from two different families i.e., SmtA from cyanobacterium *Synechococcus* and MymT from pathogenic *Mycobacterium tuberculosis*. This chapter examines the contextual and conceptual grounds, which underpin this research.

1.1 Metal ions in biology and their homeostasis

Metal ions are important in biological systems and serve as critical cofactors in physiological processes such as respiration, growth, gene transcription, enzymatic reactions, cell production and immune function. Metal ions can also be toxic when present at higher concentrations and therefore metal import/export, trafficking and availability must be tightly regulated at the cellular levels, which is collectively called metal homeostasis (Dean et al 2012). Metal homeostasis is defined as the preservation of an optimal bioavailable concentration, facilitated by the regulation of metal uptake and intracellular trafficking with efflux/storage processes to achieve the metal ion needs of the cell i.e., the right metal is incorporated into the right macromolecule at the suitable instance (Ma et al. 2009).

Changes in metal homeostasis cause or are associated with various diseases including genetic disorders, degenerative diseases, cancer and diabetes. Since at least half of all enzymes and proteins require metal ions to perform their functions (Nelson 1999), it is crucial to maintain the balance of such essential metals because higher concentrations of metal ions can be very toxic and lower concentrations may be too low for a healthy organism (Waldron et al 2009, Blindauer 2013).

Metal ions can be categorized as essential and non-essential for the growth of an organism. This can be simply explained on the basis of the Bertrand model, which describes the relationship between the concentration of the metal and the response of an organism (Bertrand 1912, Mertz 1981). An optimum balance is required for essential metals e.g. Zn(II), and deficiency can be harmful to health. On the other hand, non-essential metal ions such as Cd(II) become toxic at a much lower concentrations as shown in Figure 1.1.

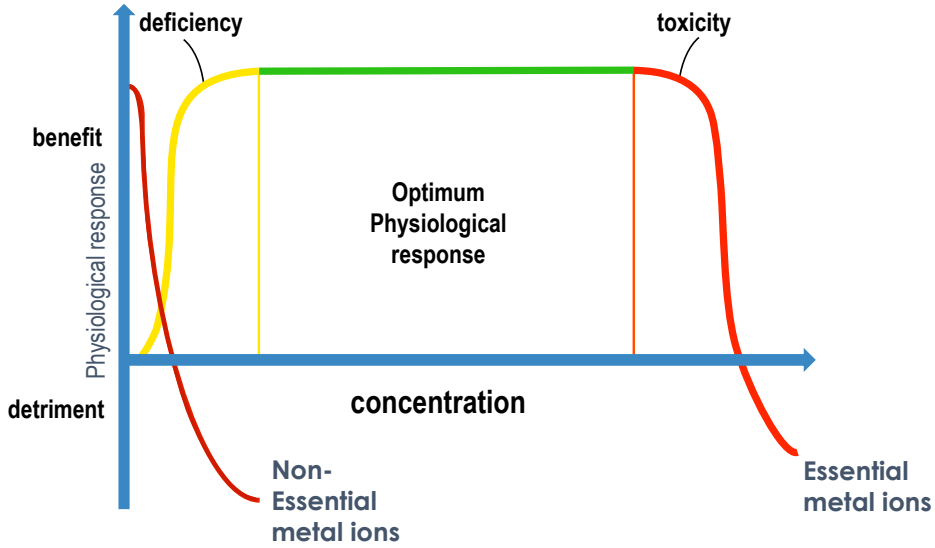

Figure 1.1 Essential and non-essential metal ions.

The plot shows the relationship of nutrient (essential and non-essential metals) to the physiological response (Figure adapted from Bertrand 1912).

It can be anticipated from the model (as shown in Figure 1.1) that any metal ion, regardless of whether it is essential or non-essential, can be hazardous and it is the concentration, which establishes its toxicity (Mertz 1981, Mertz 1998). An order of preference for thiolate containing ligands of essential and non-essential metals as provided by Irving-Williams series is Mg < Ca < Mn < Fe < Co < Ni < Cu > Zn (Foster and Robinson 2011).

1.2 Copper in biological systems

Copper is an essential trace element required by all living organisms for their growth and development (Roberts and Sarkar 2008). It plays a crucial role in cell metabolism as a cofactor for numerous enzymes, such as ceruloplasmin, cytochrome c oxidase, superoxide dismutase, dopamine-β-hydroxylase, tyrosinase, and lysyl oxidase (Cousins 1985) (Table 1.1). Copper proteins are widely involved in electron transfer reactions in the presence of oxygen, because of the favorable redox potential of Cu(II)/Cu(I) (Crichton and Pierre, 2001). Table 1.1 (adapted from Kim et al 2008) gives an overview of important copper binding proteins.

Table 1:1 Cu dependent proteins in biological systems

Examples of Cu dependant proteins.					
Protein	**Protein**	**Bacteria**	**Fungi**	**Animals**	**Plants**
Ethylene receptor	Uses Cu as a cofactor for ethylene signalling				X
Oxidoreductases					
Ascorbate oxidase	Reduction of L-ascorbate			X	
Dopamine-monooxygenase	Tyrosine metabolism			X	
Galactose oxidase	Reduction of galactose		X		
Amine oxidase	Oxidation of diamines	X	X	X	X
Electron transfer/energy production/blue Cu proteins					
Cytochrome *c* oxidase	Necessary for the last step of respiration	X	X	X	X
Plastocyanin	Electron transfer during photosynthesis	X			X
NADH dehydrogenase	Electron transfer from NADH to coenzyme Q	X	X	X	X
Nitrite reductase	Reduces nitrite to nitric oxide	X			
Amicyanin	Electron-accepting intermediate in the conversion of methylamine to formaldehyde and ammonia	X			
Free radical scavenging					
Cu/Zn SOD	Free radical scavenging	X	X	X	X
Oxidases					
Laccase	Melanine production	X	X	X	X
Lysyl oxidase,	Catalyzes the formation of collagen and elastin precursors extracellular			X	
Ceruloplasmin	MultiCu oxidase			X	
Hephaestin	Transmembrane ferroxidase, transports iron from the intestine to the circulatory system			X	
Multicopper ferroxidase	Cu-dependent iron uptake		X	X	X
Monooxygenases					
Methane monooxygenase	Oxidizes C–H bond in methane	X			
Phenylalanine hydrolase	Hydroxylation of the aromatic side chain of phenylalanine to generate tyrosine			X	
Tyrosinase	Monophenol monooxygenase, catalyzes the oxidation of phenols, melanin synthesis	X	X	X	X

Although required in trace amounts, excess copper has the ability to generate reactive oxygen species or free radicals (Seth et al. 2004), discussed in more detail in section 1.2.2, which oxidize cellular components and disrupt cellular metabolism if present in levels above the required amounts (Halliwell 1994). Therefore it is critical to tightly regulate cellular copper concentrations.

1.2.1 Copper in biology: Coordination aspects

In biological systems, Cu ions can exist in two oxidation states, Cu(I) and Cu(II) (reduced and oxidized respectively). The redox activity of copper is being exploited by organisms to use it as a catalytic cofactor for a variety of metalloenzymes involved in many diverse processes (Bertinato and Abbé 2004, Kim et al 2008) (also see Table 1.1). According to the Hard and Soft Acids and Bases (HSAB) principle (Pearson 1968), Cu(I) is a soft acid while Cu(II) is a borderline acid. So the copper binding sites in proteins are anticipated to be dominated by amino acids containing side chains with soft or borderline ligands i.e., amino acids with nitrogen and sulfur donor atoms (e.g. histidine, cysteine, methionine, see Figure 1.2) would be preferred over amino acids with carboxyl, hydroxyl, or primary amine side chains (as in aspartate and glutamate, serine, threonine, tyrosine, or lysine) (Rubino and Franz 2012). The coordination chemistries of Cu(I) and Cu(II) are distinct, with Cu(I) displaying a preference for sulfur donor ligands such as cysteine or methionine whilst Cu(II) favors nitrogen donor ligands like histidine, but oxygen donors like glutamate and aspartate may also be encountered (Rubino and Franz 2012, Davis and O' Halloran 2008).

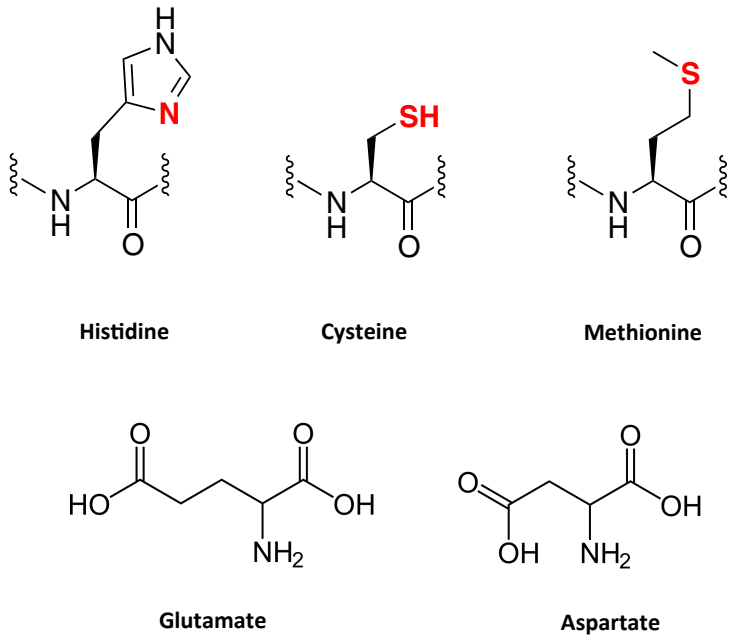

Figure 1.2 Copper binding ligands in proteins

The characteristics of the ligands such as histidine (strong binder, neutral or rarely anionic, hydrophilic with Cu(II) preferences, cysteine (anionic, hydrophilic, Cu(I) preference and methionine (no proton, neutral, hydrophobic, weak binder) favoring Cu(I) binding, oxygen donors glutamate and aspartate with Cu(II) preference. (Adapted from Rubino and Franz 2012)

Histidine comprises an imidazole functional group that contains two nitrogen atoms (both can be protonated with pK_a values of ~6 and ~14 for the free amino acid, but depending on protein environment and coordination to metals). Loss of first proton gives a neutral imidazole nitrogen donor whilst an anionic imidazole is formed after losing the second proton. Imidazolate with two nitrogen donors on opposite sides of the ring can bridge two metal ions as seen in Cu, Zn superoxide dismutase. Cysteine contains a proton in its thiol side chain, which must be removed to provide an anionic thiolate as an active metal binding site. The thiolate sulfur can also bridge two or even three metal centers. However, cysteines are redox active and can oxidize to form (amongst others) disulfide cross-linked cystine. On the contrary, methionine does not contain a protonatable side chain and does not form cross-links. The thioether functional group in methionine provides a neutral sulfur

donor with no pH dependence, unlike histidines and cysteines, and is less prone to oxidation (depending on conditions, oxidation to methionine sulfoxide and methionine sulfone can occur). Furthermore, the side chain of methionine is more hydrophobic than histidines and cysteines, which may influence solvent accessibility and protein-protein interactions (Rubino and Franz 2012).

The preferences of metal ions in binding geometry are based on the number of valence *d* electrons and the number and type of coordinating ligands. According to LFT (ligand field theory), there are likely differences in geometric preferences for Cu(II) and Cu(I). With a filled d^{10} system, Cu(I) does not exhibit geometric preferences based on ligand field stabilization energy (LFSE). Hence, it is mostly coordinated by 2, 3, or 4 ligands in linear, trigonal planar or tetrahedral geometries. Cu(II) with d^9 system experiences geometric preferences based in part on LFSE (ligand-field stabilisation energy), with coordination numbers 4, 5 or 6 in square planar, square pyramidal, or axially distorted octahedral geometries respectively, the latter as result of Jahn-Teller distortion.

The reduction potential of a metal ion depends on both its ligands and coordination number. Soft donors such as thiolates lead to more positive reduction potentials and may stabilize Cu(I). The cytoplasm is a reducing environment and is rich in thiolates such as glutathione, which is also capable of binding Cu(I). Therefore copper compounds in the cytoplasm are overwhelmingly present as Cu(I)-complexes. Also the major transporter in mammals, Ctr1, transports Cu(I) which implies the reduction of Cu(I) outside the cell (Nevitt et al. 2012).

1.2.2 Mechanisms for copper toxicity

If Cu(II) enters the cytoplasm of a cell, it will be reduced, and depending on the molecule being oxidized, this may result in formation of a positively charged organic radical which may furthermore lead to formation of reactive oxygen species (ROS). The major toxic effect of copper is, however, thought to be mediated by Cu(I) and is the formation of ROS in

Fenton type reactions, leading to the formation of hydroxyl radicals (OH·), hydrogen peroxide (H_2O_2) and superoxide (O_2^-) (Liochev and Fridovich 2002, Hodgkinson and Petris 2012, Chaturvedi and Henderson 2014).

(a) $Cu^+ + H_2O_2 \rightleftharpoons Cu^{2+} + OH^- + \cdot OH$

(b) $Cu^{2+} + O_2 \rightleftharpoons Cu^+ + O_2^-$

In addition, the depletion of sulfhydryl by reactions as shown below (c, d) has also been suggested as a cell damaging mechanisms (Solioz et al 2010).

(c) $2Cu^{2+} + 2RSH \rightleftharpoons 2Cu^+ + RSSR + 2H^+$

(d) $2Cu^+ + 2H^+ + O_2 \rightleftharpoons 2Cu^{2+} + H_2O_2$

ROS are detrimental to cellular components such as proteins, lipids and nucleic acids and have been associated with aging, neurological disorders and cancer (Finkel and Holbrook 2000, Banci et al 2010, Solioz et al 2010). Although oxidative stress has been reported *in vitro* as a mechanism of copper toxicity, another possibility responsible for primary toxic effects of copper *in vivo* was suggested by Solioz et al 2010. These findings were based on the copper specific damage of iron-sulfur clusters of an enzyme (isopropylmalate dehydratase) in *E. coli* both *in vivo* and *in vitro*. This enzyme of the branched chain amino acid biosynthesis pathway contains an iron-sulfur cluster, from which copper can displace iron under anaerobic conditions. Copper efflux systems as well as cluster repair by assembly systems improve cell resistance to this type of copper toxicity (Solioz et al 2010).

Cu(I) ions also need to be kept away from metal binding sites where they are not needed owing to the higher affinity of Cu(I) compared to other essential metals such as Zn(II) (Robinson 2011, Foster and Robinson 2011). For these reasons, intracellular copper concentrations must be kept extremely low, and copper trafficking must be controlled such that copper ions are transported to essential enzymes, but cells do not store detrimental amounts owing to copper's redox active properties. In humans, improper copper

homeostasis is associated with diseases such as Wilson and Menkes disorders, prion disease (Barnes et al. 2005, Bie et al. 2007, Richardson 2007), and Parkinson and Alzheimer's diseases (Christen 2000, Desai and Kaler 2008, West et al. 2008, Davies et al. 2014).

1.3 Copper homeostasis

To avoid copper exerting any of the above effects, there is a complex and sophisticated network of copper-trafficking proteins including metallo-chaperones, metallothioneins and copper-transporting ATPases (Rae et al. 1999; Harrison et al. 2000; O'Halloran and Culotta 2000; Lutsenko et al. 2002, Robinson and Winge 2010, Robinson 2011). Table 1.2 gives an overview of important proteins involved in copper homeostasis. These proteins not only ensure the transport of copper to the correct macromolecule and cellular compartments for fundamental functions but also help with detoxifying excess copper (Boal and Rosenzweig 2009, Waldron and Robinson 2009).

Table 1:2 Copper homeostasis proteins (adapted from Kim et al 2008).

Examples of Cu homeostasis proteins.					
Protein	**Function**	**Bacteria**	**Fungi**	**Animals**	**Plants**
Transcriptional regulators					
Ace1	Transcriptional activation in high Cu conditions		X		
CopY	Bacterial Cu metalloregulatory repressor	X			
CsoR	Bacterial Cu metalloregulatory repressor	X			
Mac1	Transcriptional activator in low Cu conditions		X		
CueR	Bacterial Cu metalloregulatory repressor	X			
Mtf1	Metalloregulatory transcription factor			X	
Spl7	Transcriptional activator responding to Cu deficiency				X
Chaperones/storage					
Atox1	Metallochaperone delivering Cu to P-type ATPases		X	X	X
Ccs	Delivers Cu to the Cu/Zn SOD1		X	X	X
CopZ	Bacterial Cu chaperone	X			
Metallothionein	Low molecular weight, cysteine-rich metal-binding and detoxification	X	X	X	X
Cell surface/secretory compartment transporters and receptors					
P1B-type ATPases	Cu+-exporting proteins	X	X	X	X
Ctr	Cu+-importing proteins		X	X	X

A representation of copper regulation and trafficking in plants, cyanobacteria, Gram-positive bacteria (*E. hirae*) and Gram-negative bacteria (*E. coli*) is shown in Figure 1.3 (adapted from Banci et al. 2010).

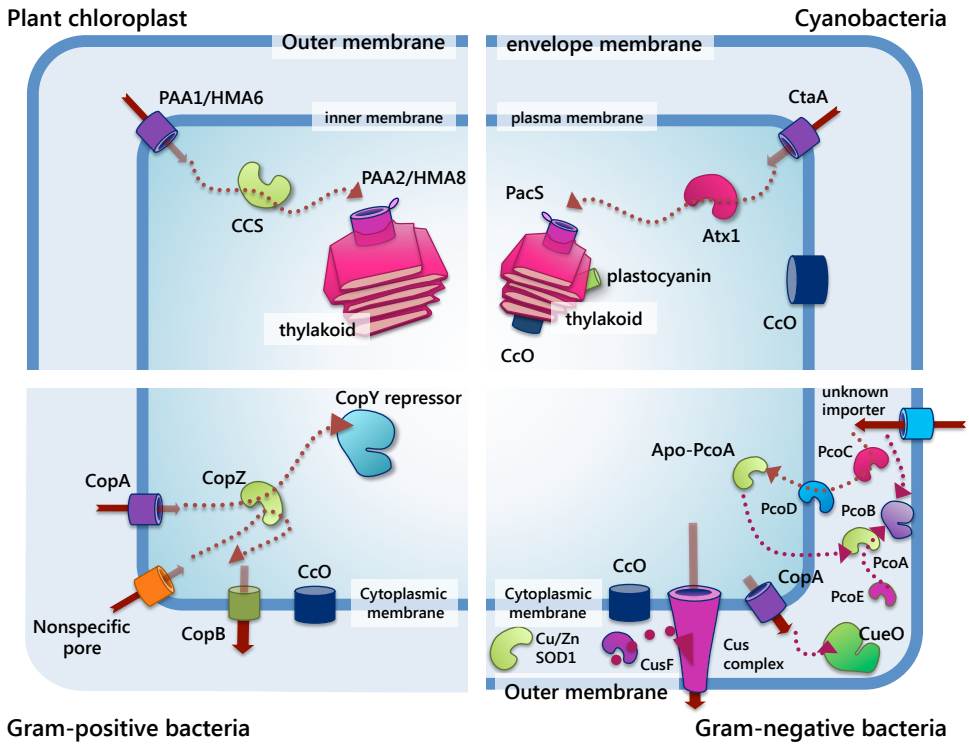

Figure 1.3 Diagrammatic representation of copper pathways in biological systems

In the plant chloroplast, copper is taken by PAA1/HMA6 and carried via CCS to the thylakoid, where it is imported through PAA2/HMA8. In cyanobacteria, CtaA imports copper and Atx1 carries it to the thylakoid, where it is imported through PacS. In *E. hirae* (a Gram-positive bacterium), copper CopA or a nonspecific pore uptakes copper where (in cytoplasm) it binds to CopZ, which delivers copper to CopB for export, or to the CopY repressor to induce the cop operon. In *E. coli* (a Gram-negative bacterium), CopA transports copper from the cytoplasm into the periplasmic space, where it can be oxidized by the multi-copper oxidase CueO. However it must be noted that *E. hirae* CopA and *E. coli* CopA (despite of the same name) transport copper in opposite directions; *E. coli* CopA is functionally equivalent to *E. hirae* CopB. The Cus system can also expel Cu(I), which then delivered to the efflux system by the soluble protein CusF. In the periplasm, PcoC transport Cu(I) to PcoD, which leads to incorporation into the multi-copper oxidase PcoA. The

metallated PcoA can oxidize Cu(I) from PcoC to Cu(II) in the periplasm, which may be exported by the outer membrane protein PcoB. PcoE also transports Cu(I) to PcoA or can act as a copper storage element. However the mechanism through which copper enters the periplasmic space is not known (Banci et al. 2010).

1.4 Copper homeostasis at the macrophage-pathogen interface

Early observations suggested that the toxicity of free Cu(I) in the presence of hydrogen peroxide may be used by the human immune system to fight bacterial pathogens (Prohaska and Lukasewycz, 1981, Newberne et al, 1968). Although copper is important for the immune system of mammals, the requirement of copper resistance for full virulence of pathogenic bacteria has only been recently established. For instance, *E. coli* copper efflux deficient mutants are more prone to killing by macrophages (White et al. 2009, Festa et al. 2011). Macrophages are important cells of the immune system that are formed in response to an infection or accumulating damaged or dead cells. Macrophages are a type of white blood cell that can engulf and digest cellular debris, microbes, and other cells throught the process of phagocytosis. Phagocytosis is an essential cellular process in unicellular organisms by which cells or phagocytes engulf and ingest other cells or particles to form a phagosome. It is an important cellular function, which allows cells to take up nutrients or act as a defence mechanism against infection by microorganisms such as bacteria. It has hence been suggested that one of the resistance strategies that macrophages employ for killing phagocytosed bacteria consists in the loading of the phagosomes with higher levels of copper. Therefore, copper resistance mechanisms in pathogens are of high current interest. In particular, recent work has revealed that *Mycobacterium tuberculosis* has highly efficient copper homeostasis and resistance mechanisms, which include the production of a metallothionein. The following sections summarize current knowledge in this area.

1.4.1 Mycobacterium tuberculosis

Mycobacterium tuberculosis (Mtb) is a highly efficient pathogen and a global health threat infecting about one third of the human population which results in annual casualties of ~2 million people worldwide (Dye et al. 1999, Ward et al. 2008, Ward et al. 2012, Chang and Yew 2013). The ability of Mtb to survive and cause disease is strongly related to their ability to escape immune defence mechanisms. Although antimycobacterial therapy exists, the currently available drugs are only partially effective because of the impermeable nature of the mycobacterial cell wall (see Figure 1.4 for detailed comparison) and the tendency of Mtb to develop resistance. (Warner and Mizrahi 2006, Warner and Mizrahi 2013).

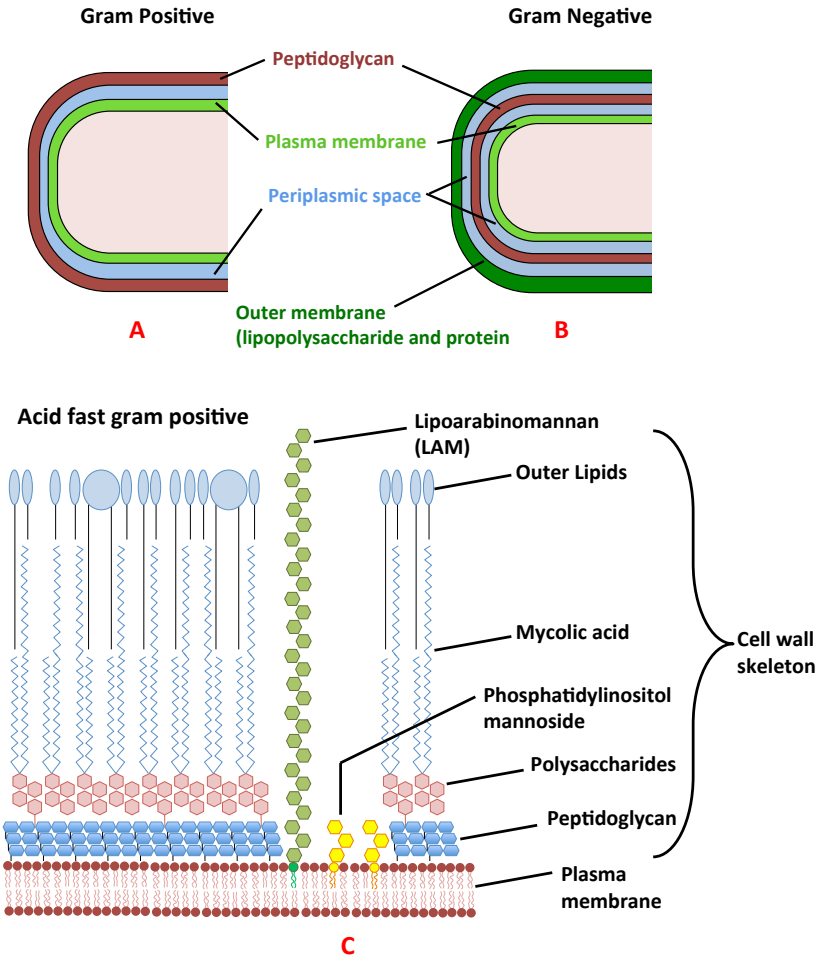

Figure 1.4 Cell wall structure for gram-positive, gram-negative bacteria and acid-fast gram positive for *mycobacterium*.

Gram-positive and Gram-negative bacteria differ mainly by their cell wall composition (Figure 1.4 A, B). A Gram-negative bacterium contains a cytoplasmic membrane, a thin peptidoglycan layer which is more thicker in gram positive bacteria. A characteristic outer membrane, that contains lipopolysaccharides (absent in Gram positive bacteria) on the outside and phospholipids on its inner leaflets, along with porins (play as pores for specific molecules). Periplasmic space is a space between peptidoglycan layer and secondary cell membrane. Surface layer is directly attached to the outer membrane instead of peptidoglycan layer. *Mtb* do not retain crystal violet stain well and classed as acid fast gram positive (Figure 1.4 C) due to lack of outer cell membrane. The characteristic cell wall is thicker, hydrophobic, waxy and rich in mycolic acids. It contains hydrophobic mycolic acid layer and a peptidoglycan layer held together by polysaccharides. The cell wall makes a substantial contribution to the robustness of this genus. In addition, Mtb has the remarkable capacity to survive within the adverse macrophage environment and also the ability to remain viable within infected hosts for prolonged times (Pieters 2008, Jayachandran et al. 2013).

This balance of Mtb maintenance within macrophages is critical in understanding Mtb pathogenesis, and the characterization of the environment to which the bacilli are exposed within the phagosomes and determination of the bacterial response to this environment are fundamental to understanding how *M. tuberculosis* is such a successful pathogen (Wolschendorf et al. 2011, Rowland and Niederweis 2012).

1.4.2 Copper trafficking in activated macrophages and Mtb

A fundamental component of the immune response to Mtb is the interferon (IFN-ϒ) mediated activation of macrophages as shown in Figure 1.5. IFN-ϒ serves as essential macrophage activator and is important for adaptive immunity against infections. This activation results in efficient maturation of phagosomes with greater capacity to kill

intracellular pathogens by utilizing a range of hydrolytic enzymes, bactericidal peptides, and reactive oxygen and nitrogen intermediates (Nathan and Shiloh, 2000).

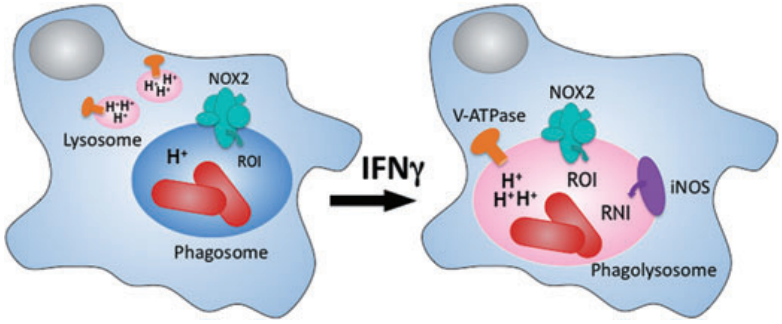

Figure 1.5 Activation of macrophage in response to *Mycobacterium tuberculosis* (Mtb).

Macrophage activation in response to Mtb caused by IFN-ϒ leads to maturation and exposure to reactive oxygen/nitrogen intermediates (ROI, RNI) (Ehrt and Schnappinger, 2009).

The phagosome matures after activation by IFN-ϒ and interacts with lysosomes. Mtb withstands phagosome maturation and inhibits phagosome-lysosome fusion in a resting macrophage which results in a mild acidic compartment leading to exposure to reactive oxygen intermediates (ROI) from phagocyte oxidase (NOX2). This causes Mtb exposure to protons from the vacuolar ATPase, RNI from iNOS and ROI from NOX2. However, Mtb has developed mechanisms not only to cope with these interdependent forms of stress but also permitting its survival within the acidic, nitro-oxidative phagolysosome of activated macrophages (Ehrt and Schnappinger, 2009). Recent *in vitro* experiments with macrophages have shown that IFN-ϒ stimulated trafficking of the copper transporter ATP7A to vesicles that fuse with phagosomes, increasing their copper content along with their bactericidal activity against *E. coli* (White et al., 2009). In addition, IFN-ϒ induced expression of the high-affinity copper importer CTR1 in macrophages (White et al., 2009), and hypoxic conditions, granulomas formed in host after lung infections with Mtb induced expression of CTR1 and the chaperone ATOX1 along with the copper transporter ATP7A, all

of which are thought to transmit copper to the Mtb containing phagosome. The evidence of the immune system using copper to control growth of mycobacteria was specified by the fact that copper concentrations were significantly increased within the phagosomal compartment of macrophages infected with *M. avium* (Wagner et al. 2005).

1.4.2.1 Copper resistance mechanisms in Mtb

Transcriptome analysis recognized 30 copper responsive genes in *M. tuberculosis*, which suggests that Mtb experiences critical concentrations of copper during its life cycle (Ward 2008, Wolschendorf 2011). For instance, the CptV gene (rv0969) is a part of copper-induced operon organized by the transcriptional regulator CsoR and possibly encodes a copper specific inner membrane efflux pump (Festa et al 2011, Ward 2008, Liu et al. 2007). CsoR, also referred to as copper sensitive operon regulator, represents a new class of copper responsive regulators, which is more widely distributed in prokaryotes compared to the well characterized CueR (from *E. coli*) or CopY (from *E. hirae*). The transcriptional regulator CsoR binds to equimolar amounts of Cu(I) using two cysteines and one histidine for coordination. Apo-CsoR represses *cso* (copper sensitive operon, induced by Cu(I)) and allows transcription of the operon by losing its affinity to its operator after Cu(I) binding. CsoR in Mtb regulates its own promoter and expression of *cso* (Festa et al. 2011, Rowland and Niederweis 2012). In addition, MctB (Rv1698), a pore-forming outer membrane protein, was also detected which may play a role in copper resistance. It was suggested that the loss of MctB led to higher amounts of copper entering the periplasm/cytoplasm of Mtb by changing the outer membrane. However, the direct role of MctB in copper efflux is not clear (Rowland and Niederweis 2012).

Furthermore, RicR, a further copper-sensing repressor was also identified and a role in protection against copper toxicity was suggested. RicR has been shown to repress gene expression under low copper concentrations, whilst excess copper exposures leads to dissociation of RicR from DNA and induction of five genes (*IpqS,* Rv2963, *ricR, socAb* and

mymT). Based on the fact that RicR regulates various genes exclusively in pathogenic *Mycobacteria,* it was proposed that these genes may be required for growth and survival within the host (Festa et. al 2011). However, the role of these proteins (except MymT) is not clear, but it may be assumed that the proteins encoded by these genes are important for virulence (Rowland and Niederweis 2012). The copper-trafficking pathways in macrophages and Mtb and proteins involved are illustrated in Figure 1.6.

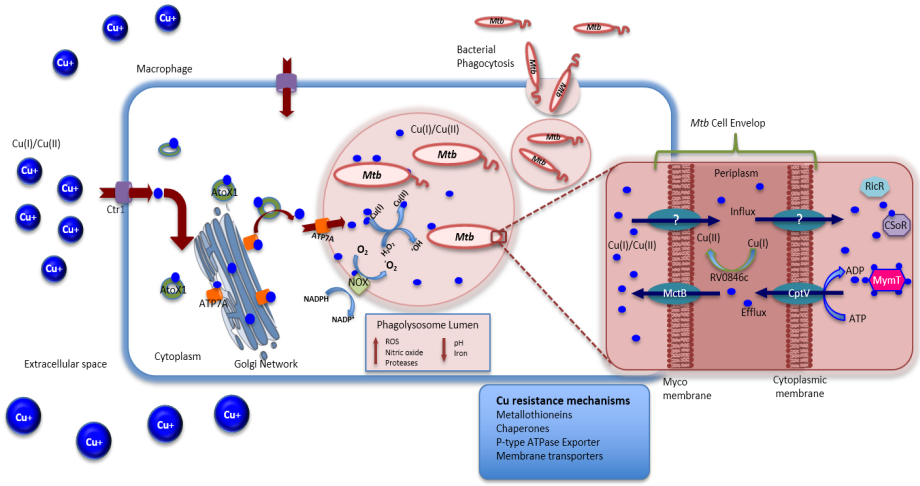

Figure 1.6 Copper delivery from the macrophage to the pathogen and Mtb resistance mechanisms

Copper uptake stimulated by Inflammatory agents (e.g., lipopolysaccharides) after inducing the expression of Cu(I) importer Ctr1 at the plasma membrane. Cytoplasmic copper is bound to copper chaperone ATOX1 to transport Cu(I) to ATP7A copper pump on Golgi network to deliver Cu to copper requiring proteins. Under copper stress, ATP7A transported to the membrane for copper export. Ctr1 and ATP7A expression increases with the maturation and activation of phagolysosome and ATP7A is trafficked to the phagolysosomal compartment, where it delivers copper. The NADPH oxidase (NOX) produces superoxide, which generates hydrogen peroxide, the bactericidal strength of which is increased via translation to the hydroxyl radical by Cu(I)-catalyzed Fenton Chemistry and cause Fe-S clusters disruption as a bactericidal agent. In *M. tuberculosis,* the outer membrane or mycomembrane proteins involved in efflux are not fully known. CtpV (inner membrane transporter, expression regulated by CsoR) serves as a copper efflux pump. Rv0846c is a putative multi-copper oxidase. *MymT* encodes a cytoplasmic copper metallothionein (expression regulated by RicR). CsoR and RicR are both repressors, which de-repress on copper binding. (Figure adapted from Wolschendorf et al. 2010, Hodgkinson and Petris 2012, Festa and Thiele 2012).

1.4.3 MymT: the first copper binding bacterial metallothionein

MymT, discovered by Gold et al. in 2008, is encoded by *mymT,* which is the only characterized gene regulated by RicR. The expression of *mymT* gene was induced in the presence of copper, a characteristics of metallothioneins, which suggested its role to protect the bacterium from copper toxicity. It is the only copper binding bacterial metallothionein to be identified to date.

MTNYEAGTLLTCSHEGCGCRVRIEVPCHCAGAGDAYRCTCGDELAPVK

Figure 1.7 Amino acid sequence of MymT

Amino acid sequence of MymT with terminal methionine. MymT contains seven cysteines (Yellow) and two histidines (Blue), which may be involved in metal binding.

Biochemical characterization of the MymT protein revealed a mass of approximately 4.9 kDa and that the expression can be induced by zinc, copper, cadmium, nickel and cobalt with the exception of manganese in wild type Mtb. However, zinc was not a strong inducer of *mymT* mRNA transcription and no zinc sensitivity was observed in Mtb *ΔmymT* mutant in contrast to what is reported for *smtA* mutant of *Synechococcus* (Turner et. al 1993, Gold et al. 2008). Furthermore, the copper hyper-susceptibility of Mtb *ΔmymT* mutant was similar to that of the *cup1* mutant of the *S. cerevisiae* (Hamer et al. 1985, Gold et al. 2008). It has been suggested that mildly acidic conditions, nitric oxide production, cell wall perturbation, oxidative stress and reactive oxygen intermediates can also induce MymT expression. This is based on the observation that increases of ~1000-fold abundance of *mymT* transcripts was induced by ROI, RNI and SDS. However, the fact that the *ΔmymT* mutants were not hypersensitive to these stressors, led to the conclusion that there was a, higher redundancy of Mtb's defence against NO, SO and SDS than redundancy against copper. It is also possible that some of the other stimuli involved in increased *mymT* expression exert their effect by displacing copper from MymT or other unknown copper binding proteins.

This resulting free copper was assumed to activate a common route for the induction of *mymT* (Gold et al. 2008). These observations were further rationalized by considering the role of CsoR, a *mymT* regulator, that represses the *mymT* transcription in the absence of copper and allows *mymT* transcription by liberating an operator site as consequence of a conformational change resulting from copper binding (Gold et al. 2008).

Studies on recombinant and chemically synthesized MymT indicated that it has a higher affinity for copper compared to zinc (Gold et al 2008, Robinson 2008). However, although mass spectrometric studies were conducted in the original study, the metal binding capacity of MymT has remained unclear, and the composition and structure of the metal cluster was not revealed by these studies. The present study is partially aimed towards elucidating the copper-binding properties of MymT. In the following, metallothioneins and in particular other bacterial metallothioneins are discussed.

1.5 Metallothioneins

Metallothioneins (MTs) are small mostly intracellular proteins found in vertebrates, invertebrates, fungi including yeast, and some bacteria, which are characterized by high cysteine contents (Kägi and Kojima 1987, Vasák 2005). Exposure of an organism to Zn(II), Cu(I), Cd(II) and Hg(II) ions often results in induction at the transcriptional level of rapid *de novo* synthesis of one or more metallothioneins, to bind metals (Saquibb et al, 1977, Bremner and Young 1976, Andersen and Weser 1978, Ohi et al, 1981, Durnam et al, 1981). They are mostly found in the cytoplasm but their presence in blood plasma and cerebrospinal fluid of higher organisms has also been reported. Mammalian MTs also occur in the nucleus during developing stages (Blindauer and Leszczyszyn 2010, Kägi and Kojima 1987, Kägi and Schäffer 1988). Margoshes and Vallee discovered the first metallothionein in 1957 whilst studying cadmium binding proteins in horse kidney cortex (Margoshes and Vallee 1957). It was later isolated as a cadmium-binding cysteine-rich protein containing 4.1% sulfur. Since then, metallothioneins were isolated from primary tissues of animals

(liver, kidney, pancreas, intestines), plants (Rauser and Curvetto 1980), fungi (Prinz and Weser 1975), and from bacteria (Olafson et al 1979, Higham et al 1986).

1.5.1 Classification of metallothioneins

On the basis of their primary structures, metallothioneins were initially classified into three classes; mammalian MTs and other vertebrate MTs form class-I, and contain 20 cysteine residues. In addition, crustacean MTs were also counted as class I. Class II MTs are phylogenetically distant from class I MTs, and include MTs from plants, fungi, invertebrates and bacteria. Class III MTs are the phytochelatins, which are not products of translation and contain multiple γ-glutamylcysteinyl units. Based on sequence similarities and phylogenetic relationships, class I and class II metallothioneins are further classified into 15 families (Binz and Kägi 1999, Valls et al. 2001, Vasák 2005).

However, an additional classification has recently been proposed in which metallothioneins are classified into two groups; Zn-Thioneins and Cu-Thioneins, based on metal stoichiometries, and spectrophotometric and spectrometric properties of the recombinant product (Capdevila et al. 2010, Capdevila and Atrian 2011), a concept reviewed further below. Besides differences in classes, all MTs have some prominent characteristics in common which define the protein super family (Fowler et al. 1987, Kägi and Kojima 1987) including:

(i) Low molecular weight (<10 kDa),

(ii) High cysteine contents,

(iii) Few or no aromatic residues,

(iv) Optical features characteristic of metal-sulfur bonds,

(v) Bridging sulfur ligands,

(vi) Induced by chemical and physical stress (Fowler et al. 1987, Kägi and Kojima 1987).

Metallothioneins can exist in three different forms *in vivo* i.e., metallated or holo form (metallothionein), metal free or apo-form (thionein) and oxidized form (thionin) (Jacob et al 1998, Krezel and Maret 2007). Due to the wide diversity and occurrence in almost every phylum, metallothioneins are reported to play very diverse and critical roles in biological systems. The biological functions of MTs include zinc and copper regulation, as well as detoxification of toxic metals and removal of free radicals.

MT synthesis induction is stimulated by such factors as metallic ions, free radicals and oxidative stress (Akashi et al. 2004; Thornalley et al. 1985), drought, osmotic, and temperature stresses in plants (Chatthai et al. 1997), which suggests involvement of many MTs in stress responses. In addition, a number of mammalian MTs have been linked to immune responses. Furthermore, in mammals down-regulation of MTs has been associated with neurodegenerative disorders such as Alzheimer's disease (Aschner and West 2005) and amyotrophic lateral sclerosis (Ono et al. 2006; Tokuda et al. 2007). Mammalian MTs are best characterized so far, although tertiary structures of some class II MTs are also published (as shown in Table 1.3). The bacterial Cu-MTs have been discovered only recently (Gold et al. 2008) and are under-studied MTs with likely distinct properties compared to any other MTs, therefore research is needed to reveal the structures and biochemical properties of bacterial Cu-MTs to fully recognize their mode of action.

1.5.1.1 Functional classification: Cu- and Zn thionein character of MTs

A new classification of MTs was proposed by Valls et al. 2001, on the basis of observations revealed by spectroscopic, stoichiometric, and spectrometric characteristics of recombinant metallothioneins, produced by binding to the physiologically essential metal ions Zn(II) or Cu(I). This classification grades MTs into two categories, in which Zn-thioneins are those which are isolated with bound Zn(II) upon (recombinant) *in vivo* folding, even at higher concentrations of Cu(I), and then often producing heterometallic Zn, Cu- mixed metal species. Cu-thioneins, on the other hand, are capable of forming homo-metallic Cu(I)-

MT species in similar conditions (Bofill et al 2009). This has been explicitly tested on invertebrates MTs (Bofill et al. 2009), however, there is no systematic information on Zn(II) or Cu(I)-thionein character of bacterial MTs.

1.5.2 Structures and metal binding characteristics of MTs

Mammalian and other vertebrate MTs contain 20 cysteines conserved in 60—68 amino acid long sequences. One prominent feature of MTs is their cysteine arrangement in the primary structure e.g., CXC and CXXC motifs (where X is any neighbouring amino acid other than cysteine, C). In addition, CC and CCC arrangements are also common in MTs (Blindauer and Leszczyszyn 2010). Another common characteristic of MT primary structure is the scarcity of aromatic and hydrophobic amino acids such as Trp and Phe, which are related to structural rigidity of other proteins whilst presence of Gly and Ala, which are abundant in MTs, provide structural flexibility. However, histidine is found in bacterial and some invertebrate and plant MTs and some mammalian MTs also contain Phe and Tyr in their amino acid chains. A lack of elements of secondary structure was also reported previously, although plant MTs and bacterial SmtA contain some β-sheets and to a lesser extent, α-helices (Freisinger 2011, Blindauer et al. 2007, Blindauer et al. 2002, Blindauer et al. 2001).

The 3D structures of MTs depend on metal ions and their coordination to the corresponding ligands (Figure 1.8). However, lack of aromatic and hydrophobic amino acid residues, high glycine content and low complexity of primary sequence make the tertiary structure determination of MTs rather hard. This is obvious when searching for metallothioneins in the Protein Data Bank (PDB), as it contains only 32 records of MTs of which 15 refer to the structures of seven different vertebrate MTs with very similar structural configurations. (Table 1.3).

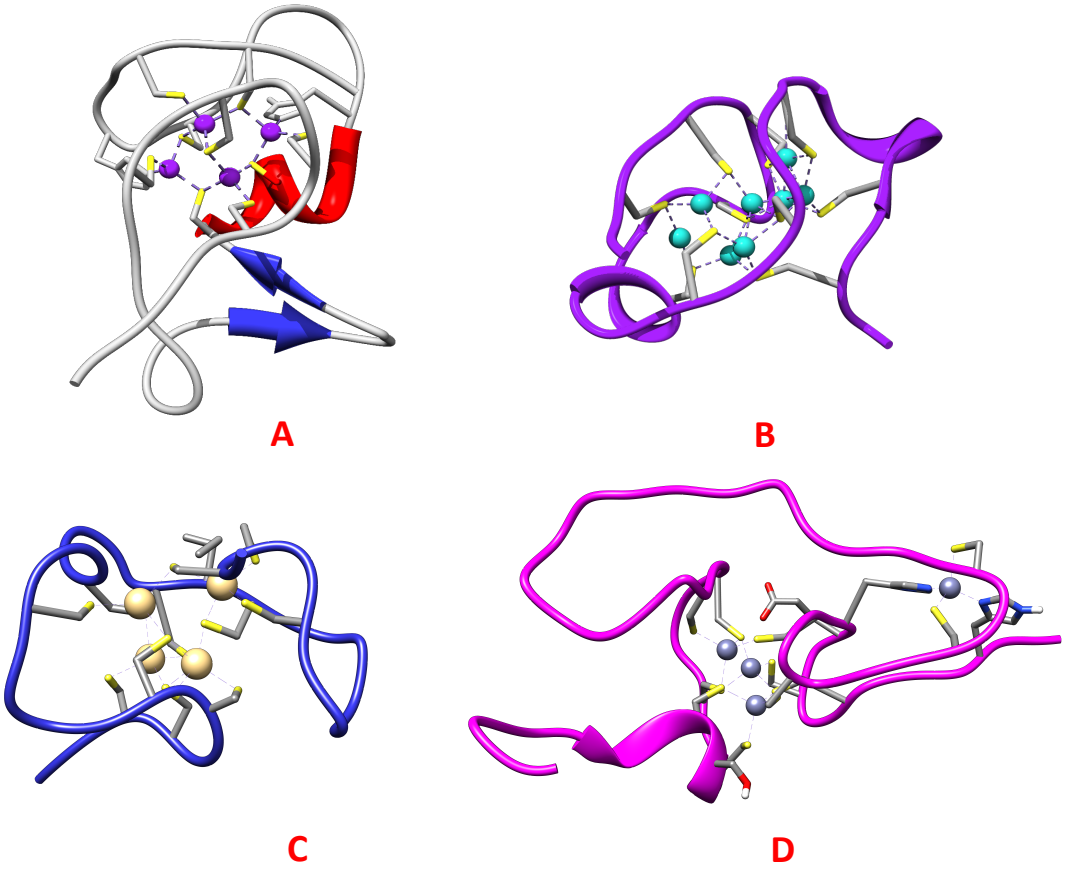

Figure 1.8 Structures of MTs

3D structures of (A) bacterial zinc binding SmtA (pdb 1jjd) containing four zinc ions, (B) Yeast Cup1 (pdb 1rju) containing eight copper ions, (C) Mammalian rabbit MT2 (α domain, pdb 1mrb) with four cadmium ions and (D) Plant wheat Ec (α domain pdb 2kak) containing four zinc ion.

Table 1:3 Summary of 3D structures of MTs.

PDB entries of 19 3D structures for 14 MTs found in vertebrates and invertebrates. Table adapted from Blindauer and Leszczyszyn 2010).

MT Source	Metal content	Method	PDB code	References
Mouse MT1	Cd_4 (α), Cd_3 (β) MT1	NMR	1dfs, 1dft	Zangger et al 1999.
Rat MT-2	Cd_3 (α), Cd_4 (β) MT2 Cd_5Zn_2MT2	NMR X-ray	1mrt, 2mrt 4mt2	Braun et al 1992.
Mouse MT3	Cd_4 (α)MT3	NMR	1ji9	Zangger et al 2001.
Rabbit MT2A	Cd_4 (α), Cd_3 (β) MT2A	NMR	1mrb, 2mrb	Arseniev et al 1988.
Human MT2	Cd_4 (α), Cd_3 (β) MT2	NMR	1mhu, 2mhu	Messerle et al 1992.
Human MT3	Cd_4 (α), Cd_3 (β) MT3	NMR	2f5h 2fj4, 2fj5	Wang et al 2006.
***N. coriiceps* MT**	Cd_4 (α), Cd_3 (β) MT	NMR	1mg0g, 1m0j	Capasso et al. 2003
***C. sapidus* MT1**	Cd_3 (α), Cd_3 (β) MT1	NMR	1dmc, 1dmd, 1dme, 1dmf	Narula et al. 1995
Lobster MT1	Cd_3 (α), Cd_3 (β) MT1	NMR	1j5l, 1j5m	Munoz et al. 2002
***S. purpuatus* MTA**	Cd_6MTA	NMR	1qjk, 1qil	Riek et al. 1999
Wheat Ec	Zn_4-Ec	NMR	2kak	Peroza et al. 2009.
Wheat Ec	Zn_2-Ec	NMR	2161/2162	Loebus et al. 2011
Yeast Cu-MT	Ag_7-Cup1	NMR	1aoo, 1aqq	Peterson et al. 1996.
	Cu_7-Cup1	NMR	1aqr, 1aqs	Bertini et al. 2000
	Cu_7 (no metal)	NMR	1fmy	
	Cu_8-Cup1	X-ray	1rju	Calderone et al. 2005.
N. crassa	Cu_6-MT	NMR	1t2y	Cobine et al. 2004.
Synechococcus PCC 7942 SmtA	Zn_4-SmtA	NMR	1jjd	Blinduaer et al. 2001.

In Table 1.3, eight further entries belong to three structures for invertebrates MTs with structural resemblance to vertebrate MT structures (crab, lobster, sea urchin). The remaining four structures (10 pdb entries) from yeast, plant and cyanobacteria show distinct features (Blindauer and Leszczyszyn 2010).

1.5.3 Metal-thiolate clusters in MTs

Metal ions bind to MTs predominantly through sulfur coordination from the cysteine residues forming clusters containing terminal and bridging thiolates. For divalent metal ions, one of the basic cluster compositions is M_3Cys_9 in which a six membered ring is formed by the coordination of three metal ions with three bridging sulfur ligands. Each of the three metal ions is bound to two further sulfurs resulting in six terminal thiolates (such clusters are found in the so-called β-domains of vertebrates, crustaceans and echinoderms).

Another common cluster motif is M_4Cys_{11} found in the α-domain of vertebrate and echinoderm MTs. In this cluster, two metal ions are bound to two terminal and two bridging thiolates whilst the remaining two metal ions are coordinated to one terminal and three bridging thiolates resulting in two fused six-membered rings as shown in Figure 1.9. Moreover, a very similar $M_4Cys_9His_2$ cluster is also reported in bacterial SmtA, where two histidine residues take part in metal coordination through their imidazole nitrogens.

More recently, a M_2Cys_6 cluster has been discovered in the γ-domain of wheat E_C (Loebus et al. 2011).

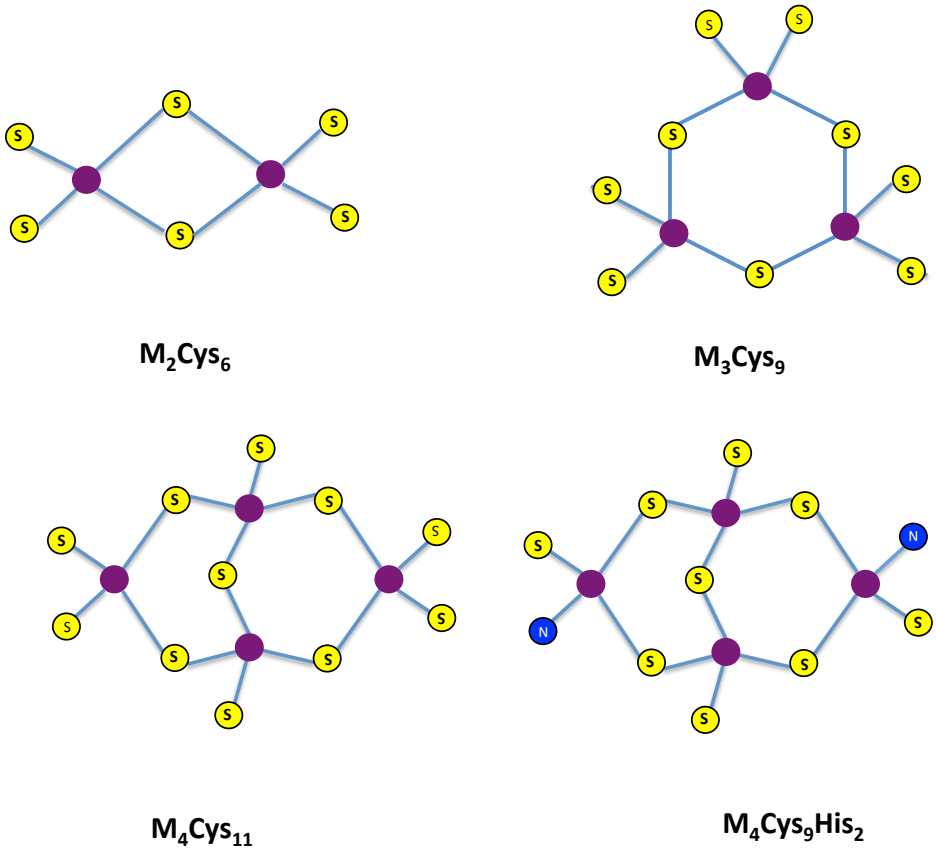

Figure 1.9 Metal-thiolate clusters in MTs

Structural arrangement of metal clusters in MTs containing divalent metal ions such as cadmium or zinc (purple balls) bound to cysteines (yellow balls) or histidines (Blue balls) (Adapted from Blinduaer et al 2001, Loebus et al. 2011).

For monovalent metal ions such as Cu(I) and Ag(I), a $M_{7\text{-}8}Cys_{10}$ cluster structure has been reported for a copper binding metallothionein (Cup1) from yeast and hence the only copper binding MT cluster structure published so far (the structure for the *Neurospora crassa* MT does not contain metal ion-specific information). In the X-ray crystal structure of Cup1, six metal ions of this cluster bind to the sulfurs forming trigonal planar sites and two are coordinated to thiolate ligands with linear or digonal geometry as shown in Figure 1.10A.

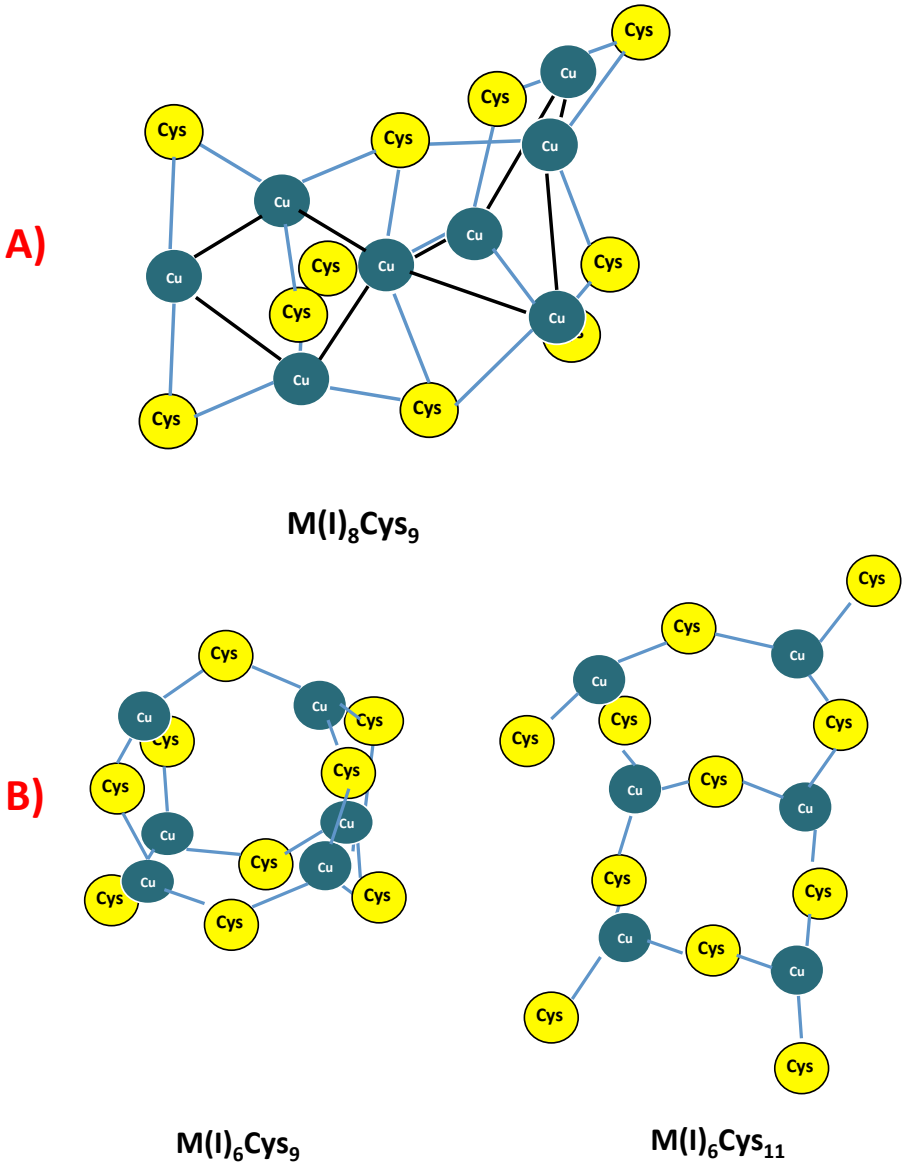

Figure 1.10 Experimentally determined and modelled metal-thiolate cluster in Cu-MTs.

A) Structural arrangement of Cu_8-Cup1 metal cluster containing copper in monovalent state (Adapted from Calderone et al. 2005). B) Modelled M_6Cys_9 and M_6Cys_{11} metal thiolate clusters in the β- and α-domain of rabbit liver MT 2A where Cu(I) is trigonally coordinated to cysteinyl S atoms (adapted from Presta et al. 1997, Merrifield et al. 2002).

The prominent feature of this cluster arrangement is that it lacks terminal thiolates, with each thiolate forming two or three bridging bonds with Cu(I). Other observed but not structurally characterized Cu-thiolate clusters are Cu_6Cys_9 and Cu_6Cys_{11} in rabbit liver metallothionein, and suggested models are shown in Figure 1.10B (Presta et al. 1997,

Merrifield et al. 2002). Previously, copper-metallothioneins (Cu-MT) had been proposed as one of the major metal-transport systems, which might be used by newly synthesized protein as a source of copper (Aggett 1999, Petering et al, 1986), although this idea has been mostly replaced by the discovery of copper chaperones. Metallothionein binding to copper is, however, thought to play a protective role by suppressing copper toxicity because copper-metallothionein reduces the ability of the metal ions to participate in harmful intracellular interactions.

1.5.3.1 Effect of pH and Cu(I) speciation

The pH stability of metal binding is a distinguishing property of MTs compared to other metalloproteins and is reported as "pH of half-dissociation". The pH of half dissociation has been extensively studied for zinc binding MTs with pH 4.3—4.4 for mammalian MTs (Jiang et al. 2000) and pH 4.1 for the cyanobacterial SmtA (Blindauer et al. 2002). For Cu(I), on the other hand, the pH of half displacement for Cu(I) is considerably lower, with 2.7 reported for rat and other mammalian MTs (Artells et al. 2013, Oh et al. 1999, Nielson et al. 1985), however pH low as pH 0.3, 0.8 and 1.6 was also suggested for Cu(I) binding MTs for instance, *S. cerevisiae* MT, *C. glabrata* MT-II and *C. albicans* respectively (Byrd et al. 1988, Mehra and Bremner 1984, Nielson et al. 1985, Oh et al. 1999). Cu(I) binding studies on sea urchin MT (SpMTA, SpMTB) and snail MT (Cu-HpCuMT) for the metal binding abilities have been done at pH 2.5 and pH 7 (Tomas et al 2013, Pérez-Rafael et al 2013).

1.6 Bacterial Metallothioneins

There are two known unrelated sub-families of bacterial metallothioneins, i.e., zinc binding bacterial metallothioneins of the BmtA family, and copper binding MymT, which are exclusively found in pathogenic mycobacteria. First discovered in cyanobacteria, it was suggested that BmtAs deal with altered metal availability, toxicity and utilization (Robinson et al. 1990, Shi et al. 1992). Initially, prokaryotic metallothionein was isolated from the marine cyanobacterium *Synechococcus* RRIMP N1 that had a high percentage of cysteine and metal ion content i.e., Cd, Zn and Cu (Olafson et al. 1979). Spectroscopic studies revealed the presence of metal-thiolate clusters, probably in one single domain (Olafson et al. 1988). This protein was later named SmtA (for *Synechococcus* MT A), and is a founding member of the BmtA family (Blindauer et al. 2002). The sequence of copper binding MymT differs considerably from SmtA, with very little sequence similarity.

1.6.1 SmtA: A prototype for zinc binding bacterial metallothionein

In *Synechococcus* PCC7942, SmtA is most strongly induced by Zn(II), suggesting it mainly functions in the homeostasis of this metal ion. This notion is strongly borne out by its structural features discussed below, and SmtA (as well as its homologues in other bacteria) is expected to display Zn-thionein character, although this has not yet been formally tested. The transcription of *smtA* is regulated by a zinc-responsive transcription factor, SmtB. In the presence of zinc, an operator site upstream of *smtA* is released by Zn(II)-SmtB that permits RNA polymerase to initiate transcription, whilst apo-SmtB represses *smtA* transcription in the absence of zinc (Morby et al. 1993, Robinson et al. 2001).

Although fulfilling a number of the criteria (as described in section 1.5.1) for being classified as an MT, SmtA (from *Synechococcus* PCC7942) has a number of distinct features. It not only contains a smaller amount of cysteine residues (16%) than mammalian MTs (33%), but also has two tyrosine and three histidine residues, and two of the latter are involved in metal coordination. It has previously been established that SmtA binds four zinc ions

(Blindauer et al 2001) in a single cluster. The sequence and metal-to-ligand connectivities are shown in Figure 1.11.

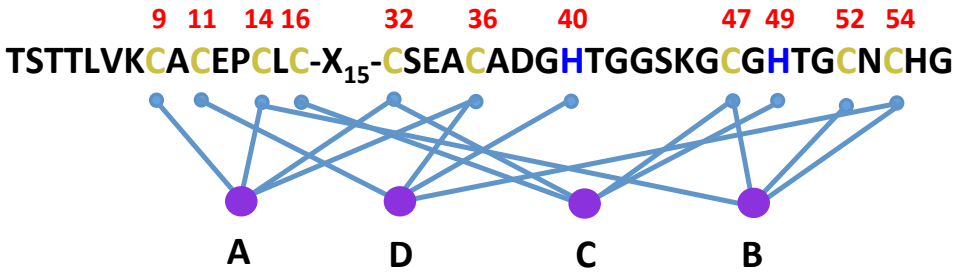

Figure 1.11 Sequence and metal binding sites in SmtA

Sequence of SmtA showing four metal binding sites and the residues involved in metal coordination. The yellow and blue colors are used to highlight the cysteine and histidine residues respectively (adapted from Blindauer et al 2001).

SmtA has a well-defined backbone for a significant part of the protein (residues 6—40) followed by a more flexible loop region (41—45) which was evident from absence of long range NOE cross peaks in ^{1}H NMR spectra. The NMR structure encloses a cleft lined with the Zn(II) ligands i.e., the side chains of cysteine and histidines residues. The side chains of charged residues (e.g. Arg, Lys, Asx, Glu) are positioned on the protein surface (Blindauer et al 2001). The structure of SmtA (Figure 1.12) is rather unusual for a metallothionein, i.e., it contains well-defined secondary structure elements with a short α-helix from Glu-34 to Gly-39 along with two small antiparallel β-sheets formed by residues Val-7, Lys-8, Asn-17, Val–18 and residues Ile-24 to Tyr-31 respectively whilst Asn-27 and Gly-28 form a turn (Blindauer et al 2001). Furthermore, there is a prominent similarity in the arrangement and orientation of site A and the connected α helix and antiparallel β-sheets of Zn_4SmtA to the secondary structures elements in so-called treble-clef zinc fingers (Grishin 2001). Beside the two metal-binding His residues (and its confirmed biological function) the main feature leading to the prediction that SmtA would display Zn-thionein character.

1.6.1.1 Inertness of site A

The exchange reaction of Zn_4SmtA with Cd(II) ions showed inertness of one metal binding site evidenced by the presence of one Zn(II) ion even after long incubation times with Cd(II) (Blindauer et al., 2003). This result had been surprising because the metal ions in MTs reported to date were kinetically labile and prone to rapid metal exchange. In addition, Cd(II) binds to cysteines more strongly than Zn(II) due to their higher affinity for sulfurs (Irving and Williams 1953), and stoichiometric amounts of Cd(II) are normally sufficient to replace Zn(II) under similar conditions (Foster and Robinson 2011).

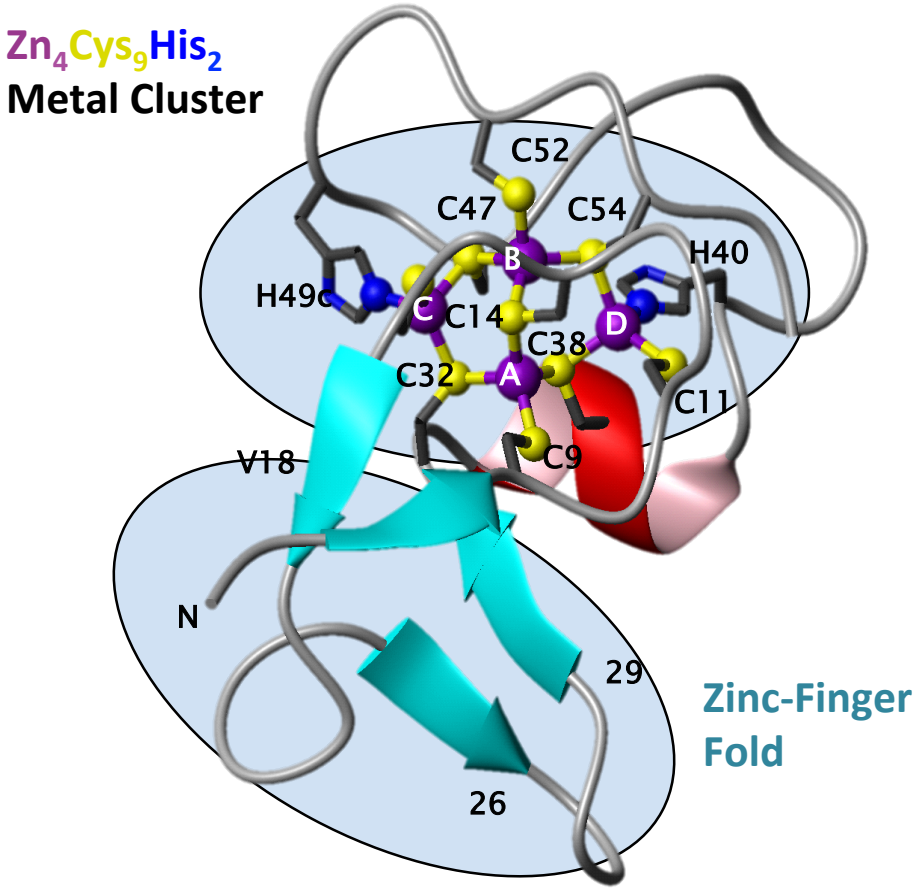

Figure 1.12 Structure and metal cluster composition of SmtA

Structure of SmtA along with composition of metal binding cluster $Zn_4Cys_9His_2$ and zinc finger fold.

Cd(II) replaced Zn(II) preferably from the Cys_4 binding site B (Figure 1.10), followed by CCHC sites D and C, but did not readily replace Zn(II) from Cys_4 site A. However, Cd(II) occupation of site A is possible when the apo protein is reconstituted with Cd(II), and Zn_4SmtA and Cd_4SmtA are isostructual (Blindauer 2008). Although site specific displacement of Zn(II) by Cd(II) had been reported previously, complete inertness is, so far, unique to SmtA as it has not been observed in other MTs (Blindauer et al. 2003). One structural explanation is that site A is surrounded by elements of secondary structure (i.e., α-helix and anti-parallel β-sheets) absent in mammalian MTs, which shield Cys-9 from surface attack. The metal in site A is protected from the other side by the three other metal ions; the fact that no metal exchange could be detected even after prolonged incubation times suggested that intra-molecular exchange did also not take place in the fully formed $M(II)_4$ cluster. This important inert site A may be useful to explore Zn(II) or Cu(I) thionein behavior of bacterial metallothioneins.

1.7 Aims and objectives of the study

There is very little structural, thermodynamic and kinetic data available for Cu-MTs. One factor may be that Cu(I) is not stable in the presence of oxygen; this makes copper binding proteins difficult to work with. This may partially account for the fact that only one copper metallothionein structure is solved so far and that this took more than four decades (i.e., yeast Cup1).

The current project concerns the copper binding properties of two bacterial metallothioneins from two different families. SmtA is clearly a Zn-MT, as Zn is the strongest inducer of SmtA expression, and because it contains a zinc-finger, and MymT is a Cu-MT, considering that it is part of a copper regulon (RicR). Although, there is clear data on biological functions available for both metallothioneins that allow their predicted

assignment as Zn-thionein (SmtA) and Cu-thionein (MymT), and it will be interesting to compare the behavior of these two proteins.

MymT displays little amino acid homology with other known eukaryotic and prokaryotic MTs. However, it has a Cys-X-His-X-X-Cys-X-Cys motif similar to a motif found in bacterial SmtA, but a second motif Cys-His-Cys-$(X)_2$-G-$(X)_2$-Tyr-Arg-Cys-Thr-Cys is unique to MymT only. There is little if any sequence homology between the two bacterial MTs (MymT and SmtA) as shown in Figure 1.13 below.

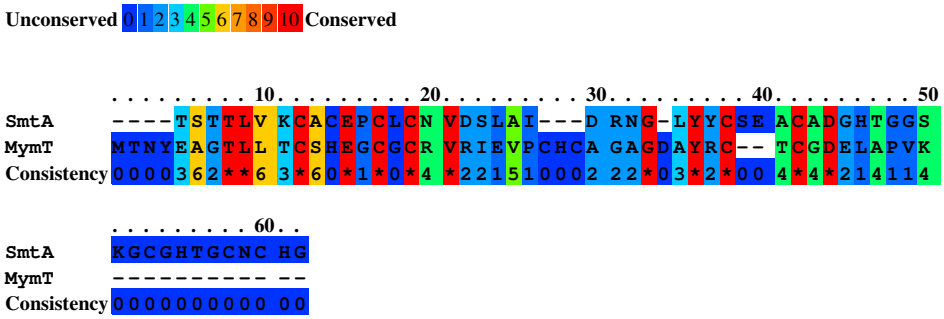

Figure 1.13 Sequence alignment of bacterial SmtA and MymT.

Alignment for the amino acid conservation between MymT and SmtA. Conservation scoring was performed by PRALINE. The scoring scheme works from 0 being the least conserved alignment position, up to 10 for the most conserved alignment position.

The residues 5—26 in MymT can be aligned with the residues 2—22 of SmtA, with full or semi-conservation of the first four metal binding residues (Cys and His) and some conservation of other residues. The CHC insertion in MymT dissects the beta hairpin of SmtA and little conservation is observed in that region, so it is highly unlikely that MymT adopts similar structure as SmtA in this region. Alignment of the remaining residues requires the introduction of two further gaps. In particular C32XXXC36 motif in SmtA is not present in MymT.

A major objective of this project was to develop and optimize sample preparation methods for reconstitution of bacterial metallothioneins, i.e., SmtA from *Synechococcus* PCC7942

and MymT from *M. tuberculosis*, with copper. SmtA was used as a model protein in order to establish methods and techniques for the preparation and analysis of copper-MT complexes, which were employed for the characterization of MymT.

This objective was facilitated by the fact that an expression construct is available for SmtA. Secondly, although the Zn(II) and Cd(II) binding properties of SmtA have been extensively studied previously, there was no information on its Cu(I) binding properties.

Hence, SmtA provides an ideal model system to

i) Develop methods for the preparation of Cu(I)-bound MTs, enabling their study

ii) Study M(I)/M(II) metal exchange reactions in an MT

iii) Study the structural consequences of binding the "wrong" metal ion to a (predicted) Zn-thionein

The experimental procedures developed were then applied to study the properties of the presumed Cu-thionein MymT *in vitro* (with a chemically synthesized MymT peptide). Since metal homeostasis is crucial for virulence of *M. tuberculosis*, obtaining information on structure and properties of Cu-MymT may provide further insight into copper handling in this particular bacterial species.

2

Experimental Methods

2.1 Reagents and Chemicals

All reagents and chemicals used in this study, unless stated otherwise, were purchased from Fisher Scientific (Loughborough, Leicestershire, UK) and Sigma-Aldrich (Gillingham, Dorset, UK). All chemicals were of the highest grade available for use in analytical or chemical biology studies and used without any further purification. Each experiment was repeated atleast three times to establish reproducibility.

2.2 Buffers

All buffers used in this study were prepared from nitrogen purged distilled water (dH_2O, Millipore), filtered through 0.22 µM filters (Millipore) and degassed using degassing flask connected directly to pump. Ammonium hydrogen carbonate buffers (10 and 20 mM, pH 8.4) were used in protein purification, 1 mM phosphate buffer at pH 7.0, 2 mM HEPES, 0.1 NaCl buffer at pH 7.4 for circular dichroism (CD) and UV-vis measurements. Deuterated Tris buffer solution (50 mM [D_{11}] Tris-Cl (CKgas, UK), 50 mM NaCl, 10% D_2O at pH 7.4) was used in the preparation of NMR samples. The Cu(I) sources used in this study were from Cu(II) acetate in presence of 100 mM DTT or 1% β-mercaptoethanol (BME) and Tetrakis(acetonitrile)copper(I)hexafluorophosphate ($[Cu(CH_3CN)_4]PF_6$).

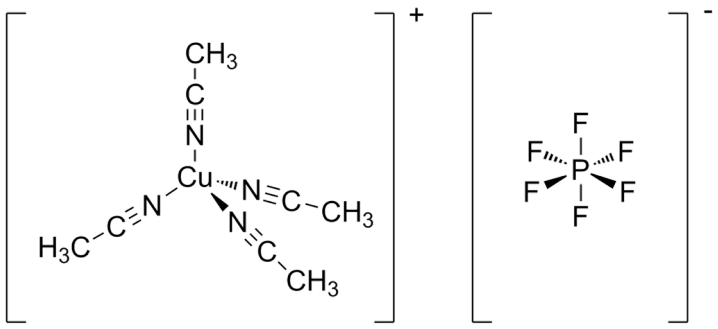

Figure 2.1 Chemical structure of Tetrakis (acetonitrile) copper (I) hexafluorophosphate

The Cu(I) ion in Tetrakis (acetonitrile)Cu(I)hexafluorophosphate is coordinated with four acetonitrile ligands which protect it from oxidation to Cu(II). Since Cu(I) is weakly bound to acetonitrile, this complex can be used as a source of Cu(I).

2.3 Bacterial Transformation

Plasmid DNA (pMHNR2.1, containing the *smtA* gene from *Synechococcus* PCC 7942 cloned into pET29a (Blindauer et al 2002) donated by N. Robinson, Newcastle University) (1 µL) was added to a 50 µL aliquot of competent cells (DH5α strain for plasmid storage and amplification, and BL21(DE3) pLys for protein expression) and incubated on ice for 5 minutes. The cell/DNA mix was heat-shocked for 30 seconds at 42 °C and then incubated on ice for 2 minutes. 250 µL of sterile LB medium was added to the transformation mixture and placed in a shaker incubator for 45 minutes at 37 °C at 180 rpm. Agar plates selective for 34 µg mL^{-1} chloramphenicol and 50 µg mL^{-1} kanamycin were used as a growth medium for *E. coli* following transformation. Typically, several dilutions of the transformation mixture were plated in a total volume of 100 µL and plates were incubated at 37 °C for 12—16 hours. *E. coli* cultures were stored on LB agar plates at 4°C for a maximum of 4 weeks.

2.4 Growth and storage of E. coli cultures

2.4.1 Standard growth conditions

E. coli cells were cultured using Luria-Bertani (LB) medium with antibiotics chloramphenicol (34 μg mL^{-1} solution in ethanol) and kanamycin (50 μg mL^{-1} solution in distilled water). Medium was pre-warmed to 37 °C before inoculation with a single bacterial colony taken from an agar plate. Liquid cultures were grown at 37 °C in a shaking incubator overnight i.e. for approximately 12—16 hours. Glycerol stocks of *E. coli* cultures were prepared for long-term storage by mixing two parts of liquid culture with one part of 50% (v/v) glycerol. Cultures were frozen with liquid nitrogen and then stored at –80 °C.

2.5 Protein Expression and purification

2.5.1 Protein expression in standard medium

Starter cultures, selective for 34 μg mL^{-1} chloramphenicol and 50 μg mL^{-1} kanamycin, were inoculated with a single colony and incubated overnight at 37 °C with shaking at 180 rpm. The expression cultures (0.6 L, selective for the same antibiotics and concentration as above) were inoculated 1:100 (v/v) with cells from the starter cultures and grown at 37 °C until an OD_{600} of ~ 0.7 was achieved. Protein expression was induced with the addition of 0.5 M IPTG (isopropyl β-D-1-thiogalactopyranoside) along with the supplement of 0.5 M $ZnSO_4$ and protein expression was continued at 37 °C for 5—6 hours. Cells were harvested by centrifugation at 5000 × g at 4 °C for 30 minutes.

2.5.2 Protein expression in minimal medium

In order to perform heteronuclear NMR studies, the incorporation of ^{15}N into the SmtA protein was required. Therefore protein (Zn_4SmtA) was expressed in minimal media

enriched with $^{15}NH_4Cl$ using the standard protein expression procedure as described above in section 2.5.1. Table 2.1 lists the recipe for the minimal medium solution that was used for Zn_4SmtA expression.

Table 2:1 Minimal medium recipe (M9 salts) used for expression of labelled protein.

Quantities for 1 L of dH2O are given. The medium was sterilized and filtered through 0.22 µm filter (Sambrook, J et al 1989).

Chemicals	Na_2HPO_4	KH_2PO_4	NaCl	$^{15}NH_4Cl$	Glucose	$MgSO_4.7H_2O$	$CaCl_2.2H_2O$	Thiamine	$FeSO_4.7H_2O$
Quantity used (g)	12.8	3.0	0.5	1.0	2.0	0.494	0.015	0.010	0.010

2.5.3 Cell disruption

The resulting cell pellet from protein expression was re-suspended in 3 mL g^{-1} of the sonication buffer (50 mM Tris-Cl, 0.1 M KCl, 3 mM DTT, 1 mM $ZnSO_4$ and 150 µL protease inhibitor cocktail without EDTA at pH 8.5). Cell lysis was attained by pulsed sonication (sonicated for 1 minute, with 30 seconds rest time on ice) at 15 W until the solution turned translucent. The resulting mixture was centrifuged at 45,000 × g at 4 °C for 30 minutes. The supernatant was separated and used in the purification steps below.

2.5.4 Ethanol chloroform precipitation

The volume of protein solution (supernatant) was measured and an equal volume of ice-cold ethanol:chloroform (100:8), added drop-wise, was used to precipitate undesired contaminants. The mixture was centrifuged at 5000 × g for 10 minutes. Three equivalent volumes of ice-cold ethanol:chloroform were then added drop-wise (with stirring on ice) to the resultant supernatant. The mixture was centrifuged again for 10 minutes at 5000 × g and precipitated protein was re-suspended in 20 mM ammonium hydrogen carbonate buffer (2.5 mL) and filtered through a 0.22 µm syringe filter for further purification via Fast Protein Liquid Chromatography (FPLC).

2.5.5 Size Exclusion Chromatography (SEC)

Protein samples were loaded onto a size exclusion column (16/60 HiLoad™ 75 Superdex™ prep grade, Amersham Biosciences) for further purification. Proteins were isocratically eluted with 20 mM ammonium hydrogen carbonate buffer (pH 8.4) with a flow rate of 0.5 mL min^{-1} (ÄKTA Purifier, Amersham Biosciences) and 4 mL fractions were collected. The elution of protein was monitored by absorbance at 220 and 280 nm.

2.6 Protein characterization: SDS-PAGE gel electrophoresis

A 15% SDS-PAGE (Pre-cast gels NuPage 10 well, 15% gradient Bis-Tris Gels, Invitrogen) gel was run according to the protocols set out in the "protocols and applications guide" (Promega 1996). Samples were made up by mixing in 1:1 Laemmli Buffer (Sigma Aldrich) and then placed in a heating block at 80 °C for 5 minutes. The denatured samples were then vortexed gently for 5 seconds and loaded onto the gel (15 µL). Electrophoresis was carried out under constant voltage (200 mV) for approximately 30 minutes at room temperature. Following electrophoresis, the gel was stained using the silver stain method described below.

2.6.1 Silver Staining of SDS-PAGE gels

Gels were soaked in 7% acetic acid for seven minutes with continuous agitation, followed by soaking in 50:50 methanol:water for 20 minutes. The previous step was repeated with a change of methanol and then gels were soaked in distilled water for 10 minutes (with agitation). Subsequently, gels were stained with a staining solution for 15 minutes. This staining solution contained two solutions, A and B. Solution A was prepared with 0.8 g silver nitrate in 4 mL of distilled water and solution B included 30% sodium hydroxide (0.25 mL), ammonium hydroxide (1.4 mL) and water (21 mL). Solution A and B were mixed and diluted with 75 mL of distilled water. After gels had been stained for the given time, they were rinsed thoroughly with water twice (5 minutes each wash) and then placed in the

developing solution (1% citric acid (1 mL), 37% formaldehyde (0.1 mL) in 200 mL water). Development was stopped soon after when the bands were visible on the gel by rinsing the gel thoroughly with stopping solution (1% acetic acid) or distilled water.

2.7 Identification of protein by mass spectrometry

25 µM protein samples were prepared in 10 mM ammonium hydrogen carbonate buffer (pH 8.5) with 10% (v/v) methanol, for the acquisition of mass spectra for fully metal loaded protein. However, in the case of Zn_4SmtA, acidification of the sample mixture with 1% formic acid was required to obtain protein in the apo form. Mass spectra were recorded on a ESI-TOF (electrospray-ionisation-time-of-flight) instrument (MicroTOF, Bruker Daltonics) with ESI source. The samples were directly introduced into the source using a syringe pump with a flow rate of 240 µL/hr and ionized at a source temperature of 300 °C. Mass spectral data were acquired for 2 minutes in the positive ion mode over the m/z range of 800-2000. The resulting data were averaged and deconvoluted using the Data Analysis module supplied by Bruker Daltonics.

2.8 Protein concentration determination

2.8.1 UV-Vis absorption spectrophotometry (A_{280})

Protein concentration was estimated using UV absorbance at 280 nm using the Beer-Lambert Law (equation 1) where *A* is the absorbance at 280 nm, ε is the extinction coefficient (M^{-1} cm^{-1}), *l* is the path length of the cuvette (cm) which is 1 cm and *c* the concentration (mol L^{-1}).

$$A = \varepsilon l c \qquad (1)$$

For SmtA, the extinction coefficient at 280 nm has been determined experimentally by Eman Allafi (MSc Thesis, 2010) to be ε_{280} =4750 M^{-1} cm^{-1}.

The UV absorbance of 50 µL of purified protein in 10 mM ammonium hydrogen carbonate buffer was measured using a UV-Vis spectrophotometer (Biomate, Thermo Scientific) and the resulting protein concentration was calculated.

2.8.2 Ellman's assay (Sulfhydryl determination with DTNB)

Ellman's reagent i.e. 5,5'-dithiobis-(2-nitrobenzoic acid) or DTNB forms a mixed disulfide with thiols, releasing the chromophore 5-mercapto-2-nitrobenzoic acid (absorption maximum 412 nm, ε = 13,600 M^{-1} cm^{-1}). The reactions were conducted in 0.1 M Tris-Cl buffer pH 7.2 at 25 °C in presence of EDTA. Concentration was calculated using the molar absorption coefficient of the yellow product.

2.8.3 Determination of metal-protein stoichiometry: ICP-OES

ICP-OES (inductively coupled plasma-optical emission spectroscopy) is a type of emission spectroscopy, which is used to detect the trace metals (with moderate to low detection range ~0.2—100ppb) and certain non-metals including sulfur. The instrument uses inductively coupled plasma as an excitation source that also dissociates the sample into its integral atoms or ions, which emit light of characteristic wavelength.

The protein samples were prepared by simply diluting protein samples with 0.1 M ultrapure HNO_3 to obtain concentrations in the range of 0.2—2 ppm. The analyses were performed on a Perkin Elmer Optima 5300V. All samples were evaluated for Cu, Zn, Cd and S. Standards 0.2—2 ppm were prepared from high grade 10, 000 ppm stocks and used for calibration. The ICP-OES data (in mg/L; ppm) were divided by the appropriate atomic masses of respective elements, which give the concentration in mM of the given element in the sample. The protein concentration was obtained by dividing the sulfur concentration by the numbers of sulfurs in the proteins. Subsequently the metal to protein ratio was calculated.

2.9 Reconstitution of SmtA

For reconstitution, Zn_4SmtA was first demetallated to produce an apo-SmtA, which was further reconstituted with Cu(I) or ^{111}Cd(II) for further analysis. The Zn_4SmtA demetallation and reconstitution methods (based on method used by Calderone et al. 2005) developed are described below.

2.9.1 Zn_4SmtA demetallation:

The demetallation procedure previously established by Vasák 1991 was used. The protein in volume of 2 mL was incubated with 250 µL 100 mM DTT (~10 fold molar excess of DTT w.r.t protein) for one hour at room temperature. The excess metal and DTT contents were removed by gel filtration (PD-10 column, GE Healthcare), which was equilibrated with 0.01 M HCl. 250 µL of 1M HCl was added rapidly to the 2.25 mL of protein/DTT solution and mixed gently. The resulting solution was applied to the PD10 column and the flow through was collected. 3.5 mL of 0.01M HCl were then added to the column and the eluate was collected in the collection tube. The pH was raised to 7.5 with NH_3 and apo-SmtA (2.88 mg/3.5ml) was freeze-dried.

2.9.2 Lyophilisation

Protein (3.5 mL of 0.82 mg mL^{-1}) was lyophilised in a 5 mL round bottomed flask. The flask was swirled in a Dewar of liquid nitrogen to form thin layers inside the flask before being placed onto dry ice and attached to a high vacuum line. The flask was left under high vacuum (using Vac line) until all solvent had been removed. The resulting lyophilised protein powder was then resuspended with 10 mM ammonium bicarbonate buffer and reconstituted with required metal [Cu(I)].

2.9.3 Preparation of Cu-loaded SmtA

Samples for copper-metallothionein were prepared in strict anaerobic conditions. For this purpose, an anaerobic nitrogen glove box was used. All the buffers and metal solution used were degassed and nitrogen purged to avoid oxidation of metal or protein.

To reconstitute, the freeze dried metal free protein was dissolved to a protein concentration of 15 $mgmL^{-1}$ in 10 mM NH_4HCO_3 buffer (pH 7.6) containing 2% (vol/vol) β-mercaptoethanol, and a 7-fold molar excess of copper(II) acetate was added. β-mercaptoethanol was anticipated to reduce copper to its monovalent state. The protein+metal solution was incubated for 30 minutes at room temperature in the glove box. The Cu-substituted protein was desalted on aPD-10 column equilibrated with NH_4HCO_3 (10 mM) and lyophilized. The freeze-dried Cu-substituted protein was stored at −80 °C until further utilization.

2.9.4 Preparation of $^{111}Cd_4$ SmtA

Zn_4SmtA was recombinantly produced according to the method described in section 2.4.3. The protein concentration was calculated by Ellman's assay and from the zinc:sulfur concentration measured by ICP-OES. $^{111}Cd_4$SmtA was prepared based on a procedure summarized in (Blindauer et al 2001) with slight modifications as described in section 2.9.1. To the apo-protein fraction (in 0.01 M HCl) eluted from a PD-10 column, a 4-fold excess (with respect to protein concentration) of $^{111}CdCl_2$ was added. The pH was raised to 7.3 with the addition of ammonium hydroxide. The resulting protein solution was then lyophilized.

2.9.5 Identification and analysis of reconstituted SmtA species

The samples ($^{111}Cd_4$SmtA or Cu_7SmtA) for mass spectrometry were prepared following the MS method as described in section 2.7. ICP-OES was used to analyze protein for zinc, sulfur, cadmium and copper composition.

2.10 NMR Experiments

2.10.1 Materials and chemicals

All reagents used were of analytical grade or high purity. Buffers were prepared with nitrogen-purged MilliQ water (Millipore).

2.10.2 NMR Sample preparation

NMR samples were prepared in 50 mM [D_{11}]Tris-Cl (CKgas,UK), 50 mM NaCl, 10% D_2O (Standard NMR buffer, pH = 7.4) in the glove box. pH was adjusted with 1 M HCl or NaOH. NMR experiments were carried out in high vacuum, low-pressure thin glass air tight 3mM bore for Cu_7SmtA and 5 mM bore precision NMR tubes (Wilmad glass, USA) for Cu(I) titrations of Zn_4SmtA or $^{111}Cd_4$SmtA.

2.10.3 Cu (I) titrations NMR experiments

For Cu(I) titration experiments, sample preparations (0.8 mM) were carried out in the glove box. Equivalent amounts of Cu(I) were added to Zn_4SmtA and the NMR tubes were sealed with Parafilm before being removed from the chamber. Eight spectra (^1H,^{15}N HSQC for Zn_4SmtA or 1D and 2D ^{111}Cd NMR spectroscopy for $^{111}Cd_4$SmtA) were recorded at 35°C with addition of 0 to 7 equivalents of $[Cu(CH_3CN)_4]PF_6$.

2.10.4 NMR Instrumentation

Solution NMR spectra were recorded on a range of Bruker solution state NMR spectrometers (Bruker, Karlsruhe, Germany). The operating frequencies of the instruments are detailed in Table 2.2. Experiments were typically run at 35°C using samples in 3 mm bore Wilmad NMR vacuum tubes or 5 mm high precision NMR tubes (Wilmad Glass, USA).

Table 2:2 Operating frequencies of spectrometers used

Spectrometer	Probe	Operating frequency (MHz)		
		^{1}H	^{15}N	^{111}Cd
Bruker DRX500	BBO	500.13	50.67	106.10
Bruker Avance III 600	TXI	600.13	60.81	-
Bruker Avance 700 Ultrashield	Cryo	700.24	70.95	-

2.10.5 Referencing of NMR Spectra

^{1}H chemical shift referencing was carried out with respect to water (4.69 ppm) on the DSS scale (Wishart et al. 1995) and ^{15}N chemical shifts were referenced externally to $^{15}NH_4Cl$ standard solution. Samples contained 10% D_2O which was used for field-frequency lock of the spectrometer.

2.11 1D ^{1}H NMR experiments

SmtA 1D ^{1}H spectra were recorded at 600 MHz with a 330 ms acquisition time, 1 second recycle delay, 16 scans, and typically a 9.25 µs 90° pulse for excitation of ^{1}H with a power level of 2.2 dB. Spectra were acquired with 8 k complex data points in F_1 and a spectral window of 16 ppm. Data were Fourier transformed into 32 k complex data points and EM line broadening of 0.5 Hz was applied during processing. For MymT spectra were recorded as per SmtA but at 500 MHz and with a ^{1}H 90° excitation pulse of 11.25 µs at a power level of 6.45 dB.

2.12 2D NMR experiments

2.12.1 2D ^{1}H Homonuclear experiments

2D homonuclear experiments were recorded on Bruker Avance III 600 MHz and 700 MHz solution state NMR spectrometers (at the University of Warwick) at 35 °C. 2D [^{1}H,^{1}H] nuclear Overhauser enhancement (NOESY) and total correlation (TOCSY) spectra were acquired for SmtA with 4k complex data points in F_2, 400 increments in F_1, and 64 scans with an acquisition time of 100 ms for F_2 and 20 ms for F_1, MymT NOESY and TOCSY experiments were recorded with 512 increments in F_1 with 32 scans per slice with an acquisition time of 180 ms for F_2 and 23 ms for F_1. A spectral window of 16 ppm in F_2 and 16 ppm in F_1 was used. Spectra were acquired using 90° pulse for excitation of 8.43 µs and for Cu-MymT 12.00µs with a power level of 2.20 dB for 600 MHz and 5.9 dB for 700 MHz. The raw data were Fourier transformed into 2 k complex data points in F_2 and 2 k in F_1.

For SmtA NOESY experiments, three spectra were recorded with mixing times of 65, 100 and 200 ms and for TOCSY a spectrum with 60 ms mixing time was recorded.

2.12.2 2D ^{1}H-^{15}N Heteronuclear experiments

2D ^{1}H-^{15}N Heteronuclear single quantum coherence (HSQC) spectra (Schleucher et al. 1994) were recorded at 600 MHz with 2 k complex data points in F_2, 128 increments in F_1, and 32 scans per increment with an acquisition time of 114 ms for F_2 and 26 ms for F_1. A spectral window of 15 ppm in F_2 and 40 ppm in F_1 was used. Spectra were acquired using a 90° pulse for excitation of ^{1}H of 9.25 µs with a power level of 2.20 dB. The raw data were Fourier transformed into 2 k complex data points in F_2 and 512 in F_1.

2.13 ^{111}Cd NMR experiments

2.13.1 ^{111}Cd NMR Sample preparation

The lyophilized sample was resuspended in 50 mM [D_{11}] Tris-Cl, 50 mM NaCl, 10% D_2O, pH 7.4 with a resulting protein concentration of 1.1 mM and transferred to a 5 mm NMR tube (5 mm precision NMR tube, Wilmad USA).

2.13.2 1D ^{111}Cd NMR Spectroscopy

NMR spectra were acquired on a Bruker DRX500 500 MHz solution state NMR spectrometer (Bruker, Karlsruhe, Germany) operating at 500.13 MHz for ^{1}H and 106.03 MHz for ^{111}Cd. The spectrometer was equipped with a broad band observe (BBO) probe optimized for direct observation of ^{111}Cd nuclei. A pulse sequence using inverse gated decoupling during acquisition (GARP) was used. Data were acquired with 4 k complex data points, a spectral width of 300 ppm and 24576 scans. Spectra were acquired using 90° pulse for excitation of 7.3 µs with a power level of 3 dB. Data were Fourier transformed with 16k data points and a 100 Hz exponential line broadening was applied for apodization.

2.13.3 2D ^{1}H-^{111}Cd NMR Spectroscopy

2D ^{1}H-^{111}Cd HSQC spectra were recorded with 2 k complex data points in F_2, 96 increments in F_1, and 256 scans per increment with an acquisition time of 150 ms for F_2 and 2.2 ms for F_1. A spectral window of 14 ppm in F_2 and 200 ppm in F_1 was used. The raw data were Fourier transformed into 2 k complex data points in F_2 and 512 in F_1.

2.14 NMR data Analysis

The analysis of the 2D NMR datasets was done using software SPARKY version 3.113 (Goddard *et al,* 2008) and TOPSPIN 2.0 (Bruker, Germany) was used to analyze 1D NMR data sets.

2.15 Electrospray Ionization Mass spectrometry (ESI-MS) Analyses

All sample preparations for ESI-MS experiments involving Cu(I) were carried out using $[Cu(CH_3CN)_4]PF_6$, under strict anaerobic conditions (glove box) to avoid the oxidation of Cu(I). All the buffer and metal solution used were degassed and nitrogen purged.

2.15.1 Ag(I) titrations of Zn4SmtA

To the Zn_4SmtA solution, 0 to 8 molar equivalents of Ag(I) acetate were added. The sample solutions were incubated for 30 minutes before the MS spectra were acquired. The samples (15 μM) with 10% methanol were directly injected (4 μL min^{-1}) into an ESI-TOF mass spectrometer (MicroTOF, Bruker Daltonics) operating in positive ion mode. The MS parameters were as follows: the source temperature was 300 °C capillary exit 210 V, hexapole RF 450 V, skimmer 70 V and hexapole 119 V. Mass spectral data were recorded for 2 minutes over m/z range of 500—2500 Th. An average spectrum was produced, smoothed and deconvoluted using the Data Analysis program supplied by Bruker Daltonics (Germany).

2.16 CD spectroscopy

Circular dichroism (CD) is a spectroscopic technique that is commonly used to characterise the secondary structure of proteins. CD experiments were conducted at room temperature (~25 °C) using a Jasco J-815 spectropolarimeter (Jasco UK, Great Dunmow, Essex, UK) and 1 mm path-length quartz cuvettes (Starna; Optiglass Ltd., Hainault, UK) using a sample volume of 150 μL. Spectra were recorded in the far and near UV region between 190 and

400 nm, with a data pitch of 0.2 nm, a 1 nm bandwidth, 100 nm min^{-1} scanning speed and a response time of 2 s.

Samples for CD spectroscopy were typically prepared with a final protein concentration of 0.3 mg mL^{-1} in buffer (5 mM Tris-Cl), and spectra were collected and averaged. For each sample, a blank containing all sample constituents apart from the protein was subtracted to correct for background noise in the spectra. The buffer was purged with nitrogen to maintain reduced conditions. The pH of the reaction mixture was maintained at ~6.8 throughout.

2.17 Metal release reactions

2.17.1 Reaction with Bathocuproine disulfonate: UV Spectroscopy

Sample aliquots of 5 µM Cu_7SmtA, with 100 fold excess of BCS to protein in 25 mM Tris-Cl buffer at pH 7.4 were prepared in the anaerobic glove box. The reaction was followed by the absorbance of Cu-MT at 483 nm using a Perkin Elmer Lambda 25 UV-Vis spectrometer. The same strategy was applied for Cu-MymT.

3

Method development for preparation of Cu-bound bacterial MTs

3.1 Introduction

Copper metallothioneins isolated from mammalian liver are subject to uncontrolled oxidation leading to disulfide bridged polymeric species and often loss of copper (Brouwer et al. 1986, Hartmann and Weser 1977, Minkel et al. 1980). For example, aerobic syntheses of rat liver Cu-MT yielded preparations with 10 to 12 titrable sulfhydryl groups, whereas 18 titratable cysteines were observed after anaerobic preparations (Geller and Winge 1982). Similarly the preparation of Cu-MT from American lobster was also sensitive to oxidation (Brouwer et al 1986). These complications make it particularly challenging to work with Cu-MTs. This may also be the main reason for the absence of solved Cu-MT structures i.e., with only two Cu-MT structures (*N. crassa* Cu-MT and Cup1, later complete with connectivities) being solved to date, which took four decades to resolve (Calderone et. al 2005). Therefore, in order to study the structure of Cu-MTs such as MymT, it was crucial to develop a viable

method for preparation and characterization, which overcomes the problems arising from oxidation.

The initial aim of the present project was to over-express and characterize the newly discovered Cu-MT, MymT, from *Mycobacterium tuberculosis* (Gold et. al 2008). However, after many efforts a suitable expression system for Cu-MymT could not be established and therefore it became necessary to develop a reconstitution method that could be applied to a synthetically prepared peptide (Chapter 6). Since the supply of MymT was limited and experimental techniques for working with Cu-MTs had not been previously established in the group, therefore a model metallothionein system was needed. For this purpose, Zn_4SmtA was used.

SmtA was selected as a model bacterial metallothionein in order to develop methods to reconstitute MTs with Cu(I) and characterization of its Cu(I) form. SmtA was chosen since it has been well characterized previously with Zn (with a 3D structure already available PDB, 1JJD, Blindauer et. al 2001). This made SmtA very suitable for method development and characterization of Cu-MTs. This also provided an opportunity to study the details of copper binding either to the metal free or Zn- or Cd-containing metallothionein SmtA (Chapters 4 and 5). There are a number of studies on characterizing the copper-binding stoichiometries of mammalian MTs (Chen et. al 1996, Dolderer et. al 2007), but little is known about detailed structural effects of either complete or partial Zn/Cu replacement, or metal distribution in mixed-metal clusters (Chen et. al 1996, Dolderer et. al 2007).

In this chapter, a method was successfully developed for the anaerobic preparation of copper-reconstituted MTs, and preliminary characterization of the resulting species is described for SmtA.

3.2 Preparation of apo-SmtA and reconstitution of Cu_7SmtA

3.2.1 Reconstitution conditions

For reconstitution, Zn_4SmtA was first demetallated by lowering the pH (~2) and the resulting solution was passed through a gel filtration column (PD-10) to remove Zn(II) from protein solution (Vasák 1991). The reconstitution was carried out with re-suspending the lyophilized apo protein in buffer, containing 4% βME and adding seven mol. equivalents of Cu(II) [Cu(II)oAc] to the protein solution (Calderone et al. 2005). The reducing agent βME is anticipated to reduce Cu(II) to Cu(I) and break any disulfide bonds in the apo-protein. The reaction mixture was incubated for 30 minutes, which allows the apo-protein to bind and equilibrate required metal ions. After Incubation, the reactants were passed through gel filtration column to remove excess Cu(I) and βME. In addition, this extra purification step also allows protein elution into any desirable buffer, in this particular case, a volatile buffer for subsequent ESI-MS analysis (See chapter 4, section 4.2 for ESI-MS theory and sample preparations). This reaction was initially carried out under a continuous N_2 stream.

The ES-MS spectra of the reconstituted protein indicated formation of a Cu_7SmtA species as shown in Figure 3.1, but still suffered from low signal to noise. In addition, the multitude of peaks below m/z 1000 suggests that protein has been degraded.

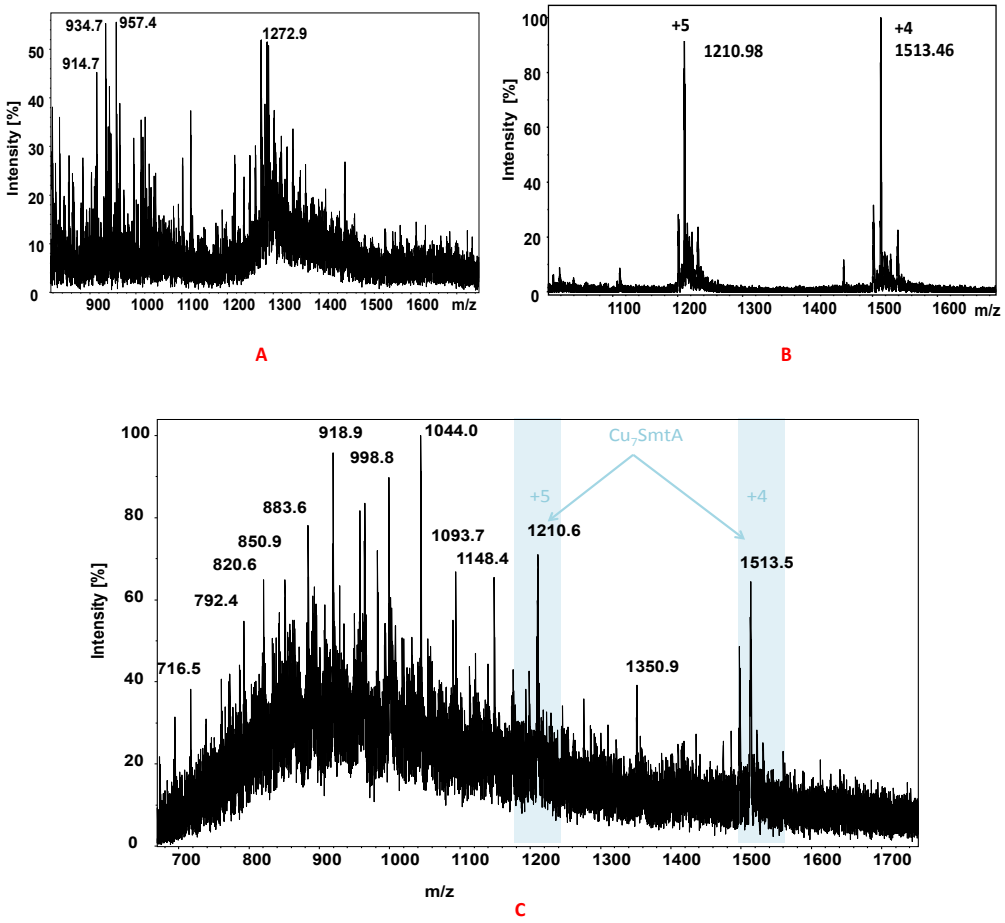

Figure 3.1 Identity of Cu_7SmtA.

A full scan ESI-MS spectra showing the product of Cu(I) reconstitution (A, C) with *in situ* reduction with reducing agent at pH 7.1. The reconstitution was carried out in fume cupboard under continuous stream of N_2. (B) ESI-MS spectrum for Cd_4SmtA prepared under N_2 stream.

The very first ESI-MS spectrum for Cu(I) reconstitution product (Figure 3.1A) has a very low signal to noise ratio and it is hard to identify any significant species from this. However, there is one low-resolution peak for metal overloaded species (~6359.5 Da which might correspond either to a 12 metal species- Cu_{12}SmtA, with theoretical mass of 6360 Da), or alternatively to a species containing mixed disulfides with BME (BME_9Cu_1SmtA, theoretical mass 6358.0 Da). One possibility for the low intensity is the formation of a complex mixture of protein degradation products along with the aggregation of protein with excess Cu(I)

binding and, above all, the possibility of oxidation. Clearly, the mere application of a stream of N_2 was not sufficient to prevent extensive oxidation.

Although attempts were made to carry out the reconstitution procedure under anaerobic conditions using an N_2 stream as a means of preventing oxidation, these precautions were not sufficient. Both apo-SmtA (at pH~7.4) along with Cu(I) has the potential to become oxidized under even small amount of oxygen. Although this method yielded an identifiable Cu_7SmtA species (Figure 3.1C), the low quality of the resulting ESI-MS data emphasize the requirement for stricter anaerobic conditions when reconstituting the apo-protein with Cu(I). Therefore the subsequent reconstitution and characterization procedures were developed under strict anaerobic conditions i.e., N_2 glove box with <1% O_2 with all buffers and reagents fully nitrogen purged.

3.2.2 Anaerobic reconstitution of SmtA

3.2.2.1 Cu(I) reconstitution of SmtA in inert atmospheric glove box

For fully anaerobic reconstitution of apo-SmtA with Cu(I), an inert atmospheric glove box was used. The lyophilized apo-SmtA protein generated by using method established by Vasák 1991 (mass spectra shown in Figure 3.2A and B) was then incubated with seven equivalents of Cu(II) (with MT concentration of 15 mg/ml) in the presence of a reducing agent (4% βME in ammonium bicarbonate buffer, pH 8.5) and this solution was passed through a gel filtration column in order to liberate loosely bound Cu(I) along with excess βME and Cu(I). ESI-MS was then used in order to identify the formation of Cu(I)-loaded SmtA. Direct injection of the sample produced the raw spectra as shown in Figure 3.2.

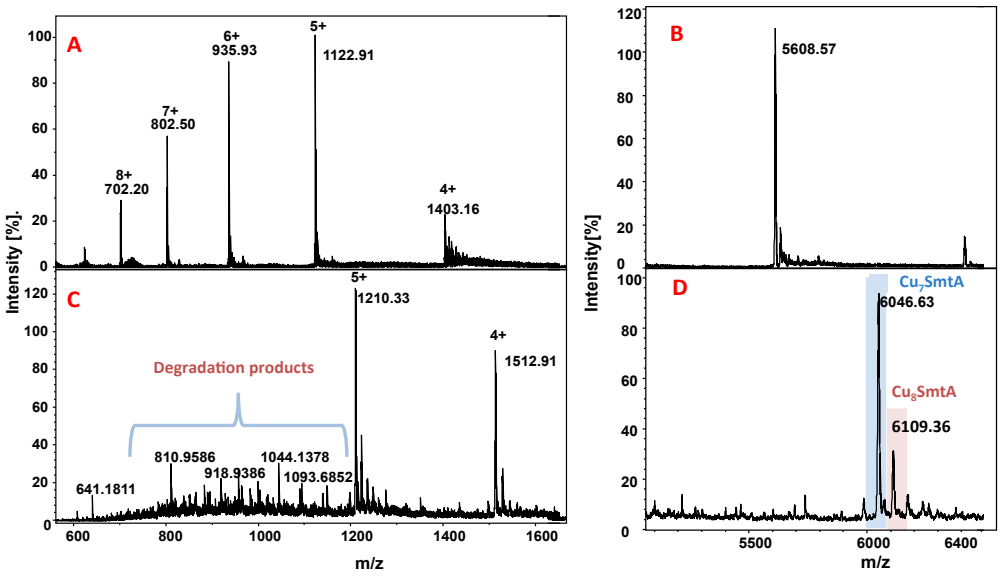

Figure 3.2 ESI-MS of apo and Cu(I) reconstituted SmtA.

Full scan (A,C) ESI-ToF-MS spectra show charge state species of apo-Smta (A) and Cu_7SmtA (C) prepared under strict anaerobic conditions. Deconvoluted spectra for neutral masses of predominant species show a monomeric apo protein (B), and SmtA with seven and eight copper(I) ions bound (D). 25 μM of both Cu_7SmtA and apo-SmtA were made up in 10 mM ammonium bicarbonate buffer at pH 6.7.

After deconvolution of the charge states one predominant peak was observed for both apo- and copper-loaded SmtA, as shown in Figure 3.2. For the apo form of SmtA, the observed experimental mass for the neutral species was 5608.57 Da, close to the theoretical mass of the SmtA protein is 5610.3 Da for the neutral species. The most abundant signal in the spectrum of Figure 3.2 (D) had a respective mass of 6046.63 Da, which is in reasonable agreement with Cu_7SmtA (theoretical mass 6047.8 Da for the neutral species). A minor species with 8 Cu(I) ions was also observed with an experimental mass 6109.36 Da which is close to theoretical mass of 6110.0 Da (neutral species) for Cu_8SmtA. It is noted that the average masses in both deconvoluted spectra were 0.6—1.7 Da lower than expected; this may be mainly due to the peak-picking routine of the program. Figure 3.3 shows the experimental and theoretical isotopic distribution for Cu_7SmtA. In these spectra, the isotopic peaks with the highest abundance were at 6046.6 (which is also the value picked in Figure 3.2) and 6047.6 Da for the experimental spectrum, and at 6046.8 and

6047.8 Da for the theoretical spectrum. The close agreement between these spectra indicates correct assignment of the Cu_7SmtA species.

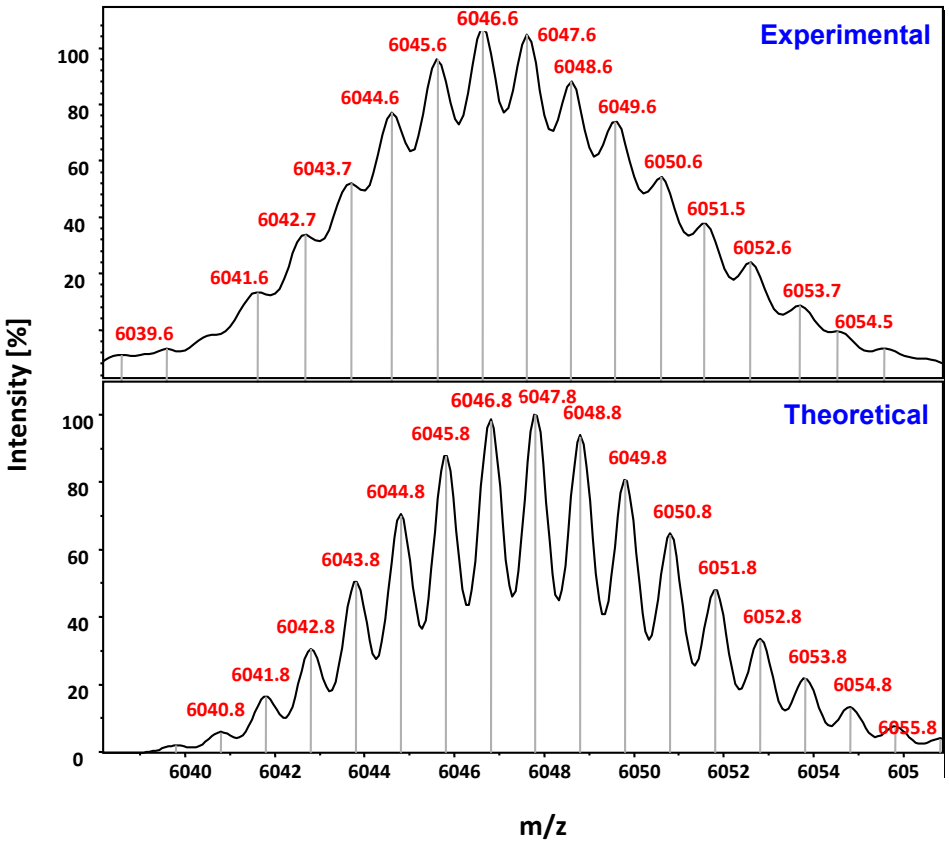

Figure 3.3 Isotopic distribution of Cu(I) reconstituted SmtA.

Isotopic distribution for 7 mol. equiv. of metal ions bound to SmtA together with a comparison to the theoretical model for the neutral species ($C_{225}H_{349}N_{70}O_{80}S_9Cu_7$).

The ESI-MS data along with isotopic distribution comparison with its theoretical model, confirmed the successful reconstitution of SmtA and the formation of Cu_7SmtA as the most prominent species.

3.3 Properties of Cu_7SmtA

3.3.1 Stability of copper reconstituted SmtA

After the successful reconstitution of SmtA with Cu(I) and formation of Cu_7SmtA as the major species, it was of interest to explore the stability of this new copper containing MT species. For this purpose, Cu_7SmtA was prepared under strict anaerobic conditions and then was exposed to air. The stability of Cu_7SmtA was monitored through the collection of a series of ESI-MS spectra, since ESI-MS can provide information on the loss of metal along with quality of sample over time. In this regard, Cu_7SmtA was exposed to air for upto four hours and aliquots were subjected to ESI-MS analysis as shown in Figure 3.4.

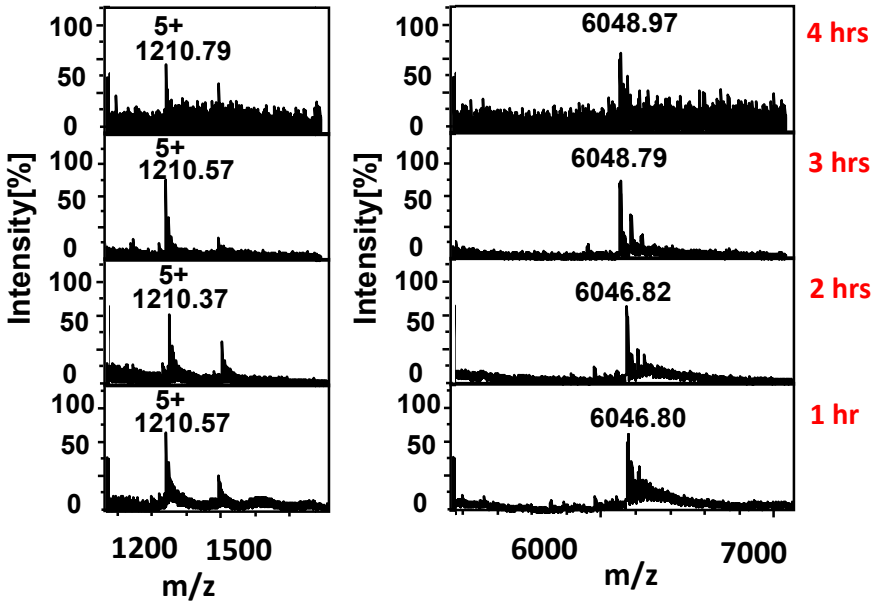

Figure 3.4 Stability of Cu_7SmtA in air.

Cu_7SmtA (25 μM in 10 mM ammonium bicarbonate buffer, pH 6.8) was exposed to air for four hours and aliquots were taken to check the stability of sample after every hour. Four spectra were acquired which show stepwise degradation of Cu-MT after three hours.

Surprisingly, the sample, which was expected to be oxygen sensitive, was relatively stable for up to three hours even in the presence of oxygen. After four hours the ESI-MS spectrum showed however a much lower signal to noise ratio for Cu_7SmtA, which may be indicative of protein degradation.

3.3.2 Competition reactions with Bathocuproine disulfonate (BCS)

The lability of Zn(II)/Cd(II) bound-MTs is often probed by reactions with chelators such as EDTA and PAR. However, these chelators are more suitable for divalent metal ions and are not appropriate for Cu(I). Instead, the Cu(I) chelator BCS (Bethocuproinedisulphonate) was used for this purpose.

BCS is a small ligand molecule that coordinates Cu(I) through nitrogen ligands to form the reddish-orange complex $Cu(BCS)_2$ with metal to ligand ratio 1:2 (Figure 3.5).

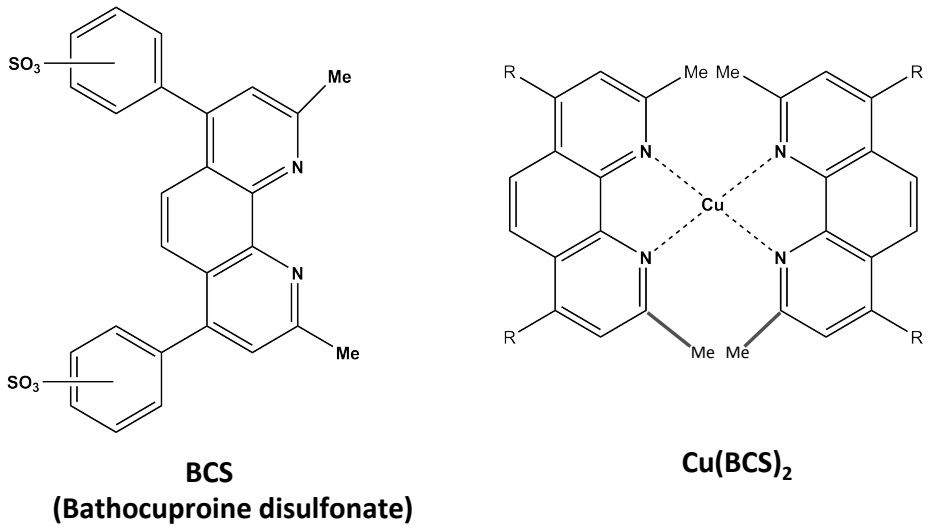

BCS
(Bathocuproine disulfonate)

$Cu(BCS)_2$

Figure 3.5 Structure of BCS and $Cu(BCS)_2$ complex.

Chemical structure of the Cu(I)-chelating ligand BCS (Bathocuproine disulfonate) and its copper complex $Cu(BCS)_2$.

A schematic diagram of BCS interaction with Cu(I)-containing proteins is shown in Figure 3.6 (adopted from Zhou et al. 2008). The schematic suggests that Cu(I) removal proceeds via formation of a ternary complex as an intermediate.

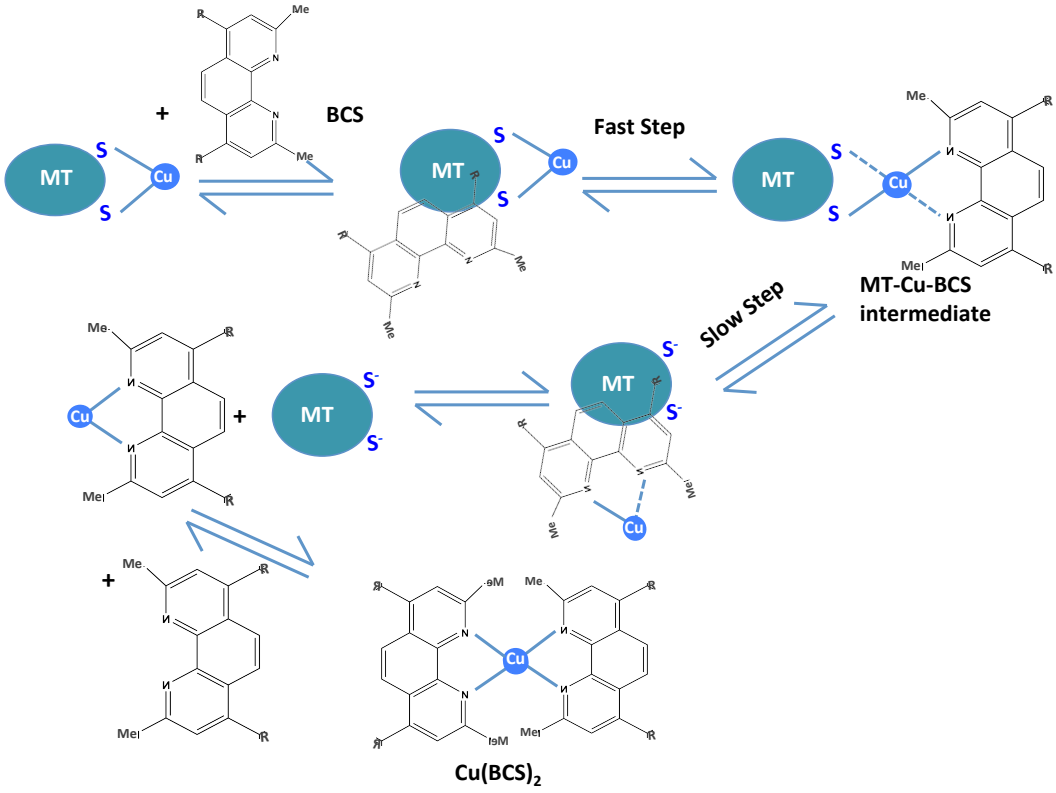

Figure 3.6 Mechanism of Cu(I) transfer between MT and BCS.

The step-wise formation of $Cu(BCS)_2$ complex is illustrated. The nature of the complex formed initially between MTs and BCS is not known (Figure adapted from Zhou et al. 2008).

The Cu(I) transfer from Cu_7SmtA to BCS under pseudo first order conditions were observed by UV-vis spectrophotometry. The fully loaded Cu(I) reconstituted MT, Cu_7SmtA, was prepared by the addition of 7 equivalents of Cu(I) to apo-SmtA as described earlier (Section 3.1). The reaction was monitored at 483 nm for the formation of $Cu(BCS)_2$. The reaction indicated that a very quick initial step occurred during mixing time and the first few minutes monitored, followed by at least one relatively slower step (Figure 3.7).

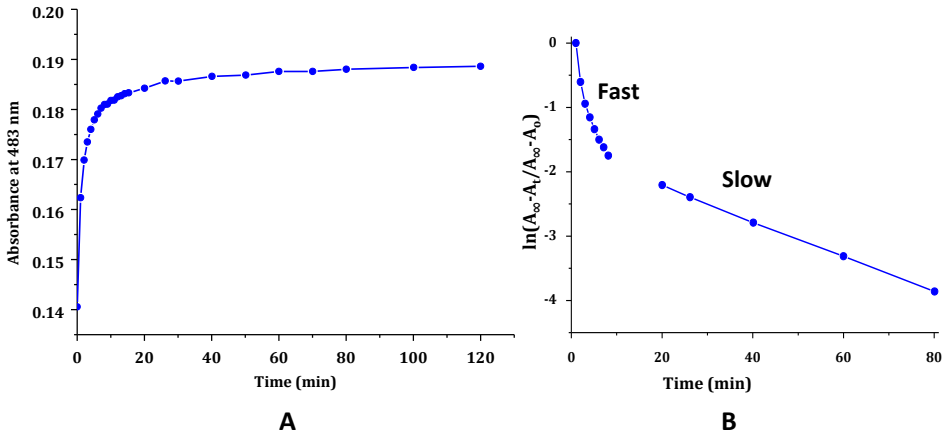

Figure 3.7 Absorbance of Cu_7MT (5 μM) with BCS (500 μM) as a function of time.

A) Time course of the formation of $Cu(BCS)_2$ complex followed by the increase in absorbance at 483 nm. B) Biphasic kinetics of copper transfer. The reaction was carried out at pH 7.5 in buffer 25 mM Tris-Cl.

The reaction of Cu_7SmtA with BCS is at least biphasic and contains both fast and slow constituents as shown in Figure 3.7B with corresponding rates of 5.3×10^{-3} and 6.9×10^{-4} s^{-1}. The first step occurs very rapidly and the rate cannot be precisely measured, unless stopped flow kinetic techniques would be employed. The second step occurs rather slowly, which is comparable to the reaction of mammalian MT with BCS (Chen et al 1996) and CopZ from *B. subtilis* (Zhou et al. 2008). This indicates that there are at least two different classes of Cu(I) sites, those with high kinetic lability, and those which are more inert - a similar situation encountered in Zn_4SmtA when reacted with EDTA (Leszczyszyn et al 2007). In the latter study, Zn_4SmtA was allowed to react with a 100 fold excess of EDTA (SmtA: EDTA ratio 1:100) under pseudo-first order conditions and the reaction was monitored by UV-Vis spectrophotometry. The initial step of the reaction was very fast followed by several slower steps. With the increase in EDTA excess to 1:150 (SmtA: EDTA), the first step could no longer be observed which shows its dependence on EDTA concentration and bimolecular nature involving a direct attack of EDTA on protein. The second step was however reported to be independent of EDTA concentration (Leszczyszyn et al. 2007).

For Zn_4SmtA, the first phase involved direct attack of EDTA on Zn containing site C with a rather complicated phase two resulting in Zn_1SmtA intermediate and phase three ended with EDTA slow reaction with Zn_1SmtA to apo-SmtA. Phase four corresponded to the degradation of unfolded apo-SmtA (Leszczyszyn et al 2007). In the reaction of Cu_7SmtA with BCS as shown in Figure 3.7, there is a fast step, which may be assumed to correspond to removal of first Cu(I) from metal cluster of protein. Obviously, since the structure of Cu_7SmtA is not known, the data cannot suggest which sites react fast and which react more slowly.

3.3.3 ^{1}H NMR spectroscopy

An approach to study the interaction of SmtA with Cu(I) in structural terms was attempted by ^{1}H NMR spectroscopy. The 1D ^{1}H NMR spectrum of Cu_7SmtA shows very little dispersion and considerable broadening of peaks as shown in Figure 3.8 A. Compared with its Cd(II) reconstituted form (Figure 3.8 B), Cu_7SmtA display a spectrum characteristic of an unfolded disordered protein with almost all residue in the NH backbone region shifted to the random coil region (i.e., 7.5 ppm-8.5 ppm) and broadened methyl peaks with no dispersion to higher field (Figure 3.8).

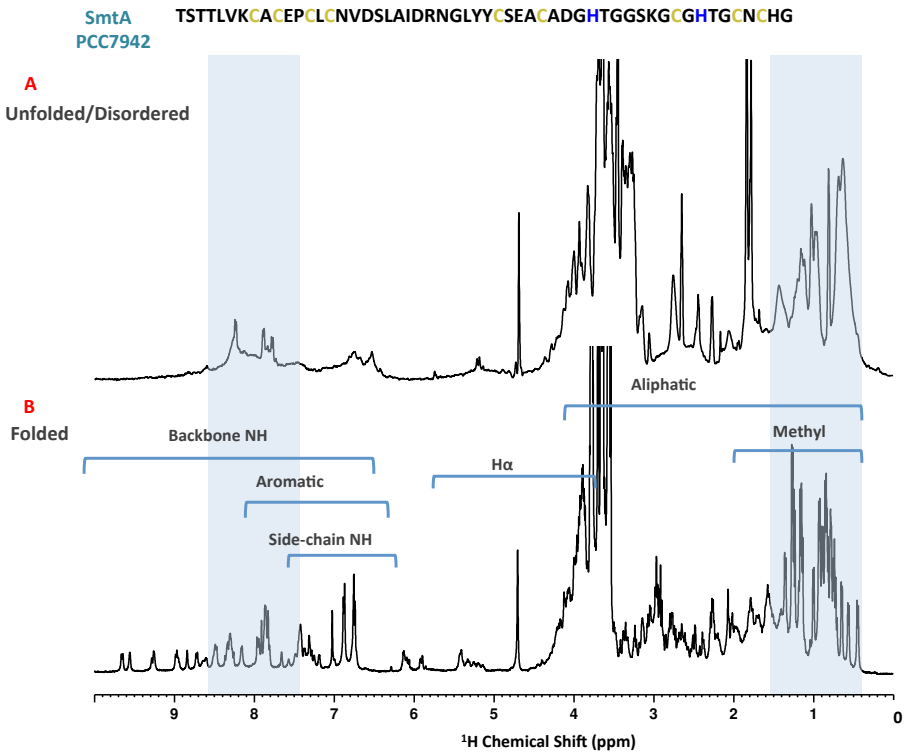

Figure 3.8 ^{1}H 1D NMR spectra of Cu_7SmtA and Cd_4SmtA.

Comparison of protein fold of (A) Cu(I) reconstituted SmtA and (B) Cd(II) reconstituted SmtA by 1D ^{1}H NMR. Samples were prepared in 50 mM Tris [D_{11}], 50 mM NaCl, pH 7.4 at 35 °C.

In addition, 2D TOCSY and NOESY were employed to obtain more detailed information on protein folding. The ^{1}H-^{1}H TOCSY is a homonuclear experiment, which gives *through bond* information for protons that are coupled together in the same spin system (i.e. all protons within one amino acid). This can be attained from scalar couplings, the magnitude of which roughly depends upon number of interfering bonds. Since there is no scalar coupling across the amide bond, protons from different amino acids give rise to different spin systems. Analysis of cross-peaks appearing from different spin systems can be used to assign each type amino acid based on the chemical shift within each system and known resonance patterns. The ^{1}H-^{1}H NOESY gives *through space* information for protons that are coupled together by dipolar couplings. The intensity of NOE signals depend on the distance between the coupled nuclei, with closer nuclei giving higher intensity NOE cross peaks and vice versa. Full 2D TOCSY and NOESY spectra of Cu_7SmtA are shown in Figure 3.9.

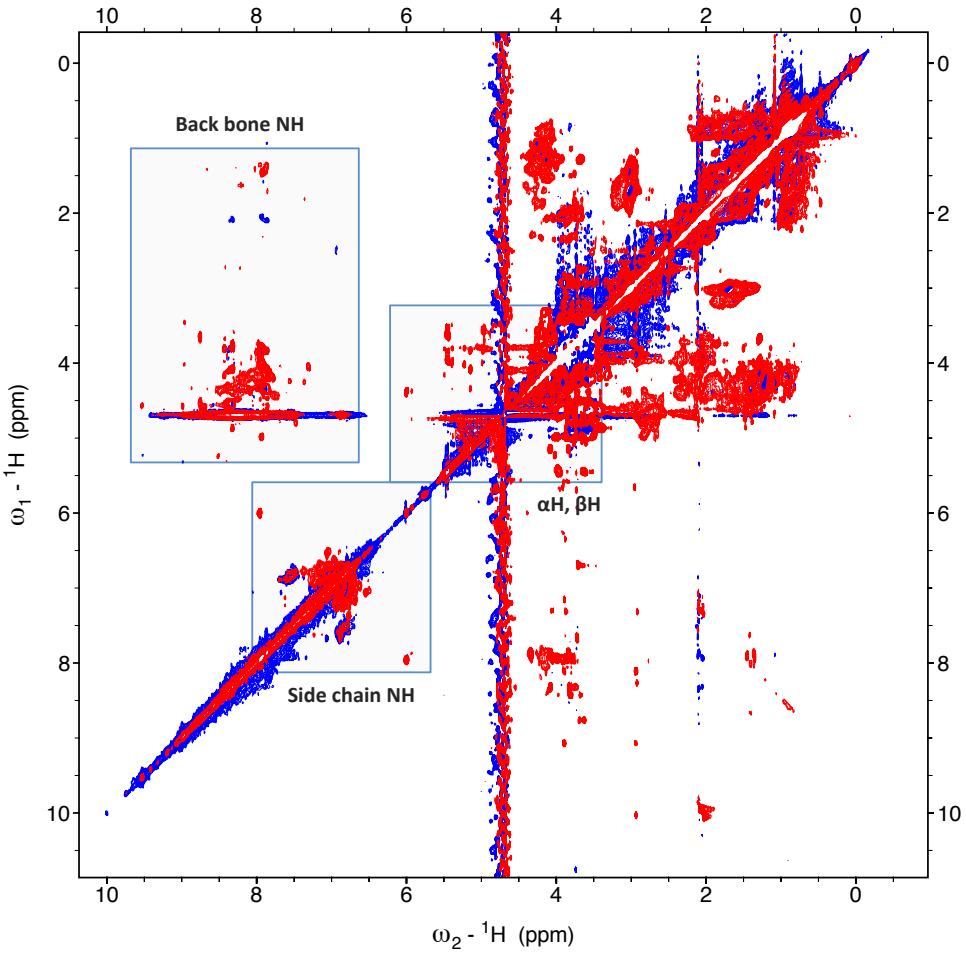

Figure 3.9 $^{1}H–^{1}H$ 2D NMR of Cu_7SmtA

An overlay of 2D $^{1}H–^{1}H$ TOCSY (red) and. $^{1}H–^{1}H$ 2D NOESY spectra of Cu_7SmtA displaying cross peaks in the fingerprint and side chain region.

Both TOCSY and NOESY spectra produced fewer peaks that expected based on the number of residues in SmtA (55). However there are prominent peaks in the side chain region of TOCSY spectrum (Figure 3.10) at 7.95 ppm and 7.54 ppm respectively.

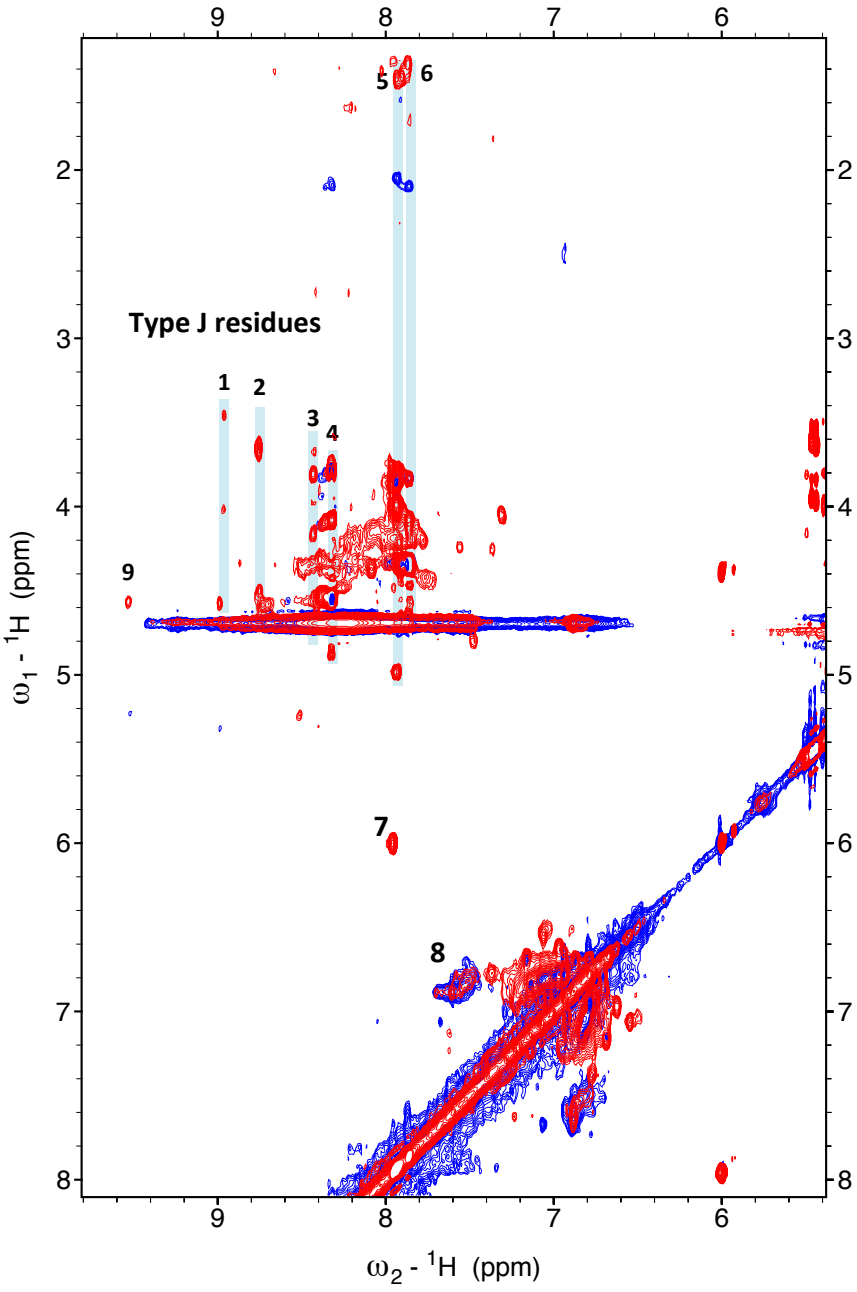

Figure 3.10 Spin system identification in ^{1}H-^{1}H 2D NMR of Cu_7SmtA

Finger print region of 2D ^{1}H–^{1}H TOCSY (red) and ^{1}H-^{1}H 2D NOESY (Blue) spectra of Cu_7SmtA highlighting six spin systems. The side chain regions of both spectra contain prominent peaks, possibly for Asn. However there is no indication of His delta and epsilon in this region.

All NH protons have very strong water exchange peaks. They are mostly in the region of random coil, most with TOCSY peaks but no NOESY peaks.

Table 3:1 Chemical shifts of resolved residues

The NH and αH chemical shifts of the residues identified in the finger print and side chain region of the TOCSY spectra.

Residue number	Chemical shift ä NH (ppm)	Chemical shift áH (ppm)
1	**8.96**	**5.22**
2	**8.74**	**5.44**
3	**8.43**	**4.96**
4	**8.32**	**5.23**
5	**7.93**	**5.14**
6	**7.86**	**4.97**
7	**7.96**	**4.93**
8	**7.58**	**6.84**
9	**9.5**	**5.20 (NOESY)** **8.5 (TOCSY)**

Since peaks are mostly not clearly defined or resolved, this may suggest there is little regular structure. At least six residues with NH resonances between 8 ppm —7.8 ppm and corresponding αH chemical shifts were observed. There are several resolved residues in the finger print region of the TOCSY spectrum. From the cross- peak patterns (or chemical shift range), it appears that the residue at 8.3 ppm most likely corresponds to a Type J residue, with chemical shifts for the β protons closest to those for Ser, and this also is true for resonance 4. They all have cross-peaks to protons around 2.10 ppm but the origin of these is not clear, although they are in the range of β or γ protons for Glu, Pro and Val (there is no Met in SmtA). The spin system of the low field shifted residue 9 at 9.5 ppm, which has a NOESY cross-peak at 5.20 ppm, could not be established due to lack of cross peaks in TOCSY

spectrum. The proton at 5.2 ppm has a TOCSY cross-peak at ca. 8.5 ppm, but again, no intra-residue TOCSY cross-peaks were identified. The chemical shifts of the NH proton at 9.5 ppm, together with the NOESY cross-peak to a proton at 5.2 ppm may indicate residual β strand character. From comparison of chemical shifts of these residues with those of Zn_4SmtA, there is a possibility that some of the resolved NH resonances belong to the sequence Asn17-Val18-Asp19-Pro20-Ser21 (within the zinc-finger fold), and that this region is less disordered than the remainder of the protein, perhaps aided by the presence of the rigid proline residue. It should be noted that this region is further away from metal binding cluster of the protein and hence may be capable of ordering itself independent of metal present.

There are also some high-field shifted resonances in Figure 3.10 with NH-CH(α) cross peaks below 7.5 ppm. The small cross-peaks to side-chain protons suggest that one of them may be an alanine, but again, lack of NOESY cross-peaks precluded further assignment.

The aromatic side-chain region should also include cross-peaks between δ and ε protons of histidines, but there was no clear indication for these at either random coil positions, or positions typical for metal-bound His residues. This may suggest that the C-terminus is also disordered because the non-metal binding residue His-55 is not observed either.

There are no cysteine residues apparent in TOCSY spectrum of Cu_7SmtA, which suggests that all cysteine residues are involved in Cu(I) binding with metal cluster of Cu_7Cys_9 i.e., 1: 1.5 for metal to cysteine ratio within the cluster. It is also a formal possibility that oligomers are formed, which may also result in disappearance of the corresponding cross-peaks (Myari et al 2004).

3.3.4 Circular dichroism of SmtA

Circular dichroism (CD) of proteins is a very useful technique and is used to study the conformation of protein or peptides via differential absorption of circularly polarized light. It is particularly helpful to observe any conformational changes induced by chelating ligands (Rodger et al. 2005, Daviter et al. 2013). CD was used to study the SmtA in the presence and absence of metal ions (i.e., Zn(II), Cd(II), Cu(I) and Apo-SmtA respectively) in order to further analyze if SmtA in presence of Cu(I) is correctly folded into its native structure e.g., Zn_4SmtA. In the Zn_4SmtA, contains the conventional elements of secondary structure i.e., α- helix and β-sheets. Figure 3.11 shows the CD spectra of SmtA. However the CD spectra of Zn_4SmtA and Apo-SmtA are very similar and unusual. The absorbance at 230 nm is because of pi-pi stalking of the two tyrosine residues. It was not possible to assign the secondary structure, which is not ideal—one reason can be different concentrations of the samples. Similarly in Cd_4SmtA CD spectrum, no evidence of secondary structure and a very prominent band at 254 nm owing to LMCT of metal. However, Cu_7SmtA CD spectrum displayed α- helical structure of the reconstitution product.

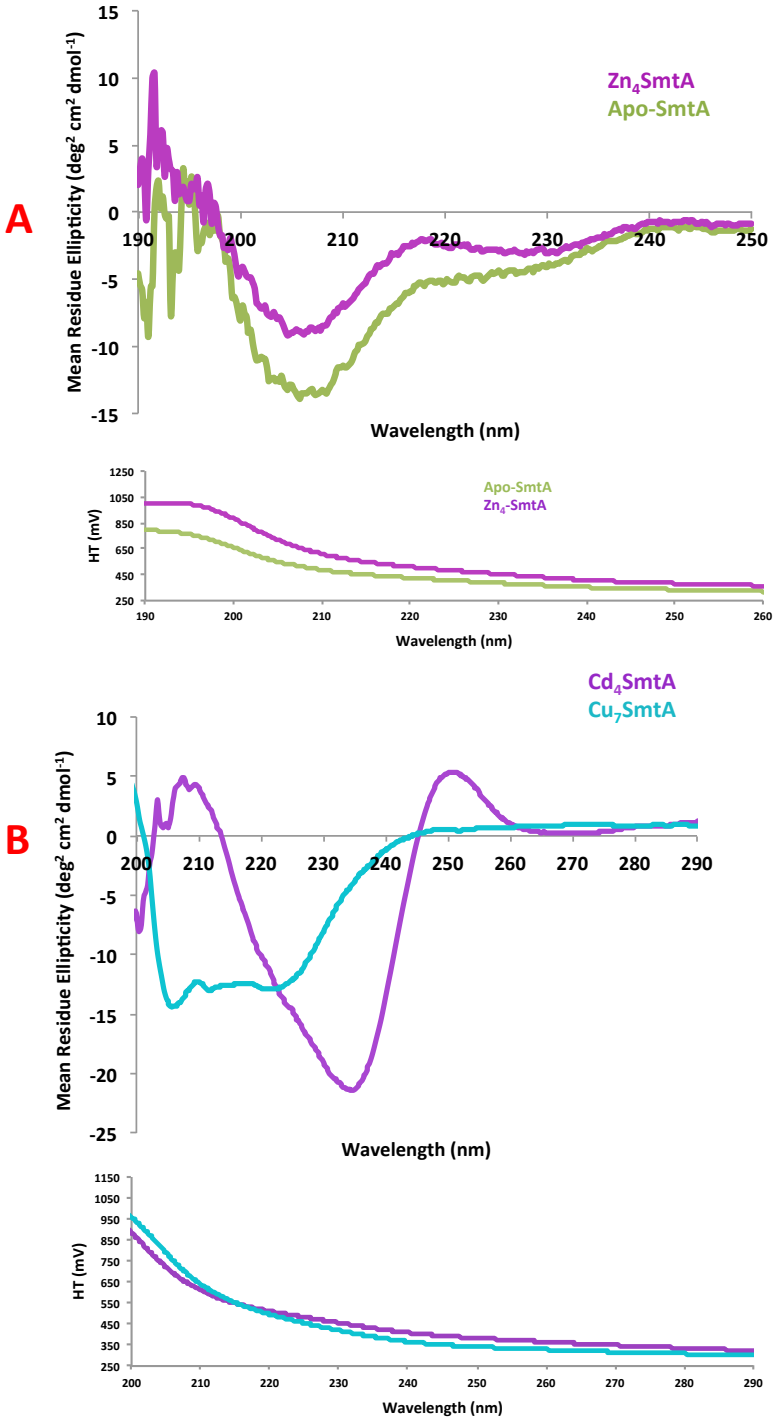

Figure 3.11 CD spectroscopy of SmtA

(A) CD spectra of SmtA in holo (containing Zn(II)) and apo-form. (B) CD spectra of reconstituted SmtA. CD spectra were recorded between 190-250 nm for Apo and Zn_4SmtA, and 200-290 nm for its reconstituted forms (Cd_4SmtA and Cu_7SmtA) obtained in 1 mM Tris-Cl, pH 6.7. The green line represents the signal for Apo-SmtA. The purple line indicates the native Zn_4SmtA. Dark purple and Cyan line is for its Cd(II) and Cu(I) bound form (Cd_4SmtA, Cu_7SmtA).

Both reconstituted products (Cd_4SmtA and Cu_7SmtA) of SmtA show different characteristics bands, but its already established by Blindauer et al. 2001, that Cd(II) does replace Zn(II) in SmtA isostructurally which was confirmed by its NMR structure. However, Cu_7SmtA shows a CD band for a α- helix structure.

The substantial change in band intensities in CD spectra of Zn_4-and Cu_7-SmtA suggests that major conformational change occurs upon metal binding of SmtA with change of structure with addition of Cu(I) in particular.

3.4 Zn-thionein and Cu-Thionein character of SmtA

The Zn- and Cu-thionein characteristics of mammalian MTs have been reported previously (Capdevila et al. 2010) with very recent studies suggesting mammalian (brain specific MT3) Zn-MT as Cu-thionein (Artells et. al 2014). However, there is no available data on Zn- or Cu-thionein characters of bacterial Zn-MTs. For this purpose, bacterial Zn_4SmtA was expressed in presence of varying concentration of Cu ($CuSO_4$) anaerobically to explore the Zn- or Cu-thionein character of this particular Zn-MT as shown in Figure 3.12.

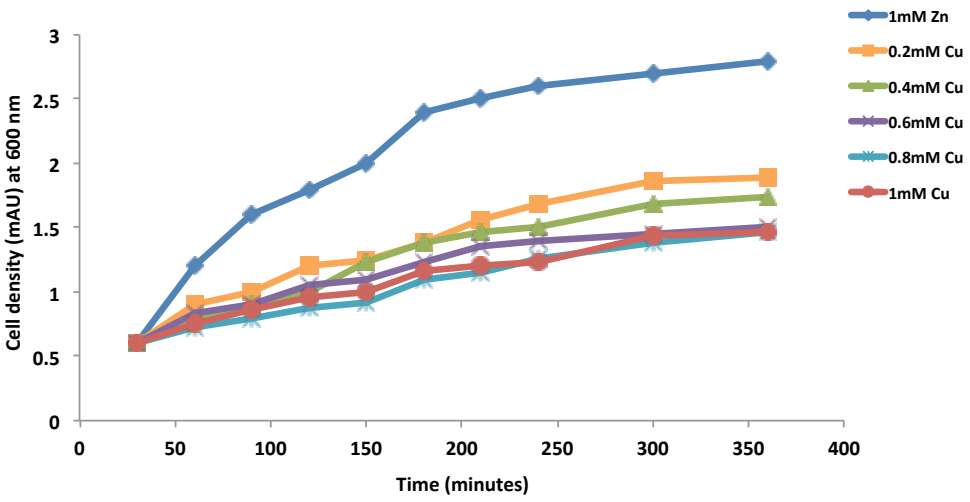

Figure 3.12 Expression curves of SmtA in presence of Cu.

SmtA was expressed by growing E. coli cells in LB medium at 37 °C (containing Kanamycin and chloramphenicol as selective markers) until it reached 0.6 optical density at 600 nm before induction by IPTG along with different concentrations of Cu (0.2–1 mM CuSO4) and 1mM ZnSO4 as control. Samples were diluted (1:200) before the absorbance was measured at 600 nm. The cells were harvested, sonicated and then resuspended in ammonium hydrogen carbonate buffer for FPLC.

The decrease in cell density absorbance was observed with increasing concentrations of Cu in media, which may suggest that the presence of Cu greatly affect the cell's ability to express desired protein.

Two samples were prepared for FPLC, each from media containing 1 mM Cu and 1 mM Zn respectively, for further analysis. The separation of protein mixtures was followed using the absorbance of peptide bonds at 220 nm.

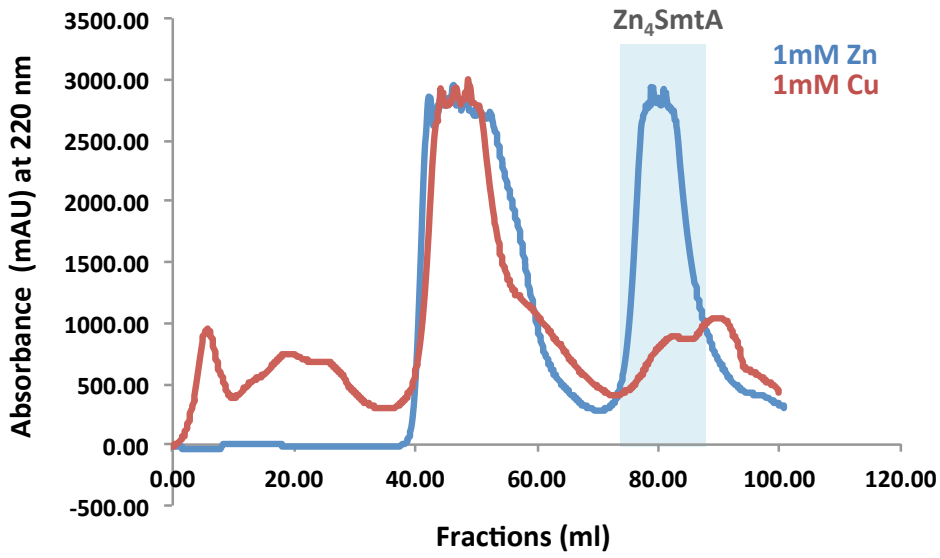

Figure 3.13 Zn- or Cu- thionein feature of SmtA

Plot of size exclusion chromatography of SmtA expressed in presence of 1mM ZnSO4 (blue) and 1mM CuSO4 (red). 2.5 mL of protein was injected onto a Superdex-75 column (16/60, HiLoad) and protein was eluted with 20 mM NH4HCO3 (pH 8.2). The separation of protein mixture was followed using the absorbance at 220 nm.

Figure 3.13 shows the overlay of chromatograms of protein expressed in Zn and Cu containing media. In case of Zn_4SmtA, the resulting chromatogram shows well-resolved peak at 80 ml for Zn_4SmtA, which confirms the presence of reasonably pure protein. The peak around 40—65 ml corresponds to higher molecular weight proteins as confirmed by early SEC elution times.

However, in the chromatogram for protein (from Cu containing media), there is a small peak eluting at similar elution times as Zn_4SmtA, which may be indicative of Zn-MT. Since there is not a big difference of molecular weight for both Zn-MT and Cu-MT, it is hard to tell from this particular experiment. In this regard, ICP-OES was used to quantify the resulting species (at similar elution time of Zn_4SmtA). ICP-OES results provided the protein to Zn ratio of 1:3.8 without any Cu in the sample. These results suggest that SmtA displays a distinct Zn-thionein character and expresses as its native Zn form, even in presence of higher amounts of copper in the culture medium, regardless of the order of affinities.

3.5 Summary and conclusion

The method development for Cu(I) reconstitution was done and tested on Zn_4SmtA due to its ready availability. The initial attempts of Cu(I) reconstitution failed due to protein oxidation, aggregation or degradation in the presence of air. However, a new method for reconstitution of Cu(I) to metallothionein was implemented under strict anaerobic conditions. An inert atmosphere glove box was used for this purpose. Subsequent ESI-MS spectrum of Cu(I)-reconstituted SmtA showed monomeric Cu_7SmtA which is moderately stable in air, although it does start to markedly degrade after four hours. The competition reaction of Cu_7SmtA with the Cu(I) chelator BCS revealed that BCS was able to abstract Cu(I) from Cu_7SmtA, with at least biphasic kinetics. The 1D and 2D ^{1}H NMR data suggested a disordered protein structure with the broadening or absence of NH peaks in a 2D TOCSY spectrum for most residues and absence of NOESY signals. In addition, CD spectroscopy showed that a major conformational change occurred on Cu(I) binding. The expression of

SmtA in copper-supplemented media produced Zn_4SmtA and lack of any Cu incorporation into the expressed protein. These data establish the clear Zn-thionein character of Zn_4SmtA. *E.coli* buffer Cu(I) may impede Cu-population, however, other MTs have been expressed in Cu-bound form.

However, the possibility of whether mixed-metal clusters can be be formed *in vitro*, and the distribution of Cu(I) and Zn(II) (or Cd(II)) in such mixed SmtA species has so far not been explored. For this purpose, SmtA in its native folded state (Zn_4SmtA or either Cd_4SmtA) will be used as starting material for titration studies with Cu(I), These studies may reveal the composition and distribution of Cu(I) within mixed-metal clusters, and are discussed in the next chapter.

4

Metal exchange reactions of metallothioneins

4.1 Introduction

The physiochemical properties of Zn and Cd-containing MTs have been studied since their discovery (Kägi and Vallee 1961, Kägi and Kojima 1987, Petering and Antholine, 1988, Blindauer et al. 2003, Freisinger and Vašák 2013). In contrast, copper bearing metallothioneins have been examined less intensively with rather less conclusive data (Bordas et al. 1982, Petering and Antholine 1988, Weser and Hartmann 1988, Weser et al. 1986, Schechinger et al. 1986, Deters et al. 1992, Sievers et al. 1996, Chen et al. 1996). The ability of endogenous metal ions to displace bound metal in MTs follows the order of stability constants for inorganic metal-thiolate complexes i.e., Ag(I)/ Cu(I)> Cd(II) > Zn(II) (Öz et al. 1998).

Attempts have been made to observe the structure and stoichiometry of zinc metallothioneins in the presence of Cu(I) (Dolderer et al. 2007, Chen et al. 1996). However, the systematic change in distribution and stoichiometries was not revealed by these

studies. The present studies focus on the stoichiometry and structural effects of binding of Cu(I) to the natively zinc binding MT SmtA from the cyanobacterium *Synechococcus elongatus* PCC7942. This protein was chosen because of its ready availability and the presence of detailed structural data for the zinc form (Blindauer et al. 2001, Blindauer et al. 2002, Blindauer et al. 2003). SmtA has been previously shown to bind four zinc ions in a $Zn_4Cys_9His_2$ cluster, with a zinc finger fold adopted by residues 6—38 (Blindauer et al. 2001). In M_4SmtA, divalent metals (Zn(II)/Cd(II)) are tetrahedrally coordinated with thiolates and imidazole sidechains in a $M_4Cys_9His_2$ metal cluster. Crucially, this tetrahedral geometry must be disrupted to accommodate the incoming, trigonally/digonally-directing Cu(I). Metallation with Cu(I) is expected to involve significant change in folding as the cysteinyl residues need to be re-oriented to provide a different (trigonal/digonal) environment.

Several studies revealed the Cu(I) stoichiometries in the two domains of mammalian zinc binding MTs (Dolderer et al. 2007, Chen et al. 1996), but there are no data available on Cu(I) binding to any of the members of the BmtA family, which are known Zn(II)/Cd(II)-binding MTs (Blindauer 2011) despite the fact that bacterial cells might experience stress from redox active but essential metals like Cu(I) from their environment. It is hence not clear how BmtAs behave with respect to other metals such as Cu(I). In the present research, experiments have been carried out to explore Cu(I) binding to SmtA from *Synechococcus* sp. PCC7942 mainly by determining the point of complete displacement of zinc ions from Zn_4SmtA upon metal exchange reactions.

Previous studies of metal exchange reactions of Zn_4SmtA have shown that titration of Cd(II) only leads to partial displacement of Zn(II), and that the Cys_4Zn zinc finger site A in folded SmtA is inert towards M(II) exchange (Figure 4.1). This specific site A is critical, keeping the metal cluster and zinc finger fold together (Blindauer et al. 2003, Blindauer 2008).

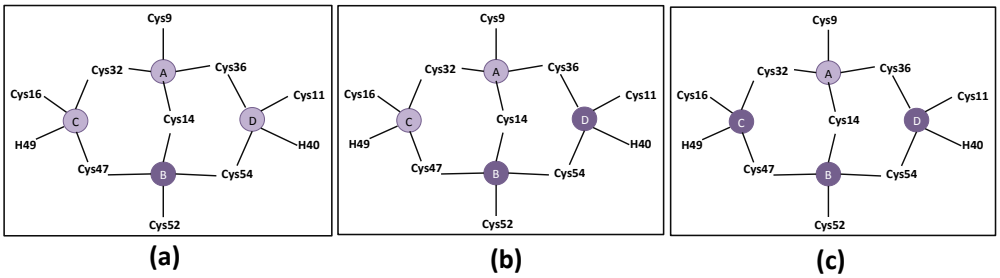

Figure 4.1 Specificity of metal clusters in Zn_4SmtA for Cd(II).

The progress of substitution reaction by Cd(II) in Zn_4SmtA with Site B (a) first to be populated, following Site D (b) and (c) Site C last to be occupied whilst site A remains inert.

The incorporation of Cd(II) in site A was attained, but only through reconstitution of apo-SmtA which generated fully exchanged Cd_4SmtA (Blindauer et al. 2001). Despite all the knowledge about the inertness of site A in Zn_4SmtA during Cd(II) titrations it is not clear how this inert site behaves in the presence of high affinity and biologically relevant Cu(I) ions. Furthermore, mixed-metal metallothioneins are found to be more dominant *in vivo* with metal composition depending on various physiological factors (Li and Otvos 1996). There is not much information about formation mechanism of these species and the effects on the chemical properties of one metal by the binding of another metal to the same protein. In the mammalian MTs, the formation of mixed metal species has been suggested as a product of an intermolecular metal exchange reaction between Zn_7MT and Cd_7MT (Nettesheim et al. 1985, Li and Otvos 1996). However, upon Cu(I) addition to mammalian MT, it showed the ability to rapidly displace both divalent ions from their native binding sites, resulting in protein structural disruption (Li and Otvos 1996).

As the structure and cluster specificity is well established for Zn_4SmtA, it was of interest to shed some light upon its reactivity towards Cu(I), and on the effect that Cu(I) incorporation has on protein structure and dynamics. In this chapter the characterization and metal binding ability of Zn_4SmtA, the starting material for all subsequent studies, are briefly discussed. Subsequently, UV-vis spectrophotometry, ESI-MS and NMR spectroscopy (chapter 5) have been used for the determination of metal:protein stoichiometries of

mixed species and effect of Cu(I) binding on protein folding. However, studying Cu(I) binding to a protein is a particular challenge due to the oxygen sensitivity of Cu(I) as the formation of Cu(II) in the presence of oxygen may lead to oxidation of MT. Therefore, all experimental procedures had to be carried out under strict anaerobic conditions, and new protocols for sample preparations had to be developed (as described in Chapter 3). These conditions were implemented in all experiments carried out in this research.

4.1.1 Spectrophotometric titration of Zn_4SmtA with $[Cu(I)(CH_3CN)_4]PF_6$

Spectrophotometric observations provide a very sensitive probe for the metal-thiolate clusters that form when metals such as Cu(I) are added to a metallothionein (Stillman et al. 1994, Presta and Stillman 1994). Owing to their filled d shells, the hydrated metal ions Cd(II), Zn(II) and Cu(I) exhibit no optical transitions within the UV-vis wavelength range, but the presence of the thiolate ligand results in ligand to metal charge transfer (LMCT) transitions. These LMCT transitions lie in the region between 230 nm and 400 nm. When metals bind either directly to the metal-free (=apo) MT or when an added metal displaces an existing metal, for example when Cu(I) is added to Zn-MT, the new metal-thiolate cluster structures that form lead to changes in absorbance (Stillman et al. 1994).

The spectrophotometric titrations were carried out to study the exchange of Zn(II) with Cu(I) in the folded protein (Zn_4SmtA). For this purpose, samples of bacterial Zn_4SmtA were titrated with Cu(I) under anaerobic conditions. To study the binding capacity of Zn_4SmtA with Cu(I) ions, the metal-protein complexes formed with different molar equivalents of Cu(I) were observed by UV-vis spectroscopy (Figure 4.2). UV-Vis spectra of the reaction mixture were recorded after each addition of Cu(I) to follow the progress of the reaction.

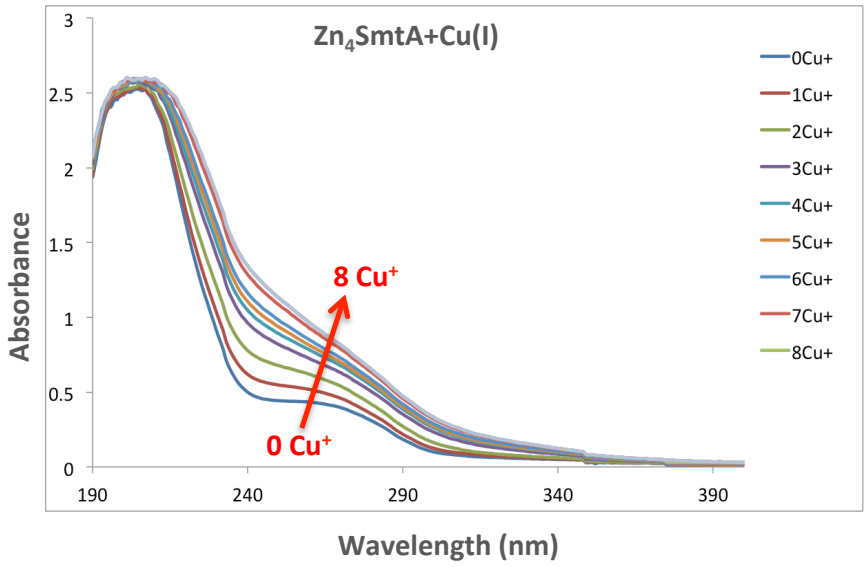

Figure 4.2 UV-Vis absorption spectra of Zn_4SmtA as a function of increasing Cu(I) equivalents.

Full scan of UV-Vis spectra of molar equivalent addition of Cu(I) to Zn_4SmtA at 25°C in 25 mM Tris-Cl, pH 7. Samples were prepared anaerobically under N_2.

With the addition of Cu(I), an increase in absorbance was observed above 250 nm, with a very prominent band observed at about 270 nm. This band is the S-Cu(I) LMCT band and reflects the number of thiolates involved in Cu(I) binding (Presta and Stillman 1994, Chen et al. 1996). The absorbance at 270 nm in dependence on equivalents Cu(I) added is shown in Figure 4.3. The intensity of the 270 nm shoulder increases more or less linearly with increasing Cu(I) equivalents (up to seven Cu(I) equivalents). Further incremental addition of Cu(I) led to no further changes.

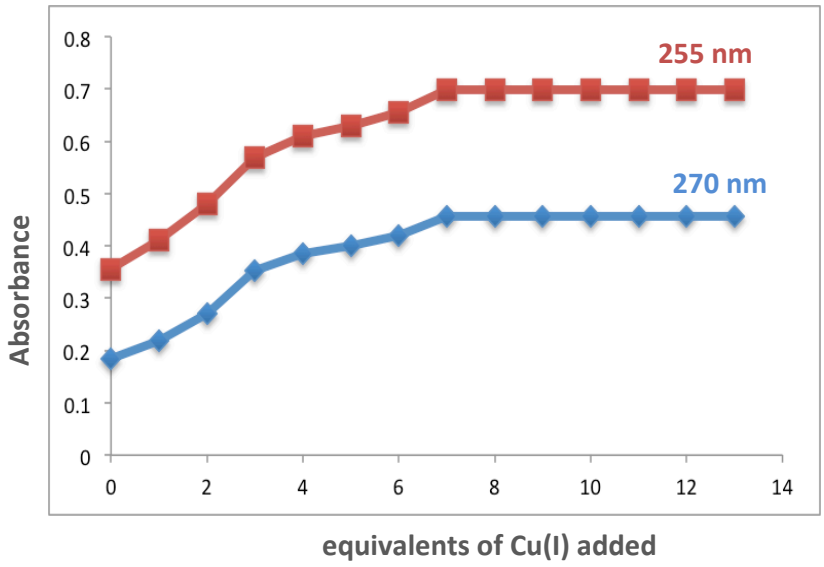

Figure 4.3 Plot of absorbance against molar equivalent of Cu(I) added.

Plot of absorbance at 255 nm and 270 nm against molar equivalent of Cu(I) added to Zn_4SmtA

The progressive increase in absorbance from 1 to 7 Cu(I) added per mol of MT shown in Figure 4.3 indicated that Cu(I) continued to form interactions with the MT until a 7:1 ratio was reached. This may suggest that up to seven equivalents of Cu(I) can be bound to SmtA, compared to up to four divalent metal ions. This increase in metal:protein stoichiometry is expected, due to the different coordination geometries i.e., tetrahedral for M(II) and linear or trigonal for Cu(I) respectively. This is also reflected in the stoichiometries for other MTs, e.g. Cu_8- and Cu_6 (metal clusters) are found for yeast and mammalian MTs (Ding et al. 1994, Pountney et al. 1994, Calderone et al. 2005).

Cu_7SmtA was the major species observed after reconstitution of apo-SmtA with copper (Chapter 3). The fact that the UV-Vis titration also is completed at 7 equivalents of Cu(I) may suggest that Zn(II) has been quantitatively displaced by Cu(I). However, the UV-Vis data do not inform about whether or not any Zn(II) has remained bound, therefore, further analyses will be necessary to confirm complete loss of Zn(II). Also, it is not possible to determine which species with which stoichiometries are present in solution at a given titration point after addition of each equivalent of Cu(I) because of the very limited

resolution of UV-vis spectroscopy. In this regard, ESI-MS is one of the most important and successfully employed techniques to characterize the composition of metallothioneins and was used to attempt answers to the above questions.

4.2 Electrospray ionization Mass spectrometry (ESI-MS) to study metallothioneins

ESI-MS is a soft ionization technique, which allows quantitative detection of various complexes in the same sample including both minor and major species. It has thus become an important method for the direct observation of individual and partially metallated species of metallothioneins under varied conditions or during metal uptake, metal exchange or metal release and transfer reactions (Leszczyszyn and Blindauer 2010). In this technique, large charged molecules are brought to the gas phase without breaking covalent bonds or even non-covalent interactions such as metal-ligand coordinative bonds under suitable experimental conditions. In addition, ESI-MS allows the production of multiply charged ions permitting the observation of higher masses at lower m/z (mass to charge ratio of ions in gas phase) values (Chan et al 2002, Blindauer and Leszczyszyn 2010), which is less demanding in terms of instrumentation. The most distinguished features of ESI-MS include; 1) the atmospheric pressure ionization system that produces a series of multiply charged ions (both negative or positive ions). 2) transfer of analytes from solution into the gas phase, giving the option to connect with separation techniques such as liquid chromatography (LC-MS) and capillary electrophoresis (CE-MS) and making it ideal to study biological molecules. 3) a soft ionization process, which means that it introduces positive or negative charges to intact molecules, instead of inducing fragmentation of the analyte molecule. This may permit to preserve non-covalent interactions between molecules in solution and is important in maintaining the structure of metal binding domains inside the spectrometer (Chan et. al 2002).

In principle, it is also possible to examine metallothioneins by Matrix-Assisted-Laser Desorption Ionization Mass Spectrometry (MALDI-MS). However, the sample preparation methods involving the use of acidic matrices, and organic solvents in most cases, result in predominantly denatured apo-MTs with partially metallated species only present in negligible amounts. Therefore, with the advantage of one easily modified MS technique to study proteins under near-native conditions, most MS investigations of metallothioneins heavily rely upon the use of ESI-MS (Ngu and Stillman 2009, Blindauer and Leszczyszyn 2010), most frequently at around neutral pH to preserve metal-ligand bonds. Nevertheless, careful experimental design is critical for ESI-MS of metalloproteins because the gaseous environment experienced by metal-protein complexes after electrospray ionization may affect the non-covalent interactions and consequently protein structure. Furthermore, a fundamental idea behind the success of native ESI-MS of metalloproteins is the fact that the species observed in the gas phase are related to speciation and structure in solution (Breuker and McLafferty 2008). Initially, electrostatic interactions are enhanced in the gas phase whereas hydrophobic interactions are weakened. ESI-MS is well suited for metal ligand analysis, because the stability constants of metal-MT complexes are high, with large electrostatic contributions to metal-ligand bonds, which in turn govern the structure and folding stability of MTs. Also, ESI-MS is particularly ideal to study d^{10} metal ions complexes such as those with Zn(II) and Cu(I), as it is independent of any spectroscopic features (Blindauer and Leszczyszyn 2010).

The disadvantages of ESI-MS include limitations of quantitative kinetics, no information on ionization efficiencies for the different species in solution, inability to monitor fast reactions directly and only detecting the end points at equilibrium.

4.2.1 Sample preparation for Electrospray ionization Mass spectrometry (ESI-MS)

Sample preparation and conditions including instrumental conditions are the most important parameters that dominate the results of an ESI-MS experiment. In the case of metal-protein complexes, one of the crucial factors is the pH of the sample solution. For example the pH of the solution for the holo protein must be maintained in the neutral range, to avoid demetallation by competition with protons. In addition, any non-volatile compounds (i.e. salts, detergents and most buffers) must be avoided in the sample solution. This may be done by chromatographic methods (mostly gel filtration, PD–10 desalting columns) or dialysis whilst making sure that the bound metals are still present. However, it is also possible to observe non-specific adducts when the holo protein is prepared by reconstitution with an excess of metal ions without removing any excess adducts in sample, so sample clean up is essential. Also, the use of an organic modifier, such as methanol, can facilitate ionization but it should be only added in small amounts (<10%) to avoid protein denaturation, which can also lead to loss of metal (Blindauer and Leszczyszyn 2010). However, the analyses of metal binding features of MT are rather complex and require careful consideration when preparing and analyzing MT samples for replacement studies. For instance (a) use of higher concentrations of buffer used in protein solution because of lowering pH of the protein solution due to metal addition and (b) presence of several M_x-MT aggregates in the solution. Figure 4.4 shows typical ESI-Mass spectra for holo and apo-SmtA.

The charge states are associated with the surface area of the protein and the number of available basic sites (Sutherland et al. 2012). The observed charge states under different conditions may be correlated to protein conformation/folding. Higher charge states are observed for unfolded proteins because unfolding allows the basic sites to become more accessible to protons and in turn fewer charge states result from folded proteins, which can only accept fewer charges (Chowdhury and Chait 1990, Chowdhury et al. 1990). In the mass

spectrum of Zn_4SmtA using native conditions, two peaks were observed corresponding to the charge states +4 and +5 (Figure 4.4 A). At the lower pH of 2, higher charge states were observed for apo-SmtA, from +4 through +8 because of protein unfolding (Figure 4.4 C) with the experimental mass of 5608.4 Da which is in close agreement with the theoretical mass of 5610.3 Da for the neutral mass of apo-SmtA.

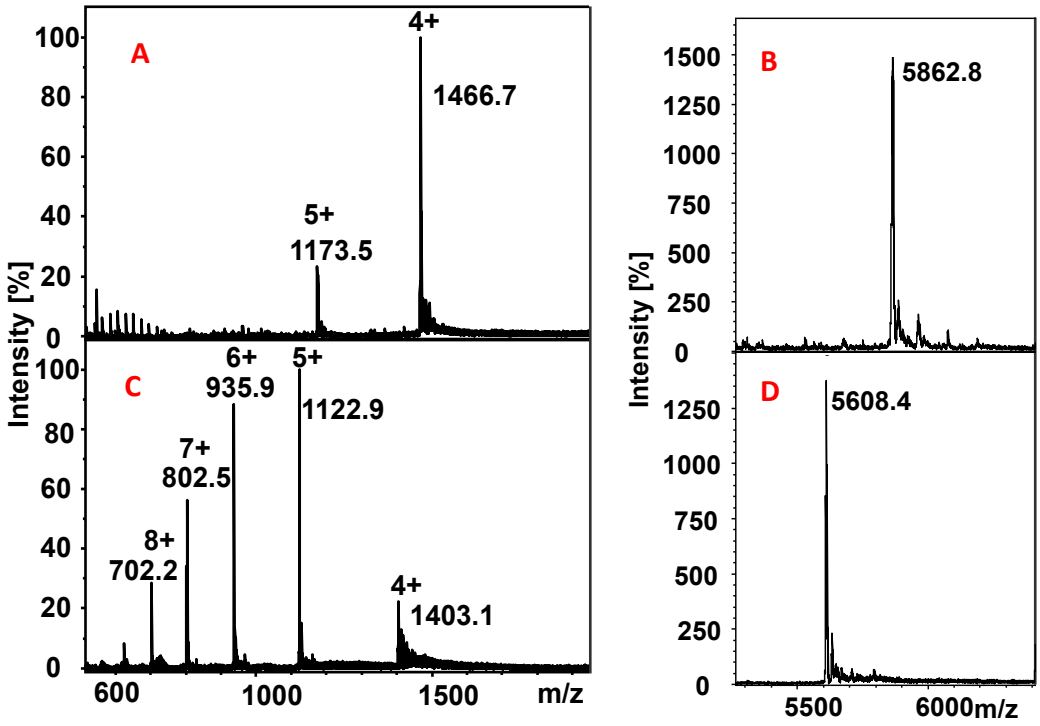

Figure 4.4 ESI-MS of holo and apo SmtA.

Mass spectra of holo Zn_4SmtA (A) and apo-SmtA (C) along with deconvoluted mass spectra of holo Zn_4SmtA (B) and apo-SmtA (D). Sample conditions: 25 µM of fully metallated pure Zn_4SmtA (pH= 7.0) and apo SmtA (pH 2) in 10 mM ammonium hydrogen carbonate.

The theoretical neutral masses of apo SmtA and Zn_4SmtA are 5610.3 Da and 5863.8 Da (5610.3 + 4*65.4 - 8), respectively. The experimental mass for the neutral Zn_4SmtA species is 5862.6 Da, which corresponds reasonably well to the theoretical mass, albeit somewhat lower than expected, and deviating by 1.2 Da. The deviations are likely due to inaccurate calibration of the TOF mass spectrometer, although partial oxidation of the apo-protein during the electrospray process is also a possible cause.

ICP-OES analysis (inductively coupled plasma-optical emission spectroscopy) was used to determine both the protein and bound metal ion concentrations. For Zn_4SmtA, the zinc-protein ratio was 4.2 ± 1.0, which is in agreement with the mass spectral analysis of Zn_4SmtA.

4.2.2 Cu(I) binding ability of Zn_4SmtA: An ESI-MS titration study

The Zn/Cu replacement reaction was studied in detail with ESI-MS with the hope that this would shed light on the behavior of the zinc-specific bacterial MT Zn_4SmtA. Figure 4.5 shows the sequence of mass spectra recorded as Cu(I) was added in microliter aliquots to provide single molar equivalent increases in Cu(I) to Zn_4SmtA at pH 6.9.

The stepwise addition of Cu(I) to Zn_4SmtA resulted in mixtures of Zn_xCu_ySmtA species of gradually increasing complexity. At one equivalent of Cu(I), both Zn_4SmtA and Cu_xZn_ySmtA (M_5) species co-exist as fully metallated species in the solution while at two equivalents, M_5 species are overwhelmingly dominant. Since the mass differences pertaining to [Cu(I) $-H^+$] and [Zn(II) $-2H^+$] are very close (62.5 vs. 63.4 Da), it is not straightforward to distinguish the composition of metal clusters, so the identity of x and y would only be resolvable with high-resolution mass spectrometry. M_6 species of heterometallic Cu_xZn_ySmtA appeared after addition of the third equivalent of Cu(I). After addition of the fourth equivalent of Cu(I), M_7 became the main species, and remained the major species at higher Cu(I) ratios. With the addition of more Cu(I), the presence of an M_8 and an M_9 species was observed, with disappearance of M_6.

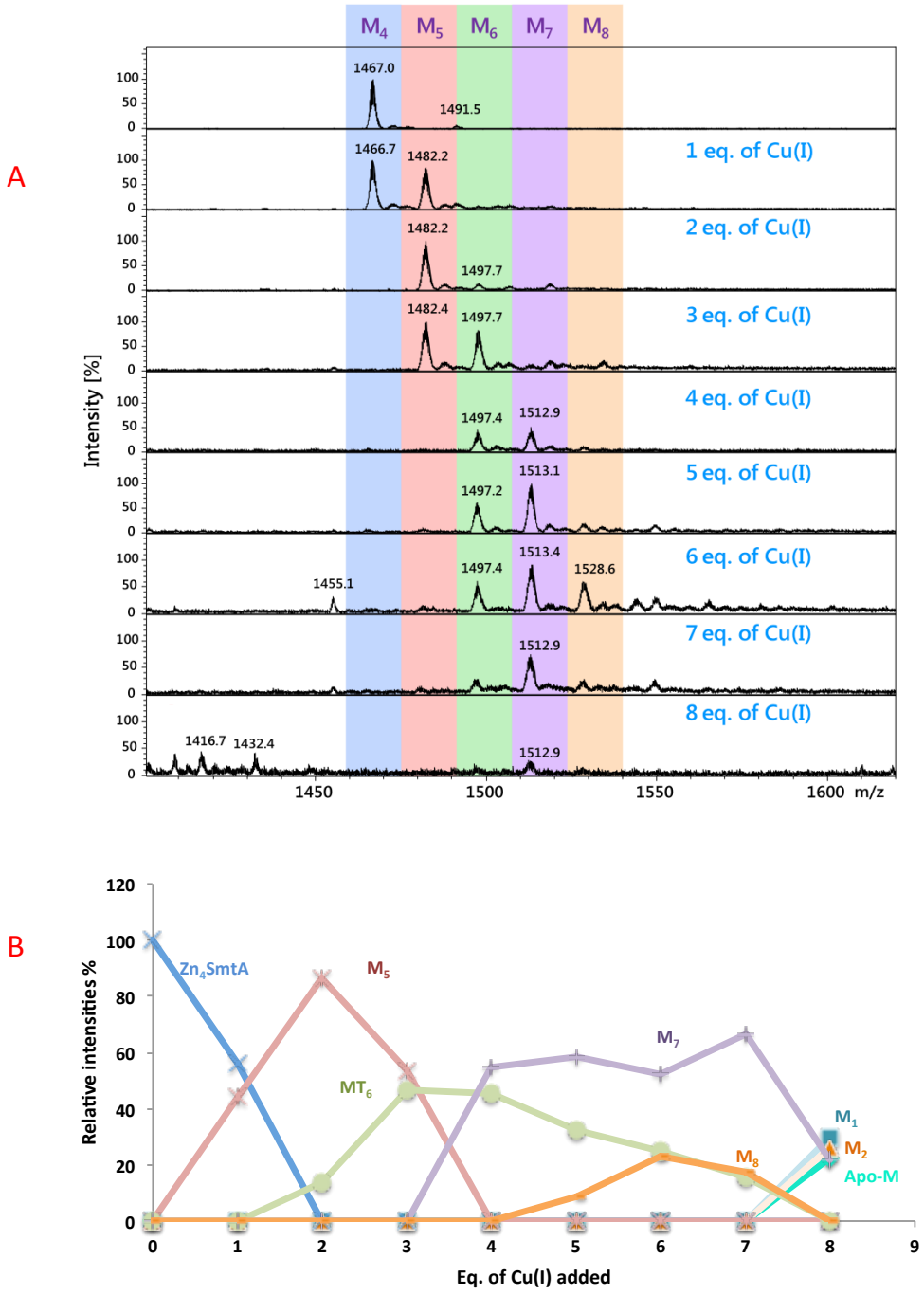

Figure 4.5 Cu(I) metallation and speciation of Zn_4SmtA.

(A) ESI mass spectra for titration of Zn_4SmtA (25 μM solution in 10 mM ammonium bicarbonate buffer with 10% methanol at pH 6.9) with Cu(I). Only the +4 charge state is shown. Aliquots of Cu(I) were added to the protein as 1, 2, 3, 4, 5, 6, 7 and 8 equivalents. The colored blocks show the formation of new species with the addition of Cu(I). (B) Summary of stepwise Cu(I) addition and speciation of Zn_4SmtA. Each line corresponds to formation of a different species: Zn_4SmtA (blue), M_5 (red), M_6 (green), M_7 (purple), M_8 (orange). The experimental and theoretical masses of the resulting species are given in appendix A1.

At 8 equivalents, the spectral quality deteriorated significantly, and only M_7, with a very low signal:noise ratio was observed. However, inspection of the lower m/z range revealed the presence of under-metallated and oxidized species (Figure 4.6).

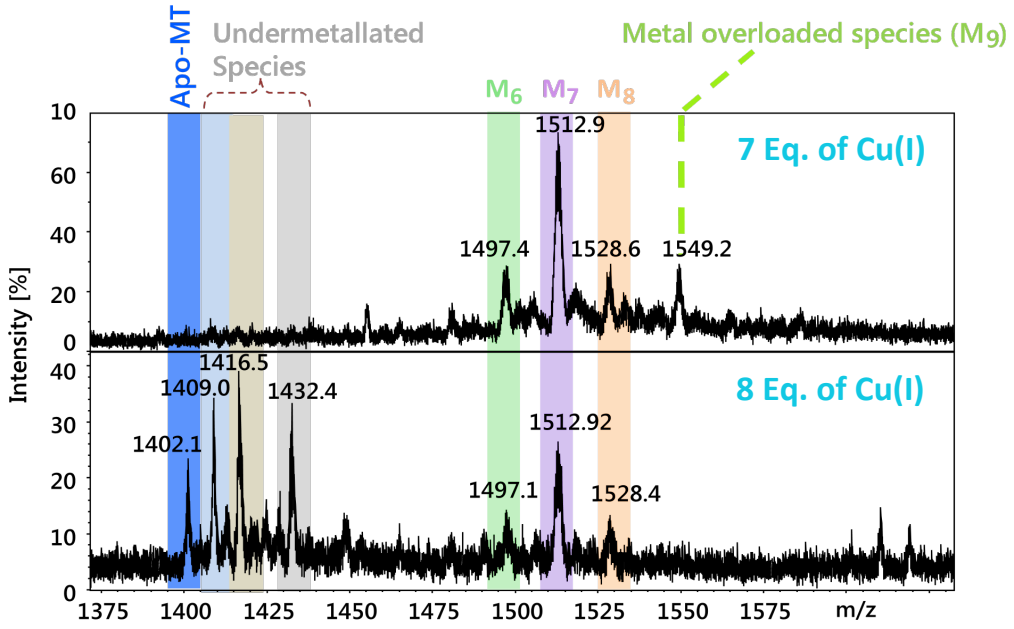

Figure 4.6 ESI mass spectra of Zn-MT containing 7 and 8 eq. of Cu(I).

ESI mass spectra after addition of seven and eight equivalents of Cu(I) to Zn_4SmtA (25 µM solution in 10 mM ammonium bicarbonate buffer with 10% methanol at pH 6.9) showing the presence of most stable M_7 species and under-metallated species including apo-MT.

The species observed at 1409.0 may correspond to an oxidized apo-SmtA with a mass of 5632.4 Da with the loss of one hydrogen and addition of 2 oxygen atoms. It is also possible that these species are resulting from the over metallated Cu_8 and Cu_9 species. The latter are likely the result of weak binding of one Cu(I) ions to one cysteine thiolate, and it is possible that these highly nucleated species may not support the ESI-MS ionization conditions well, leading to the generation of under-metallated and oxidized species. In addition, the possibility of oxidation of this particular sample during the course of the titration cannot be excluded

resulting in degraded protein and highlighting the importance of strict anaerobic conditions in Cu(I) involving experiments.

Since the composition of the resulting heterometallic Cu_xZn_y-SmtA species was not straightforward to resolve, the isotopic distribution for the M_5, M_6 and M_7 species were compared to possible theoretical models (Figure 4.7). Considering their formation at Cu:Zn_4SmtA ratios as low as 1:1, two possible combinations for metal:metal stoichiometries within a M_5 metal cluster, i.e. Cu_2Zn_3- or Cu_3Zn_2-SmtA, may be considered. Similarly, considering their occurrence at higher Cu:Zn_4SmtA ratios, for M_7 the most likely stoichiometries are either purely Cu(I) loaded Cu_7SmtA or Zn_1Cu_6-SmtA. In the previous chapter, it was shown that SmtA, when reconstituted with Cu(I), formed Cu_7SmtA as a major species, but the Zn_1Cu_6-SmtA species cannot be excluded in the present experiments. This is related to the inert site A containing the last Zn(II) and holding the structure (with zinc finger fold and metal cluster) together since, in fully loaded $M(II)_4$SmtA clusters, it is not easily accessible for the incoming metal ions (Blindauer et al. 2003).

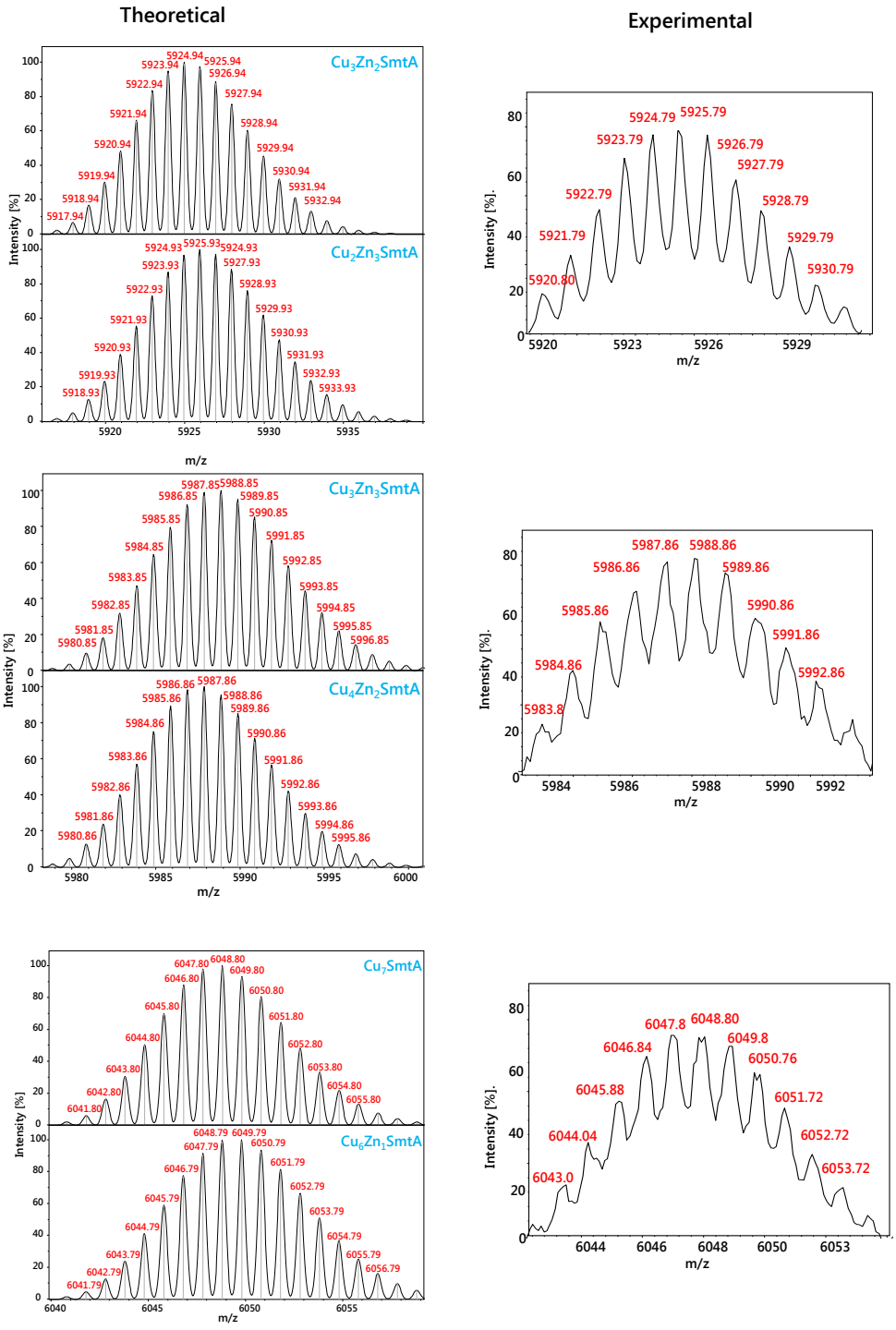

Figure 4.7 Theoretical and experimental isotopic distribution of Cu,Zn-SmtA species.

Isotopic distribution for A) M_5SmtA (after 2 eq.) together with the comparison to the theoretical models for Cu_3Zn_2SmtA ($C_{225}H_{349}N_{70}O_{80}S_9Cu_3Zn_2$), Cu_2Zn_3SmtA ($C_{225}H_{348}N_{70}O_{80}S_9Cu_2Zn_3$). B) M_6SmtA (after 3 eq.) with the comparison to the theoretical model for Cu_3Zn_3SmtA ($C_{225}H_{347}N_{70}O_{80}S_9Cu_3Zn_3$), Cu_2Zn_4SmtA ($C_{225}H_{350}N_{70}O_{80}S_9Cu_2Zn_4$), C) M_7SmtA (after 7 eq.) with the comparison to the theoretical models for Cu_7SmtA ($C_{225}H_{349}N_{70}O_{80}S_9Cu_7$) and Cu_6Zn_1SmtA($C_{225}H_{348}N_{70}O_{80}S_9Cu_6Zn_1$).

Although the isotopic envelopes for Cu_3Zn_2SmtA and Cu_2Zn_3SmtA are very similar (as shown in Figure 4.7), the isotopic distribution of M_5 species suggested that the most probable species is Cu_2Zn_3SmtA because the mass pattern observed in experimental isotopic distribution is closer to the theoretical model of Cu_2Zn_3-SmtA. Similarly, for the M_7 species, the experimental mass is closer to the isotopic distribution model of Cu_7SmtA than to that for Cu_6Zn_1SmtA. A caveat to be considered is the fact that the mass for the original Zn_4SmtA had also been lower (by 1.2Da) than expected (Figure 4.4).

The results presented here can be compared with mammalian rabbit MT1 from which is one of the zinc binding MT studied in detail for its binding ability towards monovalent metals such as Cu(I) or Ag(I). Addition of Cu(I) to Zn-mMT1 yielded heteronuclear Zn-Cu complexes, for example, after addition of sub-stoichiometric Cu(I), Cu_7Zn_3-mMT1 for the full length mMT1 and Zn_1Cu_4-αmMT1 in the α domain and homonuclear $Cu_{6\text{-}7}$-βmMT1 in the β domain form were observed, which agrees with the Cu-thionein character of mammalian β domains. However, in mammalian MT2, unfolded apo protein was also observed when Cu(I) was added gradually (Artells et al. 2013).

4.2.2.1 Cd(II) as a probe for Zn(II) to aid analyses

SmtA has been previously shown to bind Cd(II) in the same manner as Zn(II). Zn(II) exchange reactions of SmtA with Cd(II) revealed the importance and inertness of site A leading to inaccessibility of Cd(II) to replace the last remaining Zn(II) (Blindauer et al 2008). Cd(II) and Zn(II) exchange reactions have been studied in detail in the past by Blindauer et al., but the reactivity of Cd_4SmtA towards Cu(I) is unknown. Furthermore, the heterometallic species observed for Cu/Cd exchange reactions may help to better understand the Cu/Zn exchange reactions, as the observed stoichiometries are likely to be similar, but the mass differences are much more clearcut (+Cd–2H = 110.4 Da; +Cu–H = 62.5 Da) than for Zn/Cu. In particular, it should be possible to probe whether site A is inert in exchange reactions with Cu(I). In this

respect, Cd(II) reconstituted SmtA (Cd_4SmtA) was titrated with eq. molar amounts of Cu(I) to explore the stoichiometries of metal clusters in Cd(II)/Cu(I) exchange reactions. Cd_4SmtA was prepared by reconstitution of apo-SmtA with Cd(II) ions. ESI-MS of Cd-reconstituted SmtA (M_w= 6051.6 Da; neutral mass) showed that the most abundant peak at 6052.04 Da (neutral mass) corresponded to Cd_4SmtA (Figure 4.8 top; only the +4 charge state is shown), confirming that the reconstitution had generated a fully exchanged protein (Blindauer et al 2001, Blindauer et al 2008). Figure 4.8 displays the +4 charge state for the series of mass spectra acquired during Cu(I) addition to Cd_4SmtA.

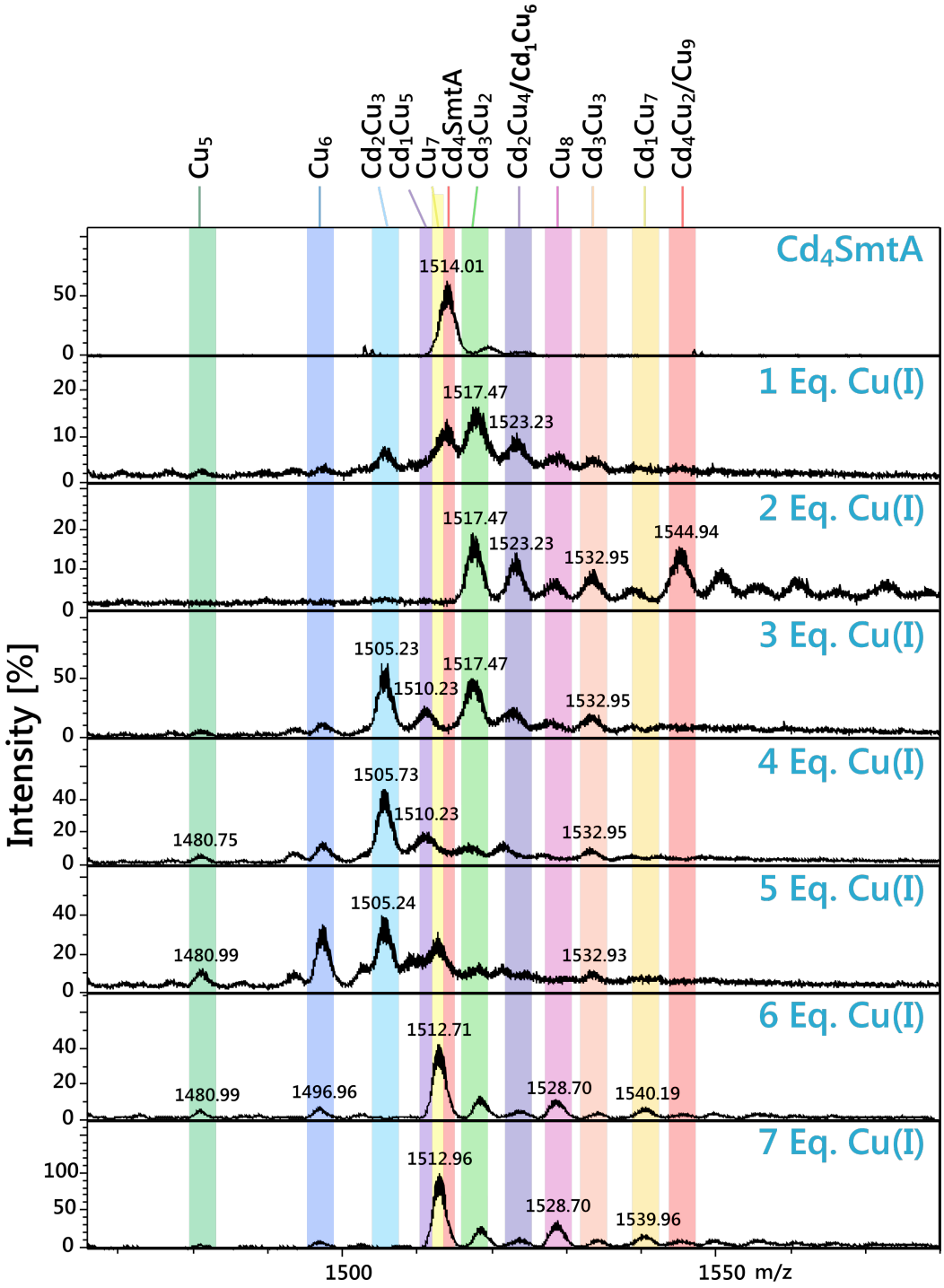

Figure 4.8 Cu(I) titration of Cd_4SmtA.

ESI mass spectra for titration of Cd_4SmtA (25 μM solution in 10 mM ammonium bicarbonate buffer with 10% methanol at pH 6.9) with Cu(I). Only the +4 charge state is shown. Aliquots of Cu(I) were added to the protein as 1, 2, 3, 4, 5, 6 and 7 equivalents. The colored blocks follow the metal binding and showing the formation of new species with the addition of Cu(I). The experimental and theoretical m/z values are given in Appendix A2.

Addition of the first equivalent of Cu(I) produced a mixture of heterometallic species i.e., M_5 [Cd_2Cu_3, Cd_3Cu_2, Cu_5] and M_6 [Cd_3Cu_3, Cd_2Cu_4, Cu_6] with a slight indication of M_8 (Cu_8), although the spectrum is quite noisy. This is intriguing because addition of one equivalent of Cu(I) to Zn_4SmtA resulted in M_5 species only, with an about equal amount of Zn_4SmtA remaining. Cd_4SmtA is also still present along with these mixed metal species, but crucially Cd_3Cu_2 is the most abundant species. Like Zn_4SmtA, Cd_4SmtA has fully disappeared after the addition of two equivalents of Cu(I), and M_6 species (Cd_3Cu_3, Cd_2Cu_4), along with the most prominent M_5 species (Cd_3Cu_2 and Cd_2Cu_3), are observed. A new metal loaded species was observed with the *m/z* of 1544.94 for +4 and 6175.76 for the neutral mass. There may be two possibilities for this fully loaded species i.e., either Cd_4Cu_2 or Cu_9 (with masses of 6176.6 and 6172.5, respectively). Cd_4Cu_2 is closer to the experimental mass for this specific species, and this mass peak was only observed in significant amounts at this relatively low Cu:Cd_4SmtA ratio of 2:1, therefore, this composition is more likely. On addition of the third equivalent of Cu(I), the spectrum is still dominated by M_5 species (Cd_3Cu_2 and Cd_2Cu_3), along with minor amounts of M_6 species (Cd_3Cu_3, Cd_2Cu_4 and the newly formed Cd_1Cu_5 species). Although present in lower amounts, the Cd_1Cu_5 species was still observed until the fifth Cu(I) equivalent was added. The Cu_6 species was also prominent at 5 eq.

After addition of the fifth equivalent, the Cu_7 species emerged and then remained the most abundant species until the final equivalent of Cu(I) was added. However, the Cd_3Cu_2 species was also still detectable. Further species present at 6 and 7 eq. included M_8 (Cd_1Cu_7, Cu_8) species. Beyond seven Cu(I) equivalents, complex mixtures of heavily loaded MT were observed which disappeared with addition of up to nine Cu(I) equivalents. The only species observed after addition of 9 eq. were degradation products as shown in Figure 4.9. The isotopic distributions clearly indicate that these are +1 species.

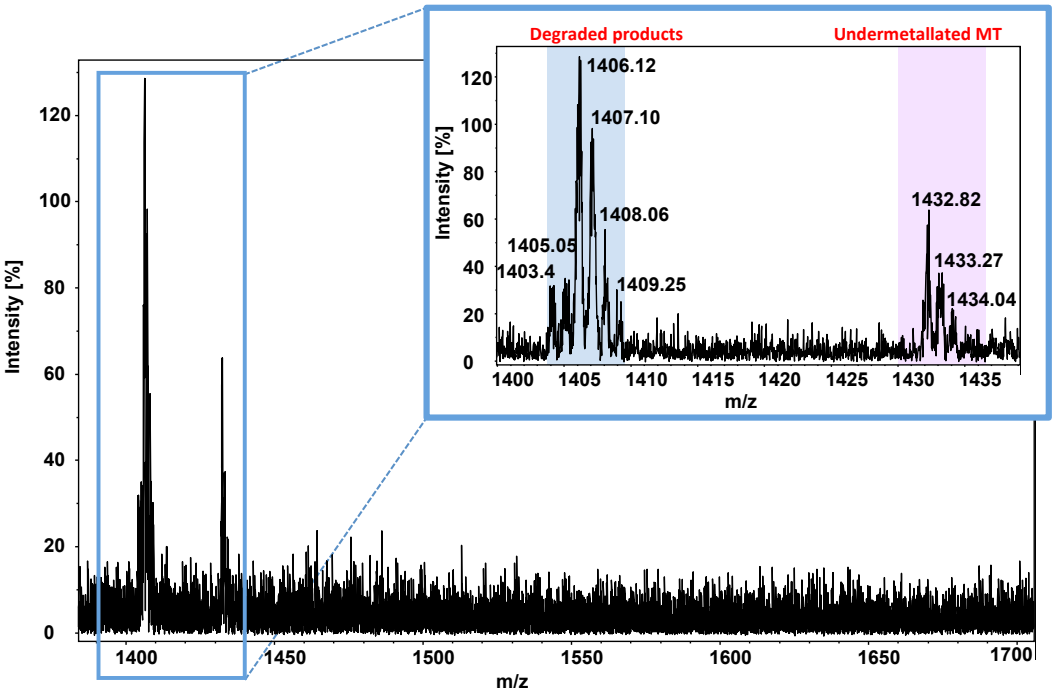

Figure 4.9 ESI mass spectrum of Cd-MT after addition of 9 eq. of Cu(I).

ESI mass spectrum after addition of nine equivalents of Cu(I) to Cd_4SmtA (25 µM solution in 10 mM ammonium bicarbonate buffer with 10% methanol at pH 6.9). Inset contains the enlarged boxed region displaying the degraded products after addition of 9 eq. of Cu(I).

It is significant to note that Cd_2Cu_3 was the most abundant species over the range of 3—5 equivalents. Concomitantly, the under-metallated species Cu_5 was present at 4-6 equivalents along with various M_6 species (Cu_6, Cd_3Cu_3). Remarkably, the Cd_3Cu_2 species was also still present at 7 eq., coexisting with the Cu_7 and Cu_8 species. In contrast, only relatively small quantities of any Cd_1 species were observed at any titration point: Cd_1Cu_5 at 3 and 4 equivalents, and Cd_1Cu_6 and Cd_1Cu_7 at 6 and 7 equivalents. In summary, the early emergence of the Cu_7 species argues against intertness, but the persistence of the Cd_3Cu_2 species at 7 equivalents of Cu(I) may indicate particular stability of this species.

Taking the results from the Cu(I) titrations of Zn_4SmtA and Cd_4SmtA together suggests that the observed M_5 species in the Zn/Cu titration may correspond to Cu_5, Zn_3Cu_2, and Zn_2Cu_3, whilst the M_6 species may include Zn_3Cu_3, Zn_2Cu_4, Zn_1Cu_5 and Cu_6, depending on the number of equivalents added. Both titrations yielded Cu_7 as the most abundant species at about

stoichiometric ratio, clearly indicating that the inertness of site A is not maintained in mixed M(II),Cu(I) clusters. In addition, it appears that compared to Zn(II), Cd(II) competes efficiently with Cu(I) ions at somewhat higher Cu(I) ratios, likely owing to its higher relative affinity to thiolates.

Since in both cases the end product was oxidized and/or degraded protein, which may be because of redox active property of Cu(I) and possibly prolonged exposure to air, it was of interest to use another non-redox active monovalent metal ion instead of Cu(I). Since Ag(I) has been previously used to provide information on Cu(I) binding to MT, including the use of Ag(I) as an NMR active analogue of Cu(I) in structural studies (Pountney et al. 1994, Li and Weser 1992, Li and Otvos 1996, Bofill et al. 1999), it was used in the metal exchange reactions for Zn_4SmtA. Since Ag(I) has higher difference of molecular mass compared to Cu(I) and Zn(II), it may be used to identify the composition of the metal clusters in Zn_4SmtA after Ag(I) addition, and also help to further rationalize the Cu/Zn titration results.

4.2.3 Characterization of Cu(I) metal clusters: Ag(I) a probe of Cu(I)?

The binding features of Ag(I) to MTs have attracted attention for structural studies of Cu-MTs because of the unsuitability of ^{63}Cu and ^{65}Cu isotopes for NMR studies. Cup1 from *S. cerevisae* is the only reported structure of Cu-MT with an Ag-substituted derivative. The NMR structures of both copper- and silver-substituted Cup1 were relatively similar with a high degree of conservation of structural elements in both MTs, containing the polypeptide backbone around a single seven-metal cluster. In addition, the metal-to-Cys stoichiometries resulting for Ag(I) substituted MT was similar to its Cu(I) substituted form (Narula et al. 1991, Peterson et al. 1996, Bertini et al. 2000). Calderone et al later revealed the full X-ray structure of Cu(I)-reconstituted Cup1 containing eight Cu(I) in its Cu_8- metal cluster (Calderone et al. 2005) instead of Cu_7 reported previously (Bertini et al. 2000).

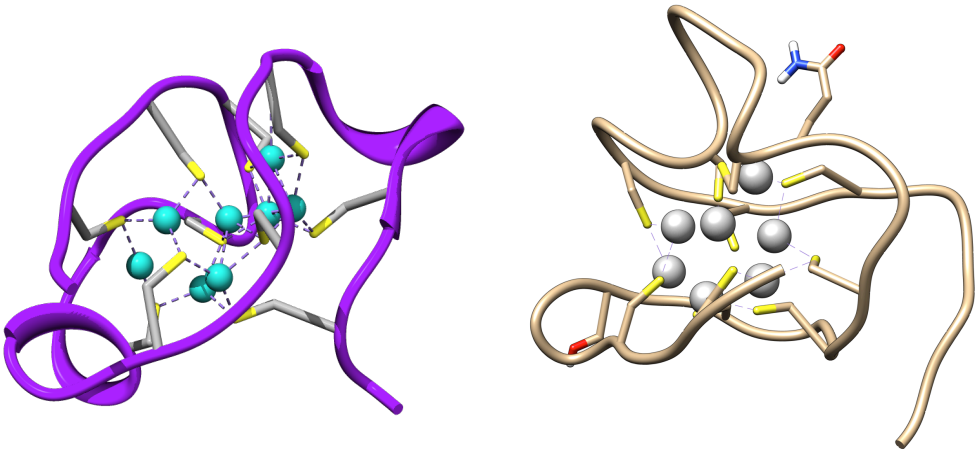

Figure 4.10 Metal cluster s for the copper binding MT Cup1 from *Saccharomyces cerevisiae*.

Cu_8Cup1 metal cluster (PDB 1rju; Calderone et al. 2005) for copper MT from *Saccharomyces cerevisiae* and the Ag_7Cup1 structure based on NMR analysis (PDB,1AQQ, Peterson et al 1996)

Nevertheless, the binding abilities of Ag(I) to mammalian MT–1 have also been studied previously with the aim of analyzing the suitability of Ag(I) as a Cu(I) probe in Cu-MT studies (Palacios et al. 2003, Bofill et al. 2001). In addition, Ag(I) has also been used for stepwise incorporation of Ag(I) into apo-MTs and mammalian zinc containing MTs, forming Zn-Ag-MT mixed metal species (Palacios et al. 2003). It is also noteworthy that Ag(I) has a higher tendency for linear coordination, i.e. two ligands, compared to Cu(I) where trigonal planar is more frequent. Overall, Ag(I) has been shown to interact in a similar but not necessarily identical manner to Cu(I) in MT metal clusters. In the present study, Ag(I) was directly titrated into Zn_4SmtA and the resulting products were analyzed by Electrospray Ionization Mass Spectrometry.

The studies of Cu(I) binding abilities of Zn_4SmtA provided insufficient information about the metal cluster composition. In this regard, Ag(I) was used with the ultimate aim of identifying the composition and stoichiometries of metal ions within bacterial SmtA metal cluster during

metal ions titrations, considering Ag(I) as a probe of Cu(I) binding and to facilitate data interpretation - in analogy to the previous section in which Cd(II) was used as a probe for Zn(II). Figure 4.11 shows the series of ESI-Mass spectra recorded during the addition of Ag(I) acetate to Zn_4SmtA at pH 6.9. The data provide valuable information concerning specific Ag-Zn-MT and Ag-MT species. This will support the suggested stoichiometries for mixed metal SmtA, which is important to enable the evaluation of structural changes with Zn/Ag and Zn/Cu replacement in bacterial SmtA. Molar equivalents of Ag(I) were added to Zn_4SmtA and the mass spectra were recorded immediately after the addition of Ag(I).

Figure 4.11 shows the formation of several Ag(I) containing species. From the data it can be clearly seen that the dominant metallation state is a direct result of the number of equivalents of Ag(I) added to the solution. Just a small addition of Ag(I) to the Zn_4SmtA led to unique and clearly identifiable mixed-metal species, for instance two M_5 [Ag_2Zn_3SmA and Ag_3Zn_2SmtA] species after addition of one eq. Ag(I), and two M_6 [Ag_3Zn_3SmtA and Ag_4Zn_2SmtA] species after addition of the second equivalent of Ag(I), all of which coexisted after 3 eq., together with unreacted Zn_4SmtA, which could still be observed at 5 eq. This is remarkable, and in contrast to the Cu(I) titrations, where Zn_4SmtA or Cd_4SmtA had both disappeared after the second molar addition of Cu(I). A Zn_1Ag_7 species also emerged already after 2 eq., along with very minor amounts of the Zn_1Ag_6 species. The two dominant species at 6 and 7 eq. were Zn_2Ag_4 and Zn_1Ag_7.

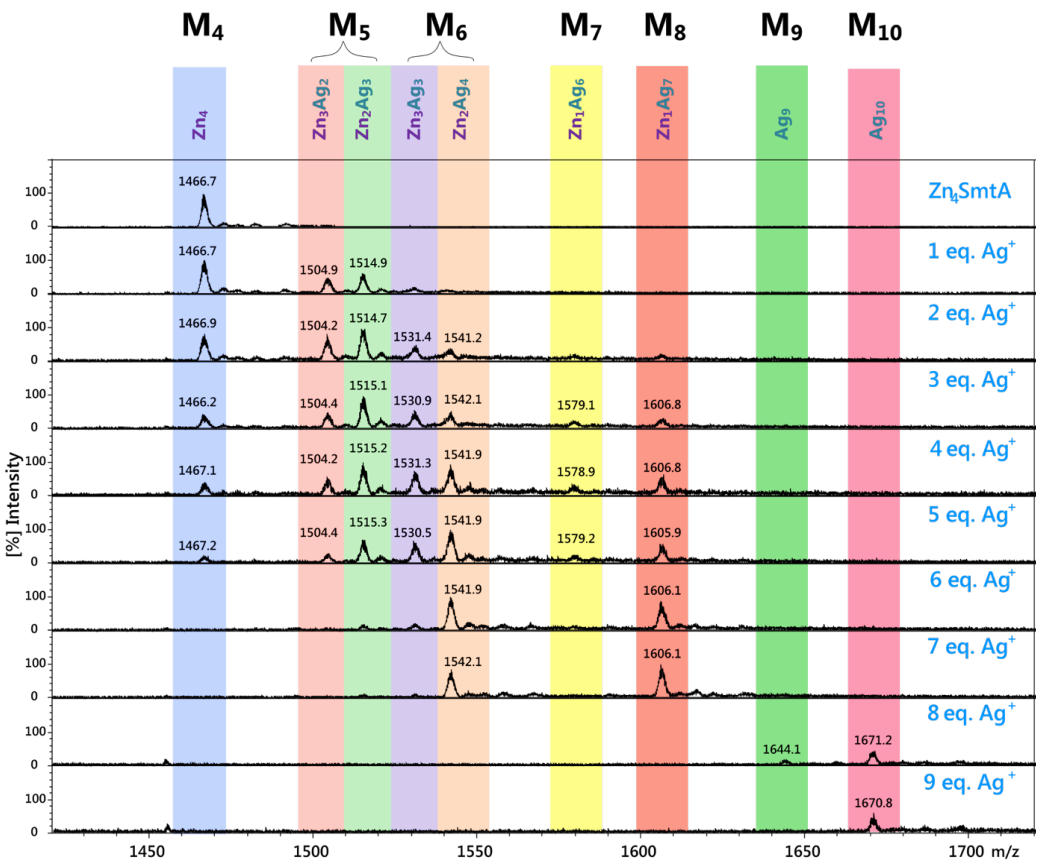

Figure 4.11 ESI-MS titration of Zn_4SmtA with Ag(I).

ESI mass spectra for titration of Zn_4SmtA (25 µM solution in 10 mM ammonium bicarbonate buffer with 10% methanol at pH 6.9) with Ag(I) at pH 6.9. Aliquots of Ag(I) were added to the protein as 1 to 9 equivalents. The colored blocks show the formation of new species with the addition of Ag(I). [Appendix A3 for experimental and theoretical m/z].

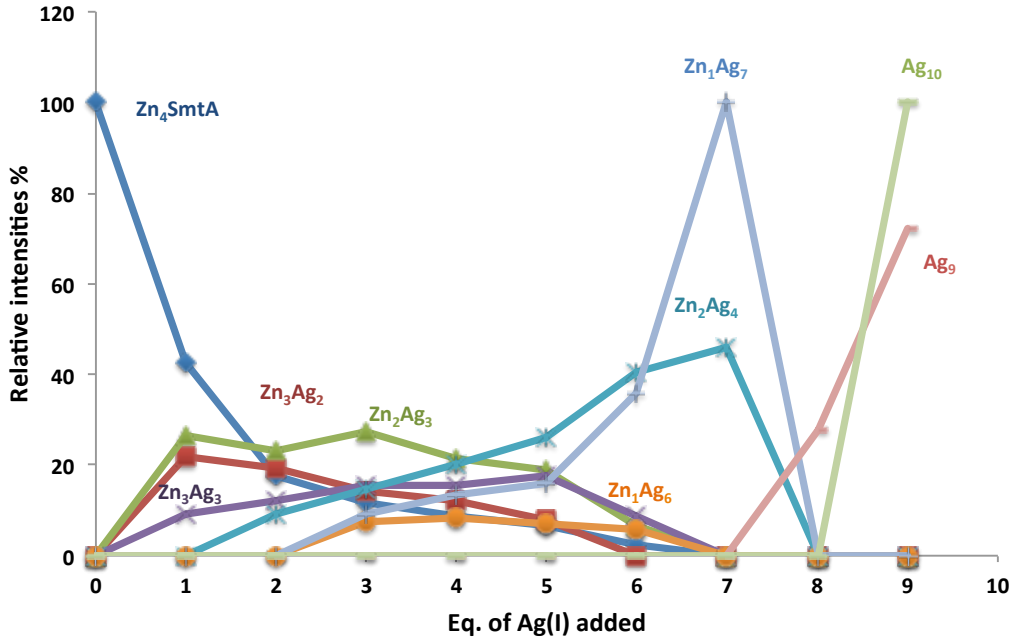

Figure 4.12 Zn_4SmtA metallation and speciation on Ag(I) addition

The relative abundance and speciation of the species based on the relative intensity of each peak in ESI-mass spectra are plotted against the equivalents of species formed during the course of the Ag(I) titration. Each line corresponds to formation of a different hetero- or homo-metallic species on incremental addition of Ag(I).

Further addition of Ag(I) resulted in loss of Zn(II) from the protein and formation of homonuclear metal clusters with M_9 and M_{10} [Ag_9SmtA and Ag_{10}SmtA] which is because of saturation of all thiolates with one Ag(I) each, and somewhat contrasts with the maximal Cu(I):MT ratios (8:1 or 9:1) observed in the titrations with Cu(I). The Ag_9-MT species may correspond to a fully unfolded protein; the binding site for the 10^{th} equivalent is unclear.

A direct comparison of the Cu/Zn and the Ag/Zn titration data reveals a tendency towards higher nuclearity for the latter - consistent with the linear coordination preference of Ag(I). Although Cu(I) and Ag(I) may interact differently within metal clusters, one important characteristic of the Zn_4SmtA metal cluster is the Zn(II) in metal binding site A of the protein which holds the protein structure together and previously has been reported to be inert towards metal exchange (Blindauer et al 2008). The persistence of the Zn_1Ag_7 species may

suggest that this one structurally essential zinc ion, along with up to seven Ag(I) ions, may keep the zinc finger structure intact until the subsequent additions of eight and nine equivalents of Ag(I). Further addition of Ag(I) only gave rise to higher noise in the spectra along with negligible amounts of apo and under-metallated species, as shown in Figure 4.13. It is important to note that at this stage, the protein had lost its last structurally critical Zn(II) ion, giving rise to only homo-metallic Ag_9 and Ag_{10}SmtA.

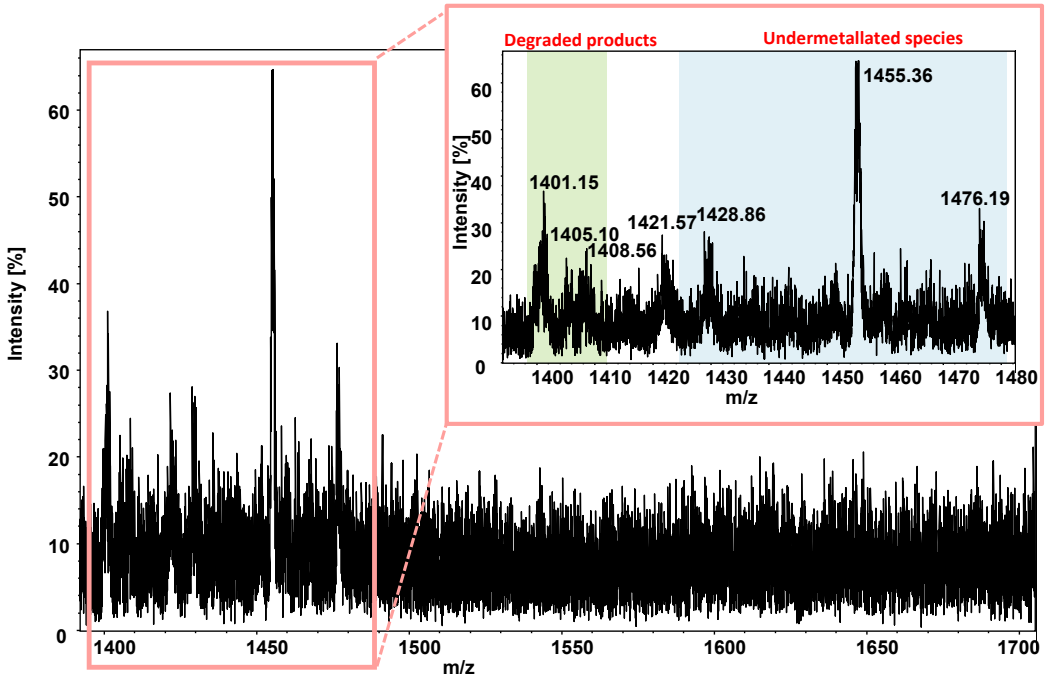

Figure 4.13 ESI mass spectrum of Zn-MT containing 11 eq. of Ag(I).

ESI mass spectra after addition of eleven equivalents of Ag(I) to Zn_4SmtA (25 μM solution in 10 mM ammonium bicarbonate buffer with 10% methanol at pH 6.9). Inset contains the enlarged boxed region to avoid overlap of peaks and labels.

Another persistent species of interest is the Zn_2Ag_4 species, which was still present at 7 eq. Ag(I). This may suggest that this and the Zn_1Ag_6 species are more stable than alternative homometallic configurations, including Ag_7 and Ag_8. Ultimately however, both heterometallic

clusters are destroyed, with complete loss of Zn(II), so in this case again, the Zn(II) in site A was unable to withstand the substitution reaction.

4.3 Summary and Conclusions

Cu(I) binding to Zn_4SmtA was studied by UV-vis absorption spectroscopy and ESI-MS. UV-Vis spectroscopy revealed saturation with Cu(I) after seven equivalents. This suggested that the final product of the metal exchange reaction contained 7 Cu(I), similar to the product of the reconstitution of apo-SmtA with copper. However from UV-vis data it was not clear whether the resulting species was Cu_7SmtA with complete displacement of Zn(II) from SmtA, or whether the product still contained Zn(II), e.g. in the inert site A. For this purpose, quantitative detection of the number and type of species formed during Cu(I) addition, ESI-MS was used. ESI-mass spectra suggested the formation of mixed metal species e.g., M_5, M_6, M_7 and M_8. Furthermore, addition of more Cu(I), i.e. eight equivalents, caused the formation of under-metallated and oxidized species, presumably as a product of unfolding of protein but the M_7 species were still the most abundant of all. Although isotopic distribution modelling of the most abundant species M_5 and M_7 indicated likely compositions of the corresponding metal clusters, it was desirable to use Cd(II) as a probe for Zn(II) in a Cu(I) titration, and Ag(I) as a substitution for Cu(I), to distinguish the composition of the hetero- and homo-metallic species formed during the titration procedure. These experiments were also of interest from a more fundamental point of view. For this purpose, Ag(I) was used as a heavier probe for Cu(I) in a ESI-MS titration of Zn_4SmtA to identify the different species forming in solution. The resulting data suggested the formation of mixed metal species with Zn_2Ag_4 and Zn_1Ag_7 (M_6 and M_8 metal species) as most abundant species. The remaining last Zn(II) in the cluster may correspond to the zinc finger site A. Although Ag(I) and Cu(I) have different coordination preferences and clearly different mixed clusters were formed, the fact that Ag(I) titrations of Zn_4SmtA also

eventually showed complete displacement then again fits with the behavior during Cu(I) titrations. It may indeed be that eventually all Zn(II) does get exchanged even if the Zn_1 species might put up a fight for some time.

Nevertheless, Cu/Cd or Zn/Ag titrations helped in understanding the stoichiometries and composition of species formed during Cu/Zn titrations. The results obtained, established that the M_5 species are combination of both Cu_2Zn_3 and Cu_3Zn_2. In addition, M_6 species could be anything from homometallic Cu_6 to Cu_5Zn_1, Cu_4Zn_2, Cu_3Zn_3 or even Cu_2Zn_4. Furthermore, the Cd/Cu titration results indicated that the M_7 species observed by the end of the Zn.Cd titrations is likely to be Cu_7: If Cd(A) is not inert, then there is no reason to assume that Zn(A) is inert, hence the inert site A is not inert with respect to Cu(I) exchange.

Whilst giving valuable insights on stoichiometries and mixed-metal species, the UV-vis and ESI-MS data give no information regarding the protein fold when the coordination geometry of the bound metals switches from tetrahedral to trigonal/digonal. To observe structural changes in dependence on metal composition of MTs, solution NMR spectroscopy is the best available method. Furthermore, neither ESI-MS nor UV-vis spectroscopy allow us to conclude whether different sites are reacting preferentially, and if so, which sites are the first to exchange the bound divalent metal. Multinuclear NMR spectroscopy has proven to be a very promising technique to study effects of metal binding to protein structure, and corresponding experiments and results for metal-exchanged SmtA are discussed in the next chapter.

5

Metal exchange reactions of Zn_4SmtA and Cd_4SmtA with Cu(I): Structural effects

5.1 Introduction

The characteristics of rapid metal exchange of metallothioneins might be important to a role in mediating inter protein metal transfer reactions (Wang et al 1996, Öz et al 1998). Although there is a range of structural data available for the MT family, only the structures for two MTs containing Cu(I) are known to date i.e., yeast MT and *N. crassa* MT (Bertini et al. 2000, Peterson et al. 1996, Calderone, Dolderer et al. 2005, Cobine et al. 2004), the latter without information regarding the location of copper ions. However, there is not a single MT for which different structures with both mono- and divalent metal ions such as Zn(II) and Cu(I) have been studied in detail. For example, for yeast Cup1, structures are available with Cu(I) and Ag(I) (Bertini et al. 2000, Calderone et al. 2005), for mammalian MTs, structures exist with only Zn(II) and Cd(II) (Vašák et al. 1987, Vašák and Meloni 2011), and for wheat Ec MT, structures with Zn(II) and Cd(II) are available (Peroza et al. 2009, Loebus et al. 2011).

NMR spectroscopy is a very crucial technique for probing protein structure and their native metal binding sites. NMR spectroscopy along with X-ray crystallography is the only technique that is capable to determine high-resolution molecular structures. NMR is particularly suitable for protein studies as it permits the determination of protein structures in solution, in near native or physiological relevant conditions. In addition, NMR has been successfully employed to investigate protein-ligand interactions, thermodynamic and kinetic properties of proteins, protein folding, and dynamics.

In NMR spectra that show backbone amide protons, qualitative information regarding the protein fold can be deduced from the distribution of the chemical shifts in a protein, referred to as chemical shift dispersion. A well-dispersed spectrum contains many different chemical shifts, which show the nuclei in many different environments, as expected for a protein containing elements of secondary structures such as α-helix and β-sheet along with a tertiary fold. However, in an unfolded protein, all nuclei of similar chemistries are in similar environments and therefore, their chemical shifts are all in the same region of the spectrum, e.g. in the case of backbone amide protons, they occur at or near random coil values, resulting in a very narrow dispersion.

This chapter describes the solution state NMR analysis of ^{15}N isotopically labelled Zn_4SmtA and cadmium (Cd(II)) reconstituted Cd_4SmtA following Cu(I) titrations. The first section of this chapter explains the use of two-dimensional (2D) heteronuclear NMR spectroscopy to investigate the effects of Cu(I) addition on protein fold and protein-metal interactions by chemical shift perturbation analyses. ^{1}H-^{15}N-HSQC spectra were used for mapping conformational changes in residues affected by Cu(I) addition. Subsequently, Cd reconstitution into apo-SmtA and further analysis of Cd_4SmtA by one-dimensional (1D) ^{111}Cd and two-dimensional ^{111}Cd-^{1}H heteronuclear NMR experiments were employed specifically to identify the order or Cd(II) replacement, and to explore metal-cysteine connectivities in mixed-metal species.

5.2 HSQC (Heteronuclear Single Quantum Correlation) NMR Spectroscopy

A protein contains protons and other magnetically active nuclei. ^{15}N and ^{13}C are of importance especially in the structure determination of larger proteins. These heteronuclei occur in low abundance. Therefore, two strategies are employed to obtain information from these nuclei:

- Isotopic enrichment of these nuclei in proteins and
- Enhancement of the signal to noise ratio by the use of inverse NMR experiments in which the magnetization is transferred from protons to the hetero nucleus.

HSQC (heteronuclear single quantum correlation) is one of the most important NMR experiments. A 2D heteronuclear single quantum correlation (HSQC) spectrum, where "heteronuclear" refers to nuclei other than ^{1}H, has one peak for each ^{1}H bound to a heteronucleus (if ^{1}J couplings are selected, often true for ^{15}N-^{1}H and ^{13}C-^{1}H, but for ^{111}Cd-^{1}H ^{3}J couplings are used). Typical protein ^{1}H,^{15}N-HSQC spectra contain the signals of the NH protons in the protein backbone, and since there is only one backbone NH per amino acid, each HSQC signal represents one single amino acid with the exception of proline, which has no amide hydrogen due to the cyclic nature of its structure. A protein ^{1}H,^{15}N-HSQC spectrum also contains signals from the NH_2 groups of the side chains of Asn and Gln, and depending on the chemical shift range, potentially aromatic HN protons of Trp and His.

5.3 Chemical shift perturbation

Chemical shift perturbation (CSP, also referred as chemical shift mapping or CIS, or complexation-induced changes in chemical shift) is a useful NMR technique to explore the binding of small molecules or macromolecules to a ^{15}N labelled protein. In this technique the

small molecules or macromolecules are titrated into a labelled protein solution and any effects on the protein are monitored at every stage of the titration by recording a $^{1}H,^{15}N$-HSQC spectrum. Since chemical shift is very sensitive to structural changes and can be measured precisely, all authentic binding interactions will generate chemical shift perturbations. The analysis is done by measuring the chemical shift at each titration point, following the movement of the peaks and measure the moving pattern of each peak during the titration (Golovanov et al. 2007, Williamson 2013). However it is important to keep the experimental conditions as similar and consistent as possible including the pH and compositions of the buffer for both protein and binding small/macro molecule solution, because any change in pH and salt concentration can also affect especially amide proton chemical shifts and confuse the analysis (Williamson 2013).

Chemical exchange has important effects on what is observed during a chemical shift perturbation experiment. For instance, in a 2D HSQC spectrum of a protein as the ligand is titrated in, the signal for a particular proton may fade with the appearance of a new signal, which indicates slow or intermediate exchange between the original and the new species, whilst in the fast exchange regime, the signal will move smoothly from their original position in the spectrum towards the position corresponding to the bound spectrum with the signal frequency at any point of titration being the weighted average of free and bound chemical shifts (Williamson 2013). An illustration of these fast and slow exchange regimes during chemical shift perturbation experiments are shown in Figure 5.1.

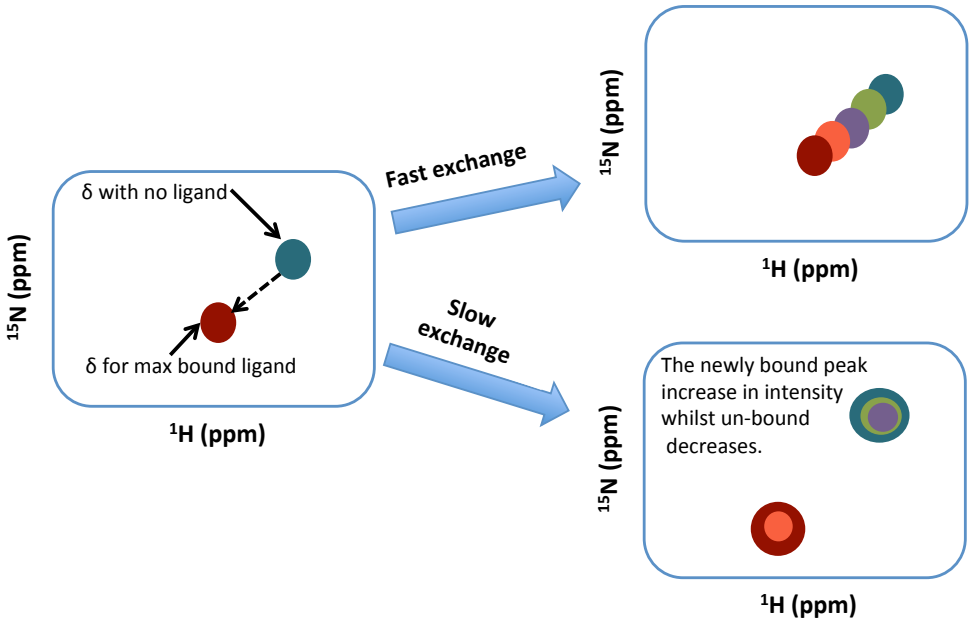

Figure 5.1 Description of chemical shift perturbations in slow and fast exchange.

Metal binding causes a change to the chemical environment of chemical shift leading to change in position of bound and unbound chemical shift. With the increase in concentration of the bound state the intensity of unbound states decreases. Figure partially adapted from Williamson 2013).

For comparing two titration points, it is often useful to calculate weighted chemical shift perturbation values. First, the chemical shifts of both ^{1}H and ^{15}N (in ppm) for each peak in both spectra are measured, and their difference is calculated, after the ^{15}N shift is multiplied by a scaling factor α as shown by equation below.

$$d = \sqrt{\frac{1}{2\left[\delta_H^2 + \left(\alpha.\delta_N^2\right)\right]}}$$

A further possible observation during such experiments is the complete disappearance of peaks - in particular if the new species suffers from structural disorder, or if the co-existing species are in intermediate exchange, which generally leads to line-broadening (and also disappearance of peaks). In these cases, chemical shift perturbation cannot be quantified.

Different peaks in the same spectrum can display different exchange regimes, related to differences in frequency and to rate of exchange. In this regard, chemical shift perturbation

studies can (in principle) provide information on the lifetime of protein-metal complexes and can also be used to determine affinity.

5.4 NMR Cu(I) titrations of Zn_4SmtA: $^{1}H–1^{5}N$ HSQC NMR

Figure 5.2 shows the $^{1}H–1^{5}N$ 2D HSQC NMR spectrum of Zn_4SmtA recorded at 35 °C. The signals are well dispersed indicating that the uniformly labelled protein was well-folded (also established by comparing experimental data with the published BMRB entry as shown in Figure 5.2) and hence the suitability of the protein for further NMR analysis. The near-complete assignment of Zn_4SmtA resonances was achieved with the aid of published ^{1}H-^{15}N data (Blindauer et al. 2001, Blindauer personal communication). The unassigned peaks in the ^{1}H-^{15}N HSQC spectrum of Zn_4SmtA are due to a contaminating peptide. The residues (marked with asterisks) 2—4, 43, 42, 50, 51 were not observed, as reported in previous studies (Blindauer et al. 2001).

The assigned ^{1}H-^{15}N HSQC spectrum of Zn_4SmtA (Figure 5.2) can be used as a map. Since the backbone chemical shifts are sensitive to changes in chemical environment for a given nucleus, either through direct binding event, conformational change or change in dynamics, the assigned HSQC spectrum is a powerful tool for probing Cu(I) binding to the Zn(II) bound protein.

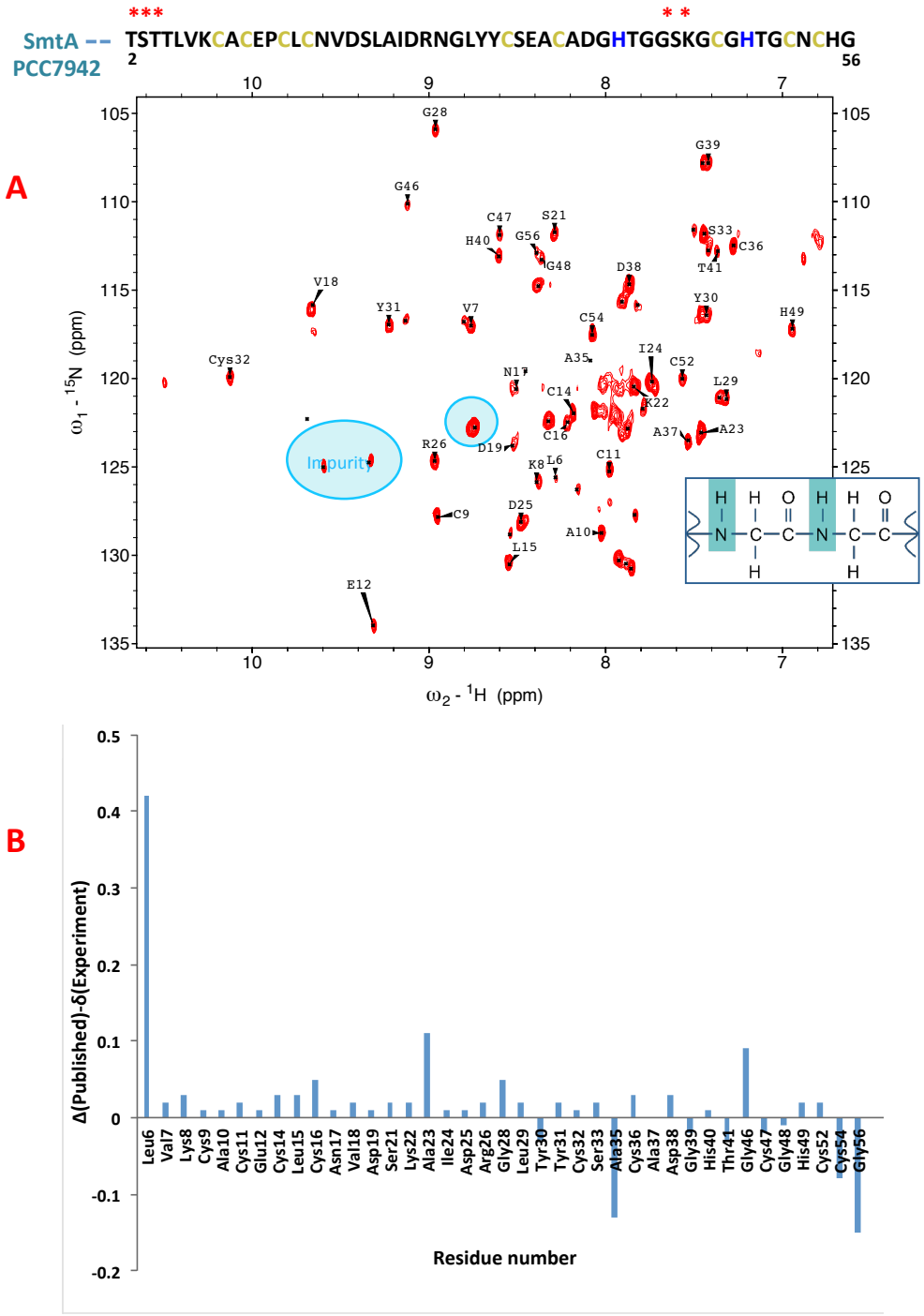

Figure 5.2 ^{1}H-^{15}N 2D HSQC NMR spectrum of Zn_4SmtA.

(A) Sequence of Zn_4SmtA-asterisks indicates unassigned residues. ^{1}H-^{15}N HSQC spectrum of Zn_4SmtA at 35 °C, pH= 7.4 in NMR buffer (50 mM Tris-Cl, 50 mM NaCl). The inset shows the protein backbone NH protons and nitrogens. B) Plot of difference of experimentally derived chemical shifts of Zn_4SmtA to the published chemical shifts.

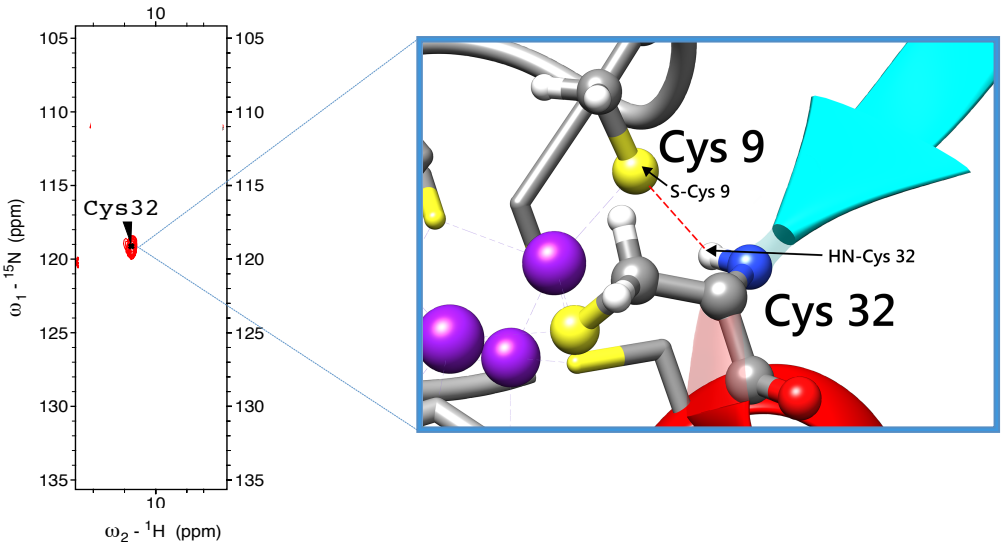

Figure 5.3 Cross-peak and environment of HN of Cys-32.

Part of HSQC spectrum showing the high chemical shift ~10.2ppm for Cys-32. This is caused by the hydrogen bond between Cys-32 NH and the Cys-9 thiolate sulfur.

The higher chemical shift of the very important residue Cys-32, which is involved in direct metal binding, is partially due to the hydrogen bond between NH of Cys-32 and sulfur of Cys-9. Cys-32 is one of the residues forming the inert site A which also stabilises the zinc-finger fold of the protein. Previous studies (Blindauer 2008) have shown that the NH proton of this residue is highly sensitive to cluster composition in mixed Zn/Cd SmtA species. Hence, it is possible that this residue will sense any incoming metal and will help in determining the changes that occur in the metal cluster of Zn_4SmtA.

5.4.1 Cu(I) binding induces significant conformational and dynamic changes throughout Zn_4SmtA

^{1}H-^{15}N HSQC spectra were recorded at each point during a titration of Zn_4SmtA with Cu(I) (added as tetrakis(acetonitrile)copper(I) hexafluorophosphate). This series of spectra (Figures 5.4, 5.5,

5.6 and 5.9) made it possible to assign Cu_xZn_ySmtA spectra (i.e., with the addition of up to three molar equivalents of Cu(I) to Zn_4SmtA) which enabled the detection of chemical shift changes in response to copper binding on a per residue basis. The assignment of the Zn_4SmtA spectrum can be superimposed on the spectra resulting from Cu(I) addition, allowing a tentative assignment of residues that are unperturbed or only slightly perturbed. Peaks that were not perturbed by addition of Cu(I) and peaks, with no neighboring chemical shifts, where there was no ambiguity as to the corresponding peak in the Zn_4SmtA HSQC spectrum were thus assigned in the subsequent Cu_xZn_ySmtA spectra. This provisional assignment facilitated a preliminary investigation of Cu(I) binding.

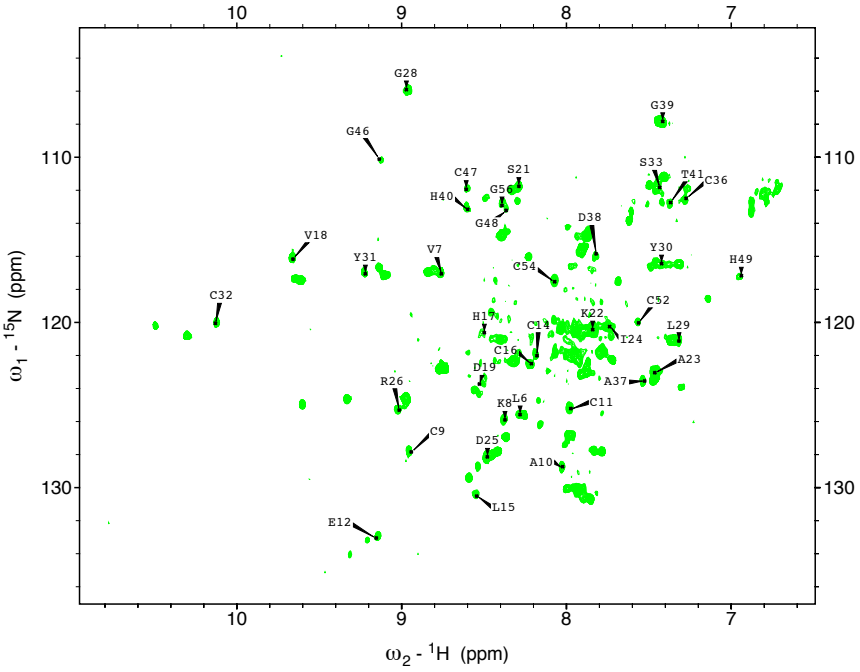

1 eq. of Cu(I)

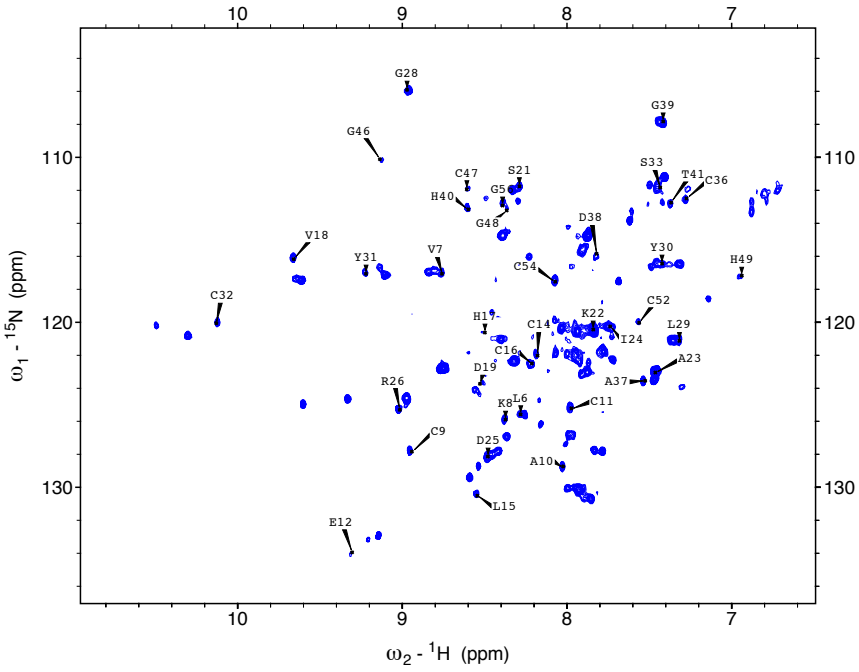

2 eq. of Cu(I)

Figure 5.4 ^{1}H-^{15}N 2D HSQC NMR spectra of Zn_4SmtA after addition of 1 and 2 eq. of Cu(I).

^{1}H-^{15}N HSQC spectra (Zn_4SmtA at 35 °C, pH= 7.4 in NMR buffer (50 mM Tris-Cl, 50 mM NaCl)) after addition of 1 and 2 eq. of Cu(I). (Chemical shifts are provided in Appendix A4)

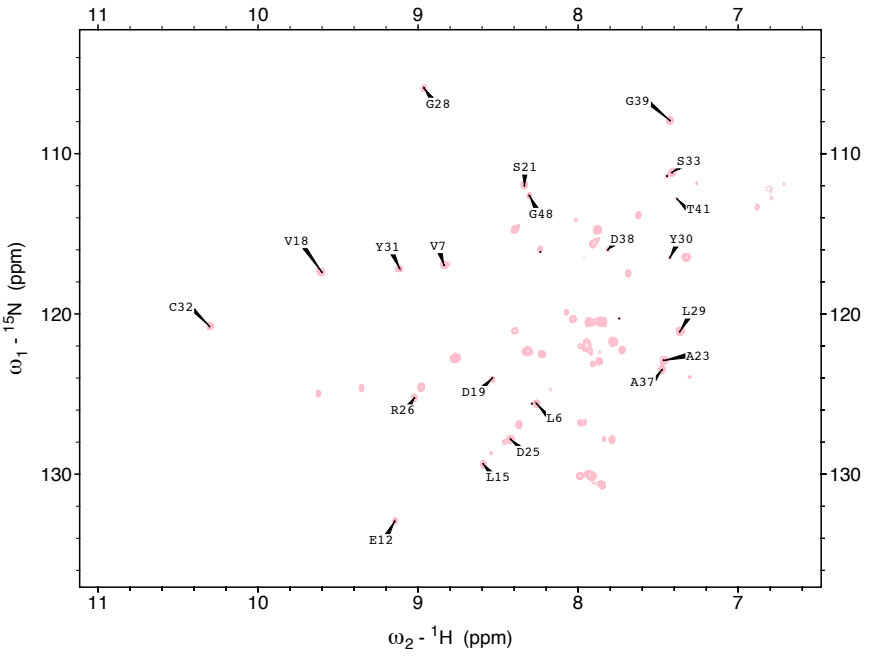

3 eq. of Cu(I)

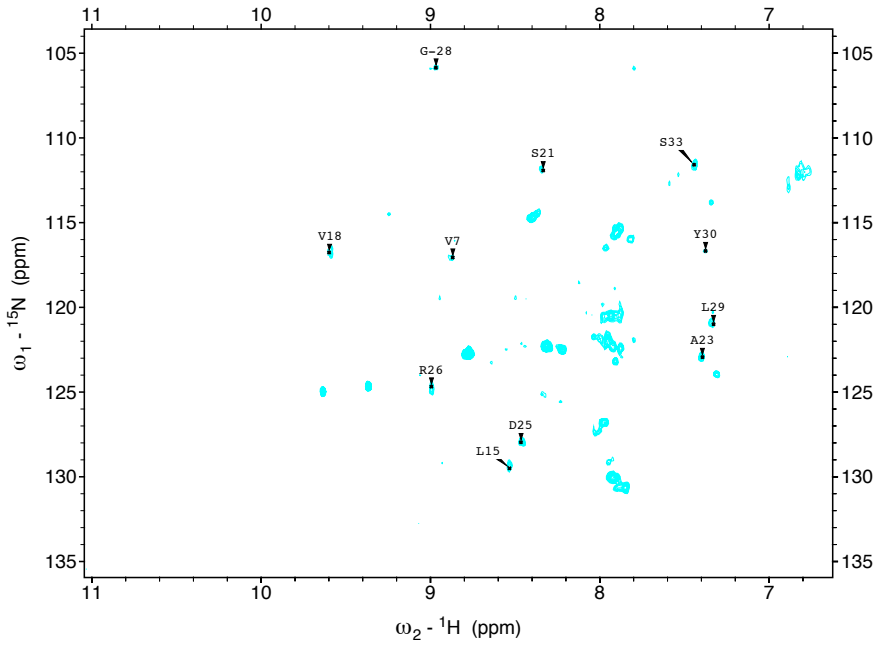

4 eq. of Cu(I)

Figure 5.5 ^{1}H-^{15}N 2D HSQC NMR spectra of Zn_4SmtA after addition of 3 and 4 eq. of Cu(I).

^{1}H-^{15}N HSQC spectra (Zn_4SmtA at 35 °C, pH= 7.4 in NMR buffer (50 mM Tris-Cl, 50 mM NaCl)) after addition of 3 and 4 eq. of Cu(I). (Chemical shifts are given in Appendix A5)

^{1}H-^{15}N HSQC NMR spectra for Zn_4SmtA and Cu(I)-bound states are overlaid in Figure 5.6, and Figure 5.7 shows an enlarged section containing residues Cys-32 and Val–18, in which five spectra have been offset by 0.1 ppm to better observe individual peaks.

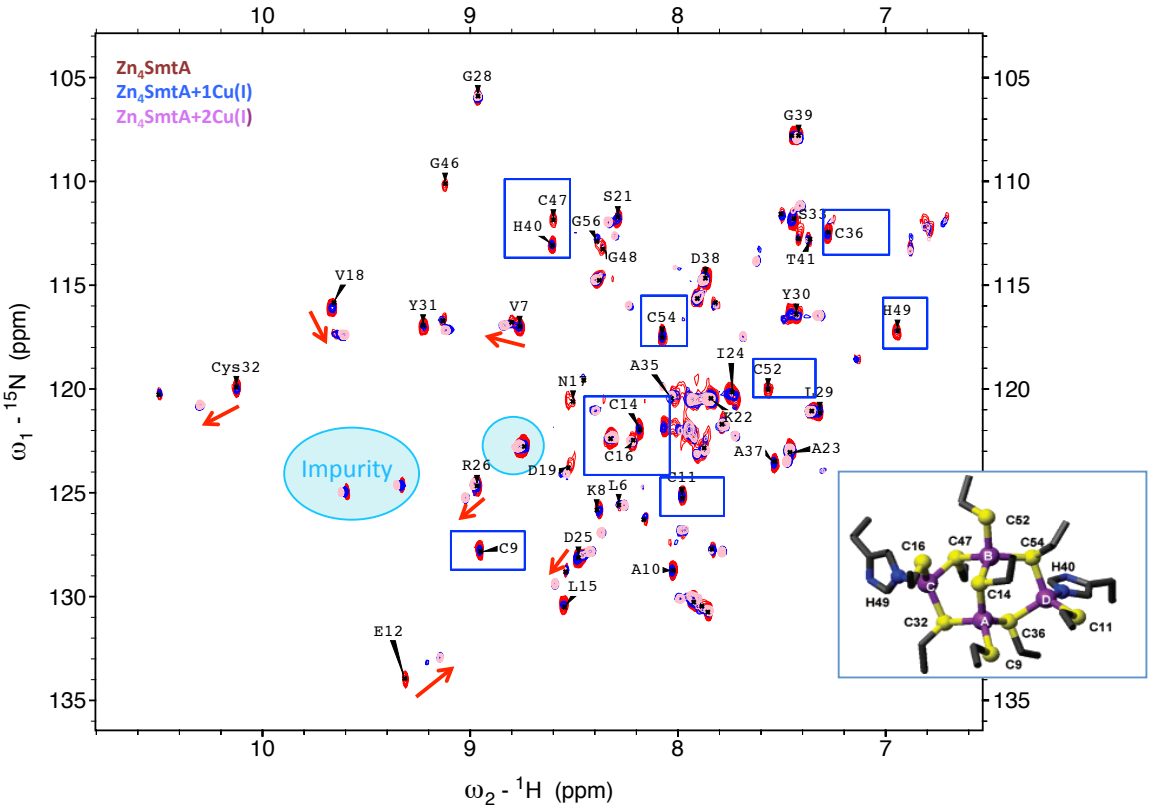

Figure 5.6 Overlaid ^{1}H-^{15}N HSQC NMR spectra for Zn and Cu(I)-bound states of SmtA.

Overlay of ^{1}H-^{15}N HSQC spectra (35 °C) of Zn_4SmtA (red), after addition of 1 (blue) and 2 (purple) mol equiv. of Cu(I) to Zn-SmtA. Boxes highlighting selected metal binding residues, and arrows show the new set of peaks after each Cu(I) addition.

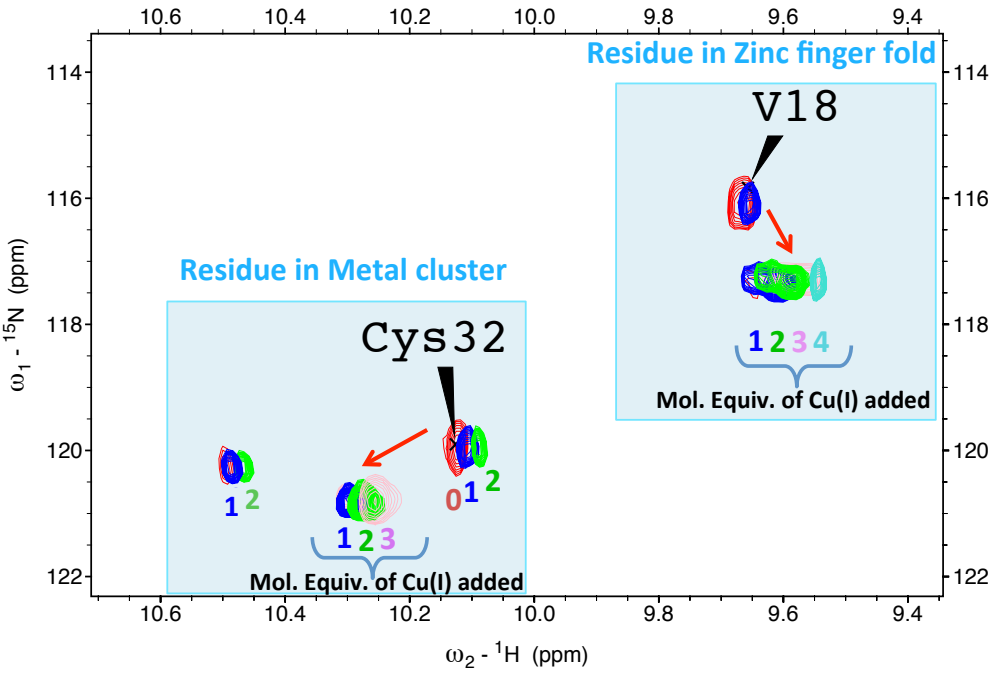

Figure 5.7 Chemical shift perturbation of residues Cys-32 and Val–18

Overlaid HSQC spectra of titrations of Zn_4SmtA with up to 4 mol. eq. of Cu(I). The five spectra are offset by 0.1 ppm in this Figure.

It can be observed that the cross peaks corresponding to the Zn_4SmtA species diminish in intensity upon addition of the first molar equivalent of Cu(I). Notably, the Zn_4SmtA species has almost completely disappeared after addition of the third equivalent, which is in good agreement with the ESI-MS titration data (Chapter 4, Figure 4.5), which showed exclusive presence of M_5 species.

For many residues, new cross peaks emerge, as indicated by red arrows in Figure 5.6, and also illustrated in Figure 5.7. All residues, for which new cross-peaks were observable, belong to the zinc finger fold and site A (Figure 5.8). These new cross peaks must correspond to one or more of the M_5 and M_6 species observed by ESI-MS. The peaks for C-terminal residues, including Cys-47, -52, and -54, and His-40 and His-49, involved in metal binding sites B, C and D, diminished in intensity, without the emergence of clearly corresponding new peaks, suggesting major structural changes upon partial replacement of Zn(II).

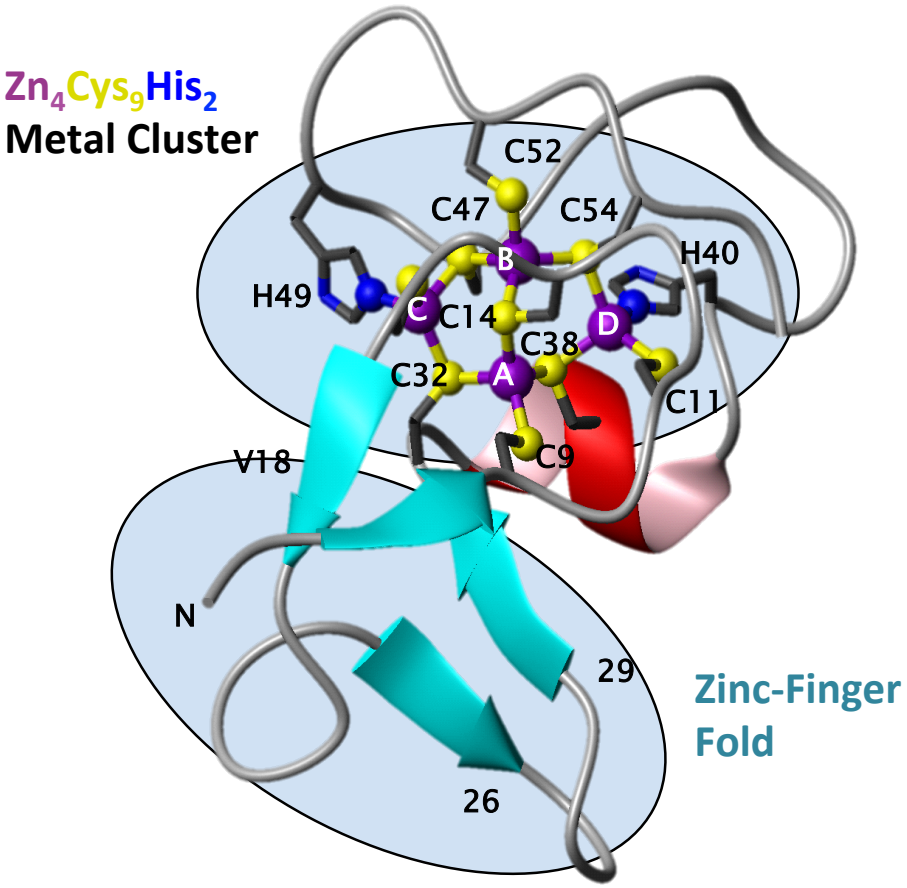

Figure 5.8 Structure of Zn_4SmtA.

Figure detailing the structure of Zn_4SmtA showing the number positions of each residue in the metal binding C terminus domain and zinc finger fold of the protein (adopted from Blindauer et al 2002).

It may be concluded that with Cu(I) titration of Zn_4SmtA (Figure 5.6) and formation of Cu_2Zn_3SmtA (and/or Cu_3Zn_2SmtA), the secondary structure elements of the zinc finger fold are initially only mildly affected, although the corresponding residues "perceive" the addition of up to four Cu(I) to the protein, and hence, the new peaks have slightly different chemical shifts. For Cys-32, there are three sets of defined peaks as marked by boxes in Figure 5.6 (one of the sets present in the original spectrum is thought to correspond to a minor Zn_1SmtA species e.g. Cys-32 NH shift at ca. 10.5 ppm; Figure 5.7), which has been previously observed in NMR spectra (C. Blindauer, personal communication), although it is unclear why this species did not take up Cu(I) during the first two titration points (which would lead to the disappearance of the corresponding

peaks). This species is only lost after 3 eq., so in principle, was capable of Cu(I) binding.

A more dramatic impact was observed after addition of 4 Cu(I) resulting in the disappearance of numerous cross-peaks, especially for the residues involved in metal binding such as Cys and His residues, in the 2D ^{1}H-^{15}N HSQC NMR spectra, without the appearance of clear new cross-peaks. The residues involved in the zinc finger fold, however, such as Val–18, Gly-28 and Leu-29 were still present after the addition of 5 mol. equiv of Cu(I), showing that structural order in this region was still maintained as shown in Figure 5.9.

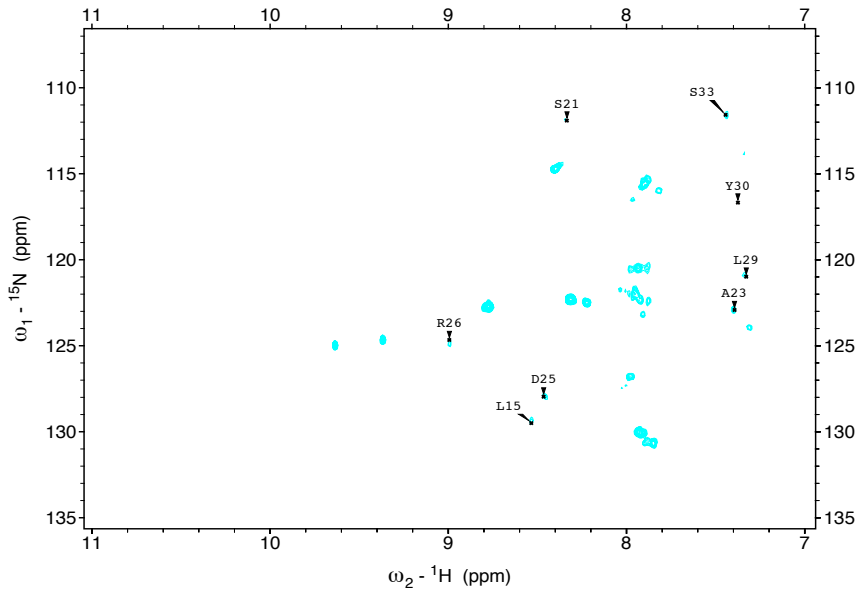

Figure 5.9 ^{1}H-^{15}N HSQC NMR spectra for Cu(I)-bound states of SmtA.

^{1}H-^{15}N HSQC spectra after addition of 5 equiv. of Cu(I) to Zn-SmtA showing disappearance of most residues.

Addition of the sixth equivalent of Cu(I) led to the complete disappearance of all remaining resonances. The overall extent of the perturbations induced by the addition of four mol. eq. of Cu(I) are illustrated in Figure 5.10. It is clear that significant chemical shift perturbations are observed in the metal binding region of SmtA upon binding of Cu(I). The standard deviation of the chemical shift perturbation across all residues (as indicated by dashed line in Figure 5.10) was used (Schumann et al. 2007) to determine residues most affected by binding. Perturbations

above this threshold were considered significant.

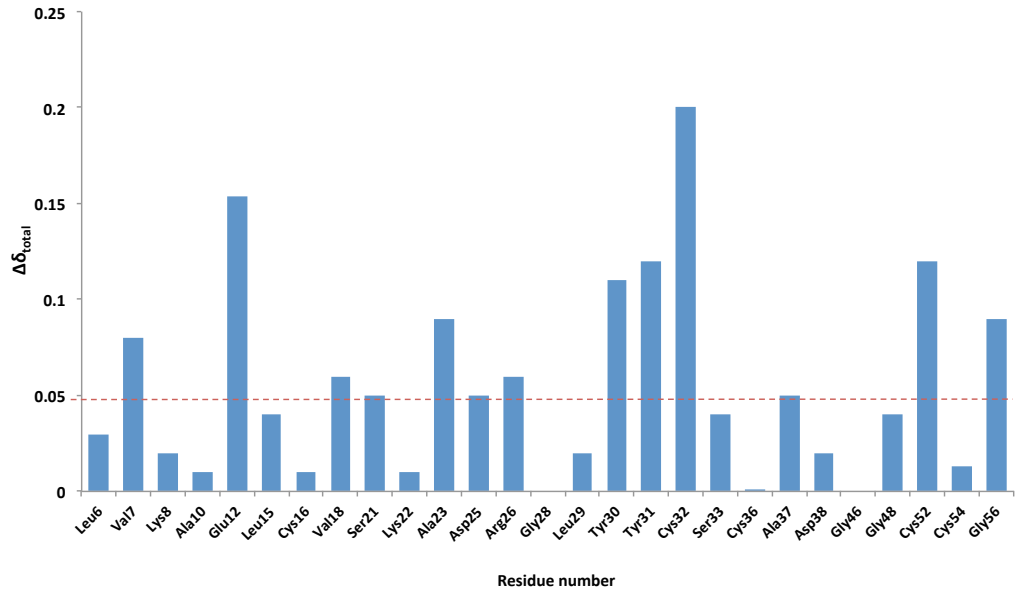

Figure 5.10 Total chemical shift difference per residue upon Cu(I) addition.

The total chemical shift perturbation upon addition of 4 equivalents of Cu(I) is plotted per residue. Dashed lines represent the standard deviation across all residues, perturbations above this line are considered to be significant. The residues not listed (including Cys–11, Cys–14, His-40, Cys-47 and His-49) are diminished completely.

Cys-32 along with residues Arg-26, Tyr-30, Tyr-31, Glu-12 and Cys-52 were perturbed very significantly. The residues involved in binding are mapped and highlighted on to the Zn_4SmtA solution structure as shown in Figure 5.11 which displays binding of Cu(I) induced perturbation of some regions in the protein near metal cluster. Specifically residues that make up the metal binding domain are significantly perturbed. Furthermore residues in β-sheet and α-helix also responded to addition of Cu(I).

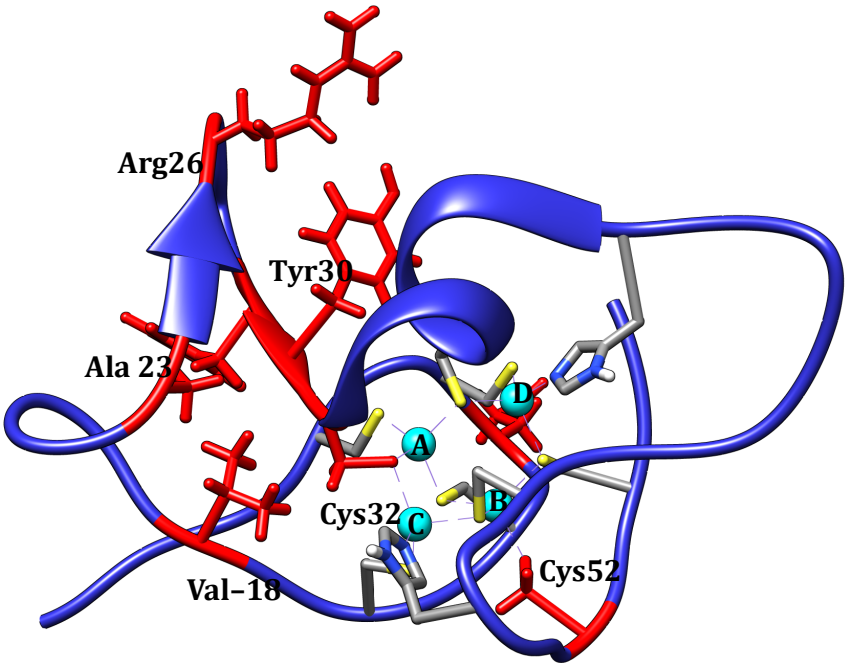

Figure 5.11 Residues involved in chemical shift perturbation following the addition of Cu(I).

Cysteines and Histidines are the most perturbed (shown in the metal cluster) and disappear after Cu(I) addition. Residues with total chemical shift perturbations greater than the standard deviation cut-off are highlighted in red. Cu(I) causes the perturbation of metal binding residues.

In the $^{1}H,^{15}N$-HSQC spectrum of SmtA in the presence of more that 5 mol eq. Cu(I), no residues could be assigned due to absence of any signals. These observations suggest that the interaction of Cu(I) with SmtA leads, eventually, to structural disorder irrespective of whether the corresponding species (fully Cu-substituted SmtA) are generated by mass action or by reconstitution as discussed in Chapter 3. The fact that all signals of the protein NH protons were subject to broadening suggests that the whole molecule was affected by Cu(I) binding above 5 mol equivalents. A similar effect was observed for the interaction of Cu(I) in the study of the metal thiolate clusters in both domains of vertebrate Zn-metallothionein (Dolderer et al. 2007) and N-terminal domain of neuronal growth inhibitory factor (Faller and Vašák 1997). However, since the entire C terminus (which includes residues for binding sites B,C and D) became significantly perturbed already in the early stages of the titration, it was not possible to determine which metal site is exchanged first from these ^{1}H-^{15}N NMR data. However, the

presence of Zn(II) in site A is highly likely for up to five Cu(I) added, as the zinc-finger fold residues are still observable.

To pinpoint the order of metal exchange, the native Zn(II) ions were replaced by ^{111}Cd(II) ions (nuclear spin I = ½) to produce $^{111}Cd_4$SmtA, and this was titrated with Cu(I) and studied by ^{111}Cd NMR spectroscopy.

5.5 ^{111}Cd NMR Spectroscopy for metal-ligand connectivities

This section details the use of nuclear magnetic resonance methods of ^{111}Cd(II) to probe Cu(I) exchange of Cd_4SmtA (see also Chapter 4, Figure 4.8). To probe the ligand coordination chemistry of bio metals, the native metal ion may be replaced iso-structurally with another metal nucleus with suitable properties to study by nuclear magnetic resonance (Öz et al. 1998, Coleman 1993, Maret and Vallee 1993, Armitage et al. 1982, Armitage et al. 2013).

^{111}Cd NMR spectroscopy is the most effective method to investigate metal ligand connectivities in metallothioneins (Vašák 1998). The binding sites in metallothioneins containing Zn(II) are not responsive to direct observation by the most spectroscopy methods due to the spectroscopically silent nature of Zn(II) with filled *d*-shell (Maret 2004) and EXAFS is not useful to investigate individual metal ions in polynuclear clusters (PhD Thesis, Leszczyszyn 2008) and unsuitable for determining connectivities. However cadmium has been shown to replace zinc iso-structurally in bacterial SmtA used in this present study (Blindauer et al. 2001, Blindauer 2008). Moreover, the chemical shifts of cadmium nuclei are significantly perceptive to the coordination environment i.e., geometry, bond lengths, coordinating ligands, and neighbouring metal ions, as shown previously in Zn/Cd exchange reactions (Blindauer 2001 and 2008). Therefore, these relatively similar cadmium ions in metallothionein polynuclear sites may be distinguished which makes ^{111}Cd NMR spectroscopy a very powerful tool to determine the structures of metallothionein clusters (Coleman 1993, Öz et al. 1998, Nazorova and Hemming 2004).

The NMR studies on mixed Cd-Zn-SmtA had established that iso-structural replacement of Zn(II)

by Cd(II) has no discernible effect on protein dynamics, a conclusion which was based on the fact that all residues observed for Zn_4SmtA were also observed for Cd_4SmtA (Blindauer et al. 2001, Blindauer 2008). Figure 5.12 displays the full comparison of the structure of Zn_4SmtA and Cd_4SmtA backbone along with ^{1}H chemical shift difference on a per residue basis.

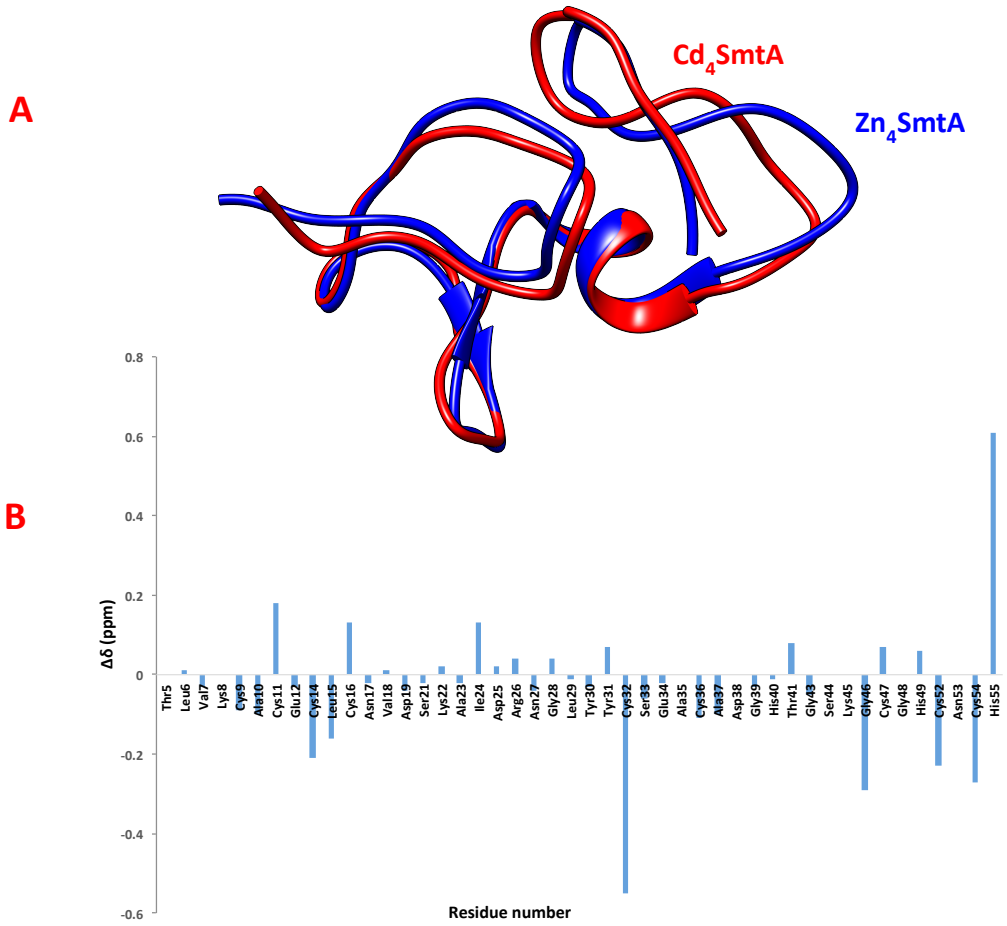

Figure 5.12 Comparison of Zn_4SmtA and Cd_4SmtA.

(A) Comparison of the backbone fold of Zn_4SmtA (Blue; pdb 1jjd) and Cd_4SmtA (Red). (B) chemical shift difference between backbone HN protons of Cd and Zn bound SmtA. (Blindauer et al 2008, Blindauer personal communication).

The difference in chemical shifts of several backbone NH and CH(α) resonances for residues linked to the cluster structure arise from small changes in the backbone conformation due to the larger size of Cd(II) compared to Zn(II) with tetrahedral ionic radii of 0.92 Å and 0.74 Å,

respectively (Blindauer et al. 2001). Such small structural differences are also observed in other MTs such as mammalian zinc and cadmium binding MT2 (Messerle et al. 1992). The difference in M-S bond lengths (i.e. average M-S 2.32 Å for Zn(II) and 2.53 Å for Cd(II) in MTs) contributes to an extended coordination sphere volume (Blindauer et al. 2001). An extreme example of such an effect is Cys-32, which is very sensitive towards metal exchange and the composition of the whole cluster (Blindauer 2008), as already mentioned in section 5.4 and shown in Figure 5.13.

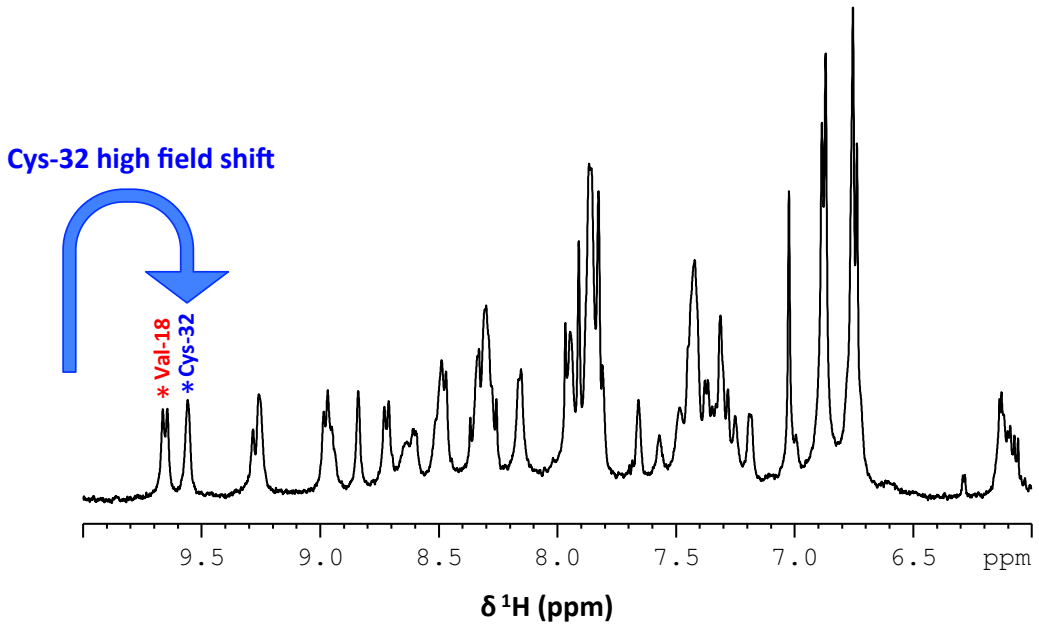

Figure 5.13 1D ^{1}H NMR spectrum of Cd_4SmtA.

Fingerprint region of 1D 1H NMR of Cd4SmtA (pH 7.3, 35 °C in 10% D2O 50 mM Tris-HCl, 50 mM NaCl) showing the high field shift of Cys-32 after exchanging Zn for Cd.

This very low field ^{1}H chemical shift Cys-32 (10.09 ppm) shifts to higher field by 0.5 ppm (to 9.56 ppm) on Cd(II) exchange due to the larger coordination sphere of Cd(II) causing the elongation of an NH-S H-bond (Blindauer et al. 2001, Blindauer et al. 2003, Blindauer et al. 2008) as discussed earlier.

5.5.1 Preparation of $^{111}Cd_4SmtA$

$^{111}Cd_4SmtA$ was prepared by reconstitution of apo-SmtA with $^{111}Cd(II)$ ions following the previously established method (Vašák 1991). ESI-MS of ^{111}Cd reconstituted SmtA showed that the most abundant peak had a Mw= 6045.84 Da (for neutral species) corresponding to Cd_4SmtA (calculated mw= 6046.3 amu) as shown in Figure 5.14.

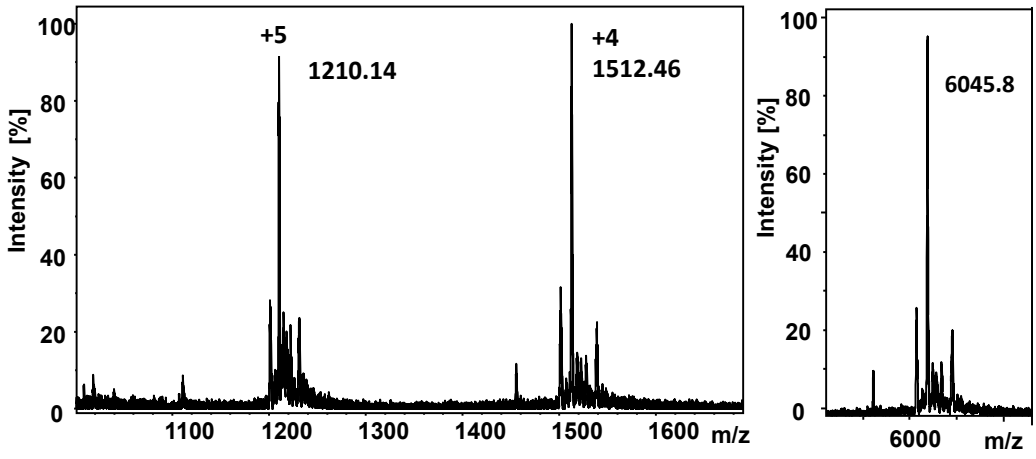

Figure 5.14 ESI-MS spectrum of $^{111}Cd_4SmtA$

$^{111}Cd_4SmtA$ prepared by reconstitution of apo-SmtA with $^{111}Cd(II)$ ions and buffer exchanged to 10 mM ammonium bicarbonate (25 μM of protein) for ESI-ToF MS.

ESI-MS and a subsequent 1D ^{111}Cd NMR spectrum (Figure 5.15) confirmed the homogeneity of the preparation and that the reconstitution had generated a fully exchanged folded protein with NMR spectra of Cd(II) loaded protein comparable to published spectra (Blindauer et al. 2001, Blindauer 2008).

5.5.2 ^{111}Cd 1D NMR and metal cluster characteristics of Cd(II)-substituted SmtA

The 1D ^{111}Cd NMR spectrum of Cd_4SmtA showed four peaks at 712.4 ppm (Site A), 659.5 ppm (Site B), 591.8 ppm (Site C) and 564.1 ppm (Site D) as shown in Figure 5.15. These four resonances indicate Cd(II) in four metal binding sites. The present resonances for $^{111}Cd_4$SmtA are approximately matched with the published resonances as compared in Table 5.1.

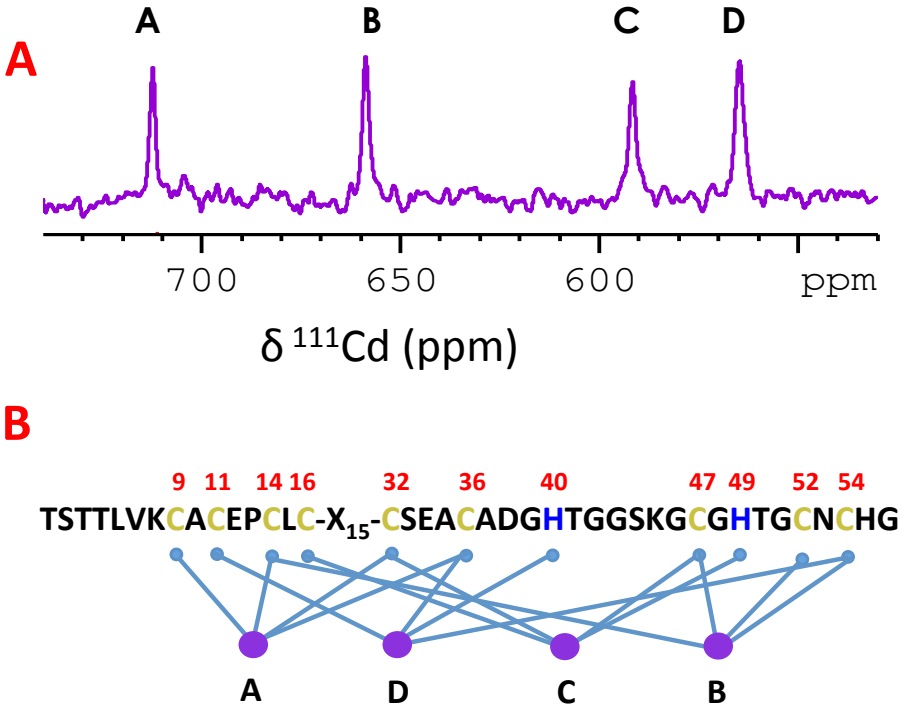

Figure 5.15 ^{111}Cd 1D NMR spectrum of ^{111}Cd reconstituted SmtA.

(A) $^{111}Cd_4$SmtA prepared by reconstitution of apo-SmtA with ^{111}Cd(II) ions (106.03 MHz, pH 7.3, 35 °C in 10% D_2O 50 mM Tris-HCl, 50 mM NaCl) displaying four peaks for individual binding sites. (B) Metal-to-ligand connectivities for SmtA (Figure adapted from Blindauer et al 2001)

Table 5:1 chemical shifts for 1D ^{111}Cd NMR of Cd_4SmtA

Comparison of published chemical shift (BMRB) of $^{111}Cd_4$SmtA with the experimental chemical shifts.

Metal binding sites in $^{111}Cd_4$SmtA	Published δ ^{111}Cd (ppm)	Experimental δ ^{111}Cd (ppm)
Site A	712	712.4
Site B	660	659.5
Site C	596	591.8
Site D	567	564.1

5.6 Metal binding sites in Cd_4SmtA

The site-specific Cd(II) incorporation into Zn_4SmtA has already been reported by Blindauer et al 2008, with Cys_4 site B being the first to be occupied, followed by the Cys_3His site D, and site C whilst site A remained inaccessible for Cd(II) and Zn(II) (Blindauer et al. 2003). Adding one molar equivalent of Cd(II) yielded Cd_1Zn_3SmtA soon after mixing and after equilibrium the ^{111}Cd NMR spectrum remained dominated by Cd_1Zn_3SmtA (Blindauer 2008). However, the last Cys_4 Zn(II) in site A was still bound to the protein together with three Cd(II) even after addition of ten mol equivalents of Cd(II) to Zn_4SmtA with long incubation times. This is one unique characteristics of Zn_4SmtA with inert Site A, which holds the associated α-helix and antiparallel β-strands together.

5.7 NMR titration of $^{111}Cd_4$SmtA with Cu(I)

To explore how Cu(I) is allocated among the clusters of bacterial metallothionein, $^{111}Cd_4$SmtA was titrated with Cu(I), which is experimentally demanding due to the air-sensitivity of Cu(I) and Cu-MTs to oxidation when compared to Zn-Cd-MTs. Strict anaerobic conditions were required to minimize the risk of oxidative damage. Figure 5.16 shows a series of 1D ^{111}Cd NMR spectra resulting from the displacement of Cd(II) from Cd-MT with Cu(I). After addition of the first eq. of

Cu(I), three new resonances (termed tentatively A*, C* and D*) were observed at 686.9 ppm, 577 ppm and 567 ppm, along with the four resonances of the original $^{111}Cd_4$SmtA. All peaks corresponding to the Cd_4 species disappeared upon the addition of a second equivalent of Cu(I), whilst the three new peaks remained. Around 570 ppm, at least two peaks are overlapping. The unequal intensities suggest that at least two different species were present at this point, one of them a Cd_3Cu_x species (as three resonances were seen). This also fits with the fact that the most prominent species in the ESI-MS spectrum for 2 equivalent was Cd_3Cu_2. , The identity of the second species remains unresolved: ESI-MS suggested a prominent Cd_2Cu_3 species at this titration point, but only one extra peak was observed in the ^{111}Cd NMR spectrum.

The question which sites are present in the Cd_3Cu_2 species will ultimately be answered using 2D $^{1}H,^{111}$Cd HSQC spectra, but at this point, the most likely site from which Cd(II) has been lost is site B: up-field shifts of ~50-60 ppm have been previously reported for calf liver MT-1 and MT-2 after Cu(I) addition in ^{113}Cd NMR (Armitage et al. 1982), but there are no new peaks in that region up-field of site B. The intensity around peak at 570 ppm became higher with the addition of the third Cu(I) equivalent whilst sites A* and C* still present at equal intensity. The spectrum at the fourth Cu(I) equivalent is similar to the three Cu(I) equivalent spectrum but overall all intensities have decreased with much lower signal to noise ratio. It may correspond to the same species but lower in concentration since the rest has reacted to unfolded or fully-exchanged species that can no longer be observed by ^{111}Cd NMR - similar to the observations in the ^{1}H-^{15}N HSQC spectra during Zn/Cu exchange.

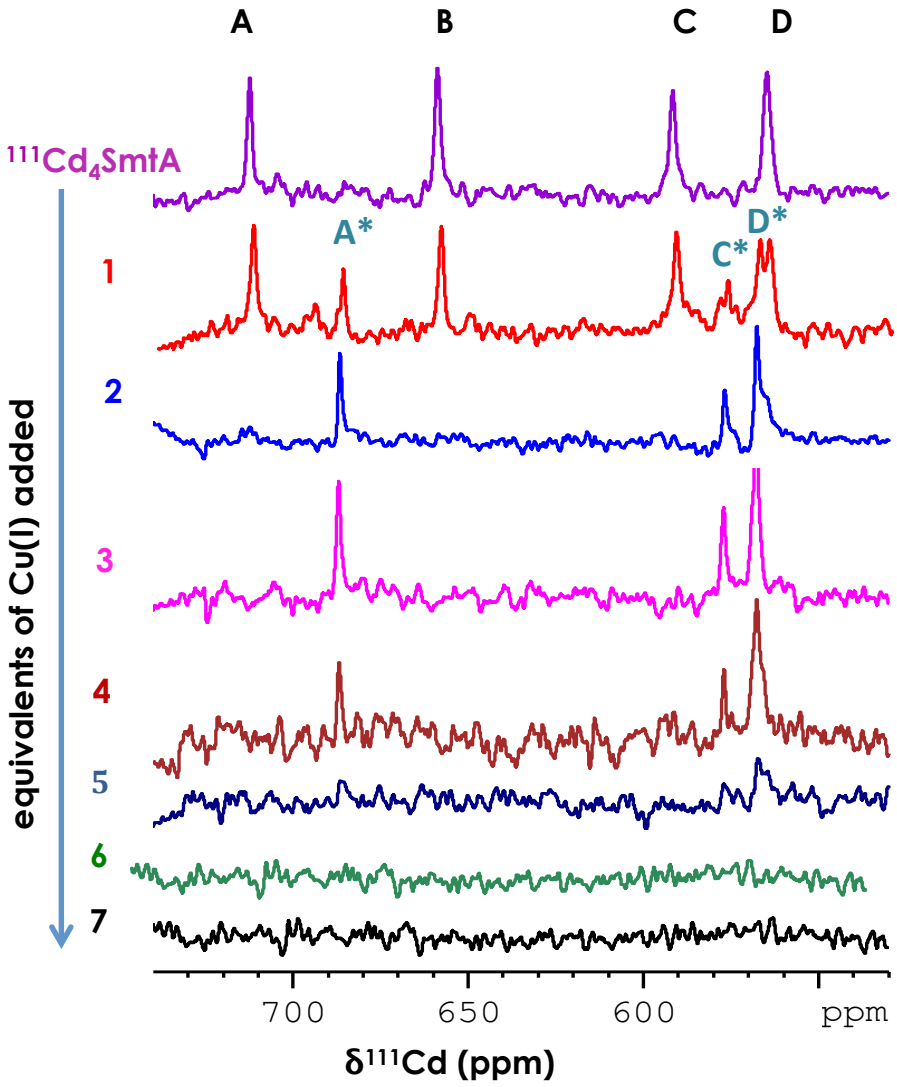

Figure 5.16 Cu(I) titrations of $^{111}Cd_4SmtA$.

Stack of ^{111}Cd 1D NMR of 111Cd4SmtA (pH 7.3, 35°C in 10% D2O 50 mM Tris-HCl, 50 mM NaCl) with step wise addition of Cu(I). The new signal marked by asterisks indicate new species formed after addition of the first equivalent of Cu(I).

In contrast, the observation of reasonably sharp peaks in the earlier ^{111}Cd spectra indicates the presence of folded species. However, further addition of Cu(I) caused a complete decrease in the intensities of the metal cluster resonances. It is clear from Figure 5.16 that Cu(I) readily displaced Cd(II), and that up to six equivalents of Cu(I) were needed in order to displace all of the Cd(II) from Cd_4SmtA - coinciding with the complete loss of resolved NH resonances in the ^{1}H,^{15}N HSQC spectrum of Zn_4SmtA after addition of six eq. Cu(I). In addition, the aggregation of the formed

species is likely as precipitates were formed at this stage.

5.7.1 ^{1}H-^{111}Cd HSQC 2D NMR for site identification

Heteronuclear two-dimensional NMR (^{1}H-^{111}Cd HSQC) of ^{111}Cd-subsituted metallothioneins provide information on identity of coordinating ligands through scalar couplings between the ^{111}Cd(II) ion and protons of amino acid ligands such as cysteine, histidine, carboxylates and methionine (Armitage et al. 1987). The heteronuclear three-bond couplings between each ^{111}Cd(II) ion and the β protons of their cysteine ligands is vital in the determination of the solution structure by two dimensional methods (Wüthrich 1991).

The formation of heterometallic cluster species is well defined for Zn/Cd-MTs (Otvos and Armitage 1979, Nettesheim et al. 1985, Good et al. 1991) but there is no information on the characteristics of heterometallic cluster species such as Cd(II) or Zn(II) sharing metal clusters with monovalent Cu(I). In order to recognize the metal binding site specificities and metal to protein connectivities in mixed metal cluster species it was necessary to analyse the coupling between ^{111}Cd(II) ions and protons directly. For this purpose, ^{1}H-^{111}Cd HSQC spectra were acquired along with ^{1}H-^{1}H 2D TOCSY and NOESY (see Appendix). Figure 5.17 displays the full ^{1}H-^{111}Cd HSQC spectrum of $^{111}Cd_4$SmtA defining individual metal binding sites showing the cysteine residues involved within each site as well as the two metal binding histidine residues in sites C and D.

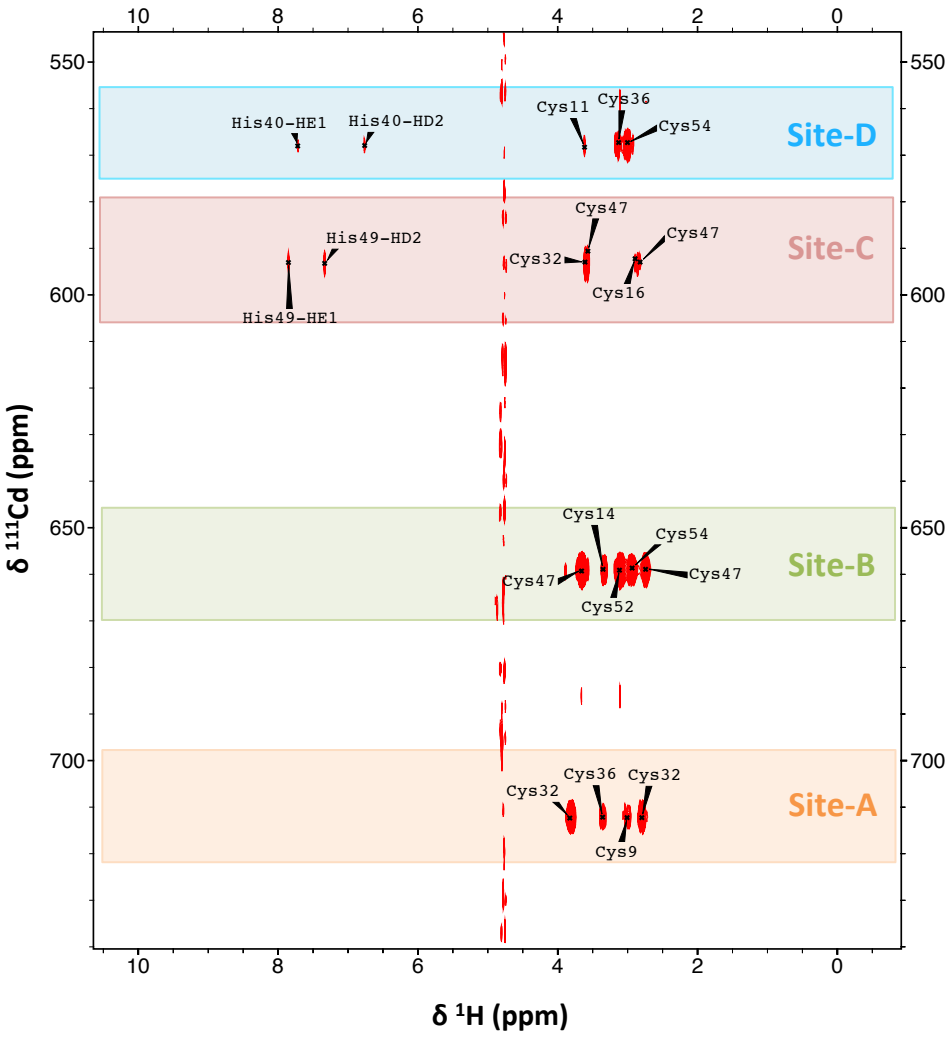

Figure 5.17 ^{1}H-^{111}Cd HSQC spectrum of $^{111}Cd_4$SmtA.

Four metal containing sites are displayed in ^{1}H-^{111}Cd HSQC spectrum of $^{111}Cd_4$SmtA (pH 7.3, 35°C in 10% D2O 50 mM Tris-HCl, 50 mM NaCl, recorded at 500 MHz, 3J= 35 Hz) .

The correlations of cysteine beta protons with four Cd(II) resonances is observed in the ^{1}H-^{111}Cd HSQC spectrum of Cd_4SmtA. It was possible to assign almost all of the resonances with the help of published chemical shifts (Blindauer et al 2001, Blindauer personal communication). This allows the identification of metal-cysteine connectivities and hence the characteristics of metal binding sites. The spectra for the Cu(I) addition of two and three equivalents to Cd_4SmtA is shown in Figure 5.18 (A,B). The observed cross peak patterns (Figure 5.18) clearly identify the new ^{111}Cd resonances in the new Cd_3Cu_x species as pertaining to sites A, C, and D, shifted by -26

ppm (from 713 to 687 ppm for site A), by –15 ppm (from 592 to 577 for site C), and by +3.2 ppm (from 564.5 to 567.7 ppm for site D). In addition, the comparison of the spectra for two and three equivalents (Figure 5.18) indicates that they pertain to the same species, as all cross peaks match perfectly.

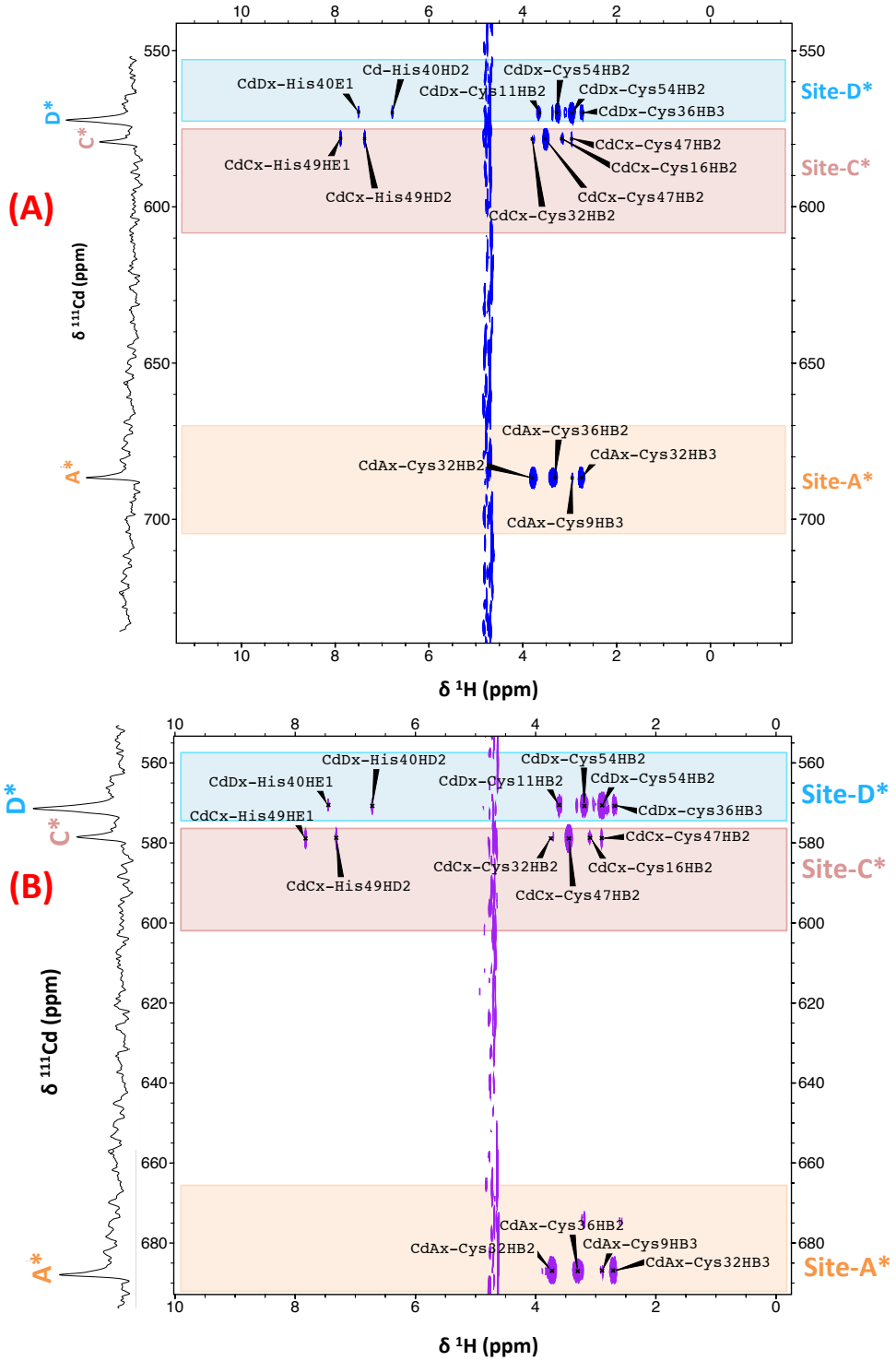

Figure 5.18 ^{1}H-^{111}Cd HSQC NMR titrations of of $^{111}Cd_4$SmtA.

^{1}H-^{111}Cd NMR of $^{111}Cd_4$SmtA (pH 7.3, 35°C in 10% D2O 50 mM Tris-HCl, 50 mM NaCl, recorded at 500 MHz, 3J = 35 Hz) produced after step-wise addition of (A) two and (B) three eq. of Cu(I) to $^{111}Cd_4$SmtA. . The metal binding sites are color coded and show up-field shift of resonances after addition of second and third equivalents of Cu(I)

In summary, the HSQC analysis has clearly revealed that the Cd(II) ion in the Cys_4 site B is the first to be displaced by Cu(I). This is reminiscent of this site also being the first to be displaced by Cd(II) in Zn_4SmtA. It is important to note here that the species observed are those present after establishment of equilibrium.

5.8 Specificity of metal binding sites and mixed metal clusters in SmtA

The binding of Cu(I) to Cd(II) and Zn(II) containing SmtA was addressed with ^{15}N and ^{111}Cd NMR studies, which demonstrate that about six to seven Cu(I) equivalents added to $Zn(II)_4$SmtA or $Cd(II)_4$SmtA displace all four divalent metal ions from the metal binding cluster. However the formation of mixed metal species was also observed during the step-wise Cu(I) titration procedures. Step-wise addition of Cu(I) to Cd_4SmtA led to up-field shifts by 15 and 25 ppm for sites C and A, respectively, following exchange of site B with the removal of first Cd(II) involving residues Cys residues 47 (bridge to site C), 14 (bridge to site A), 52. Residue Cys-54 (involved in metal binding in Site B and D) is presumably mediating a slight down-field shift (~2.8 ppm) of Site D with possible change in coordinating environment of this binding site.

Figure 5.19 summarises the Cu(I) substitution in Cd_4SmtA metal cluster along with the speciation of Cd_4SmtA on Cu(I) addition analysed by ESI-MS in the previous chapter. Together these data sets (ESI-MS and 2D NMR) provide information on composition of metal cluster and effect of Cu(I) on protein structure.

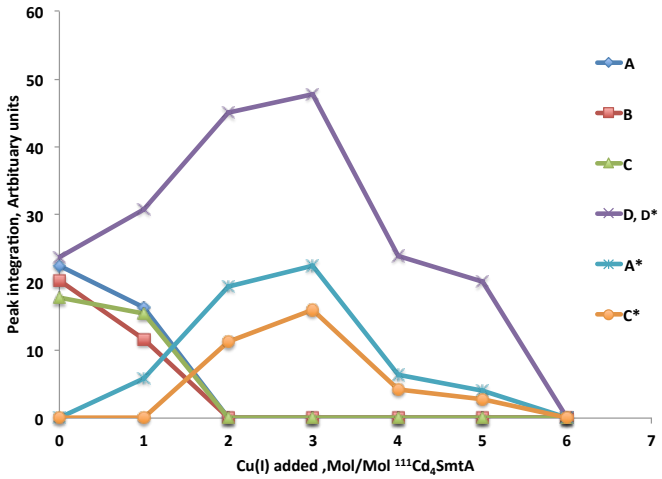

Figure 5.19 ^{111}Cd peak integrals for Cd_4SmtA on Cu(I) addition.

The displacement of Cd(II) metal binding sites by Cu(I) eq. molar addition to Cd_4SmtA. Cu(I) eliminates Cd(II) from the protein. Note that the trace for sites D, D* comprises several overlapped peaks.

The plot in Figure 5.19 re-iterates that only two equivalents of Cu(I) were required to eliminate the original 4-metal cluster Cd resonances as seen in Figure 5.18. This may suggest that the new species observed in the HSQC spectra at this stage is the 5-metal species Cd_3Cu_2SmtA, and this is also broadly in agreement with the ESI-MS data, which however also showed the pronounced presence of the Cd_2Cu_3 species at three, four, and five equivalents added. The much higher intensity of the peak (summarily labelled D, although several overlapped peaks can be assumed) around 570 ppm in the 1D ^{111}Cd spectra at two and three equivalents indicates the presence of a second species, likely the Cd_2Cu_3 species, but unfortunately, analysis of the 2D HSQC spectra did not reveal the identity of the respective binding site(s).

The Cd_3Cu_2 species remained present in the ^{111}Cd NMR spectra, albeit at decreasing levels, up to 5 equivalents added. There was no clear formation of a Cd_1Cu_x species with a Cd(II) ion in site A. This is again in agreement with the ESI-MS data, which did not indicate dominating amounts of such species at any given point. Following the addition of six equivalents of Cu(I), all NMR resonances disappeared as summarized in Figure 5.19. Consistent with this, at this point, the major species observed in the ESI-MS data was the Cu_7SmtA species. The "missing" protein may be due to partial degradation in either experiment.

The ^{111}Cd 1D NMR titration data show that for up to five equivalents of added Cu(I), Cd(II) is displaced from the protein and becomes a constituent of one or more mixed metal clusters as also clear from ESI-MS data from chapter 4. Since the environments of the Cd(II) are no longer the same as the initial M_4-cluster, the three metal resonances (A, B, and C) disappear and two new resonances (A* and C* along with slight shift of site D) appear from the Cd(II) ions in the mixed metal cluster species. Similar Cu-Cd-mixed metal clusters have also been reported elsewhere (Li and Otvos 1996). Further addition of Cu(I) leads to complete disappearance of the new resonances as the mixed metal cluster species are replaced by Cu(I), and Cd(II) ions are completely eliminated from the protein.

Since Cu(I) binding stoichiometries have been previously stated as inconsistent, probably because of cysteine oxidation and disproportionation of Cu(I) in aqueous solution (Li and Weser 1992, Li and Otvos 1996, Chen et al. 1996), the Cu(I) titrations experiments were repeated and special precautions were made to avoid oxidation. In all cases, the findings were very consistent i.e., the ^{111}Cd 1D NMR resonances from Cd_4-cluster were abolished after addition of two equivalents of Cu(I) with a similar set of new resonances appearing on further addition of Cu(I).

5.9 Summary and conclusion

The Cu(I) titrations of Zn_4SmtA (ESI-MS) showed the formation of mixed metal species and unfolding of protein (^{1}H-^{15}N 2D NMR) on addition of up to five Cu(I) equivalents with the full replacement of Zn(II) on seven Cu(I) equivalents. ^{1}H-^{111}Cd NMR provided information about site specific replacement of Cd(II) from Cd_4SmtA.

The ability to replace Zn(II) or Cd(II) by Cu(I) did not come as a surprise since the association constants for these metals are known to decrease in the order Cu>Cd>Zn. Metal coordination with cysteines in different sequence positions within metal clusters has clear effects on protein backbone. Hydrogen bonds, salt bridges and van der Waal's contact interactions within the structure contribute to the stability of the metal cluster. The resulting expansion or contraction of the cluster, and more importantly, the change in coordination geometry, leads to changes in

protein structure (Good et al 1991). The magnitude of the perturbation of the metallothionein structure, induced by binding of Cu(I), was illustrated by the complete loss of resolved resonances in either ^{1}H,^{15}N and ^{111}Cd NNMR spectra. Figure 5.20 summarizes the likely cluster species present at different titration points.

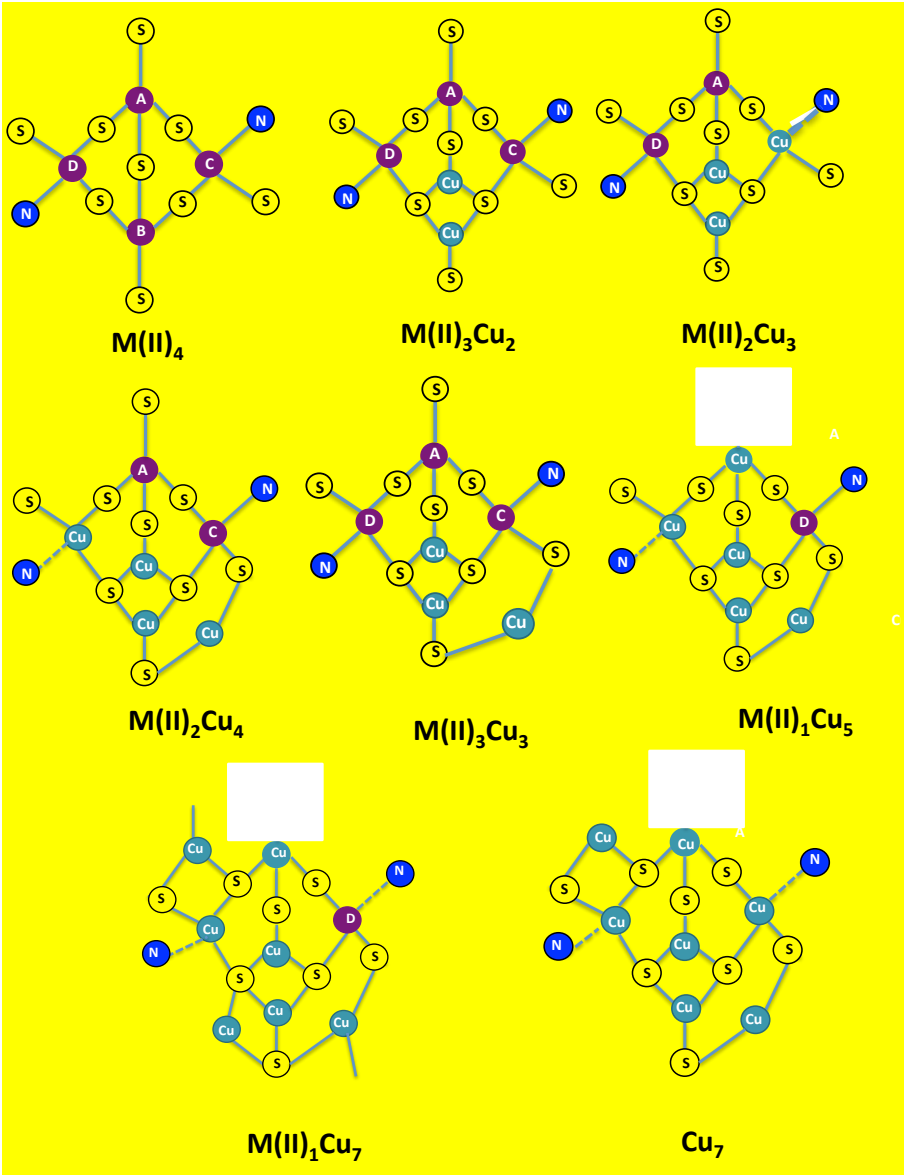

Figure 5.20 Likely composition of metal clusters in mixed M(II)/Cu(I) species.

Composition and stoichiometry of metal clusters in SmtA on Cu(I) addition, based on ESI-MS analysis of Cu(I) addition to Zn(II)/Cd(II)-SmtA.

The NMR and ESI-MS data (Chapter 4) have provided an insight into the composition and stoichiometries of M(I)/M(II)-mixed-metal clusters in SmtA, along with information on protein folding. Since SmtA is a native Zn(II) binding metallothionein, addition of Cu(I) caused major changes in the structure owing to its different coordination geometry. However, it was also evident that the $M(II)_3Cu(I)_2$, and perhaps also the $M(II)_2Cu_3$ and $M(II)_2Cu_4$ species, still retain a partial fold. The necessary rearrangements to accommodate further Cu(I) ions however resulted in the formation of disordered structure(s), as is evident from all three sets of experiments.

6

Characterization of the copper binding metallothionein MymT from *Mycobacterium tuberculosis*

6.1 Introduction

Recently new mechanisms involving direct impacts on the metal homeostasis of pathogenic microorganisms have been revealed as important components of the immune system (Osman et al. 2010, Braymer and Giedroc 2014, Cavet 2013) especially against *Mycobacterium tuberculosis.* In addition, components of copper homeostasis in pathogenic bacteria have been characterized as critical microbial virulence determinants (Ward et al. 2008, Wolschendorf et al. 2011, Samanovic et al. 2012).

Mycobacterial metallothionein (MymT) is a copper binding metallothionein from *Mycobacterium tuberculosis* and is important in protecting the bacterium against copper toxicity (Gold et al. 2008, Festa et al. 2011). The biochemical characterization carried out by Gold et al suggested that this protein binds up to six Cu(I) ions and stepwise addition of Cu(I) ions resulted in species between four and five Cu(I) ions bound to MymT. However, the published luminescence data suggested the five Cu(I) species (Cu_5MymT) as the fully loaded species (Gold et al. 2008, Blindauer 2011), so clarification on the metal stoichiometry is necessary. Furthermore, structural

characterization of the Cu-MymT complex(es) would be desirable to significantly shed light on metal binding and effects of histidine residues in Cu-MTs .

An expression system for MymT could not be established, although attempts were made to sub-clone a synthetic *mymT* gene into a pET vector (Appendix A6). Therefore, the experiments described in this chapter were done on a chemically synthesized MymT peptide (donated by Prof. Ben Gold). Figure 6.1 shows the amino acid sequence of MymT with potential metal binding residues, seven cysteines and two histidines, highlighted.

MTNYEAGTLLTCSHEGCGCRVRIEVPCHCAGAGDAYRCTCGDELAPVK

Figure 6.1 Amino acid sequence of MymT

Amino acid sequence of MymT with terminal methionine. MymT contains seven cysteines (Yellow) and two histidines (Dark blue), which may be involved in metal binding.

In this chapter, more detailed work on the copper binding properties of MymT, reconstitution of this newly discovered metallothionein with Cu(I) and its analysis by ESI-MS and ^{1}H NMR spectroscopy is reported. All the preparations and characterizations were carried out under strict anaerobic conditions, which is crucial when working with Cu-MTs (See chapter 3).

6.2 Reconstitution of apo-MymT

The MymT peptide (donated by Prof Ben Gold, New York) was used without further purification as the seven cysteine residues in the peptide may lead to difficulties during HPLC purification. The peptide was first resuspended in buffer containing 4% of the reducing agent β-mercaptoethanol (βME), to break any disulfide bonds in apo-MymT, and this was then evaporated off by using a vac-line. The resulting lyophilized Cu-MymT was resuspended in buffer (10 mM ammonium hydrogen carbonate). ESI-MS was used to identify the apo-MymT. Figure 6.2 shows the full scan ESI-MS for the synthetic peptide (apo-MymT).

The mass of 5063.16 Da observed as a major species is for apo-MymT including the N-terminal methionine, which corresponds to its theoretical mass of 5063.6 Da (+1 species). A second minor peak with mass of 4961.16 Da shows the loss of one cysteine residue (theoretical mass 4960.6 Da) probably resulting from errors during solid phase synthesis of the MymT synthetic peptide. Although errors introduced by this impurity cannot be excluded, its influence on the subsequent studies by ESI-MS and NMR spectroscopy can be considered minor, as the first technique allows distinguishing any peaks related to this species (including any metallated species), and major peaks in NMR spectra will pertain to the major species, too.

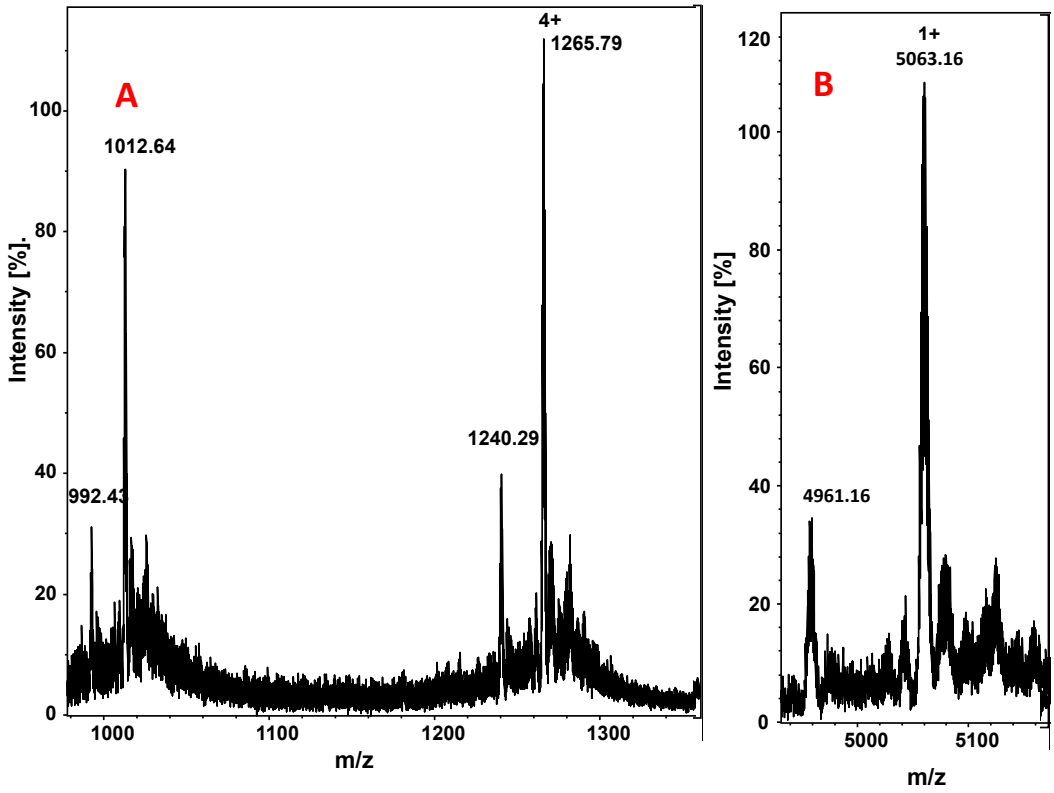

Figure 6.2 ESI-MS of Apo-MymT.

(A) Full scan ESI-ToF-MS spectrum shows charge state species of apo-MymT. (B) Deconvoluted spectrum for +1 masses of predominant species shows MymT with terminal methionine. 25 μM of Apo-MymT sample was prepared anaerobically (in glove box) in 10 mM ammonium bicarbonate buffer at pH 7.1.

The Cu(I) reconstitution experiment for MymT followed the methods developed in chapter 3 (section 3.2). Apo-MymT (synthetic peptide, Figure 6.2) was reconstituted with Cu(I), prepared under strict anaerobic conditions by in situ reduction with βME. ESI-MS was used in order to identify the Cu(I)-loaded MymT. Direct injection of he sample produced the raw spectrum as shown in Figure 6.3A where at least two charge states were observed corresponding to +4 and +3. Deconvolution of the raw spectrum provided clear indication of the components of the Cu(I) reconstituted MymT as presented in Figure 6.3B.

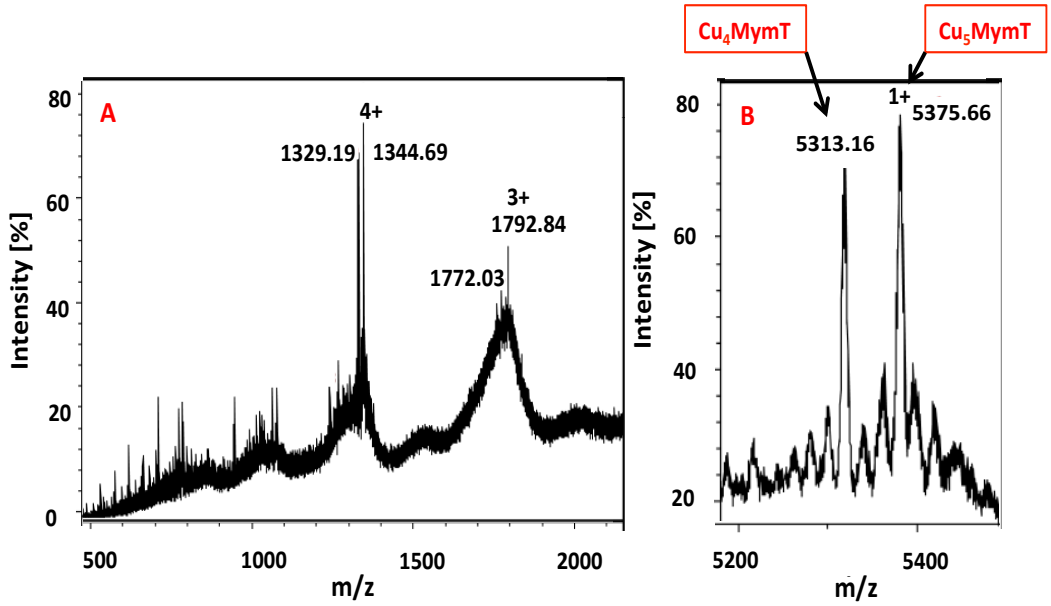

Figure 6.3 ESI-MS of Cu(I) reconstituted MymT.

(A) Full scan ESI-ToF-MS spectrum shows charge state species of Cu(I) reconstituted MymT prepared under strict anaerobic conditions. Deconvoluted spectrum for +1 masses of predominant species show MymT with five copper(I) ions bound along with four copper species. 25 μM of Cu-MymT sample was prepared anaerobically (glove box) in 10 mM ammonium bicarbonate buffer at pH 7.1.

After deconvolution of the charge states, two main peaks were observed for Cu(I) reconstituted MymT, as shown in Figure 6.3B. The most abundant signal in the spectrum of Figure 6.3 (B) had a respective mass of 5375.66 Da, which may correspond to Cu_5MymT with a theoretical mass 5375.3 Da. The mass of 5313.16 Da for the second most abundant species is close to the theoretical mass of 5313.6 Da for Cu_4MymT. The theoretical isotopic distribution was simulated

for one of the resulting Cu-loaded MymT species (Cu_5MymT, Figure 6.4B) and compared with its theoretical model as presented in Figure 6.4A.

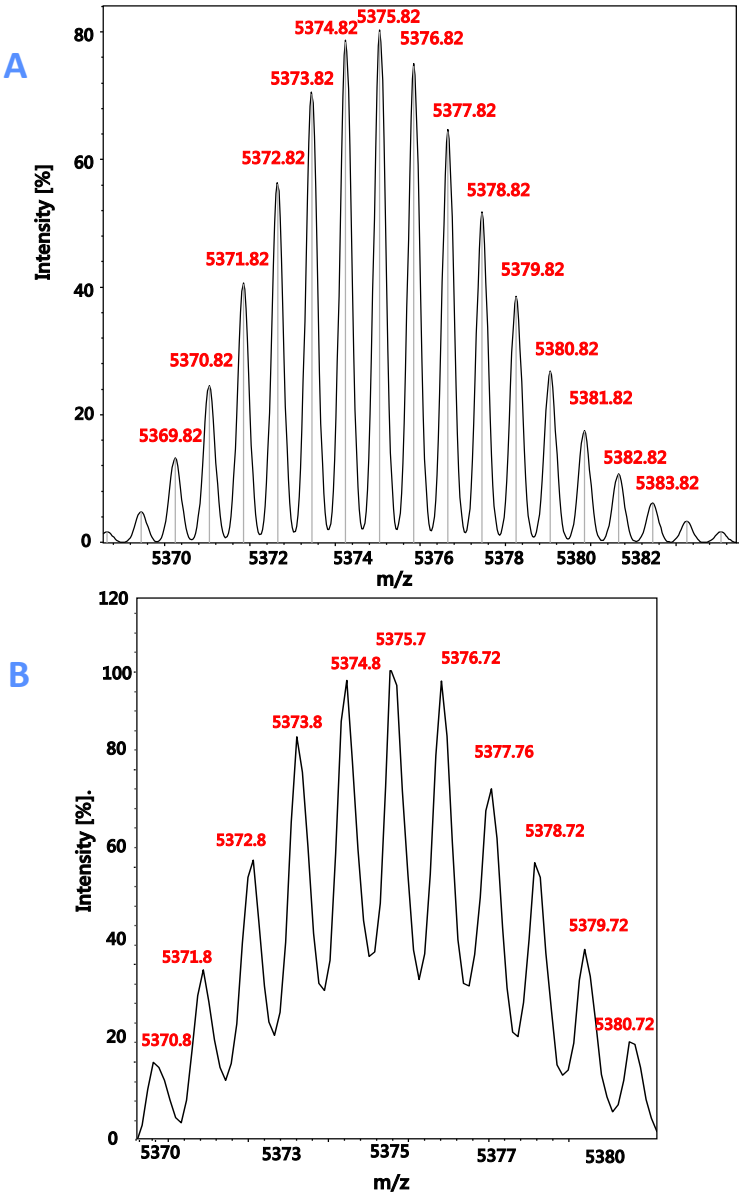

Figure 6.4 Deconvoluted ESI-TOF spectrum and isotopic pattern for Cu_5MymT.

(B) The isotopic distribution of the isotopic envelope at 5375.7 Da is shown together with a comparison to the (A) theoretical model ($C_{205}H_{327}N_{63}O_{69}S_8Cu_{5+}$). Both are for +1 species.

The molecular formula for Cu_5MymT is fully compatible with the Cu_5MymT experimental data. However, further analysis is essential to explore metal to protein stoichiometries quantitatively and identification of the most stable species.

6.3 Cu(I) titration of apo-MymT

ESI-MS is crucial for evaluating the metallation of MymT on Cu(I) addition. In this regard, apo-MymT was titrated with incremental addition of Cu(I) under strict anaerobic conditions at near neutral pH 6.9 and was analyzed via ESI-MS. Figure 6.5 displays the +4 charge state from mass spectra of step-wise incremental addition of Cu(I) to apo-MymT acquired for the species observed.

The addition of the first equivalent of Cu(I) gave rise to a very prominent Cu_5-MymT species along with Cu_1MymT and apo-MymT. The two species, apo-MymT and Cu_5MymT, coexisted in solution at 1-4 equivalents, however the fourth equivalent of Cu(I) resulted in Cu_5MymT as the major species along with lower intensity peaks for apo-MymT, Cu_1MymT, and Cu_4MymT as shown in Figure 6.5. Addition of the fifth Cu(I) equivalent produced a range of species i.e., Cu_2MymT, Cu_4MymT, and Cu_5MymT, along with heavily loaded Cu_7MymT and Cu_8MymT. The much higher noise levels of this and the subsequent spectra may suggest the loss of sample at higher Cu(I):peptide ratios. This may be because of protein aggregation and/or air sensitivity. These samples were not tested by ICP-OES due to limited amount of sample. Although Cu_5MymT was the major and rather consistent species during the entire course of the Cu(I) titration, Cu_7MymT and Cu_8MymT were also detected after addition of six and seven equivalents of Cu(I). In contrast, the Cu_6MymT species was only abundant in one spectrum, after addition of 6 mol. eq, together with about the same amount of the Cu_4 species. The Cu_5 species is only a minor peak in this spectrum.

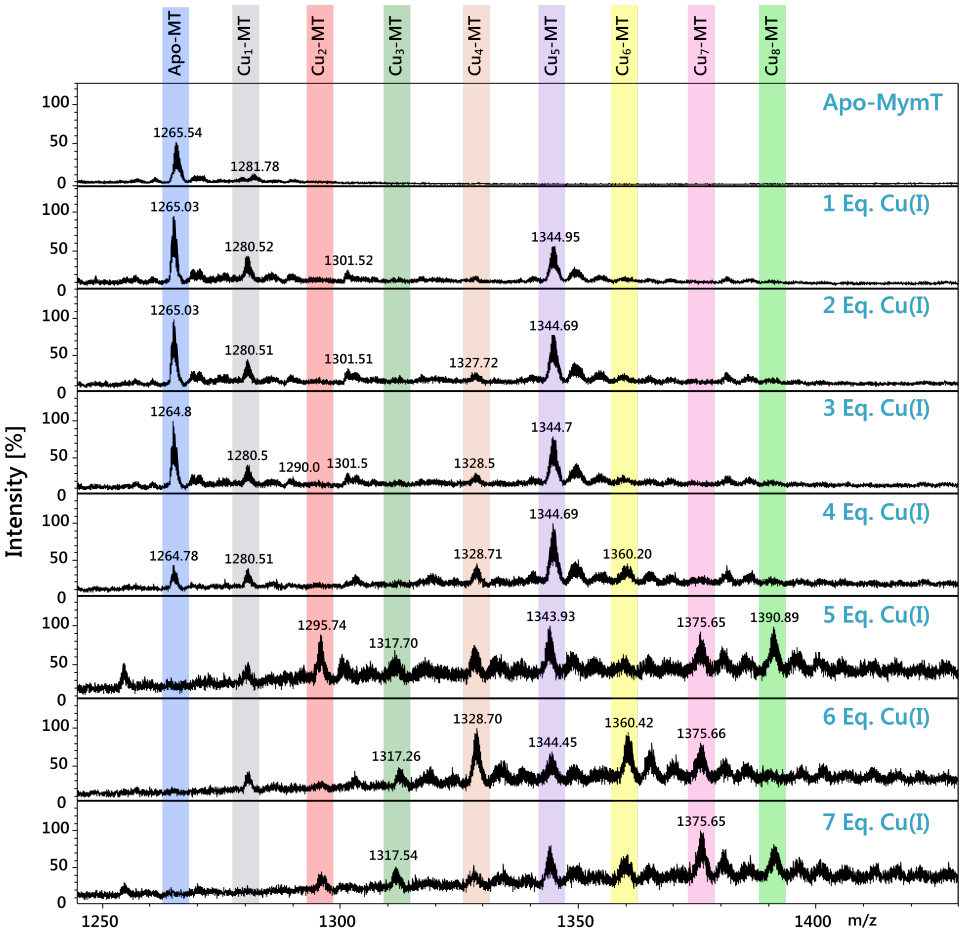

Figure 6.5 ESI-MS titration of MymT with Cu(I).

ESI mass spectra for titration of Apo-MymT (25 µM solution in 10 mM ammonium bicarbonate buffer with 10% methanol at pH 6.9) with Cu(I). Only the +4 charge state is shown. Aliquots of Cu(I) were added to the protein as 1, 2, 3, 4, 5, 6 and 7 equivalents. The colored blocks follow the metal binding and show the formation of new species with the addition of Cu(I). (Experimental and theoretical m/z values are provided in Appendix A9).

The most important observation resulting from these data was the cooperative formation of Cu_5MymT at Cu(I) to peptide ratios of 1-4:1. Cooperative binding is caused if the number of occupied binding sites of protein is a non-linear function of the metal's concentration that can be due to the affinity for the metal depending on the amount of metal bound. In this regard, Cu_5MymT already formed after addition of the first equivalent of Cu(I) and remained as the most dominant species until addition of five equivalents of Cu(I). However, some observations are difficult to understand, for example the remarkable decrease of the Cu_5 species in the spectrum

after 6 mol. eq. If this species has a special stability, as suggested by the data in the preceding spectra, then its low abundance in the presence of significant and almost equal quantities of the Cu_4 and the Cu_6 species is distinctly odd, as the latter two could "combine" to form similar amounts of the Cu_5 species. It may be that there were unknown problems or differences with either preparation or measurement for this sample.

The titration data acquired here may be compared with previous work on synthetic MymT titrated with Cu(I) (Gold et al. 2008). The data reported here differ from the previous work in the points presented in Table 6.1.

Table 6:1 Comparison of metal to peptide ratio of present study and published ESI-MS data.

The formation (with metal to peptide ratios) of the species formed in the present study can be compared to the species reported previously by Gold et al. 2008.

Cu(I) added	Present study	Published ESI-MS data
Low ratios	Dominance of Cu_5 species at 1-4 eq.	Dominance of Cu_4 species at 3 eq.
5 eq. of Cu(I)	2,3,4, 5, 7 and 8	-
6 eq of Cu(I)	4-7, dominant 4 and 6	4-6, 5 most abundant
7 eq. of Cu(I)	5, 7 and 8	4-6, 6 most abundant
10 eq. of Cu(I)	-	6,7

It is notable that also in the published spectra, an increase in noise is visible at higher Cu(I):peptide ratios. Some of the dominating species are observed in either study, but otherwise, there are some remarkable differences in the observed speciation: whilst in the present work, the Cu_5 species played a prominent role throughout, the Cu_4 species was more abundant at low ratios, and the Cu_6 was more abundant at higher ratios in the studies carried out by Gold et al.

Only one of the spectra here features a dominant Cu_6 species. Two of the spectra here feature the Cu_8 species (even at 5 mol.eq.), which was never observed in the previous study (Gold et al. 2008).

At this point, it is difficult to explain these discrepancies. The only notable difference in experimental conditions was the buffer used (10 mM NH_4HCO_3 in this study, and 50 mM NH_4Ac in the published study), and the instrumentation. These observations may serve as a caveat when using ESI-MS as the only technique.

6.3.1 Metal to Cysteine stoichiometry and histidine coordination

The stoichiometries of Cu-MTs have been problematic in the past. The stoichiometries of Cu_7- and Cu_8- have been debated for copper binding MT (Cup1) from *Saccharomyces cerevisiae*. Cup1 from *Saccharomyces cerevisiae* contains twelve cysteines accommodating eight Cu(I) ions in its Cu_8Cys_{12} metal cluster (Calderone et al. 2005) although there had been rather convincing previous evidence of Cu_7MT as a stable species from Ag_7MT and Cu_7MT structural data (Bertini et al. 2000).

A Cu_4 metal cluster was also observed in *Neurospora crassa* containing seven cysteine residues exclusively involved in metal coordination although Cu_6MT (Cu_6NcMT) was revealed as the main species (Cobine et al. 2004). Cysteine residues are the main contributors to the metal-thiolate interactions leading to formation of metal-clusters in all MTs along with involvement of histidine in some cases. The contribution of histidine ligands in stabilizing the metal cluster has been previously reported in cyanobacterial metallothionein SmtA with metal cluster $Zn_4Cys_9His_2$. Histidine residues in SmtA play important roles in stability of protein fold and reducing the charge of the metal cluster, and are involved in refining the reactivity of the bound metal ions (Blindauer et al. 2007).

However, the histidine residues in copper binding metallothioneins from yeast *Saccharomyces cerevisiae* and yeast *Candida glabrata* do not participate in metal ion coordination, establishing

the cysteine residues as sole coordinating residues (Berger et al. 1997, Bertini et al. 2000, Calderone et al. 2005). Nevertheless, the histidine residue in HpCuMT from *Helix pomatia* was reported to increase the copper binding ability of this particular CuMT, which may specify the role of histidine to enhance copper binding ability and copper release, essential for copper transfer to other biomolecules requiring copper (Pérez-Rafael et al. 2013). For Cu_5MymT, the metal cluster composition of Cu_5Cys_7 is proposed as seven cysteines are sufficient to bind five Cu(I) ions without involvement of His residues, as discussed below.

It is possible to predict the number of metal ions bound in fully loaded MT species from the number of ligands (Freisinger 2008), and in turn, it may be instructive to see whether the observed species are compatible with either Cys-only coordination or require the recruitment of His residues as well. Table 6.2 shows observed Cu:Cys ratio values for copper bound MTs.

Table 6:2 The metal ion contents of Cu containing MTs

Cu(I) to Cys ratio of copper binding metallothioneins calculated for experimentally observed metal-thiolate clusters.

Species	Metal cluster composition	Cu(I): Cysteine ratio	Reference
N. crassa	Cu_6Cys_7	1:1.2	Cobine et.al 2004
S. cerevisiae	Cu_8Cys_{12}	1:1.5	Calderone et.al 2005
C. sapidus	$Cu_{12}Cys_{21}$	1:1.75	Serra-Batiste et.al 2010
C. elegans			Bofill et. al 2009
CeMT-1	$Cu_8Cys_{19}His_4$	1:2.4	
CeMT-2	$Cu_8Cys_{18}His$	1:2.25	
Mouse Cu-MT	αCu_6Cys_{11}	1:1.5	Bofill et.al 2001
	βCu_6Cys_9	1:1.2	
Mouse MT-4	$Cu_{10}Cys_{20}$	1:2	Tio et. al 2004

Table 6.2 shows that Cu:Cys ratios vary from 1:1.2 (for true Cu-thioneins) up to 1:2.4.

MymT contains seven cysteines and two histidines, so nine potential ligands. For Cu_5MymT, the metal ion-to-cysteine ratio calculated for the M_5Cys_7 metal-thiolate cluster is 1:1.4 (based on 7 Cys), or 1:1.8 (based on 9 ligands). Both values are in principle within observed ranges, although this analysis indicates that it is not necessary to invoke His coordination for the Cu_5MymT species. For a Cu_6 species, the values are 1.2 for Cys-only coordination (the same ratio as for the *N. crassa* MT), or 1.5 for Cys+His coordination (i.e. the same value as for Cup1). Again, both modes are possible, but it is also clear that His is not strictly required in the Cu_6 species either. As evident from the Cu(I) reconstitution and ESI-MS data it may be concluded that MymT binds five Cu(I) ions in a relatively stable form, with a likely Cu_5Cys_7 metal cluster as proposed in Figure 6.6.

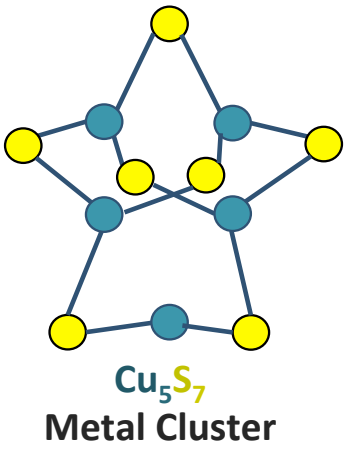

Figure 6.6 Metal cluster composition of MymT.

Geometrical model of the metal-sulfur framework for a Cu_5Cys_7 –cluster. Blue balls represent Cu(I) and yellow are for cysteine sulfurs. Both trigonal and linear coordination is possible.

6.4 Circular dichroism of Cu_5MymT

Circular dichroism (CD) was used as an independent method to check the holo protein conformation at lower concentrations. The CD spectrum of Cu_5MymT (Figure 6.7) shows a negative band at 197 nm and a slight positive band with a maximum at 230 nm (as shown in Figure 6.7), later as a result of tyrosine coupling. However, it was not possible to use standard secondary structure analysis for backbone CD.

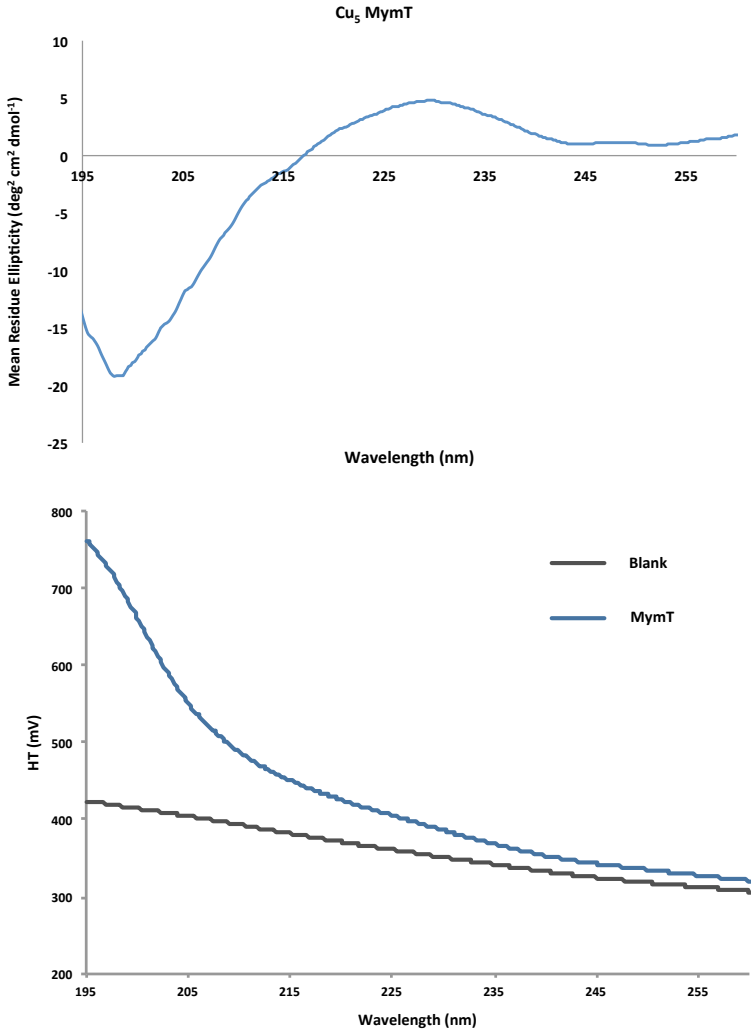

Figure 6.7 Far-UV region CD spectrum of Cu_5MymT.

CD spectrum of 100 μM Cu_5MymT in 5 mM Tris-Cl buffer, pH 7.1. Far-UV CD provides information on the environment of stereochemically active residues, which is important for assessing secondary structure contents.

6.5 NMR spectroscopy of MymT

MymT peptide was revealed to coordinate predominantly five Cu(I) ions, likely by seven cysteinyl sulfurs as described in the previous sections (6.2 and 6.3), but the involvement of histidine residues in metal coordination of this particular MT is not fully explored as yet. ^{1}H NMR studies are a prerequisite for structural work and may also aid in answering question of His contribution in metal coordination; therefore attempts were made to study Cu(I)-reconstituted MymT by ^{1}H NMR spectroscopy.

6.5.1 1D ^{1}H NMR of Cu_5MymT

1D ^{1}H NMR of Cu(I) reconstituted MymT at 35 °C showed a mixture of sharp and broad peaks as shown in Figure 6.8B, which suggests a partially folded structure when compared to, for example, the spectrum for folded Cd_4SmtA (Figure 6.8A). By using the chemical shifts for the NH and methyl groups, the protein fold can be assessed. For example, “ring current shifts” are caused when the methyl groups are shifted from their random coil position via spatially close aromatic groups, although in the case of MTs with fewer aromatic residues (Phe, Tyr and Trp) it is harder to assess the fold by methyl group dispersion. The backbone amide protons (NH) are shifted up-field or down-field through hydrogen bonding, depending on secondary structure. Compared to alpha helices, the hydrogen bonding is stronger in beta sheets, and amide protons are shifted further away (downfield) from the random coil shifts.

In the 1D ^{1}H NMR spectrum of Cd_4SmtA all peaks are sharp and fully resolved compared to that of Cu_5MymT spectrum (Figure 6.8B). This may lead to the conclusion that the present Cu_5MymT has at best a partially folded structure and lacks secondary structure elements, which is not unusual for MTs.

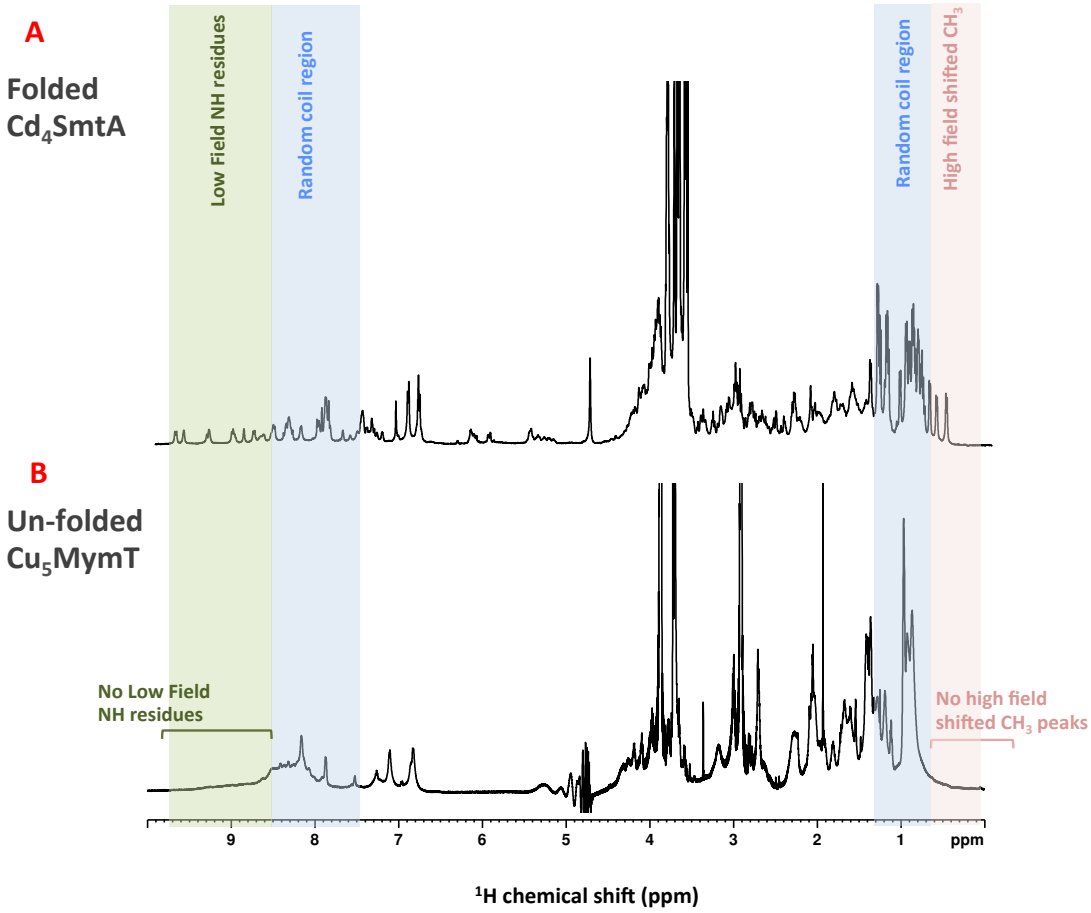

Figure 6.8 1D ^{1}H NMR spectra for folded Cd_4SmtA and Cu_5MymT

1D ^{1}H NMR spectra for A) folded Cd_4SmtA and B) structurally disordered Cu_5MymT displaying the broadness of peaks and lack of dispersion in Cu5MymT spectrum. The NH chemical shifts between ca. 7.5-8.5 ppm and methyl groups between 0.8–1.2 ppm are highlighted and can be used to qualitatively assess the "foldedness" of a protein. The 1D ^{1}H spectrum of copper reconstituted MymT (Cu_5MymT) was recorded for a 0.5 mM sample in 50 mM Tris [D11], 50 mM NaCl, pH 7.4, on a 700 MHz spectrometer (Bruker, Avance II) at 35 °C. MymT contains one tyrosine residue, any other aromatic proton peak will be due to the presence of the two histidine residues.

6.5.1.1 Effect of temperature

In order to improve the resolution and gain more information from the spectra, 1D ^{1}H NMR spectra were recorded at various temperatures ranging from 10 °C to 45 °C. This is also helpful to explore whether altering temperatures improves spectral quality. Temperature will have an effect on the tumbling rate, but also other motions, and N-H/H_2O exchange, and may also have an influence on protein folding behaviour.

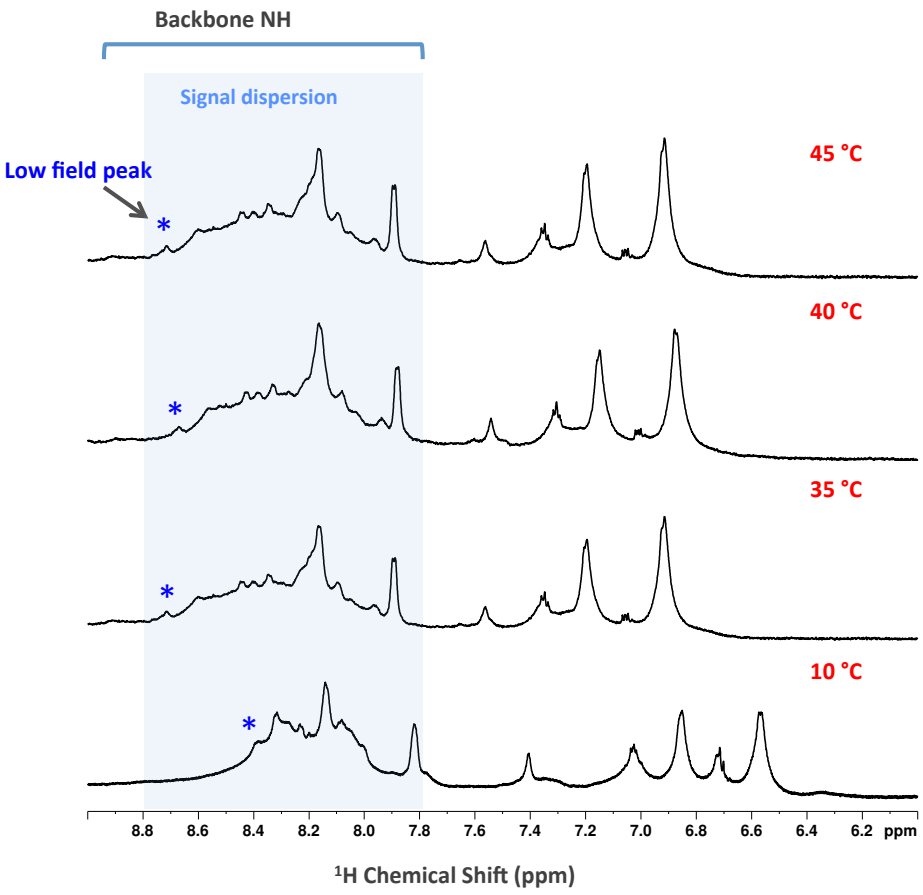

Figure 6.9 Stacked plot of 1D ^{1}H NMR spectra showing the fingerprint region of Cu_5MymT at varying temperatures.

A 0.5 mM sample was prepared in 50 mM Tris [D11], 50 mM NaCl with 10% D2O at pH 7.4 and spectra were recorded on 700 MHz Spectrometer (Bruker, Avance II) at varying temperatures from 10 °C to 45 °C. Asterisks shows a shifting low-field peak. It is clear that at higher temperatures, the dispersion is somewhat better but there is no improvement on intensity of signals.

From the spectra obtained (Figure 6.9) it was observed that there was relatively little improvement in resolution between 45 °C and 35 °C with the peak width at half height (measured on the 6.92 ppm peak) being 34.52 Hz at 45 °C, 35.75 Hz (6.87 ppm) at 40 °C. At 35 °C, it was not possible to measure the width of this peak, as a second peak overlapped with it, but qualitatively, it did not broaden significantly.

A difference was observed though when going from 35 °C to 10 °C where the resolution was seen to decrease slightly. At 10 °C there were also some new peaks around 6.7 ppm but in contrast less dispersion of backbone NH region of spectrum as shown in Figure 6.9. Due to instrument limitations it was not possible to acquire spectra at higher (than 45 °C) or lower (than 10 °C) temperatures. Since prolonged periods of temperature higher than 35 °C can compromise the performance of the cryo-probe, all experiments were performed at a temperature of 35 °C.

6.5.1.2 Cu(I) titration of MymT

Another preliminary 1D ^{1}H NMR experiment was done in order to directly investigate the effect of Cu(I) on protein folding. For this purpose, Cu(I) was added incrementally to apo-MymT and 1D ^{1}H NMR spectra were acquired after each addition. The backbone NH regions of the resulting spectra are shown in Figure 6.10. The addition of Cu(I) causes significant line broadening.

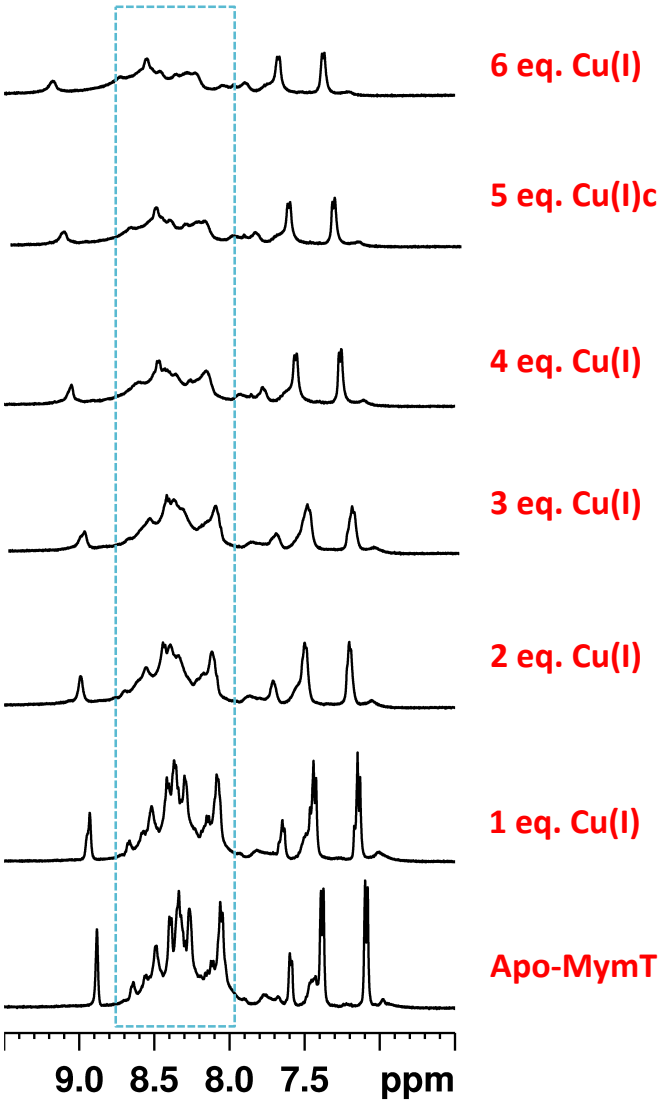

Figure 6.10 1D ^{1}H NMR spectra of stepwise addition of Cu(I) to MymT.

Stack of 1D ^{1}H NMR spectra of incremental addition of Cu(I) to apo-MymT. The 0.5 mM sample was prepared in 50 mM Tris [D11], 50 mM NaCl with 10% D2O (pH 7.4), recorded on 500 MHz Spectrometer (Bruker, Avance II) at 35 °C. The whole molecule seems to be affected by Cu(I) addition with the decrease in both signal dispersion and spectra quality with the increasing amounts of Cu(I). The most prominent region is highlighted and show the random coil shifts of backbone protons.

There is a difference of concentration when comparing ESI-MS and 1D NMR samples, but considerable information can be gained by combining information from the two techniques. ESI-MS revealed the presence of more than one species (apo-, Cu_1- and Cu_5) after addition of the

first Cu(I) equivalent; therefore, it can be assumed that the NMR spectrum recorded at this ratio may also pertain to a mixture of species. Similar considerations can be made for other Cu(I):protein ratios. Since however the 1D NMR spectra do at no point reveal the presence of two or three different sets of peaks, their appearance indicates intermediate to fast exchange, as judged from the increase in line broadening with increasing Cu(I) equivalents. It is likely that several exchange processes overlap, including exchange between differentially metallated species, and configurational and conformational exchange within particular metallospecies (Faller et al. 1999, Roschitzki and Vašák 2002, Faller 2010).

6.5.2 2D ^{1}H NMR of Cu_5MymT

2D ^{1}H-^{1}H TOCSY and ^{1}H-^{1}H NOESY were employed that may provide further information on protein folding and may also allow to give insight into side chain properties. A 2D TOCSY spectrum of reconstituted Cu_5MymT contains peaks for backbone and side chain NH protons in the random coil region along with α- and β-H protons as shown in Figure 6.11.

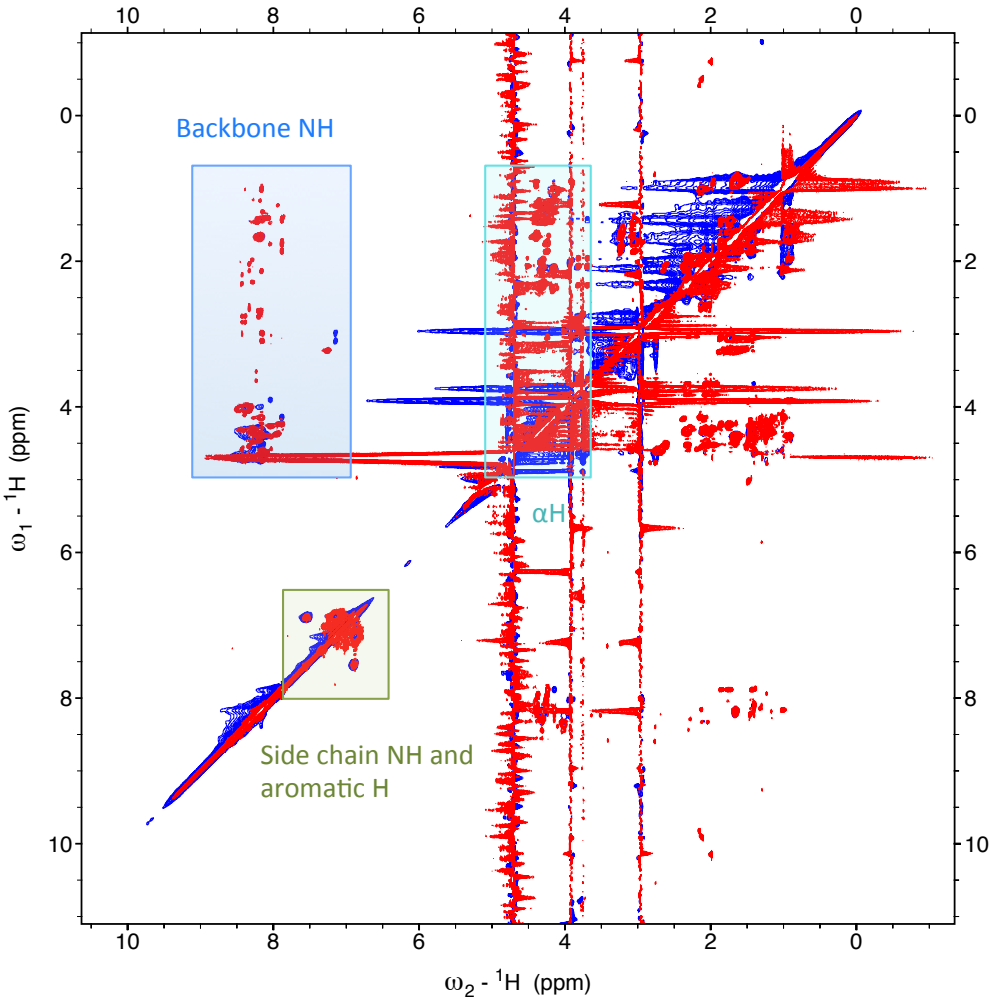

Figure 6.11 2D ^{1}H-^{1}H NMR of Cu_5MymT.

An overlay of 2D ^{1}H-^{1}H TOCSY (red) and NOESY (blue) spectra of Cu_5MymT. The 0.5 mM sample was prepared in 50 mM Tris [D11], 50 mM NaCl with 10% D2O at pH 7.4 and spectra were recorded on 700 MHz Spectrometer (Bruker, Avance II) at 35 °C.

In total, the number of amino acid resonances observed in the 2D TOCSY spectrum was 15, all in the random coil region, which is only a fraction of the number of expected resonances i.e., 48 residues minus 3 = 45 (N-terminus and two prolines). Figure 6.12 A shows the fingerprint region of overlaid 2D TOCSY and NOESY spectra of Cu_5MymT with the illustration of each type of spin system.

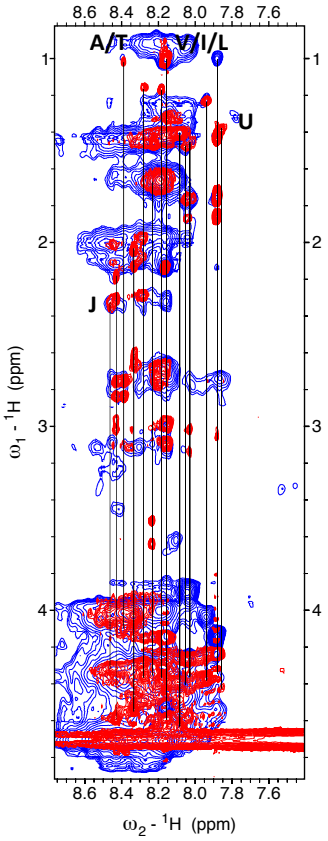

A

MTNYEAGTLLTCSHEGCGCRVRIEVPCHCAGAGDAYRCTCGDELAPVK

B

Spin System	Amino Acids
A/T	Ala, Thr
G	Gly
J	Cys, Ser, His, Asn, Asp, Tyr
V/I/L	Val, Ile, Leu
U	Lys, Arg, Met, Gln Glu

Figure 6.12 Spin system identification.

(A) Overlay of finger print region of ^{1}H-^{1}H TOCSY (red) and NOESY (blue) spectra of Cu_5MymT and (B) Spin system types and corresponding amino acids along with sequence of MymT. A total of 8 peaks belonging to J-type spin system may be identified. Peaks for spin systems A/T and U may also be observed.

Very few peaks (~15) along with sidechain NH for Asn and aromatic H for Tyr can be detected in the TOCSY and NOESY spectra of Cu_5MymT.

The side-chain cross-peak patterns suggest the presence of several type J residues (any residue with a CH_2-R group, i.e. Cys, His, Ser, Asx, Tyr, Phe, Trp), several Type U residues (longer alipahtic side chains, e.g. Lys, Glx, Arg), indications for Val/Ile/Leu as well as Ala and Thr. Except for a sequential cross peak between the C-terminal Val47 and Lys48, sequential assignments were not possible due to lack of dispersion and lack of NOESY cross peaks.

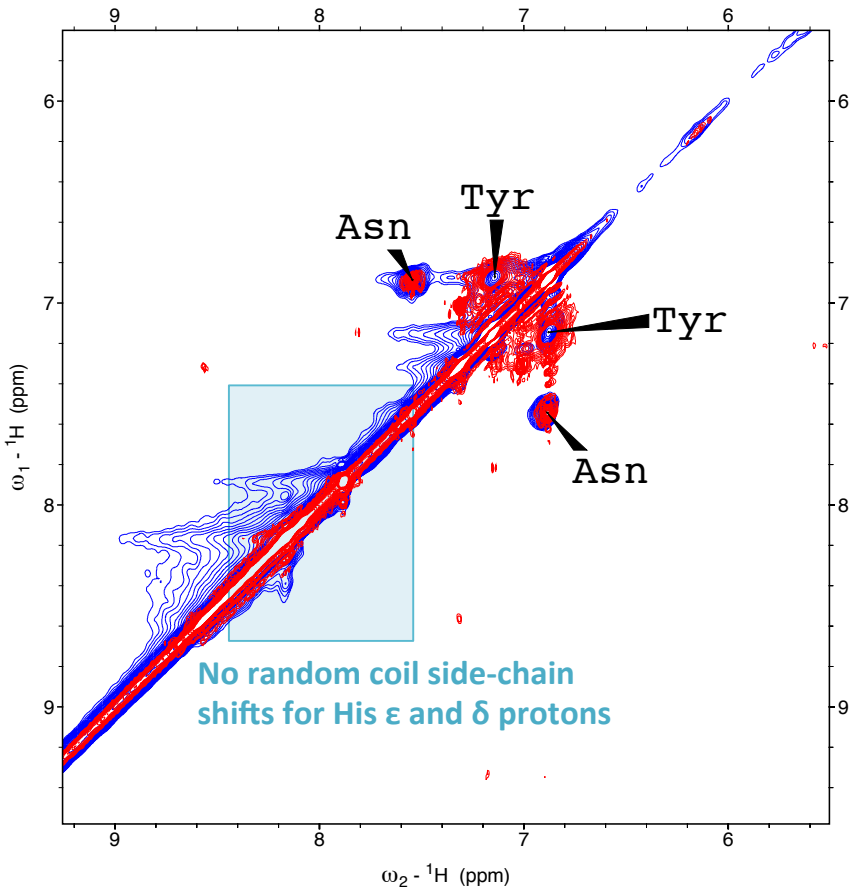

Figure 6.13 Side chain NH and aromatic H in 2D NMR.

Overlay of ^{1}H-^{1}H TOCSY (red) and NOESY (blue) spectra of Cu_5MymT showing the region for aromatic and NH side chains. However no His residues are observed.

There are two Tyr residues and one Asn residue in the MymT sequence. Only one set of cross peaks likely to pertain to Tyr δ and ε protons was observed, indicating a lack of dispersion due to not experiencing different chemical environments. However, due to the essential absence of relevant NOESY cross peaks, it is not possible to assign any connectivities between residues.

Resonances for His aromatic protons, whether metal-bound or not, are usually sharp and readily identifiable even in a 1D spectrum (e.g., His peak at 7.023 ppm in 1D ^{1}H NMR Cd_4SmtA spectrum, Figure 6.8). Inspection of the region for aromatic side-chain protons of 2D TOCSY and NOESY spectra did not reveal any cross-peaks pertaining to δ and ε protons of His residues. (typical

shifts of ~7.1 and 8.1 ppm, respectively). It is likely that these resonances are broadened beyond detection, and this in turn may indicate that they are at least temporarily interacting with metal ions.

From the titration data (Figure 6.10) it can be assumed that the presence of Cu(I) led to conformational changes of the peptide fold, but both 1D and 2D NMR data indicate that the molecule, at least under the present conditions, is too dynamic for structural studies as revealed by 1D NMR Cu(I) titrations.

6.6 Competition experiment with BCS

The displacement of copper ions by BCS was followed by the increase in absorbance due to formation of the $Cu(BCS)_2$ complex at 483 nm. Under these conditions where the BCS concentration is stoichiometric with respect to Cu (2 fold excess of BCS over protein-bound Cu), the reaction is extremely slow since the absorbance continues to increase steadily even after 5 hours as shown in Figure 6.14.

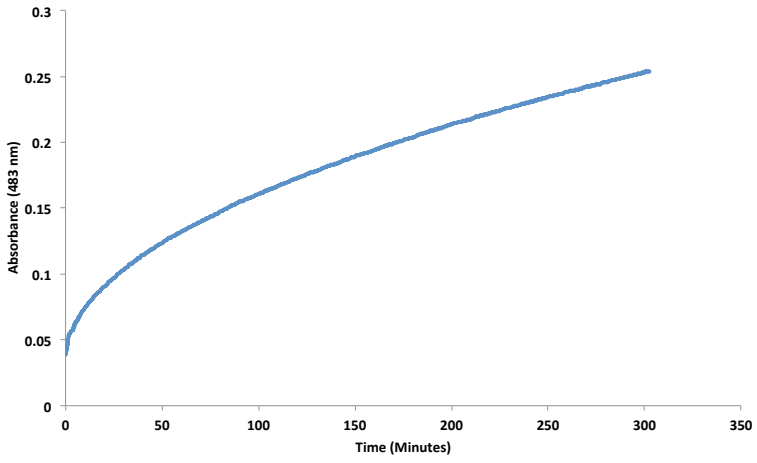

Figure 6.14 The dynamics of Cu exchange in MymT.

Time course of Cu exchange between Cu_5MymT and BCS observed by the formation of $Cu(BCS)_2$ at 483 nm. The experiment was carried out in 25 mM Tris-Cl, pH 7.1.

It is however clear that BCS is capable of abstracting Cu(I) from the protein. Further work witll be required to assess both thermodynamic and kinetic properties of MymT-boud Cu(I).

6.7 Summary and conclusion

Cu(I)-reconstituted MymT was prepared and preliminary characterization was done. The reconstitution of MymT produced predominantly Cu_5MymT along with a minor Cu_4MymT species. The cooperative formation of Cu_5MymT, even at sub-stoichiometric ratios, was revealed by titration studies followed by ESI-MS. However, Cu_6, Cu_7 and Cu_8 species were also observed in the later stages of titrations (at 5-7 Cu(I) equivalents). Although the role of histidine residues in Cu(I) binding could not be revealed, the metal cluster composition of Cu_5Cys_7 is proposed for MymT, since coordination to all seven Cys residues is sufficient to bind five Cu(I) ions with a metal to Cys ratio of 1:1.4. 1D and 2D ^{1}H NMR spectra indicated disordered protein structure with almost all amino acid residues within random coil region. 2D TOCSY and NOESY made it possible to identify resonances of backbone NH of 15 residues along with two sets for side chains of Asn and Tyr, but no clear peaks for His aromatic protons. Broadening of proton signals and lack of dispersion did not allow significant information to be gained for metal binding residues (Cys and His) in the ^{1}H-NMR studies. CD spectroscopy confirmed random coil fold for Cu_5MymT as suggested by NMR data.

One of the most important factors may still be the sample preparation method. Although the sample was prepared anaerobically, there may still be the possibility of oxidization or paramagnetism caused by resulting Cu(II) in the solution leading to broadness of signals in the NMR spectra. There is however still the possibility that a better-folded, and/or less dynamic protein can be obtained by changing the buffer composition and pH. The exchange rate of NH protons with bulk water is pH dependent and upon lowering the pH, more protons may show slow-exchange behaviour.

7

Conclusions and Future work

7.1 Summary of observations

7.1.1 Preparation of Cu(I)-MTs

The reconstitution method for Cu(I) binding to MT was developed and successfully employed on Zn_4SmtA as described in chapter 3. This proved to be challenging because of the air sensitivity of Cu(I) and apo-SmtA. However, this was overcome through the use of an inert atmosphere glove box and ensuring all sample preparation stages were carried out under strict anaerobic conditions. The successful reconstitution of apo-SmtA produced monomeric Cu_7SmtA as the predominant species. The comparison of the isotopic distribution model of Cu_7SmtA was compared to its theoretical model, which further confirmed Cu_7SmtA as a fully loaded species and the involvement of all 9 cysteine residues in Cu(I) binding was proposed.

Cu_7SmtA was further characterized for its stability and metal release. From ESI-MS spectra obtained, it was revealed that once formed, Cu_7SmtA, is moderately air-stable for up to three hours and only degraded significantly afterwards. The degradation of the sample was

very clear with lower signal to noise ratio in the ESI-MS spectrum acquired after four hours of air exposure.

To study the metal release kinetics of Cu_7SmtA, it was reacted with the Cu(I) chelator BCS. This reaction displayed biphasic reaction characteristics and contained both fast and slow reaction rates with corresponding rates of 5.3×10^{-3} and 6.9×10^{-4} s^{-1}. However, site-specific metal release and effects of Cu(I) binding on protein fold were not established by these studies. 1D and 2D ^{1}H NMR spectroscopy techniques were used for this purpose. A 1D ^{1}H NMR spectrum of Cu_7SmtA showed shifting of backbone NH peaks towards random coil region which indicates that Cu(I) binding had a very strong effect on the protein fold resulting in the formation of a disordered structure. The absence of high-field shifted CH_3 peaks and low-field NH peaks further confirmed the presence of an unfolded structure.

To further investigate the residues specifically involved or effected in Cu(I) binding 2D ^{1}H-^{1}H TOCSY and NOESY NMR spectra were acquired for Cu_7SmtA. Both spectra produced a number of cross peaks corresponding to J-type spin system. The NH_2 and aromatic side chain protons of Asn and Tyr residues displayed prominent cross peaks, but lacked dispersion. A total of 9 residues were spotted in the fingerprint region of the TOCSY spectrum. However, it was not possible to assign the residues in the fingerprint region due to a scarcity of corresponding cross-peaks in NOESY spectra. There was an interesting finding of some less disordered residues, potentially pertaining to the sequence N17-V18-D19-P20-S21, which is a short β strand followed by a loop. This region is distant from the metal binding cluster and may order itself independent of the metal present in the structure. The CD spectrum of Cu_7SmtA also supported the NMR result of a disordered structure with CD band characteristic of a random coil.

7.1.2 Zn-thionein character of Zn_4SmtA

SmtA was expressed in the presence of Zn and Cu, which resulted in the lower cell growth upon Cu addition to media. The gel filtration (SEC) chromatogram from the Cu containing media revealed a low intensity peak at the elution volume appropriate for SmtA, The fractions from FPLC were analyzed by ICP-OES, which gave rise to a protein to Zn ratio of 1:3.8 (based on 9 sulfurs pe protein) with the absence of Cu that further confirmed the Zn-thionein character of SmtA.

7.1.3 Metal exchange reactions of Zn_4SmtA: Stoichiometries

The incremental addition of Cu(I) to Zn_4SmtA showed the binding of up to eight metal ions to SmtA, although the closeness of the masses of zinc and copper did not allow an unambiguous identification of the species formed. Table 7.1 summarizes the species observed in ESI-MS titrations of equimolar addition of Cu(I) to Zn_4SmtA.

Table 7:1 Speciation of Zn_4SmtA on Cu(I) addition

Summary of the species formed after Cu(I) addition to Zn_4SmtA analyzed by ESI-MS (pH6.9)

	Cu(I) equivalents added								
	0	1	2	3	4	5	6	7	8
M1	-	-	-	-	-	-	-	-	
M2	-	-	-	-	-	-	-	-	
M3	-	-	-	-	-	-			
M4			-	-	-	-	-	-	-
M5	-				-	-	-	-	-
M6	-	-							-
M7	-	-	-	-					-
M8	-	-	-	-					-
Oxidized	-	-	-	-	-	-	-	-	

7.1.3.1 Characterization of metal clusters

In order to help with distinguishing the composition of mixed Zn, Cu clusters in SmtA, two further ESI-MS titrations were carried out: titration of Zn_4SmtA with Ag(I) instead of Cu(I), and titration of Cd_4SmtA with Cu(I).

Table 7.2 summarizes the results from the titration with Ag(I). The formation of mixed metal species with Zn_2Ag_4 and Zn_1Ag_7 (M_6 and M_8 metal species) composition was established as most abundant species.

Table 7:2 Metal to protein stoichiometries

Summary of the species formed after Ag(I) addition to Zn4SmtA analyzed by ESI-MS (pH6.9)

Metal cluster composition	Ag(I) equivalents added										
	0	0.5	1	2	3	4	5	6	7	8	9
Zn_4MT	▲	▲	▲	▲	▲	▲	▲	-	-	-	-
Ag_2Zn_3-MT	-	◆	◆	◆	◆	◆	◆	-	-	-	-
Ag_3Zn_2-MT	-	⬠	⬠	⬠	⬠	⬠	⬠	-	-	-	-
Ag_3Zn_3-MT	-	-	○	○	○	○	○	○	-	-	-
Ag_4Zn_2-MT	-	-	-	⬭	⬭	⬭	⬭	⬭	⬭	-	-
Ag_6Zn_1-MT	-	-	-	▱	▱	▱	▱	-	-	-	-
Ag_7Zn_1-MT	-	-	-	⬢	⬢	⬢	⬢	⬢	⬢	-	-
Ag_9-MT	-	-	-	-	-	-	-	-	-	⬢	
Ag_{10}-MT	-	-	-	-	-	-	-	-	-	⬢	⬢

Although Zn(II) was eventually completely replaced by Ag(I), the persistence of the Zn_1 species suggests that at least in the highly-loaded M_7 and M_8 species, some inertness is retained. The remaining last Zn in the cluster may correspond to the zinc finger site A, which has previously been shown to be inert towards metal exchange, and holds the protein structure together.

Since Cd_4SmtA has been previously shown to have a similar structure like the native Zn_4SmtA form, it was also analyzed for its Cu(I) binding ability and also to explore the

inertness of site A for metal exchange. Cu(I) did replace Cd(II) from the protein completely towards the end point of the titrations, suggesting that mixed Cu(I),Cd(II) clusters in SmtA did not contain an inert site. Notably, no Cd_1Cu_6 or Cd_1Cu_7 species were observed, contrasting with the Ag/Zn data.

Both Cd/Cu and Zn/Ag titrations indicated that there were several M_5 and M_6 species, namely $M(II)_3M(I)_2$ and $M(II)_2M(I)_3$ for M_5, and $M(II)_3M(I)_3$ and $M(II)_2M(I)_4$ for M_6. Whether the M_7 species in the Zn/Cu titration pertains to Cu_7 (as observed in the Cd/Cu data), or Zn_1Cu_6 (as observed in the Zn/Ag data), remains unresolved.

The impact of Cu(I) incorporation into SmtA was further analyzed by titrations followed by 2D ^{1}H-^{15}N and (1D, 2D) ^{111}Cd NMR spectroscopy.

7.1.4 Structural effects of metal exchange

The Cu(I) titration of Zn_4SmtA monitored by $^{1}H–1^{5}N$ 2D NMR revealed the loss of protein fold upon the addition of the fourth equivalent of Cu(I), although at lower ratios, the formation of one or more new folded heterometallic species along with presence of Zn_4SmtA was also observed. However, the complete loss of resolved resonances at seven Cu(I) was consistent with the full replacement of Zn(II). $^{1}H/^{111}Cd$ NMR was used to explore the site specific replacement of Cd(II) from Cd_4SmtA. Sub-stoichiometric quantities of Cu(I) selectively displaced Cd(II) from site B, likely forming a Cd_3Cu_2 and/or a Cd_3Cu_3 species (as suggested by ESI-MS) which were not distinguishable by 1D or 2D ($^{1}H,^{111}Cd$ HSQC) data. The MS analysis also suggested formation of a Cd_2Cu_4 species, but no specific information on this species could be derived from either 1D or 2D ($^{1}H,^{111}Cd$ HSQC) NMR data either, although the presence of one or more high-field-shifted peak around 570 ppm was evident. Both ESI-MS and NMR titrations indicated that neither Zn- nor Cd-based clusters retained an inert site upon replacement with Cu(I).

In summary, it has been established by these studies that SmtA is a Zn-thionein and addition of Cu(I) causes major changes within the structure. The necessary rearrangements results in the formation of a predominantly disordered structure, which is evident from the ^{1}H-^{15}N 2D NMR data as well as the 2D ^{1}H NMR data of reconstituted Cu_7SmtA.

7.1.5 Reconstitution and characterization of MymT

In chapter 6, the reconstitution of metallothionein MymT with Cu(I) and its characterization for its metal cluster composition and protein fold was reported. The anaerobic reconstitution with Cu(I) produced predominantly Cu_5MymT. The cooperative formation of Cu_5MymT was revealed by incremental addition of Cu(I) to the apo-MymT peptide when the species formed were monitored by ESI-MS. This confirmed the composition of the Cu_5Cys_7 metal cluster with a metal to cysteine ratio of 1:1.4, with cysteine sufficient as the sole contributor to metal binding.

The addition of Cu(I) to MymT caused signal broadening and a loss of dispersion in 1D ^{1}H NMR spectra. 2D ^{1}H NMR spectra showed only few cross-peaks for residues, mostly in the random coil region. A total of ^{15}NH resonances were identified for this protein. The CD spectrum of Cu_5MymT was consistent with a random coil structure. In consequence, the distribution of metal in protein fold was not established by the present data and further work is necessary to fully explore the structure of MymT.

7.2 Future directions

7.2.1 SmtA: Characterization of heterometallic species

There is much evidence present for a Zn-thionein character of SmtA, so the characterization and structure determination of corresponding heterometallic species will give deeper insight into the structural consequences of Zn(II)/Cu(I) replacement. The 2D NMR TOCSY was acquired for heterometallic (Cd_3Cu_2, Cd_3Cu_3)- SmtA and data displayed a mostly folded

protein with reasonable signal dispersion in the finger print region. Peaks were already assigned to the TOCSY spectrum but it would be desirable to acquire the corresponding 2D NOESY spectrum of the same species. This would help in the structure determination of such mixed metal species. In addition, the modeling of the mixed species may provide some information on their biological relevance.

The Cu(I) reconstitution method is now established in the laboratory, and hence can be applied to any MT where there is physiological room for studying Cu(I) binding.

7.2.2 MymT: A new insight into macrophage resistance

7.2.2.1 Expression construct

The present studies of MymT were carried out on synthetic peptide, however, for further characterization and structure elucidation, in particular, the synthesis of the corresponding expression construct would be highly desirable. Furthermore, once the expression construct is available, it would facilitate to establish the Cu-thionein character of protein, in terms of studying expression and "in vivo" (in the heterologous host *E. coli*) metallation in the presence of different metal ions (as shown for SmtA in Chapter 3). In addition, it will also allow the expression of MymT in isotopically labelled minimal media, which is critical for NMR sample preparation and essential for structural determination of MymT.

7.2.2.2 NMR structure elucidation of MymT

The change and optimisation of MymT sample preparation of conditions such as pH, salt concentration, different NMR buffers and acquiring NMR at higher or lower temperatures to stabilize protein fold is necessary in ^{1}H-^{1}H NMR analyses. Solid state NMR of MymT may be another possibility to avoid the fast solution state dynamics of this MT.

8

References

Aggett, P. J. (1999). "An overview of the metabolism of copper." *Eur J Med Res* **4**(6): 214-216.

Akashi, K., N. Nishimura, Y. Ishida and A. Yokota (2004). "Potent hydroxyl radical-scavenging activity of drought-induced type-2 metallothionein in wild watermelon." *Biochem. Biophys. Res. Commun.* **323**(1): 72-78.

Andersen, R. D. and U. Weser (1978). "Partial purification, characterization and translation in vitro of rat liver metallothionein messenger ribonucleic acid." *Biochem. J* **175**(3): 841-852.

Armitage, I. M., D. C. Dalgarno and B. A. Johnson (1987). "NMR analysis of the structure and metal sequestering properties of metallothioneins." *Experientia Suppl* **52**: 159–169.

Armitage, I. M., T. Drakenberg and B. Reilly (2013). "Use of (113)Cd NMR to probe the native metal binding sites in metalloproteins: an overview." *Met Ions Life Sci* **11**: 117–144.

Armitage, I. M., J. D. Otvos, R. W. Briggs and Y. Boulanger (1982). "Structure elucidation of the metal-binding sites in metallothionein by 113Cd NMR." *Fed Proc* **41**(13): 2974-2980.

Arseniev, A., P. Schultze, E. Worgotter, W. Braun, G. Wagner, M. Vasak, J. H. Kagi and K. Wuthrich (1988). "Three-dimensional structure of rabbit liver [Cd7]metallothionein-2a in aqueous solution determined by nuclear magnetic resonance." *J. Mol. Biol.* **201**(3): 637-657.

Artells, E., O. Palacios, M. Capdevila and S. Atrian (2013). "Mammalian MT1 and MT2 metallothioneins differ in their metal binding abilities." *Metallomics* **5**(10): 1397–1410.

Artells, E., O. Palacios, M. Capdevila and S. Atrian (2014). "In vivo-folded metal-metallothionein 3 complexes reveal the Cu-thionein rather than Zn-thionein character of this brain-specific mammalian metallothionein." *FEBS J.* **281**(6): 1659–1678.

Aschner, M. (1998). "Metallothionein (MT) isoforms in the central nervous system (CNS): regional and cell-specific distribution and potential functions as an antioxidant." *Neurotoxicology* **19**(4-5): 653-660.

Aschner, M. and A. K. West (2005). "The role of MT in neurological disorders." *J Alzheimers Dis* **8**(2): 139–145; discussion 209–115.

Babula, P., M. Masarik, V. Adam, T. Eckschlager, M. Stiborova, L. Trnkova, H. Skutkova, I. Provaznik, J. Hubalek and R. Kizek (2012). "Mammalian metallothioneins: properties and functions." *Metallomics* **4**(8): 739-750.

Banci, L., I. Bertini, F. Cantini, C. T. Chasapis, N. Hadjiliadis and A. Rosato (2005). "A NMR study of the interaction of a three-domain construct of ATP7A with copper(I) and copper(I)-HAH1: the interplay of domains." *J. Biol. Chem.* **280**(46): 38259-38263.

Banci, L., I. Bertini, F. Cantini and S. Ciofi-Baffoni (2010). "Cellular copper distribution: a mechanistic systems biology approach." *Cell. Mol. Life Sci.* **67**(15): 2563-2589.

Banci, L., I. Bertini, S. Ciofi-Baffoni, R. Del Conte and L. Gonnelli (2003). "Understanding copper trafficking in bacteria: interaction between the copper transport protein CopZ and the N-terminal domain of the copper ATPase CopA from *Bacillus subtilis*." *Biochemistry* **42**(7): 1939–1949.

Banci, L., I. Bertini, S. Ciofi-Baffoni, T. Kozyreva, K. Zovo and P. Palumaa (2010). "Affinity gradients drive copper to cellular destinations." *Nature* **465**(7298): 645-648.

Banci, L., I. Bertini, S. Ciofi-Baffoni, X. C. Su, G. P. Borrelly and N. J. Robinson (2004). "Solution structures of a cyanobacterial metallochaperone: insight into an atypical copper-binding motif." *J. Biol. Chem.* **279**(26): 27502-27510.

Banci, L., I. Bertini, C. Luchinat and M. Mori (2010). "NMR in structural proteomics and beyond." *Prog. Nucl. Magn. Reson. Spectrosc.* **56**(3): 247-266.

Banci, L., I. Bertini, K. S. McGreevy and A. Rosato (2010). "Molecular recognition in copper trafficking." *Nat. Prod. Rep.* **27**(5): 695-710.

Banci, L. and A. Rosato (2003). "Structural genomics of proteins involved in copper homeostasis." *Acc. Chem. Res.* **36**(3): 215-221.

Barnes, N., R. Tsivkovskii, N. Tsivkovskaia and S. Lutsenko (2005). "The copper-transporting ATPases, menkes and wilson disease proteins, have distinct roles in adult and developing cerebellum." *J. Biol. Chem.* **280**(10): 9640-9645.

Beltramini, M., K. Lerch and M. Vasak (1984). "Metal substitution of *Neurospora* copper metallothionein." *Biochemistry* **23**(15): 3422-3427.

Berger, B., R. Dallinger, P. Gehrig and P. E. Hunziker (1997). "Primary structure of a copper-binding metallothionein from mantle tissue of the terrestrial gastropod *Helix pomatia* L." *Biochem. J* **328 (Pt 1)**: 219-224.

Berson, G. (1983). "Silver staining of proteins in polyacrylamide gels: increased sensitivity by a blue toning." *Anal. Biochem.* **134**(1): 230-234.

Bertinato, J. and M. R. L'Abbe (2004). "Maintaining copper homeostasis: regulation of copper-trafficking proteins in response to copper deficiency or overload." *J Nutr Biochem* **15**(6): 316-322.

Bertini, I., H. J. Hartmann, T. Klein, G. Liu, C. Luchinat and U. Weser (2000). "High resolution solution structure of the protein part of Cu7 metallothionein." *Eur. J. Biochem.* **267**(4): 1008–1018.

Bertrand G. (1912) *8th Int. Congr. App. Chem*. New York.

Binz, P. A., J. H. R. Kägi (1999) “Metallothionein: Molecular evolution and classification”. In: Metallothionein IV (ed. CD Klassen), 7–13. Birkhäuser Verlage Basel.

Blindauer, C. A. (2008). "Metallothioneins with unusual residues: Histidines as modulators of zinc affinity and reactivity." *J. Inorg. Biochem.* **102**(3): 507-521.

Blindauer, C. A. (2011). "Bacterial metallothioneins: past, present, and questions for the future." *J. Biol. Inorg. Chem.* **16**(7): 1011–1024.

Blindauer, C. A. (2013). "Lessons on the critical interplay between zinc binding and protein structure and dynamics." *J. Inorg. Biochem.* **121C**: 145–155.

Blindauer, C. A., M. D. Harrison, J. A. Parkinson, A. K. Robinson, J. S. Cavet, N. J. Robinson and P. J. Sadler (2001). "A metallothionein containing a zinc finger within a four-metal cluster protects a bacterium from zinc toxicity." *Proc Natl Acad Sci U S A* **98**(17): 9593-9598.

Blindauer, C. A., M. D. Harrison, A. K. Robinson, J. A. Parkinson, P. W. Bowness, P. J. Sadler and N. J. Robinson (2002). "Multiple bacteria encode metallothioneinsand SmtA-like zinc fingers." *Mol. Microbiol.* **45**(5): 1421–1432.

Blindauer, C. A. and O. I. Leszczyszyn (2010). "Metallothioneins: unparalleled diversity in structures and functions for metal ion homeostasis and more." *Nat. Prod. Rep.* **27**(5): 720-741.

Blindauer, C. A., N. C. Polfer, S. E. Keiper, M. D. Harrison, N. J. Robinson, P. R. Langridge-Smith and P. J. Sadler (2003). "Inert site in a protein zinc cluster: isotope exchange by high resolution mass spectrometry." *J. Am. Chem. Soc.* **125**(11): 3226-3227.

Blindauer, C. A., M. T. Razi, D. J. Campopiano and P. J. Sadler (2007). "Histidine ligands in bacterial metallothionein enhance cluster stability." *J. Biol. Inorg. Chem.* **12**(3): 393-405.

Blindauer, C. A. and R. Schmid (2010). "Cytosolic metal handling in plants: determinants for zinc specificity in metal transporters and metallothioneins." *Metallomics* **2**(8): 510-529.

Boal, A. K. and A. C. Rosenzweig (2009). "Structural biology of copper trafficking." *Chem. Rev.* **109**(10): 4760-4779.

Bofill, R., M. Capdevila and S. Atrian (2009). "Independent metal-binding features of recombinant metallothioneins convergently draw a step gradation between Zn- and Cu-thioneins." *Metallomics* **1**(3): 229-234.

Bofill, R., M. Capdevila, N. Cols, S. Atrian and P. Gonzalez-Duarte (2001). "Zinc(II) is required for the in vivo and in vitro folding of mouse copper metallothionein in two domains." *J. Biol. Inorg. Chem.* **6**(4): 405-417.

Bofill, R., R. Orihuela, M. Romagosa, J. Domenech, S. Atrian and M. Capdevila (2009). "Caenorhabditis elegans metallothionein isoform specificity--metal binding abilities and the role of histidine in CeMT1 and CeMT2." *FEBS J.* **276**(23): 7040-7056.

Bofill, R., O. Palacios, M. Capdevila, N. Cols, R. Gonzalez-Duarte, S. Atrian and P. Gonzalez-Duarte (1999). "A new insight into the Ag+ and Cu+ binding sites in the metallothionein beta domain." *J. Inorg. Biochem.* **73**(1-2): 57-64.

Bordas, J., M. H. Koch, H. J. Hartmann and U. Weser (1982). "Tetrahedral copper-sulphur coordination in yeast Cu-thionein. An EXAFS study." *FEBS Lett.* **140**(1): 19-21.

Boulanger, Y., I. M. Armitage, K. A. Miklossy and D. R. Winge (1982). "113Cd NMR study of a metallothionein fragment. Evidence for a two-domain structure." *J. Biol. Chem.* **257**(22): 13717–13719.

Braun, W., M. Vasak, A. H. Robbins, C. D. Stout, G. Wagner, J. H. Kagi and K. Wuthrich (1992). "Comparison of the NMR solution structure and the x-ray crystal structure of rat metallothionein-2." *Proc Natl Acad Sci U S A* **89**(21): 10124–10128.

Braymer, J. J. and D. P. Giedroc (2014). "Recent developments in copper and zinc homeostasis in bacterial pathogens." *Curr. Opin. Chem. Biol.* **19C**: 59-66.

Bremner, I. and N. T. Davies (1976). "Studies on the appearance of a hepatic copper-binding protein in normal and zinc-deficient rats." *Br J Nutr* **36**(1): 101–112.

Bremner, I. and B. W. Young (1976). "Isolation of (copper, zinc)-thioneins from the livers of copper-injected rats." *Biochem. J* **157**(2): 517-520.

Breuker, K. and F. W. McLafferty (2008). "Stepwise evolution of protein native structure with electrospray into the gas phase, 10(–12) to 10(2) s." *Proc Natl Acad Sci U S A* **105**(47): 18145–18152.

Briggs, R. W. and I. M. Armitage (1982). "Evidence for site-selective metal binding in calf liver metallothionein." *J. Biol. Chem.* **257**(3): 1259–1262.

Brouwer, M., P. Whaling and D. W. Engel (1986). "Copper-metallothioneins in the American lobster, *Homarus americanus*: potential role as Cu(I) donors to apohemocyanin." *Environ. Health Perspect.* **65**: 93–100.

Bulheller, B. M., A. Rodger and J. D. Hirst (2007). "Circular and linear dichroism of proteins." *PCCP* **9**(17): 2020-2035.

Butcher, L. A. and J. K. Tomkins (1985). "A comparison of silver staining methods for detecting proteins in ultrathin polyacrylamide gels on support film after isoelectric focusing." *Anal. Biochem.* **148**(2): 384-388.

Byrd, J., R. M. Berger, D. R. McMillin, C. F. Wright, D. Hamer and D. R. Winge (1988). "Characterization of the copper-thiolate cluster in yeast metallothionein and two truncated mutants." *J. Biol. Chem.* **263**(14): 6688-6694.

Calderone, V., B. Dolderer, H. J. Hartmann, H. Echner, C. Luchinat, C. Del Bianco, S. Mangani and U. Weser (2005). "The crystal structure of yeast copper thionein: The solution of a long-lasting enigma." *Proc Natl Acad Sci U S A* **102**(1): 51-56.

Capasso, C., V. Carginale, O. Crescenzi, D. Di Maro, E. Parisi, R. Spadaccini and P. A. Temussi (2003). "Solution structure of MT_nc, a novel metallothionein from the Antarctic fish *Notothenia coriiceps*." *Structure* **11**(4): 435-443.

Capdevila, M. and S. Atrian (2011). "Metallothionein protein evolution: a miniassay." *J. Biol. Inorg. Chem.* **16**(7): 977-989.

Capdevila, M., O. Palacios and S. Atrian (2010). "The zn- or cu-thionein character of a metallothionein determines its metal load when synthesized in physiological (metal-unsupplemented) conditions." *Bioinorg Chem Appl*: 541829.

Cavet, J. S (2013) *Metals in Bacterial Pathogenicity and Immunity*. Encyclopedia of Inorganic and Bioinorganic Chemistry. 1–12.

Cavet, J. S., G. P. Borrelly and N. J. Robinson (2003). "Zn, Cu and Co in cyanobacteria: selective control of metal availability." *FEMS Microbiol. Rev.* **27**(2-3): 165–181.

Chan, T. W., L. Duan and T. P. Sze (2002). "Accurate mass measurements for peptide and protein mixtures by using matrix-assisted laser desorption/ionization Fourier transform mass spectrometry." *Anal. Chem.* **74**(20): 5282-5289.

Chang, K. C. and W. W. Yew (2013). "Management of difficult multidrug-resistant tuberculosis and extensively drug-resistant tuberculosis: update 2012." *Respirology* **18**(1): 8-21.

Chatterjee, D. (1997). "The mycobacterial cell wall: structure, biosynthesis and sites of drug action." *Curr. Opin. Chem. Biol.* **1**(4): 579-588.

Chatthai, M., K. H. Kaukinen, T. J. Tranbarger, P. K. Gupta and S. Misra (1997). "The isolation of a novel metallothionein-related cDNA expressed in somatic and zygotic embryos of Douglas-fir: regulation by ABA, osmoticum, and metal ions." *Plant Mol. Biol.* **34**(2): 243-254.

Chaturvedi, K. S. and J. P. Henderson (2014). "Pathogenic adaptations to host-derived antibacterial copper." *Front Cell Infect Microbiol* **4**: 3.

Chen, P., P. Onana, C. F. Shaw, 3rd and D. H. Petering (1996). "Characterization of calf liver Cu,Zn-metallothionein: naturally variable Cu and Zn stoichiometries." *Biochem. J* **317 (Pt 2)**: 389-394.

Chevallet, M., S. Luche and T. Rabilloud (2006). "Silver staining of proteins in polyacrylamide gels." *Nat Protoc* **1**(4): 1852–1858.

Chowdhury, S. K. and B. T. Chait (1990). "Analysis of mixtures of closely related forms of bovine trypsin by electrospray ionization mass spectrometry: use of charge state distributions to resolve ions of the different forms." *Biochem. Biophys. Res. Commun.* **173**(3): 927-931.

Chowdhury, S. K., V. Katta and B. T. Chait (1990). "Probing conformational changes in proteins by mass spectrometry." *J. Am. Chem. Soc.* **112**(24): 9012-9013.

Christen, Y. (2000). "Oxidative stress and Alzheimer disease." *Am. J. Clin. Nutr.* **71**(2): 621S-629S.

Cobine, P. A., G. N. George, D. J. Winzor, M. D. Harrison, S. Mogahaddas and C. T. Dameron (2000). "Stoichiometry of complex formation between Copper(I) and the N-terminal domain of the Menkes protein." *Biochemistry* **39**(23): 6857-6863.

Cobine, P. A., R. T. McKay, K. Zangger, C. T. Dameron and I. M. Armitage (2004). "Solution structure of Cu-6 metallothionein from the fungus *Neurospora crassa*." *Eur. J. Biochem.* **271**(21): 4213-4221.

Coleman, J. E. (1993). "Cadmium–113 nuclear magnetic resonance applied to metalloproteins." *Methods Enzymol.* **227**: 16-43.

Cousins, R. J. (1983). "Metallothionein--aspects related to copper and zinc metabolism." *J Inherit Metab Dis* **6 Suppl 1**: 15-21.

Crichton, R. R. and J. L. Pierre (2001). "Old iron, young copper: from Mars to Venus." *BioMetals* **14**(2): 99–112.

Dainty, S. J., C. J. Patterson, K. J. Waldron and N. J. Robinson (2010). "Interaction between cyanobacterial copper chaperone Atx1 and zinc homeostasis." *J. Biol. Inorg. Chem.* **15**(1): 77-85.

Dallinger, R., B. Berger, P. Hunziker and J. H. Kagi (1997). "Metallothionein in snail Cd and Cu metabolism." *Nature* **388**(6639): 237-238.

Daniels, M. J., J. S. Turner-Cavet, R. Selkirk, H. Sun, J. A. Parkinson, P. J. Sadler and N. J. Robinson (1998). "Coordination of Zn2+ (and Cd2+) by prokaryotic metallothionein. Involvement of his-imidazole." *J. Biol. Chem.* **273**(36): 22957-22961.

Davies, K. M., S. Bohic, A. Carmona, R. Ortega, V. Cottam, D. J. Hare, J. P. Finberg, S. Reyes, G. M. Halliday, J. F. Mercer and K. L. Double (2014). "Copper pathology in vulnerable brain regions in Parkinson's disease." *Neurobiol. Aging* **35**(4): 858-866.

Davis, A. V. and T. V. O'Halloran (2008). "A place for thioether chemistry in cellular copper ion recognition and trafficking." *Nat. Chem. Biol.* **4**(3): 148–151.

Daviter, T., N. Chmel and A. Rodger (2013). "Circular and linear dichroism spectroscopy for the study of protein-ligand interactions." *Methods Mol Biol* **1008**: 211-241.

de Bie, P., P. Muller, C. Wijmenga and L. W. Klomp (2007). "Molecular pathogenesis of Wilson and Menkes disease: correlation of mutations with molecular defects and disease phenotypes." *J. Med. Genet.* **44**(11): 673-688.

Dean, K. M., Y. Qin and A. E. Palmer (2012). "Visualizing metal ions in cells: an overview of analytical techniques, approaches, and probes." *Biochim. Biophys. Acta* **1823**(9): 1406–1415.

Desai, V. and S. G. Kaler (2008). "Role of copper in human neurological disorders." *Am. J. Clin. Nutr.* **88**(3): 855S-858S.

Deters, D., H. J. Hartmann and U. Weser (1994). "Transient thiyl radicals in yeast copper(I) thionein." *Biochim. Biophys. Acta* **1208**(2): 344-347.

Ding, X. Q., C. Butzlaff, E. Bill, D. L. Pountney, G. Henkel, H. Winkler, M. Vasak and A. X. Trautwein (1994). "Mossbauer and magnetic susceptibility studies on iron(II) metallothionein from rabbit liver. Evidence for the existence of an unusual type of $[M_3(CysS)_9]_3$- cluster." *Eur. J. Biochem.* **220**(3): 827-837.

Dolderer, B., H. Echner, A. Beck, H. J. Hartmann, U. Weser, C. Luchinat and C. Del Bianco (2007). "Coordination of three and four Cu(I) to the alpha- and beta-domain of vertebrate Zn-metallothionein–1, respectively, induces significant structural changes." *FEBS J.* **274**(9): 2349-2362.

Dunn, M. J. and S. J. Crisp (1994). "Detection of proteins in polyacrylamide gels using an ultrasensitive silver staining technique." *Methods Mol Biol* **32**: 113–118.

Durnam, D. M. and R. D. Palmiter (1981). "Transcriptional regulation of the mouse metallothionein-I gene by heavy metals." *J. Biol. Chem.* **256**(11): 5712-5716.

Dye, C., S. Scheele, P. Dolin, V. Pathania and M. C. Raviglione (1999). "Consensus statement. Global burden of tuberculosis: estimated incidence, prevalence, and mortality by country. WHO Global Surveillance and Monitoring Project." *JAMA* **282**(7): 677-686.

Ehresmann, B., P. Imbault and J. H. Weil (1973). "Spectrophotometric determination of protein concentration in cell extracts containing tRNA's and rRNA's." *Anal. Biochem.* **54**(2): 454-463.

Ehrt, S. and D. Schnappinger (2009). "Mycobacterial survival strategies in the phagosome: defence against host stresses." *Cell. Microbiol.* **11**(8): 1170–1178.

Faller, P. (2010). "Neuronal growth-inhibitory factor (metallothionein-3): reactivity and structure of metal-thiolate clusters." *FEBS J.* **277**(14): 2921-2930.

Faller, P. and M. Vasak (1997). "Distinct metal-thiolate clusters in the N-terminal domain of neuronal growth inhibitory factor." *Biochemistry* **36**(43): 13341–13348.

Festa, R. A., M. B. Jones, S. Butler-Wu, D. Sinsimer, R. Gerads, W. R. Bishai, S. N. Peterson and K. H. Darwin (2011). "A novel copper-responsive regulon in *Mycobacterium tuberculosis*." *Mol. Microbiol.* **79**(1): 133–148.

Festa, R. A. and D. J. Thiele (2012). "Copper at the front line of the host-pathogen battle." *PLoS Pathog* **8**(9): e1002887.

Finkel, T. and N. J. Holbrook (2000). "Oxidants, oxidative stress and the biology of ageing." *Nature* **408**(6809): 239-247.

Foster, A. W. and N. J. Robinson (2011). "Promiscuity and preferences of metallothioneins: the cell rules." *BMC Biol.* **9**: 25.

Fowler, B. A., D. W. Engel and M. Brouwer (1986). "Purification and characterization studies of cadmium-binding proteins from the American oyster, *Crassostrea virginica*." *Environ. Health Perspect.* **65**: 63-69.

Fowler, B. A., C. E. Hildebrand, Y. Kojima and M. Webb (1987). "Nomenclature of metallothionein." *Experientia Suppl* **52**: 19-22.

Freisinger, E. (2008). "Plant MTs-long neglected members of the metallothionein superfamily." *Dalton Trans*(47): 6663-6675.

Freisinger, E. (2011). "Structural features specific to plant metallothioneins." *J. Biol. Inorg. Chem.* **16**(7): 1035–1045.

Freisinger, E. and M. Vasák (2013). "Cadmium in metallothioneins." *Met Ions Life Sci* **11**: 339-371.

Geller, B. L. and D. R. Winge (1982). "Metal binding sites of rat liver Cu-thionein." *Arch. Biochem. Biophys.* **213**(1): 109–117.

Geller, B. L. and D. R. Winge (1982). "Rat liver Cu,Zn-superoxide dismutase. Subcellular location in lysosomes." *J. Biol. Chem.* **257**(15): 8945-8952.

Giancotti, V. and G. H. Goodwin (1986). "A method for silver staining HMG chromosomal proteins in polyacrylamide electrophoretic gels." *J. Biochem. Biophys. Methods* **12**(5-6): 265-269.

Goddard T.D and Kneller D.G (2007) SPARKY 3. San Francisco, University of California.

Gold, B., H. Deng, R. Bryk, D. Vargas, D. Eliezer, J. Roberts, X. Jiang and C. Nathan (2008). "Identification of a copper-binding metallothionein in pathogenic mycobacteria." *Nat. Chem. Biol.* **4**(10): 609-616.

Goldberg, H. A. and K. J. Warner (1997). "The staining of acidic proteins on polyacrylamide gels: enhanced sensitivity and stability of "Stains-all" staining in combination with silver nitrate." *Anal. Biochem.* **251**(2): 227-233.

Golovanov, A. P., R. T. Blankley, J. M. Avis and W. Bermel (2007). "Isotopically discriminated NMR spectroscopy: a tool for investigating complex protein interactions in vitro." *J. Am. Chem. Soc.* **129**(20): 6528-6535.

Good, M., R. Hollenstein and M. Vasak (1991). "Metal selectivity of clusters in rabbit liver metallothionein." *Eur. J. Biochem.* **197**(3): 655-659.

Good, M., M. Vasak and J. H. R. Kagi (1987). "Effects of Cluster Formation on Co(Ii)-Thiolate and Fe(Ii)-Thiolate Excitations in Metallothionein." *Recueil Des Travaux Chimiques Des Pays-Bas-Journal of the Royal Netherlands Chemical Society* **106**(6-7): 186–186.

Grass, G., C. Rensing and M. Solioz (2011). "Metallic copper as an antimicrobial surface." *Appl. Environ. Microbiol.* **77**(5): 1541–1547.

Grimsley, G. R. and C. N. Pace (2004). "Spectrophotometric determination of protein concentration." *Curr Protoc Protein Sci* **Chapter 3**: Unit 3 1.

Grishin, N. V. (2001). "Treble clef finger--a functionally diverse zinc-binding structural motif." *Nucleic Acids Res.* **29**(8): 1703–1714.

Halliwell, B. (1994). "Free radicals and antioxidants: a personal view." *Nutr. Rev.* **52**(8 Pt 1): 253-265.

Halliwell, B. (1994). "Free radicals, antioxidants, and human disease: curiosity, cause, or consequence?" *Lancet* **344**(8924): 721-724.

Hamer, D. H., D. J. Thiele and J. E. Lemontt (1985). "Function and autoregulation of yeast copper thionein." *Science* **228**(4700): 685-690.

Harrison, M. D., C. E. Jones, M. Solioz and C. T. Dameron (2000). "Intracellular copper routing: the role of copper chaperones." *Trends Biochem. Sci* **25**(1): 29-32.

Hartmann, H. J., Y. J. Li and U. Weser (1992). "Analogous copper(I) coordination in metallothionein from yeast and the separate domains of the mammalian protein." *BioMetals* **5**(3): 187–191.

Hartmann, H. J. and U. Weser (1977). "Copper-thionein from fetal bovine liver." *Biochim. Biophys. Acta* **491**(1): 211-222.

Higham, D. P., P. J. Sadler and M. D. Scawen (1986). "Cadmium-binding proteins in *Pseudomonas putida*: pseudothioneins." *Environ. Health Perspect.* **65**: 5–11.

Hochstrasser, D. F., A. Patchornik and C. R. Merril (1988). "Development of polyacrylamide gels that improve the separation of proteins and their detection by silver staining." *Anal. Biochem.* **173**(2): 412-423.

Hodgkinson, V. and M. J. Petris (2012). "Copper homeostasis at the host-pathogen interface." *J. Biol. Chem.* **287**(17): 13549–13555.

Irving, H. M. N. H, R. J. P (1953) " The stability of transition metal complexes." *J. Chem. Soc.* 3192-3210.

Jacob, C., W. Maret and B. L. Vallee (1998). "Control of zinc transfer between thionein, metallothionein, and zinc proteins." *Proc Natl Acad Sci U S A* **95**(7): 3489-3494.

Jayachandran, R., S. Bosedasgupta and J. Pieters (2013). "Surviving the Macrophage: Tools and Tricks Employed by *Mycobacterium tuberculosis*." *Curr. Top. Microbiol. Immunol.* **374**: 189-209.

Jiang, L. J., M. Vasak, B. L. Vallee and W. Maret (2000). "Zinc transfer potentials of the alpha - and beta-clusters of metallothionein are affected by domain interactions in the whole molecule." *Proc Natl Acad Sci U S A* **97**(6): 2503-2508.

Kägi, J. H. and Y. Kojima (1987). "Chemistry and biochemistry of metallothionein." *Experientia Suppl* **52**: 25-61.

Kägi, J. H. and A. Schaffer (1988). "Biochemistry of metallothionein." *Biochemistry* **27**(23): 8509-8515.

Kägi, J. H. and B. L. Vallee (1961). "Metallothionein: a cadmium and zinc-containign protein from equine renal cortex. II. Physico-chemical properties." *J. Biol. Chem.* **236**: 2435-2442.

Kägi, J. H., M. Vasák, K. Lerch, D. E. Gilg, P. Hunziker, W. R. Bernhard and M. Good (1984). "Structure of mammalian metallothionein." *Environ. Health Perspect.* **54**: 93–103.

Kim, B. E., T. Nevitt and D. J. Thiele (2008). "Mechanisms for copper acquisition, distribution and regulation." *Nat. Chem. Biol.* **4**(3): 176–185.

Klaassen, C. D., J. Liu and S. Choudhuri (1999). "Metallothionein: an intracellular protein to protect against cadmium toxicity." *Annu. Rev. Pharmacol. Toxicol.* **39**: 267-294.

Klassen, R. B., K. Crenshaw, R. Kozyraki, P. J. Verroust, L. Tio, S. Atrian, P. L. Allen and T. G. Hammond (2004). "Megalin mediates renal uptake of heavy metal metallothionein complexes." *Am J Physiol Renal Physiol* **287**(3): F393-403.

Kondrat, F. D., G. R. Kowald, C. A. Scarff, J. H. Scrivens and C. A. Blindauer (2013). "Resolution of a paradox by native mass spectrometry: facile occupation of all four metal binding sites in the dimeric zinc sensor SmtB." *Chem Commun (Camb)* **49**(8): 813-815.

Kraker, A. J., G. Krakower, C. F. Shaw, 3rd, D. H. Petering and J. S. Garvey (1988). "Zinc metabolism in Ehrlich cells: properties of a metallothionein-like zinc-binding protein." *Cancer Res.* **48**(12): 3381-3388.

Krezel, A. and W. Maret (2007). "Different redox states of metallothionein/thionein in biological tissue." *Biochem. J* **402**(3): 551-558.

Krezoski, S. K., J. Villalobos, C. F. Shaw, 3rd and D. H. Petering (1988). "Kinetic lability of zinc bound to metallothionein in Ehrlich cells." *Biochem. J* **255**(2): 483-491.

Leszczyszyn, O. I. and C. A. Blindauer (2010). "Zinc transfer from the embryo-specific metallothionein E_c from wheat: a case study." *Phys. Chem. Chem. Phys.* **12**(41): 13408–13418.

Leszczyszyn, O. I., C. D. Evans, S. E. Keiper, G. Z. L. Warren and C. A. Blindauer (2007). "Differential reactivity of individual zinc ions in clusters from bacterial metallothioneins." *Inorg. Chim. Acta* **360**(1): 3–13.

Li, H. and J. D. Otvos (1996). "HPLC characterization of Ag+ and Cu+ metal exchange reactions with Zn- and Cd-metallothioneins." *Biochemistry* **35**(44): 13937–13945.

Li, H. and J. D. Otvos (1996). "^{111}Cd NMR studies of the domain specificity of Ag+ and Cu+ binding to metallothionein." *Biochemistry* **35**(44): 13929–13936.

Lian, L. Y. and D. A. Middleton (2001). "Labelling approaches for protein structural studies by solution-state and solid-state NMR." *Prog. Nucl. Magn. Reson. Spectrosc.* **39**(3): 171–190.

Li, Y. J. and U. Weser (1992) “Circular dichroism, luminescence and electronic absorption of copper binding sites in metallothionein and its chemically characterized alpha and beta domains.” *Inorg. Chem*. **31**(26) 5526-5533.

Liochev, S. I. and I. Fridovich (2002). "Copper, zinc superoxide dismutase and H2O2. Effects of bicarbonate on inactivation and oxidations of NADPH and urate, and on consumption of H2O2." *J. Biol. Chem.* **277**(38): 34674-34678.

Liu, T., A. Ramesh, Z. Ma, S. K. Ward, L. Zhang, G. N. George, A. M. Talaat, J. C. Sacchettini and D. P. Giedroc (2007). "CsoR is a novel *Mycobacterium tuberculosis* copper-sensing transcriptional regulator." *Nat. Chem. Biol.* **3**(1): 60-68.

Loebus, J., E. A. Peroza, N. Bluthgen, T. Fox, W. Meyer-Klaucke, O. Zerbe and E. Freisinger (2011). "Protein and metal cluster structure of the wheat metallothionein domain gamma-E(c)–1: the second part of the puzzle." *J. Biol. Inorg. Chem.* **16**(5): 683-694.

Lutsenko, S., R. G. Efremov, R. Tsivkovskii and J. M. Walker (2002). "Human copper-transporting ATPase ATP7B (the Wilson's disease protein): biochemical properties and regulation." *J. Bioenerg. Biomembr.* **34**(5): 351-362.

Ma, Z., D. M. Cowart, R. A. Scott and D. P. Giedroc (2009). "Molecular insights into the metal selectivity of the copper(I)-sensing repressor CsoR from *Bacillus subtilis*." *Biochemistry* **48**(15): 3325-3334.

Ma, Z., F. E. Jacobsen and D. P. Giedroc (2009). "Coordination chemistry of bacterial metal transport and sensing." *Chem. Rev.* **109**(10): 4644-4681.

Manso, Y., J. Carrasco, G. Comes, G. Meloni, P. A. Adlard, A. I. Bush, M. Vasak and J. Hidalgo (2012). "Characterization of the role of metallothionein-3 in an animal model of Alzheimer's disease." *Cell. Mol. Life Sci.* **69**(21): 3683-3700.

Maret, W. (2004). "Zinc and sulfur: a critical biological partnership." *Biochemistry* **43**(12): 3301-3309.

Maret, W. and B. L. Vallee (1993). "Cobalt as probe and label of proteins." *Methods Enzymol.* **226**: 52-71.

Margoshes M and B. L. Vallee (1957) “A cadmium protein from equine kidney cortex.” *J. Am. Chem. Soc*. **79**(17) 4813-4814.

Mehra, R. K. and I. Bremner (1984). "Species differences in the occurrence of copper-metallothionein in the particulate fractions of the liver of copper-loaded animals." *Biochem. J* **219**(2): 539-546.

Meloni, G. and M. Vasak (2011). "Redox activity of alpha-synuclein-Cu is silenced by Zn(7)-metallothionein-3." *Free Radic Biol Med* **50**(11): 1471–1479.

Merrifield, M. E., Z. Huang, P. Kille and M. J. Stillman (2002). "Copper speciation in the alpha and beta domains of recombinant human metallothionein by electrospray ionization mass spectrometry." *J. Inorg. Biochem.* **88**(2): 153–172.

Mertz, W. (1981). "The scientific and practical importance of trace elements." *Philos Trans R Soc Lond B Biol Sci* **294**(1071): 9–18.

Mertz, W. (1981). "The essential trace elements." *Science* **213**(4514): 1332–1338.

Mertz, W. (1998). "Review of the scientific basis for establishing the essentiality of trace elements." *Biol. Trace Elem. Res.* **66**(1-3): 185–191.

Mertz, W. (1998). "A perspective on mineral standards." *J. Nutr.* **128**(2 Suppl): 375S-378S.

Messerle, B. A., A. Schaffer, M. Vasák, J. H. Kägi and K. Wüthrich (1992). "Comparison of the solution conformations of human [Zn7]-metallothionein-2 and [Cd7]-metallothionein-2 using nuclear magnetic resonance spectroscopy." *J. Mol. Biol.* **225**(2): 433-443.

Minkel, D. T., K. Poulsen, S. Wielgus, C. F. Shaw, 3rd and D. H. Petering (1980). "On the sensitivity of metallothioneins to oxidation during isolation." *Biochem. J* **191**(2): 475-485.

Molteni, C., H. K. Abicht and M. Solioz (2010). "Killing of bacteria by copper surfaces involves dissolved copper." *Appl. Environ. Microbiol.* **76**(12): 4099-4101.

Morby, A. P., J. S. Turner, J. W. Huckle and N. J. Robinson (1993). "SmtB is a metal-dependent repressor of the cyanobacterial metallothionein gene *smtA*: identification of a Zn inhibited DNA-protein complex." *Nucleic Acids Res.* **21**(4): 921-925.

Munoz, A., F. H. Forsterling, C. F. Shaw, 3rd and D. H. Petering (2002). "Structure of the ^{113}Cd(3)beta domains from *Homarus americanus* metallothionein–1: hydrogen bonding and solvent accessibility of sulfur atoms." *J. Biol. Inorg. Chem.* **7**(7-8): 713-724.

Myari, A., N. Hadjiliadis, N. Fatemi and B. Sarkar (2004). "Copper(I) interaction with model peptides of WD6 and TM6 domains of Wilson ATPase: regulatory and mechanistic implications." *J. Inorg. Biochem.* **98**(9): 1483–1494.

Narula, S. S., M. Brouwer, Y. Hua and I. M. Armitage (1995). "Three-dimensional solution structure of *Callinectes sapidus* metallothionein–1 determined by homonuclear and heteronuclear magnetic resonance spectroscopy." *Biochemistry* **34**(2): 620-631.

Narula, S. S., D. R. Winge and I. M. Armitage (1993). "Copper- and silver-substituted yeast metallothioneins: sequential ^{1}H NMR assignments reflecting conformational heterogeneity at the C terminus." *Biochemistry* **32**(26): 6773-6787.

Nathan, C. and M. U. Shiloh (2000). "Reactive oxygen and nitrogen intermediates in the relationship between mammalian hosts and microbial pathogens." *Proc Natl Acad Sci U S A* **97**(16): 8841-8848.

Nazarova, I. and M. A. Hemminga (2004). "Analytical analysis of multi-pulse NMR." *J. Magn. Reson.* **170**(2): 284-289.

Nelson, N. (1999). "Metal ion transporters and homeostasis." *EMBO J.* **18**(16): 4361-4371.

Nettesheim, D. G., H. R. Engeseth and J. D. Otvos (1985). "Products of metal exchange reactions of metallothionein." *Biochemistry* **24**(24): 6744-6751.

Nevitt, T., H. Ohrvik and D. J. Thiele (2012). "Charting the travels of copper in eukaryotes from yeast to mammals." *Biochim. Biophys. Acta* **1823**(9): 1580–1593.

Newberne, P. M., C. E. Hunt and V. R. Young (1968). "The role of diet and the reticuloendothelial system in the response of rats to *Salmonella typhilmurium* infection." *Br J Exp Pathol* **49**(5): 448-457.

Ngu, T. T., A. Easton and M. J. Stillman (2008). "Kinetic analysis of arsenic-metalation of human metallothionein: significance of the two-domain structure." *J. Am. Chem. Soc.* **130**(50): 17016–17028.

Ngu, T. T. and M. J. Stillman (2009). "Metalation of metallothioneins." *IUBMB Life* **61**(4): 438-446.

Nielson, K. B., C. L. Atkin and D. R. Winge (1985). "Distinct metal-binding configurations in metallothionein." *J. Biol. Chem.* **260**(9): 5342-5350.

Nielson, K. B. and D. R. Winge (1985). "Independence of the domains of metallothionein in metal binding." *J. Biol. Chem.* **260**(15): 8698-8701.

O'Halloran, T. J. (2000). "Membrane traffic and cytokinesis." *Traffic* **1**(12): 921-926.

O'Halloran, T. V. and V. C. Culotta (2000). "Metallochaperones, an intracellular shuttle service for metal ions." *J. Biol. Chem.* **275**(33): 25057-25060.

Oh, K. B., T. Watanabe and H. Matsuoka (1999). "A novel copper-binding protein with characteristics of a metallothionein from a clinical isolate of *Candida albicans*." *Microbiology* **145** (9): 2423-2429.

Ohi, S., G. Cardenosa, R. Pine and P. C. Huang (1981). "Cadmium-induced accumulation of metallothionein messenger RNA in rat liver." *J. Biol. Chem.* **256**(5): 2180-2184.

Olafson, R. W., K. Abel and R. G. Sim (1979). "Prokaryotic metallothionein: preliminary characterization of a blue-green alga heavy metal-binding protein." *Biochem. Biophys. Res. Commun.* **89**(1): 36-43.

Olafson, R. W., W. D. McCubbin and C. M. Kay (1988). "Primary- and secondary-structural analysis of a unique prokaryotic metallothionein from a *Synechococcus sp*. cyanobacterium." *Biochem. J* **251**(3): 691-699.

Olafson, R. W., R. G. Sim and A. Kearns (1979). "Physiological and chemical characterization of invertebrate metallothionein-like proteins." *Experientia Suppl* **34**: 197-204.

Ono, S., Y. Endo, E. Tokuda, K. Ishige, K. Tabata, S. Asami, Y. Ito and T. Suzuki (2006). "Upregulation of metallothionein-I mRNA expression in a rodent model for amyotrophic lateral sclerosis." *Biol. Trace Elem. Res.* **113**(1): 93–104.

Orihuela, R., J. Domenech, R. Bofill, C. You, E. A. Mackay, J. H. Kagi, M. Capdevila and S. Atrian (2008). "The metal-binding features of the recombinant mussel *Mytilus edulis* MT–10-IV metallothionein." *J. Biol. Inorg. Chem.* **13**(5): 801-812.

Osman, D. and J. S. Cavet (2008). "Copper homeostasis in bacteria." *Adv. Appl. Microbiol.* **65**: 217-247.

Osman, D., C. J. Patterson, K. Bailey, K. Fisher, N. J. Robinson, S. E. Rigby and J. S. Cavet (2013). "The copper supply pathway to a Salmonella Cu,Zn-superoxide dismutase (SodCII) involves P(1B)-type ATPase copper efflux and periplasmic CueP." *Mol. Microbiol.* **87**(3): 466-477.

Osman, D., K. J. Waldron, H. Denton, C. M. Taylor, A. J. Grant, P. Mastroeni, N. J. Robinson and J. S. Cavet (2010). "Copper homeostasis in Salmonella is atypical and copper-CueP is a major periplasmic metal complex." *J. Biol. Chem.* **285**(33): 25259-25268.

Otvos, J. D. and I. M. Armitage (1979). "Structural characterization of metallothionein by multinuclear NMR." *Experientia Suppl* **34**: 249-257.

Öz, G., D. L. Pountney and I. M. Armitage (1998). "NMR spectroscopic studies of I = 1/2 metal ions in biological systems." *Biochem. Cell Biol.* **76**(2-3): 223-234.

Palacios, O., K. Polec-Pawlak, R. Lobinski, M. Capdevila and P. Gonzalez-Duarte (2003). "Is Ag(I) an adequate probe for Cu(I) in structural copper-metallothionein studies? The binding features of Ag(I) to mammalian metallothionein 1." *J. Biol. Inorg. Chem.* **8**(8): 831-842.

Pearson, R. G (1968) "Hard and soft acids and bases, HSAB, Part 1; Fundamental principles." *J. Chem. Edu*. **45**(9) 581.

Perez-Rafael, S., S. Atrian, M. Capdevila and O. Palacios (2011). "Differential ESI-MS behaviour of highly similar metallothioneins." *Talanta* **83**(3): 1057–1061.

Peroza, E. A., A. A. Kaabi, W. Meyer-Klaucke, G. Wellenreuther and E. Freisinger (2009). "The two distinctive metal ion binding domains of the wheat metallothionein Ec–1." *J. Inorg. Biochem.* **103**(3): 342-353.

Peroza, E. A., R. Schmucki, P. Guntert, E. Freisinger and O. Zerbe (2009). "The beta(E)-domain of wheat E(c)–1 metallothionein: a metal-binding domain with a distinctive structure." *J. Mol. Biol.* **387**(1): 207-218.

Petering, D. H. and W. E. Antholine (1988) "Copper toxicity speciation and reactions of copper in biological systems." *Rev. Biochem. Toxic* **9**: 225-270.

Petering, D. H. and B. A. Fowler (1986). "Roles of metallothionein and related proteins in metal metabolism and toxicity: problems and perspectives." *Environ. Health Perspect.* **65**: 217-224.

Peterson, C. W., S. S. Narula and I. M. Armitage (1996). "3D solution structure of copper and silver-substituted yeast metallothioneins." *FEBS Lett.* **379**(1): 85-93.

Pieters, J. (2008). "Mycobacterium tuberculosis and the macrophage: maintaining a balance." *Cell Host Microbe* **3**(6): 399-407.

Pountney, D. L., I. Schauwecker, J. Zarn and M. Vasák (1994). "Formation of mammalian Cu_8-metallothionein in vitro: evidence for the existence of two Cu(I)4-thiolate clusters." *Biochemistry* **33**(32): 9699-9705.

Presta, A. and M. J. Stillman (1994). "Chiral copper(I)-thiolate clusters in metallothionein and glutathione." *Chirality* **6**(7): 521-530.

Presta, A. and M. J. Stillman (1997). "Incorporation of copper into the yeast *Saccharomyces cerevisiae*. Identification of Cu(I)-metallothionein in intact yeast cells." *J. Inorg. Biochem.* **66**(4): 231-240.

Prinz, R. and U. Weser (1975). "A naturally occurring Cu-thionein in *Saccharomyces cerevisiae*." *Hoppe Seylers Z Physiol Chem* **356**(6): 767-776.

Prohaska, J. R. and O. A. Lukasewycz (1981). "Copper deficiency suppresses the immune response of mice." *Science* **213**(4507): 559-561.

Rae, T. D., P. J. Schmidt, R. A. Pufahl, V. C. Culotta and T. V. O'Halloran (1999). "Undetectable intracellular free copper: the requirement of a copper chaperone for superoxide dismutase." *Science* **284**(5415): 805-808.

Rauser, W. E. (1987). "The Cd-binding protein from tomato compared to those of other vascular plants." *Experientia Suppl* **52**: 301-308.

Rauser, W. E and N. R. Curvetto (1980) "Metallothionein occurs in roots of *Agrostis* tolerant to excess copper." *Nature* **287**: 563-564.

Rensing, C. and G. Grass (2003). "*Escherichia coli* mechanisms of copper homeostasis in a changing environment." *FEMS Microbiol. Rev.* **27**(2-3): 197-213.

Riccardi, G., A. Milano, M. R. Pasca and D. H. Nies (2008). "Genomic analysis of zinc homeostasis in *Mycobacterium tuberculosis*." *FEMS Microbiol. Lett.* **287**(1): 1-7.

Richardson, D. R. and Y. Suryo Rahmanto (2007). "Differential regulation of the Menkes and Wilson disease copper transporters by hormones: an integrated model of metal transport in the placenta." *Biochem. J* **402**(2): e1-3.

Riek, R., B. Precheur, Y. Wang, E. A. Mackay, G. Wider, P. Guntert, A. Liu, J. H. Kägi and K. Wüthrich (1999). "NMR structure of the sea urchin (Strongylocentrotus purpuratus) metallothionein MTA." *J. Mol. Biol.* **291**(2): 417-428.

Rigby Duncan, K. E., C. W. Kirby and M. J. Stillman (2008). "Metal exchange in metallothioneins: a novel structurally significant Cd(5) species in the alpha domain of human metallothionein 1a." *FEBS J.* **275**(9): 2227-2239.

Roberts, E. A. and B. Sarkar (2008). "Liver as a key organ in the supply, storage, and excretion of copper." *Am. J. Clin. Nutr.* **88**(3): 851S-854S.

Robinson, N. J. (2008). "A bacterial copper metallothionein." *Nat. Chem. Biol.* **4**(10): 582-583.

Robinson, N. J. (2011). "Structural biology: a platform for copper pumps." *Nature* **475**(7354): 41-42.

Robinson, N. J., A. Gupta, A. P. Fordham-Skelton, R. R. Croy, B. A. Whitton and J. W. Huckle (1990). "Prokaryotic metallothionein gene characterication and expression: chromosome crawling by ligation-mediated PCR." *Proc Biol Sci* **242**(1305): 241-247.

Robinson, N. J., S. K. Whitehall and J. S. Cavet (2001). "Microbial metallothioneins." *Adv. Microb. Physiol.* **44**: 183-213.

Robinson, N. J. and D. R. Winge (2010). "Copper metallochaperones." *Annu. Rev. Biochem* **79**: 537-562.

Rodger, A., R. Marrington, D. Roper and S. Windsor (2005). "Circular dichroism spectroscopy for the study of protein-ligand interactions." *Methods Mol Biol* **305**: 343-364.

Roschitzki, B. and M. Vasák (2002). "A distinct Cu_4-thiolate cluster of human metallothionein-3 is located in the N-terminal domain." *J. Biol. Inorg. Chem.* **7**(6): 611-616.

Rowland, J. L. and M. Niederweis (2012). "Resistance mechanisms of *Mycobacterium tuberculosis* against phagosomal copper overload." *Tuberculosis (Edinb)* **92**(3): 202-210.

Rubino, J. T. and K. J. Franz (2012). "Coordination chemistry of copper proteins: how nature handles a toxic cargo for essential function." *J. Inorg. Biochem.* **107**(1): 129–143.

Samanovic, M. I., C. Ding, D. J. Thiele and K. H. Darwin (2012). "Copper in microbial pathogenesis: meddling with the metal." *Cell Host Microbe* **11**(2): 106–115.

Schaffer, A., M. Vasak and J. H. R. Kagi (1987). "Spectroscopic Investigation of Thiolate Transitions in Metallothionein and in a Model Peptide." *Recueil Des Travaux Chimiques Des Pays-Bas-Journal of the Royal Netherlands Chemical Society* **106**(6-7): 186–187.

Schechinger, T., H. J. Hartmann and U. Weser (1986). "Copper Transport from Cu(I)-Thionein into Apo-Ceruloplasmin Mediated by Activated Leukocytes." *Biochem. J* **240**(1): 281-283.

Schumann, F. H., H. Riepl, T. Maurer, W. Gronwald, K. P. Neidig and H. R. Kalbitzer (2007). "Combined chemical shift changes and amino acid specific chemical shift mapping of protein-protein interactions." *J. Biomol. NMR* **39**(4): 275-289.

Serra-Batiste, M., N. Cols, L. A. Alcaraz, A. Donaire, P. Gonzalez-Duarte and M. Vasák (2010). "The metal-binding properties of the blue crab copper specific CuMT-2: a crustacean metallothionein with two cysteine triplets." *J. Biol. Inorg. Chem.* **15**(5): 759-776.

Seth, R., S. Yang, S. Choi, M. Sabean and E. A. Roberts (2004). "In vitro assessment of copper-induced toxicity in the human hepatoma line, Hep G2." *Toxicol. In Vitro* **18**(4): 501-509.

Shi, J., W. P. Lindsay, J. W. Huckle, A. P. Morby and N. J. Robinson (1992). "Cyanobacterial metallothionein gene expressed in *Escherichia coli*. Metal-binding properties of the expressed protein." *FEBS Lett.* **303**(2-3): 159–163.

Sievers, C., D. Deters, H. J. Hartmann and U. Weser (1996). "Stable thiyl radicals in dried yeast $Cu(I)_6$-thionein." *J. Inorg. Biochem.* **62**(3): 199-205.

Solioz, M., H. K. Abicht, M. Mermod and S. Mancini (2010). "Response of gram-positive bacteria to copper stress." *J. Biol. Inorg. Chem.* **15**(1): 3–14.

Squibb, K. S. and R. J. Cousins (1977). "Synthesis of metallothionein in a polysomal cell-free system." *Biochem. Biophys. Res. Commun.* **75**(3): 806-812.

Stafford, S. L., N. J. Bokil, M. E. Achard, R. Kapetanovic, M. A. Schembri, A. G. McEwan and M. J. Sweet (2013). "Metal ions in macrophage antimicrobial pathways: emerging roles for zinc and copper." *Biosci. Rep.* **33**(4).

Stillman, M. J., A. Presta, Z. Gui and D. T. Jiang (1994). "Spectroscopic studies of copper, silver and gold-metallothioneins." *Met Based Drugs* **1**(5-6): 375-394.

Sutherland, D. E. and M. J. Stillman (2008). "Noncooperative cadmium(II) binding to human metallothionein 1a." *Biochem. Biophys. Res. Commun.* **372**(4): 840-844.

Sutherland, D. E., K. L. Summers and M. J. Stillman (2012). "Noncooperative metalation of metallothionein 1a and its isolated domains with zinc." *Biochemistry* **51**(33): 6690-6700.

Suzuki, T., H. Yamanaka, K. Nakajima, K. Kanatani, K. Suzuki, M. Kimura, Y. Nakazawa and N. Otaki (1993). "Induction of metallothionein by $CdCl_2$ administration in rat prostate." *Prostate* **22**(2): 163–170.

Thornalley, P. J. and M. Vasák (1985). "Possible role for metallothionein in protection against radiation-induced oxidative stress. Kinetics and mechanism of its reaction with superoxide and hydroxyl radicals." *Biochim. Biophys. Acta* **827**(1): 36-44.

Tio, L., L. Villarreal, S. Atrian and M. Capdevila (2004). "Functional differentiation in the mammalian metallothionein gene family: metal binding features of mouse MT4 and comparison with its paralog MT1." *J. Biol. Chem.* **279**(23): 24403-24413.

Tokuda, E., S. Ono, K. Ishige, A. Naganuma, Y. Ito and T. Suzuki (2007). "Metallothionein proteins expression, copper and zinc concentrations, and lipid peroxidation level in a rodent model for amyotrophic lateral sclerosis." *Toxicology* **229**(1-2): 33-41.

Tomas, M., J. Domenech, M. Capdevila, R. Bofill and S. Atrian (2013). "The sea urchin metallothionein system: Comparative evaluation of the SpMTA and SpMTB metal-binding preferences." *FEBS Open Bio* **3**: 89–100.

Turner, J. S., A. P. Morby, B. A. Whitton, A. Gupta and N. J. Robinson (1993). "Construction of Zn2+/Cd2+ hypersensitive cyanobacterial mutants lacking a functional metallothionein locus." *J. Biol. Chem.* **268**(6): 4494-4498.

Valls, M., R. Bofill, R. Gonzalez-Duarte, P. Gonzalez-Duarte, M. Capdevila and S. Atrian (2001). "A new insight into metallothionein (MT) classification and evolution. The in vivo and in vitro metal binding features of *Homarus americanus* recombinant MT." *J. Biol. Chem.* **276**(35): 32835-32843.

Vasák, M. (1991). "Metallobiochemistry. Part B. Metallothionein and related molecules." *Methods Enzymol.* **205**: 1-626.

Vasák, M. (1991). "Metal removal and substitution in vertebrate and invertebrate metallothioneins." *Methods Enzymol.* **205**: 452-458.

Vasák, M. (1991). "Paramagnetic resonance of metallothionein." *Methods Enzymol.* **205**: 520-528.

Vasák, M. (1991). "Standard isolation procedure for metallothionein." *Methods Enzymol.* **205**: 41-44.

Vasák, M. (2005). "Advances in metallothionein structure and functions." *J. Trace Elem. Med Biol.* **19**(1): 13–17.

Vasák, M., C. Berger and J. H. Kägi (1984). "Dynamic structure of metallothionein." *FEBS Lett.* **168**(1): 174–178.

Vasák, M. and G. Meloni (2011). "Chemistry and biology of mammalian metallothioneins." *J. Biol. Inorg. Chem.* **16**(7): 1067–1078.

Vasák, M., E. Worgotter, G. Wagner, J. H. R. Kägi and K. Wüthrich (1987). "Metal Coordination in Rat-Liver Metallothionein-2 Prepared with or without Reconstitution of the Metal-Clusters, and Comparison with Rabbit Liver Metallothionein-2." *J. Mol. Biol.* **196**(3): 711-719.

Vazquez, F. and M. Vasák (1988). "Comparative ^{113}Cd-NMR. studies on rabbit $^{113}Cd_7$-, (Zn_1,Cd_6)- and partially metal-depleted $^{113}Cd_6$-metallothionein-2a." *Biochem. J* **253**(2): 611-614.

Wagner, D., J. Maser, B. Lai, Z. Cai, C. E. Barry, 3rd, K. Honer Zu Bentrup, D. G. Russell and L. E. Bermudez (2005). "Elemental analysis of *Mycobacterium avium-, Mycobacterium tuberculosis*-, and *Mycobacterium smegmatis*-containing phagosomes indicates pathogen-induced microenvironments within the host cell's endosomal system." *J. Immunol.* **174**(3): 1491–1500.

Waldron, K. J., S. J. Firbank, S. J. Dainty, M. Perez-Rama, S. Tottey and N. J. Robinson (2010). "Structure and metal loading of a soluble periplasm cuproprotein." *J. Biol. Chem.* **285**(42): 32504-32511.

Waldron, K. J. and N. J. Robinson (2009). "How do bacterial cells ensure that metalloproteins get the correct metal?" *Nat. Rev. Microbiol.* **7**(1): 25-35.

Waldron, K. J., J. C. Rutherford, D. Ford and N. J. Robinson (2009). "Metalloproteins and metal sensing." *Nature* **460**(7257): 823-830.

Wang, H., Q. Zhang, B. Cai, H. Li, K. H. Sze, Z. X. Huang, H. M. Wu and H. Sun (2006). "Solution structure and dynamics of human metallothionein-3 (MT-3)." *FEBS Lett.* **580**(3): 795-800.

Ward, S. K., J. A. Heintz, R. M. Albrecht and A. M. Talaat (2012). "Single-cell elemental analysis of bacteria: quantitative analysis of polyphosphates in *Mycobacterium tuberculosis*." *Front Cell Infect Microbiol* **2**: 63.

Ward, S. K., E. A. Hoye and A. M. Talaat (2008). "The global responses of *Mycobacterium tuberculosis* to physiological levels of copper." *J. Bacteriol.* **190**(8): 2939-2946.

Warner, D. F. and V. Mizrahi (2006). "Tuberculosis chemotherapy: the influence of bacillary stress and damage response pathways on drug efficacy." *Clin. Microbiol. Rev.* **19**(3): 558-570.

Warner, D. F. and V. Mizrahi (2013). "Complex genetics of drug resistance in *Mycobacterium tuberculosis*." *Nat. Genet.* **45**(10): 1107–1108.

Weser, U., W. Mutter and H. J. Hartmann (1986). "The role of Cu(I)-thiolate clusters during the proteolysis of Cu-thionein." *FEBS Lett.* **197**(1-2): 258-262.

West, A. K., J. Hidalgo, D. Eddins, E. D. Levin and M. Aschner (2008). "Metallothionein in the central nervous system: Roles in protection, regeneration and cognition." *Neurotoxicology* **29**(3): 489-503.

White, C., T. Kambe, Y. G. Fulcher, S. W. Sachdev, A. I. Bush, K. Fritsche, J. Lee, T. P. Quinn and M. J. Petris (2009). "Copper transport into the secretory pathway is regulated by oxygen in macrophages." *J. Cell Sci.* **122**(Pt 9): 1315–1321.

White, C., J. Lee, T. Kambe, K. Fritsche and M. J. Petris (2009). "A role for the ATP7A copper-transporting ATPase in macrophage bactericidal activity." *J. Biol. Chem.* **284**(49): 33949-33956.

Williamson, M. P. (2013). "Using chemical shift perturbation to characterise ligand binding." *Prog. Nucl. Magn. Reson. Spectrosc.* **73**: 1–16.

Willner, H., M. Vasak and J. H. R. Kagi (1987). "Cadmium-Thiolate Clusters in Metallothionein - Spectrophotometric and Spectropolarimetric Features." *Biochemistry* **26**(19): 6287-6292.

Winge, D. R. and M. Brouwer (1986). "Techniques and problems in metal-binding protein chemistry and implications for proteins in nonmammalian organisms." *Environ. Health Perspect.* **65**: 211-214.

Winge, D. R. and K. A. Miklossy (1982). "Domain nature of metallothionein." *J. Biol. Chem.* **257**(7): 3471-3476.

Winge, D. R. and K. A. Miklossy (1982). "Differences in the polymorphic forms of metallothionein." *Arch. Biochem. Biophys.* **214**(1): 80-88.

Winge, D. R., K. B. Nielson, W. R. Gray and D. H. Hamer (1985). "Yeast metallothionein. Sequence and metal-binding properties." *J. Biol. Chem.* **260**(27): 14464–14470.

Wishart, D. S., C. G. Bigam, A. Holm, R. S. Hodges and B. D. Sykes (1995). "^{1}H, ^{13}C and ^{15}N random coil NMR chemical shifts of the common amino acids. I. Investigations of nearest-neighbor effects." *J. Biomol. NMR* **5**(1): 67-81.

Wishart, D. S., C. G. Bigam, J. Yao, F. Abildgaard, H. J. Dyson, E. Oldfield, J. L. Markley and B. D. Sykes (1995). "^{1}H, ^{13}C and ^{15}N chemical shift referencing in biomolecular NMR." *J. Biomol. NMR* **6**(2): 135–140.

Wolschendorf, F., D. Ackart, T. B. Shrestha, L. Hascall-Dove, S. Nolan, G. Lamichhane, Y. Wang, S. H. Bossmann, R. J. Basaraba and M. Niederweis (2011). "Copper resistance is essential for virulence of *Mycobacterium tuberculosis*." *Proc Natl Acad Sci U S A* **108**(4): 1621–1626.

Worgotter, E., G. Wagner, M. Vasák, J. H. R. Kägi and K. Wüthrich (1987). "Sequence-Specific ^{1}H NMR Assignments in Rat-Liver Metallothionein-2." *Eur. J. Biochem.* **167**(3): 457-466.

Wüthrich, K. (1991). "Six years of protein structure determination by NMR spectroscopy: what have we learned?" *Ciba Found Symp* **161**: 136–145; discussion 145–139.

Wüthrich, K., P. Schultze, W. Braun, E. Worgotter, G. Wagner, A. Arseniev, M. Vasák and J. H. R. Kägi (1987). "Determination of the Metal Coordination in the 3-Dimensional Structure of Metallothionein by Nuclear-Magnetic-Resonance in Aqueous-Solution." *Recueil Des Travaux Chimiques Des Pays-Bas-Journal of the Royal Netherlands Chemical Society* **106**(6-7): 183–183.

Zangger, K., G. Öz, J. D. Otvos and I. M. Armitage (1999). "Three-dimensional solution structure of mouse Cd_7-metallothionein–1 by homonuclear and heteronuclear NMR spectroscopy." *Protein Sci.* **8**(12): 2630-2638.

Zangger, K., G. Shen, G. Öz, J. D. Otvos and I. M. Armitage (2001). "Oxidative dimerization in metallothionein is a result of intermolecular disulphide bonds between cysteines in the alpha-domain." *Biochem. J* **359**(Pt 2): 353-360.

Zhou, L., C. Singleton and N. E. Le Brun (2008). "High Cu(I) and low proton affinities of the CXXC motif of *Bacillus subtilis* CopZ." *Biochem. J* **413**(3): 459-465.

9

Appendix

A1-Thesis Reference: Chapter 4, page

Table 9:1 Theoretical and experimental masses of metalloforms observed for Zn_4SmtA after Cu(I) addition.

The values are provided for neutral masses in Da.

Species	Experimental (m/z)	Theoretical (m/z)
Zn_4SmtA	5864	5862.8
M5	5924.8	5922.5
M6	5986.8	5985
M7	6047.6	6047.5
M8	6110.4	6110

A2-Thesis Reference: Chapter 4, page

Table 9:2 Experimental and theoretical masses of species observed for Cd_4SmtA after Cu(I) addition. Values given are for the neutral species.

Species	Experimental (m/z)	Theoretical (m/z)
Cd_4SmtA	6052.04	6052
Cd_3Cu_2SmtA	6065.88	6066.5
Cd_1Cu_6/Cd_2Cu_9	6088.92	6095.5/6081
Cu_8	6110.03	6110
Cd_3Cu_3	6127.08	6129
Cd_1Cu_7	6156.76	6158
Cd_4Cu_2/Cu_9	6175.76	6177/6172.5
Cu_7	6046.84	6047.5
Cd_1Cu_5	6036.92	6033
Cd_2Cu_3	6018.8	6018.5
Cu_6	5983.84	5985
Cu_5	5920	5922.5

A3-Thesis Reference: Chapter 4, page

Table 9:3 Experimental and theoretical masses of species observed for Zn_4smtA after Ag(I) addition. The masses provided are for the neutral species.

Species	Experimental (m/z)	Theoretical (m/z)
Zn_4SmtA	5862.8	5862.8
Zn_3Ag_2	6015.6	6011.5
Zn_2Ag_3	6055.6	6056
Zn_3Ag_3	6121.6	6118.5
Zn_2Ag_4	6160.8	6163
Zn_1Ag_6	6312.4	6314.5
Zn_1Ag_7	6423.2	6421.5
Ag_9	6572.4	6573
Ag_{10}	6683.2	6680

A4-Thesis Reference: Chapter 5, page

Table 9:4 ^{1}H and ^{15}N chemical shifts of Zn_4SmtA after second Eq. of Cu(I).

Residue	NH	^{1}H
G28	105.9	8.96
G39	107.9	7.41
G46	110.1	9.12
S33	111.8	7.43
S21	111.8	8.28
C47	111.9	8.6
C36	112.5	7.27
T41	112.7	7.36
G56	112.9	8.38
H40	113.1	8.6
G48	113.3	8.36
D38	115.9	7.81
Y30	116.4	7.42
V7	117	8.75
Y31	117	9.21
H49	117.3	6.94
V18	117.4	9.64
C54	117.5	8.06
C52	120	7.56
C32	120	10.12
C32”	120.2	10.49
I24	120.3	7.74
K22	120.4	7.83
C32’	120.8	10.3

L29	121	7.31
C14	122	8.17
C16	122.5	8.21
A23	123.1	7.45
A37	123.6	7.51
D19	124.1	8.55
C11	125.2	7.97
R26	125.3	9.01
L6	125.6	8.27
K8	125.9	8.37
C9	127.9	8.95
D25	128.2	8.47
A10	128.7	8.02
L15	130.4	8.54
E12	133/134.1	9.14

A6-Thesis Reference: Chapter 6, page

Residue	NH	^{1}H
G28	106	8.96
G39	107.9	7.42
S33	111.2	7.42
D38	114.8	7.87
Y30	116.4	7.42
V7	117	8.83
Y31	117.2	9.11
V18	117.4	9.6
A35	120.3	8.03
C32	120.8	10.3
L29	121.1	7.35
K22	121.8	7.78
C16	122.5	8.23
A23	122.9	7.47
A37	123.5	7.42
D19	124.1	8.54
R26	124.6	8.3
L6	125.6	8.25
K8	126.9	8.36
D25	127.9	8.41
L15	129.4	8.59
E12	133	9.14

A6-Thesis Reference: Chapter 6, page

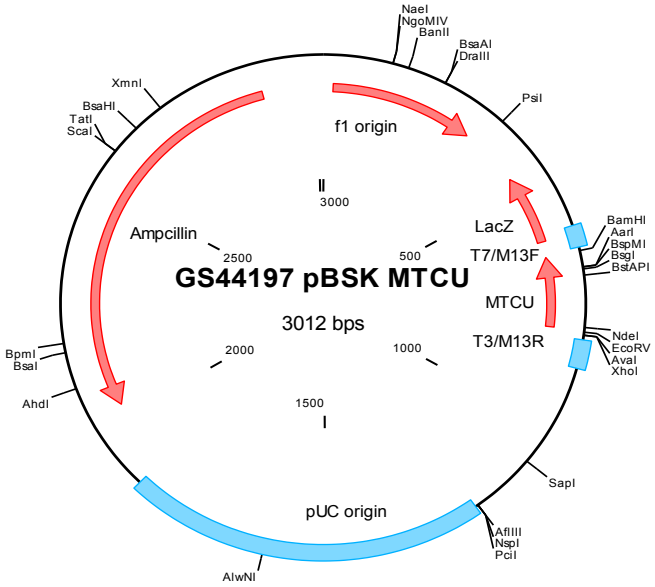

Figure 9.1 Physical map of pBSK MTCU- A synthetic MymT gene was cloned into SmaI digested pBluescript II SK by ATG biosynthesis.

The synthetic MymT (MTCU) gene, cloned in pBSK vector to creat MTCU_pBSK was purchased from ATG biosynthesis. The plasmid sequence was used to design PCR primers for amplification of the MymT gene for cloning in to a pET26b vector.

A8-Thesis Reference: Chapter 6, page

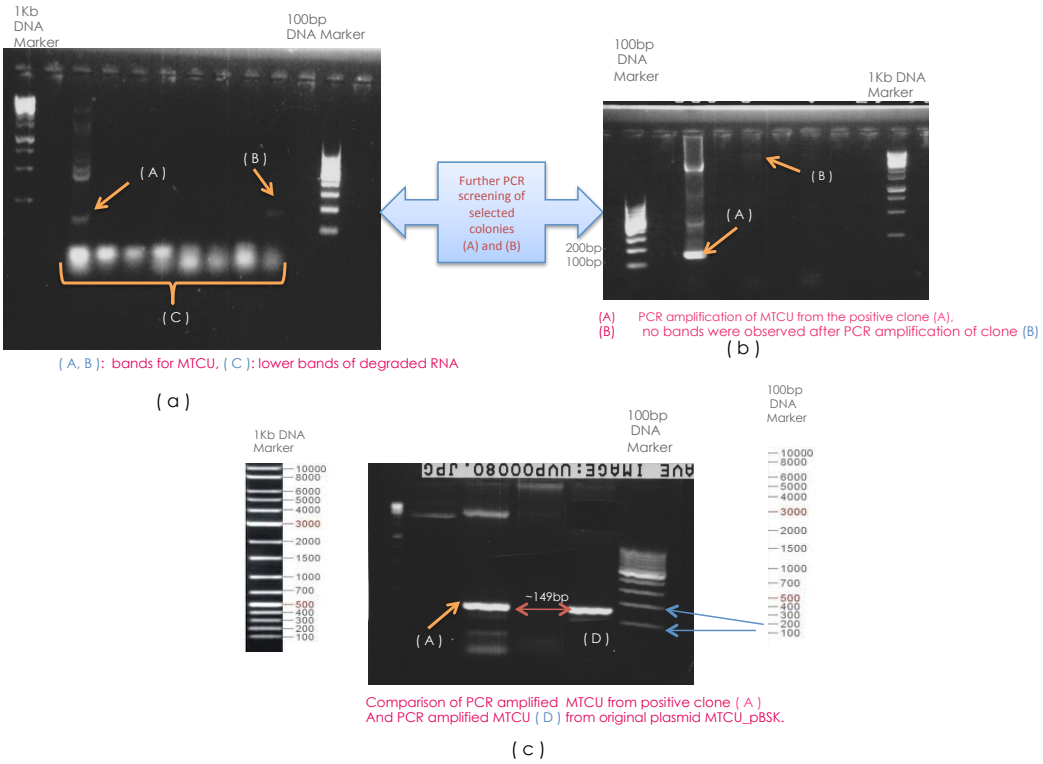

Figure 9.2 Sub-cloning of *mymT* in expression vector pET-26b.

Attempts were made to sub clone *mymT* into pET-26b. Gels displaying the PCR screening of the positive colonies obtained after ligation of *mymT* and pET 26b after restriction digest with BamH1 and Nde1 enzymes. However the construct recovered from these gels could not be sequenced for possible degradation before sequencing.

A9-Thesis Reference: Chapter 6, page

Table 9:5 Experimental and theoretical masses of species observed for Apo-MymT after Cu(I) addition.

The masses given are for the neutral species.

Species	Experimental (m/z)	Theoretical (m/z)
ApoMT	5058.16	5059.16
Cu_1MymT	5122	5122.66
Cu_2MymT	5178.8	5184.6
Cu_3MymT	5266.8	5246.6
Cu_4MymT	5310.84	5309.16
Cu_5MymT	5375.8	5371.6
Cu_6MymT	5436.8	5434
Cu_7MymT	5498.6	5496.5
Cu_8MymT	5559.56	5559